REPUBLIQUE DU CAMEROUN
PAIX-TRAVAIL-PATRIE
**********
UNIVERSITE DE YAOUNDE I
**********
ECOLE DOCTORALE DE
SCIENCES, TECHNOLOGIE
ET GEOSCIENCES
**********
DEPARTEMENT DE PHYSIQUE
**********
UNITE DE RECHERCHE ET
DE FORMATION DOCTORALE
EN PHYSIQUE ET APPLICATIONS

REPUBLIC OF CAMEROON
PEACE-WORK-FATHERLAND
**********
UNIVERSITY OF YAOUNDE I
**********
POST GRADUATE SCHOOL
OF SCIENCE, TECHNOLOGY
AND GEOSCIENCES
**********
DEPARTMENT OF PHYSICS
**********
RESEARCH AND POST
GRADUATE TRAINING UNIT
FOR PHYSICS AND APPLICATIONS

LABORATORY OF MECHANICS, MATERIALS AND STRUCTURES

# Relaxation and conductivity of exciton-polaron in transition metal dichalcogenides

Thesis

defended publicly in fulfilment of the requirements for the award of a
**Doctorate/Ph.D** in **Physics**
Option : *Mechanics and Complex Systems*



By

**TEGUIMFOUET KITIO Arthur**
*M.Sc in Physics*
*Registration number : 18W5516*

Under the supervision of :

**KENFACK**
**JIOTSA Aurelien**
*Professor*
*University of Yaoundé 1*

**KENFACK**
**SADEM Christian**
*Professor*
*University of Dschang*

Year 2024

UNIVERSITÉ DE YAOUNDÉ
THE UNIVERSITY OF YAOUNDE I

FACULTÉ DES SCIENCES
FACULTY OF SCIENCES

DÉPARTEMENT DE PHYSIQUE
DEPARTMENT OF PHYSICS

# ATTESTATION DE CORRECTION DE LA THÈSE DE DOCTORAT/PhD

Nous, Pr **FEWO Serge Ibraïd** et le Pr **NDJAKA Jean Marie Bienvenu**, respectivement Examinateur et Président du jury de la thèse de Doctorat/PhD de Monsieur **TEGUIMFOUET KITIO Arthur**, Matricule **18W5516**, préparée sous la direction du Pr **KENFACK JIOTSA Aurélien** (Université de Yaoundé I) et Pr **KENFACK SADEM Christian** (Université de Dschang), intitulée : « **RELAXATION AND CONDUCTIVITY OF EXCITON-POLARON IN TRANSITION METAL DICHALCOGENIDES** », soutenue le **mercredi, 23 avril 2025**, en vue de l'obtention du grade de Docteur/PhD en Physique, Spécialité **Mécanique, Matériaux et Structures,** option **Mécanique Fondamentale et Systèmes Complexes,** attestons que toutes les corrections demandées par le jury de soutenance ont été effectuées.

En foi de quoi, la présente attestation lui est délivrée pour servir et valoir ce que de droit.

Fait à Yaoundé, le 22 MAI 2025

| Examinateur | Le Président du jury | Le Chef de Département de Physique |
|---|---|---|
| Pr. FEWO Serge Ibraïd | Pr. NDJAKA Jean Marie | Pr. NDJAKA Jean Marie |

REPUBLIQUE DU CAMEROUN
PAIX-TRAVAIL-PATRIE
**********
UNIVERSITE DE YAOUNDE I
**********
ECOLE DOCTORALE DE
SCIENCES, TECHNOLOGIE
ET GEOSCIENCES
**********
DEPARTEMENT DE PHYSIQUE
**********
UNITE DE RECHERCHE ET
DE FORMATION DOCTORALE
EN PHYSIQUE ET APPLICATIONS

REPUBLIC OF CAMEROON
PEACE-WORK-FATHERLAND
**********
UNIVERSITY OF YAOUNDE I
**********
POST GRADUATE SCHOOL
OF SCIENCE, TECHNOLOGY
AND GEOSCIENCES
**********
DEPARTMENT OF PHYSICS
**********
RESEARCH AND POST
GRADUATE TRAINING UNIT
FOR PHYSICS AND APPLICATIONS

LABORATORY OF MECHANICS, MATERIALS AND STRUCTURES

# Relaxation and conductivity of exciton-polaron in transition metal dichalcogenides

Thesis
defended publicly in fulfilment of the requirements for the award of a
**Doctorate/Ph.D** in **Physics**
Option : *Mechanics and Complex Systems*

By

**TEGUIMFOUET KITIO Arthur**
*M.Sc in Physics*
*Registration number : 18W5516*

Under the supervision of :

**KENFACK**
**JIOTSA Aurelien**
*Professor*
*University of Yaoundé 1*

**KENFACK**
**SADEM Christian**
*Professor*
*University of Dschang*

Year 2024

# CERTIFICATION

I, the undersigned, **TEGUIMFOUET KITIO Arthur**, Registration Number : **18W5516**, hereby certify that this thesis entitled **"Relaxation and conductivity of exciton-polaron in transition metal dichalcogenides"** is the fruit of my personal research carried out in the "Laboratory of Mechanics, Materials and Structures" of the University of Yaoundé 1 under the co-direction of **Pr. KENFACK JIOTSA Aurelien** and **Pr. KENFACK SADEM Christian**, in partial fulfillment of the conditions for the award of a Doctor of Philosophy (Ph.D) degree in Physics (Option : Mechanics and complex systems). This work is authentic and has never been presented anywhere before.

The author :

**TEGUIMFOUET KITIO Arthur**

The supervisors :

**KENFACK**
**JIOTSA Aurelien**
*Professor*
*University of Yaoundé 1*

**KENFACK**
**SADEM Christian**
*Professor*
*University of Dschang*

# DEDICATION

To my parents **KITIO David** and **FOFE Denise**, and my wife **KENGNE Pierre Carole**.

# ACKNOWLEDGEMENTS

Above all, I would like to express my gratitude to the Creator since health, science, and everything come from you. This work would not have been possible without the support of many people.

I am sincerely grateful to my supervisors **Pr. KENFACK JIOTSA Aurelien** and **Pr. KENFACK SADEM Christian** for all the work done, both for academic and personal support. You were always present, open to discussion, and willing to share your knowledge. Thanks for your patience and guidance. You have become more than supervisors, you are role models to me.

I thank the jury members for accepting to evaluate my work. During the defense, I learned a lot from their feedback and shared experiences, for which I am truly thankful.

My thanks also go to the members of the pre-defense jury, whose comments and advice helped me to significantly improve the quality of this document.

I would like to express my sincere thanks to **Pr. NDJAKA Jean Marie Bienvenu**, Head of the Physics Department at the University of Yaoundé 1. I am deeply grateful for his administrative support and encouragement.

I also thank the entire staff of the Department for providing me a solid academic foundation.

My gratitude goes to the members of the laboratory of Mechanic, Material and Structures at the University of Yaoundé 1, particularly **Pr. TCHAWOUA Clement**, **Pr. FEWO Serge Ibraid** and **Pr. ZEKENG Serge**

**Sylvain** . Thank you for accepting this research topic and for the laboratory work.

I would also like to thank the members of the laboratory of Condensed Matter and Nanomaterials at the University of Dschang led by **Pr. FAI Cornelius** for the time, attention, and support they extended to me.

A special thank goes to **Pr. FEDDI Elmustapha**, member of the Optoelectronic of Semiconductors and Nanomaterials group of Mohammed V University in Morocco, for the exchanges that greatly contributed to the understanding and development of this work.

I am also grateful to my academic elders, especially **Dr. DJOKO Jean Paul**, **Dr. KEUMO TSIAZE Magloire**, **Dr. TAGOUEGNI Senghor**, **Dr. DJAZET Alain**, **Dr. FOBASSO Florette** and **Dr. DJOMOU Jules**, for the exchanges and encouragement.

I cannot forget my PhD mates. Thank you, in particular to **Dr. NGUEPNANG Valere**, **MOUNBOU Souleyman**, **NGUEMASSON Charles** and **Dr. NGOA Steve Barthelemy** for your constant availability and collaboration.

My deepest gratitude goes to my entire family, especially **KITIO David**, **FOFE Denise**, **TEGUIMFOUET Lydie**, **KENFACK Madeleine**, **DONFACK KITIO Cedric** and **AZEBAZE KITIO Fabrice**. Thank you for your unconditional support throughout my schooling.

Finally, I would like to extend my heartfelt thanks to all my friends and relatives, and to everyone who, in one way or another, contributed to the completion of this thesis, even if their names are not mentioned here.

# TABLE OF CONTENTS

# ABSTRACT

In this thesis, we investigated the exciton-polaron relaxation and conductive properties in monolayers TMDCs ($MoSe_2$, $WSe_2$, $WS_2$ et $MoS_2$) under the influence of a magnetic barrier and an electric field.

We showed that the exciton-polaron is confined in the magnetic barrier while its binding energy is weakened by the electric field. A long lifetime of exciton-polaron is favored in a strong magnetic field and a weak electric field, especially in $WS_2$. The shortest relaxation time is observed in $MoS_2$. The electric field disturbs excitonic states increasing the relaxation whereas the magnetic barrier stabilizes it. Strengthening the magnetic barrier reduces the electrical conductivity but the electric field enhances it. At low temperatures, TMDCs display good electrical conductivity and high thermoelectric efficiency, particularly in $MoSe_2$. At high temperatures, hot carriers responsible of the Seebeck current are disrupted. Moreover, TMDCs show high optical conductivity and absorption, especially $MoS_2$. This optical absorption, facilitated by the magnetic barrier, starts when the photon energy exceeds twice phonon energy.

In summary, tune the magnetic barrier, the electric field, and the temperature allows to improve the electrical and optoelectronic properties in TMDC monolayers.

**Keywords :** exciton-polaron, lifetime, magnetic barrier, relaxation time, electrical conductivity, absorption coefficient, TMDCs.

# TITLE IN FRENCH

# Relaxation et conductivité de l'exciton-polaron dans les dichalcogénures de métaux de transition.

# RÉSUMÉ

Dans cette thèse, nous avons étudié la relaxation de l'exciton-polaron et les propriétés conductrices dans des monocouches de TMDCs ($MoSe_2$, $WSe_2$, $WS_2$ et $MoS_2$), sous l'effet d'une barrière magnétique et d'un champ électrique.

Nous avons montré que l'exciton-polaron est confiné dans la barrière magnétique tandis que son énergie de liaison est fragilisée par le champ électrique. Une longue durée de vie de l'exciton-polaron est favorisée dans un champ magnétique fort et un champ électrique faible, particulièrement dans $WS_2$. Le temps de relaxation le plus bas est observé dans $MoS_2$. Le champ électrique perturbe les états excitoniques augmentant ainsi la relaxation alors que la barrière magnétique la stabilise. L'intensification de la barrière magnétique diminue la conductivité électrique mais le champ électrique la renforce. À basses températures, les TMDCs montrent une bonne conductivité électrique et une forte efficacité thermoélectrique, en particulier $MoSe_2$. À haute température, les porteurs chauds responsables du courant de Seebeck sont perturbés. De plus, les TMDCs présentent une forte conductivité et absorption optique, surtout $MoS_2$. Cette absorption, favorisée par la barrière magnétique, commence lorsque l'énergie du photon dépasse deux fois celle du phonon.

En résumé, ajuster la barrière magnétique, le champ électrique et la température permet d'améliorer les propriétés électriques et optoélectroniques dans les monocouches de TMDCs.

**Mots clés** : exciton-polaron, temps de vie, barrière magnétique, temps de relaxation, conductivité électrique, coefficient d'absorption, TMDCs.

# LIST OF ABBREVIATIONS

**BC** : Conduction Band
**GS** : Ground State
**LLP** : Lee-Low-Pines
**LA** : Longitudinal Acoustic
**LO** : Longitudinal Optical
$\boldsymbol{MoSe_2}$ : molybdenum diselenide
$\boldsymbol{MoS_2}$ : molybdenum disulfide
**1L** : monolayer
**RTA** : Relaxation Time Approximation
**3D** : Three Dimensional
**TMDCs** : Transition Metal Dichalcogenides
**TA** : Transversal Acoustic
**TO** : Transversal Optical
$\boldsymbol{WSe_2}$ : tungsten diselenide
$\boldsymbol{WS_2}$ : tungsten disulfide
**2D** : Two Dimensional
**BV** : Valence Band

# LIST OF TABLES

# LIST OF FIGURES

# GENERAL INTRODUCTION

## Context

In physics, a polaron is a quasiparticle used in a solid material to understand the interaction between electrons and atoms. The polaron is seen as an electron dressed with the phonons of the medium. It well describes the motion of the electron. When the structure is subjected to an excitation, that generates electrons and holes moving at the same speed but in opposite directions. An electron and its corresponding hole constitute a bound pair called exciton and exciton-polaron is the quasiparticle resulting from the interaction of an exciton with phonons of the structure due to lattice deformations. The concept of exciton-polaron is more important in the study of transport properties and precisely conductivity since it takes into account the hole. This quasiparticle groups polaronic and excitonic effects. Excitonic systems have been studied theoretically [1], experimentaly [2] and it is shown that the interactions with phonons highly contribute to excitonic states.

A suitable concept in the investigation of exciton-polaron systems is the relaxation, in particular for optical excitation, formation and recombination of excitons [3, 4]. The relaxation time was studied experimentally by many authors [5, 6, 7] and it follows that its range is around the femtoseconds (fs) and picosecond (ps) . The relaxation and the generation of excitons in intraconduction band were studied by El-Ballouli et al. [8]. They showed the important role of the confinement in the process of intraband relaxation since the relaxation time becomes shorter as decreases the size of the structure. Moreover, structures with small sizes favor the efficiency of transferring the energy of excess photon to carriers multiplication. Khoirunnisa et al. [9] investigating the optical conductivity demonstrated the presence of excitonic

signal and [10] showed that the role of exciton effects is crucial in the optical spectra. It is seen that for energies below the gap, it appears as a well-defined peak in the absorption spectra. Above the gap, we observed a band renormalization and an increase of the optical conductivity attributed to the Coulomb-mediated scattering of the electron-hole [11, 12]. Also, Peres et al. [13] found that excitonic resonances are responsible for some features of the experimentally measured midinfrared response of graphene such as the enhancement of the conductivity beyond the universal value above the Fermi blocked regime, the decrease of the optical conductivity at high frequencies and the broadening of the absorption at the threshold .

The miniaturization has an important place and is the subject of several works. One of the interesting 2D materials are TMDCs because of their several applications mainly related to their structures. The TMDC formula is in the form $MX_2$ where $M$ is the transition metal and $X$ the chalcogen. The $M$-atoms are sandwiched between atoms of two $X$-layers coupled to each other by Van der Waals interactions. They became particularly promising because of their semiconducting properties with high stability and large flexibility [14, 15, 16], their electronic and optical properties [17, 18] which indicate applications in photovoltaics, transistors, optoelectronics, photodetectors and molecular sensing [19, 20, 21], in spintronic and valleytronic effects [22], in photoluminescence experiments [23]. One of the problems in the modeling of exciton-polaron systems is the fact that operators are not always diagonally shaped in the Hamiltonian. Therefore, it begins necessary to use a method of diagonalization to obtain appropriate eigenvalues, eigenfunctions or other properties [24, 25, 26]. Thilagam [27] presented a model of system for 1L TMDCs. She used a unitary transformation and the variationnal method to approximatively diagonalize the operators, to determine the exciton-polaron effective mass and the ground state energy.

Yang et al. [28] investigated the electrical and optoelectronic properties in TMDCs and precisely the layer-dependence. It appears that these properties are strongly influenced by the number of layers. Monolayers provide better performances and the band gap rises when decreases the layers number. Chen et al. [29] showed the increase of electrical conductivity when

the thickness layer decreases. That leads to the probable surface dominance of electrical conduction in TMDC layer structures resulting from either the intrinsic high surface conductivity or the anisotropic conductivity. Qin et al. [30] studied the transport coefficient along different directions and highlighted the effect of electron (hole) concentration at room temperature. For electrical conductivity and thermopower they observed an anisotropic behavior. The electrical conductivity rises as increases the carrier concentration whereas the Seebeck coefficient decreases with this concentration. They found a larger asymmetry of the Seebeck coefficient for P-type doping than for N-type doping. High values of Seebeck coefficient are observed and a peak appears when the carrier concentration is about $1,25.10^{11} cm^{-2}$.

## Motivation

Since 1950, a part of the scientific community has been making a great effort to technically develop energy storage using solid materials. It is ten years after that the most important research programs in this field were developed from semiconductor materials. The desired material properties are determined through the figure of merit which depends on the transport properties of the material : Seebeck coefficient, electrical resistivity and thermal conductivity. The search for new sources of non-polluting energy has become a major challenge for our society. This is the reason why the production of electricity from waste heat using thermoelectric modules (application of the Seebeck effect) appears to date to be a very promising avenue. In addition, thermoelectric materials can be used to evacuate heat by the Peltier effect, in particular to cool the microelectronics components. Thus, thermoelectricity or conversion of energy from heat, is one of these new sources of renewable energy. The conversion of thermal energy into electrical energy is one of the mainstays of modern times because in power plants, a large part of fossil energy is lost in the atmosphere on the form of heat which cannot be efficiently exploited.

In this frame, thermoelectricity should emerge and play a role in future years by recovering the enormous quantities of lost energy (automobiles, boilers, incinerators, etc.) and contributing to sustainable development or

integrating other emerging technologies such as photovoltaic or geothermal. The majority of existing thermoelectric devices relate to modules made from materials based on solid $Bi_2Te_3$ and its derivatives, but these materials are neither biocompatible (toxic materials) nor integrable on a small scale. However, these two points are crucial aspects with a view to industrial transfers. In addition, manufacturing costs currently remain relatively high due in particular to weak production volumes and limited yield. Thus, the development of thermoelectric modules based on thin layers perfectly meets these two criteria.

Today, the consumer is also a nomad who wants to take his comfort with him, creating new needs for electrical energy sources. These needs are currently met at the cost of the pollution of our environment by the heavy metals contained in batteries. Thermoelectric conversion brings a new way to the growing demand for electrical energy source. Although the performance of thermoelectric devices is generally low, they are irreplaceable for certain applications such as the production of electrical energy for deep space probes (use of thermoelectric modules). Studies show that thin films have significantly higher thermoelectric performances than those obtained in bulk materials. However, few works have so far been devoted to thin-film materials and should improve heat-to-electricity conversion efficiencies.

Our motivation to explore the transport properties in 1L TMDCs stems from this interest in low-dimensional materials. Indeed, recent studies have shown that TMDCs are one of the best 2D compound semiconductors and good candidates for thermoelectricity since they have high-performance carrier mobility, low electrical conductivity at high temperatures and high Seebeck coefficient at low temperature [31].

## Problem statement

Several researchers have devoted themselves to the study of polaron and exciton, but few authors studied the notion of exciton-polaron and they just look at the system modelization, binding energy. Scarce are the works on exciton-polaron systems which highlight the influence of external parameters

constituting the environment.

Van der Donck et al. [32] showed that the presence of the magnetic strength reduces the electron-hole interdistance in TMDCs, leading to the increase of exciton binding energy with magnetic field . Seung-il et al. [33] proved that the role of external magnetic field is minor on the electrical conductivity for very strong magnetic strength, and it becomes relatively significant for temperatures. In addition, the electrical conductivity increases when the temperature and the relaxation time increase. Das et al. [34] revealed that the Seebeck coefficient decreases in magnetic field and globally it enhances with temperatures. Tahir et al. [35] showed that the magnetic field influence is important in the properties of magneto-optical transport in monolayer 2D phosphorene. The amplitude of optical transitions depends of the $xy$ momentum operator and the optical conductivity has an oscillatory dependence with the magnetic field . The magneto-optical response is limited for graphene and 2D electron gas to the terahertz range whereas in TMDCs it can be set in the visible, from microwave to terahertz.

Moreover, [36] studied the exciton transport in response to an in-plane electric field for 2D materials . It is showed that there is a short time regime in which the electron and the hole of exciton have velocities in the same direction. The two particles initially move in opposite directions until reach an equilibrium where the Coulomb interaction is closer to the force due to the electric field. In addition, the presence of an electric field considerably enhances the relaxation time [37] and reduces the optical absorption [38]. The binding energy of excitons decreases with the increase of the electric field [39] and can lead to the exciton dissociation.

It is clear that the temperature, the magnetic and electric fields are key parameters for the study of systems. We can ask ourselves: how can these parameters influence the electrical and optoelectronic properties in 1L TMDCs ?

## Objectives

The main objective is to investigate the relaxation and the conductivity of exciton-polaron in 1L TMDCs with the presence of some external parameters.

This will be done by explore the dynamic of exciton-polaron under a magnetic barrier and an electric field. Therefore, we project to study the exciton-polaron system in these conditions. As we are in a perturbed system, another objective is to bring out the effect of the external parameters (temperature, magnetic barrier and electric field) on the relaxation and formation of exciton-polaron as quasiparticle. From these two objectives, we will better understand the system and this is necessary before going to conductivity. By conductivity, we think of the electrical conductivity directly linked to the Seebeck coefficient and the optical conductivity which is closer to the optical absorption coefficient. We aim to show the variation of the electrical conductivity with temperature and with the system parameters ; to evaluate the impact of the magnetic barrier and the electric field on the thermoelectric property ; to look at the optical properties of the defined system.

## Outlines

To address our research objectives, we organized this thesis as follows:

Chapter one is a literature review in which we present the concepts of polaron, exciton-polaron and TMDCs. We provides an overview of the developments concerning them.

In chapter two, we present the theory and methods. The Lee-Low-Pines as variational method and the 2D theory are explained in order to obtain the 2D energy. Also, the Fermi's golden rule is used to derive the lifetime of exciton-polaron and the optical absorption coefficient while the relaxation time approximation permits to obtain the relaxation time of exciton-polaron, the electrical conductivity and the Seebeck coefficient. This chapter ends by the Kubo's formula for the determination of optical conductivity.

Chapter three is devoted to the results obtained for different TMDCs compounds under a magnetic barrier and an electric field. Here, the ground state and the first excited state eigen energies of exciton-polaron in 1L TMDCs are obtained by using the variational method. These energies allow to evaluate the Tsallis entropy of the system. Always to understand the behavior of the exciton-polaron in this environment, its lifetime and relaxation time are evaluated. Moreover, the electrical and optical properties of 1L TMDCs are determined through electrical conductivity, Seebeck coefficient, optical conductivity and optical absorption coefficient.

The thesis ends by a general conclusion which summarizes the results and we give some perspectives for future works.

CHAPTER 1

# LITERATURE REVIEW

## Introduction

This chapter is a general presentation of key concepts of the work. We focus on polaron, exciton-polaron, relaxation, conductivity and transition metal dichalcogenides. Here, we define each concept ; we explain each property ; we describe the TMDC structure and present some works done in that framework.

## 1.1 Concept of polaron

This section presents a histotical study of polaron and gives some basics important to understand this quasiparticle. We firstly look at the phonons which governe the polaron formation.

### 1.1.1 Phonons

Etymologically, the word phonon means "sound or voice" because long-wavelength phonons give rise to sound. A phonon is a quantum of vibration in a crystalline solid i.e an elememtary packet of vibration. It is associated to the collective vibrations of atoms in the lattice. The deformation is elastic and the propagating wave allows to explain the physical properties in solids. Phonons are analogous to photons.

The concept of phonon was created by Tamm [40]. In quantum mechanics, phonons are the quantum mechanical equivalent of a particular category of vibratory movements known as normal modes of vibration in classical mechanics. A normal vibration mode is a mode in which all the elements of a network vibrate at the same frequency. Phonons are quasiparticles of spin

0 and they are found only within a crystal lattice with a large number of particles, precisely in crystalline solids.

The forces acting between the different atoms in the lattice lead to move one or more atoms around their equilibrium position causing the vibration and propagation of waves through the lattice. The amplitude of the wave is given by the amplitude of atoms displacement around their equilibrium positions.

In physics, the phonon plays a crucial role. It is indeed involved in many physical properties of solids such as thermal or electrical conductivity, propagation of sound waves or the ability to store heat. In a real solid, there exist acoustic phonons and optical phonons.

*** The acoustic phonons**

They are phonons that typically correspond to sound waves in the network. Acoustic phonons have lower frequencies and there is a linear relationship between the phonon wave vector and frequency. Acoustic phonons increase with wave vector starting from zero to a saturation limit. There exist transversal and longitudinal acoustic phonons. We speak of longitudinal waves when the waves oscillate parallel to the direction of propagation. In the case of transverse waves, the oscillation is perpendicular to the waves direction.

*** The optical phonons**

These phonons are present in solids that have several atoms per cell. The word optical is because light waves (in the infrared range) easily excited them in ionic crystals. This is due to the fact that they correspond to modes of vibration for which the positive and negative ions located on adjacent sites of the network approach and move away from each other by creating an electric dipole moment oscillating with time. Optical phonons interacting with light in this way are said to be active in the infrared. The optical frequency is nearly independent of the phonon wave vector and one distinguishes longitudinal and transversal optical phonons.

### * Hamiltonian of phonon

The Hamiltonian of lattice vibrations is equal to the phonon Hamiltonian and can be written as follows:

$$H_{ph} = \frac{M}{2} \int \left[ \dot{\hat{p}}^2(r) + \omega_s^2(q) \hat{p}^2(r) \right] dr \tag{1.1}$$

with

$$\vec{p}(r) = \frac{1}{4\pi\varepsilon} \vec{D} \tag{1.2}$$

and

$$\frac{1}{\varepsilon} = \frac{1}{\varepsilon_\infty} - \frac{1}{\varepsilon_0} \tag{1.3}$$

$\vec{D}$ is the electric induction, $r$ is the position of the electron, $\omega_s(q)$ is the frequency of the phonon with wave vector $q$ in the branch index $s$ (acoustic or optic), $\varepsilon$ is the polarizability of the medium, $\varepsilon_0$ and $\varepsilon_\infty$ are respectively the polarizability of the vacuum and at infinity.
Let us consider:

$$\dot{y}(r) = \frac{\partial H_{ph}}{\partial \hat{p}(r)} = M \dot{\hat{p}}(r) \tag{1.4}$$

$$x(r) = \hat{p}(r) \tag{1.5}$$

Then we have:

$$H_{ph} = \frac{1}{2} \int \left[ \frac{y^2(r)}{M} + M\omega_s^2(q) x^2(r) \right] \tag{1.6}$$

$$\begin{aligned} H_{ph} \;=\; & \tfrac{1}{2} \sum_q \hbar\omega_s(q) \left[ \sqrt{\tfrac{M\omega_s(q)}{2\hbar}} x_q - i \sqrt{\tfrac{1}{M\hbar\omega_s(q)}} y_q \right] \times \\ & \left[ \sqrt{\tfrac{M\omega_s(q)}{2\hbar}} x_q + i \sqrt{\tfrac{1}{M\hbar\omega_s(q)}} y_q \right] \end{aligned} \tag{1.7}$$

$q$ is the wave vector of phonon, $x_q$ and $y_q$ are canonical variables. Then the Hamiltonian of the phonon takes the form:

$$H_{ph} = \frac{1}{2} \sum_q \hbar\omega_s(q) b_q^\dagger b_q \tag{1.8}$$

with

$$b_q^\dagger = \sqrt{\frac{M\omega_s(q)}{2\hbar}} x_q - i \sqrt{\frac{1}{M\hbar\omega_s(q)}} y_q \tag{1.9}$$

$$b_q = \sqrt{\frac{M\omega_s(q)}{2\hbar}}x_q + i\sqrt{\frac{1}{M\hbar\omega_s(q)}}y_q \tag{1.10}$$

where $b_q^\dagger$ ($b_q$) denotes the creation (anhilation) operator of phonons.

### 1.1.2 Polarons

The first who introduced the concept of polaron was Landau [41] and the polaron is explained by starting with the description of crystals. The crystals structure can be pictured in terms of lattice (a periodic and regular arrangement of points). Each lattice point has an associated group of atoms named basis that can be periodically repeated in space to constitute the crystal structure. At room temperature, atoms are not fixed but they vibrate around their equilibrium positions (the lattice points). These vibrations will form a displacement field that can be quantized to phonons. In the crystal, the ionic polarization appears by the electric field of a conduction electron that moves the negative and positive ions (attraction and repulsion according to Coulomb force): this movement can be described as cloud or waves of phonons.

In an ionic crystal or a polar semiconductor, a conducting electron (or hole) together with its self-induced polarization form a quasiparticle called a polaron. In the polaron formation, the electron polarizes the lattice producing a potential well around itself in which it becomes trapped: self-trapping.

In ionic semiconductors or polar crystals, the polaron is interesting because it describes the particular physical properties of an electron and represents a good theoretical model of interaction between a fermion and a boson field. As parameters that characterize it we have : the self or binding energy, the effective mass, its radius, the number of phonons in its cloud and the response to an external field. In addition, the coupling constant commonly denoted $\alpha$ represents the electron-phonon interaction strength . For $\alpha < 1$ it is weak coupling, $\alpha > 7$ strong coupling and between these ranges we speak of intermediate coupling. It is possible to classify polarons according to the size and the interacting phonons frequency.

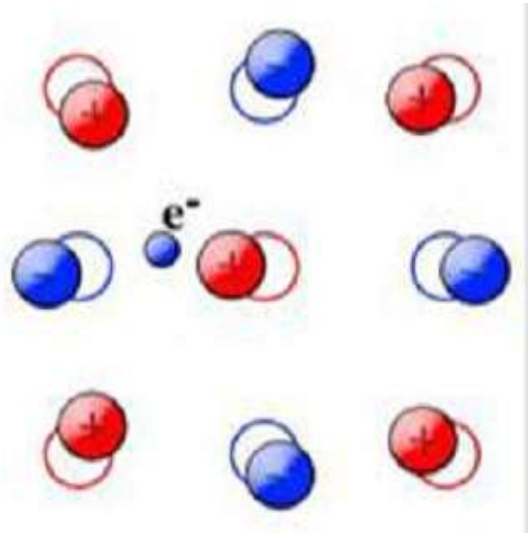


Figure 1.1: Representation of a polaronic structure.

*** Fröhlich polaron or large polaron**

One talks of Fröhlich polaron when the ion displacement is greater than the lattice constant and the lattice deformation will be large. This polaron is ruled by the long range interaction and generally the self trapped electron extends over several sites [42, 43]. Moreover, in a large polaron regime, one can change the lattice by a continuum medium but it is not appropriate for the case of small polaron.

*** Holstein polaron or small polaron**

Holtein polaron means that the ion displacement is lower than the lattice constant and the lattice deformation will be small. The self trapped electron is locked in a single site and this polaron is ruled by the short range interaction [43, 44].

*** Optical polaron**

Here, the word optical is due to the fact that this type of polaron comes from the interaction between the electron of conduction and optical modes of vibrations with high frequencies in polar materials. The optical polaron easily interplays with light.

### * Acoustic polaron

The acouctic polaron is formed in structures resulting from the interplay between the electron and acoustic phonons at lower frequencies or between electron and the short range acoustic deformation potential. In theory, for the treatment of this polaron one usually imposes a Debye cut-off wavenumber on the deformation potential interplay [27].

### * Hamiltonian of polaron

The polaron theory is governed by the Hamiltonian which can be splited into three parts [42]: the electron Hamiltonian ($H_e$), the phonon Hamiltonian ($H_{ph}$) and the Hamiltonian of electron-phonon interaction ($H_{e-ph}$) appearing as :

$$H_{pol} = H_e + H_{ph} + H_{e-ph} \tag{1.11}$$

We can write in this form :

$$H_{pol} = \frac{p_e^2}{2m_e} + \sum_q \hbar\omega_{LO} b_q^\dagger b_q + \sum_q \left[V_q b_q e^{iq.r} + V_q^* b_q^\dagger e^{-iq.r}\right] \tag{1.12}$$

where $\vec{p_e} = (p_{ex}, p_{ey}, p_{ez})$ and $m_e$ represent respectively the momentum vector and the mass of electron, $V_q$ is the amplitude of the electron-phonon interaction given by:

$$V_q = -i\left(\frac{\hbar\omega_{LO}}{q}\right)\left(\frac{4\pi\alpha}{V}\right)^{1/2}\left(\frac{\hbar}{2m_e\omega_{LO}}\right)^{1/4} \text{ in 3D} \tag{1.13}$$

$$V_q = -i\left(\frac{\hbar\omega_{LO}}{\sqrt{q}}\right)\left(\frac{2\pi\alpha}{S_{2D}}\right)^{1/2}\left(\frac{\hbar}{2m_e\omega_{LO}}\right)^{1/4} \text{ in 2D} \tag{1.14}$$

with $V\,(S_{2D})$ is the volume (surface) of crystal, $\hbar\omega_{LO}$ is the LO-phonons energy and $\alpha$ is the standard electron-phonon coupling constant given by:

$$\alpha = \frac{e^2}{2\hbar\varepsilon_0}\sqrt{\frac{2m_e}{\hbar\omega_{LO}}}\left(\frac{\varepsilon_0}{\varepsilon_\infty} - 1\right) \tag{1.15}$$

where $\varepsilon_\infty\,(\varepsilon_0)$ is the high frequency (static) dielectric constant of the medium. [42] used the first weak coupling perturbation-theory and obtained the po-

laron binding energy in the GS as:

$$E_{pol}^{3D} = -\alpha\hbar\omega_{LO} \tag{1.16}$$

Electron system in reduced dimensions as in 2D is of great interest. The polaron effect and the electron-phonon interplay are important in such systems. For a polaron confined in 2D and interacts with a 3D phonon cloud, the Hamiltonian remains on the same form but with a simple modification in $V_q$. The polaron self energy in 2D and weak coupling was first derived by [45] and provided the result:

$$E_{pol}^{2D} = -\frac{\pi}{2}\alpha\hbar\omega_{LO}. \tag{1.17}$$

For the strong-coupling [46, 47], one gets the results:

$$E_{pol}^{3D} = -\frac{\alpha^2}{3\pi}\hbar\omega_{LO} \tag{1.18}$$

$$E_{pol}^{2D} = -\frac{\pi\alpha^2}{8}\hbar\omega_{LO}. \tag{1.19}$$

It is clear that the decrease of the dimensions leads to an increase of the value of the binding energy of the polaron. This is because the confinement increases the binding energy.

### 1.1.3 Historical study of polaron

Historically, the first study on polaron is the one of [41] that described the concept of polaron. In 1937, [48] gave a discussion about electron scattering in ionic crystals and the notion of lattice displacement was introduced as a field. In 1949, the Fröhlich Hamiltonian of polaron is derived using the quantum field theory [42, 49] solved the weak coupling problem via the perturbation theory . In 1951, from the work of [42], Pekar and Landau studied the effective mass and the binding energy of polaron in strong coupling regime [44]. LLP [50] in 1953, provided a variational method which depends on a series of successive canonical transformations and obtained good results for intermediate coupling. In 1954, [51] developped the trial wave state of polaron $\psi$ appearing in two parts : the wave function of electron $\phi_e$ and the

wave function of phonon (field) $\phi_{ph}$ given by:

$$\psi = \phi_e \phi_{ph} \tag{1.20}$$

It can also take the form:

$$|\psi\rangle = |\phi_e\rangle \, |\phi_{ph}\rangle \tag{1.21}$$

Feynman, in 1955, looking the work [42] proposed the Lagrangian form of quantum mechanics for the polaron problem. He considered the polaron as two classical particles and eliminated oscillators (waves). In 1976, Huybrechts [52] suggested a change on the method of [50] and investigated the problem for all coupling. He presented a simple unitary transformation and obtained results of GS energy in agreement with those of others. Even if the problem of polaron seems to be an old subject, it remains interesting because of the physic that it represents : a theoretical model of a particle interacting with a fluctuating medium. The concept of polaron connects both the quantum field theory and the condensed matter physics.

In addition, another important concept is the magnetopolaron which shows the influence of the external magnetic field in the polaron problem. A large number of theories and experiments [53, 54, 55] investigated the polaronic effects in semiconductors with the absence of a magnetic field. In all magnetopolaron studies there exists an interrelation between the magnetic strength and the polaron coupling strength. An additional term appears in the Fröhlich Hamiltonian resulting of the magnetic field and then the self energy becomes greater due to the additional degree of localization brought about. [56] made a great contribution in the theoretical study of polarons with magnetic fields. The lattice responds to the overall motion of the faster electron in its Landau orbit [57]. The high degree of confinement and the magnetic strength lead to the pseudo increase of $\alpha$ and therefore the enhancement of the polaronic effect. Many researches and studies [55, 57] focused on the quantum systems such as magnetopolaron and polaron with reduced dimensionality in semiconductors since it is important in microfabrication technology. Other authors also explored the properties of polaron in low dimensions [58, 59, 60], in crystals and polar semiconductors [53, 61]. Despite this long history, the interest of polaron continues to be topical and has given birth to other quasiparticles.

As well as the polaron has been studied, another concept more interesting is the exciton-polaron. The latest will be the center of the next section.

## 1.2 Concept of exciton-polaron

In this second section, before going to the quasiparticle of exciton-polaron, it is necessary to explain the concept of exciton.

### 1.2.1 Excitons

In semiconductors and crystals, the absorption of an incident photon excits an electron which jumps from the valence band to the conduction band. In the valence band this creates a positive charged vacancy named a hole. Due to the Coulomb interaction between the hole and the conduction electron, a bound neutral system is formed such as a hydrogen atom. Exciton represents this bound set consisting of the conduction electron and hole.

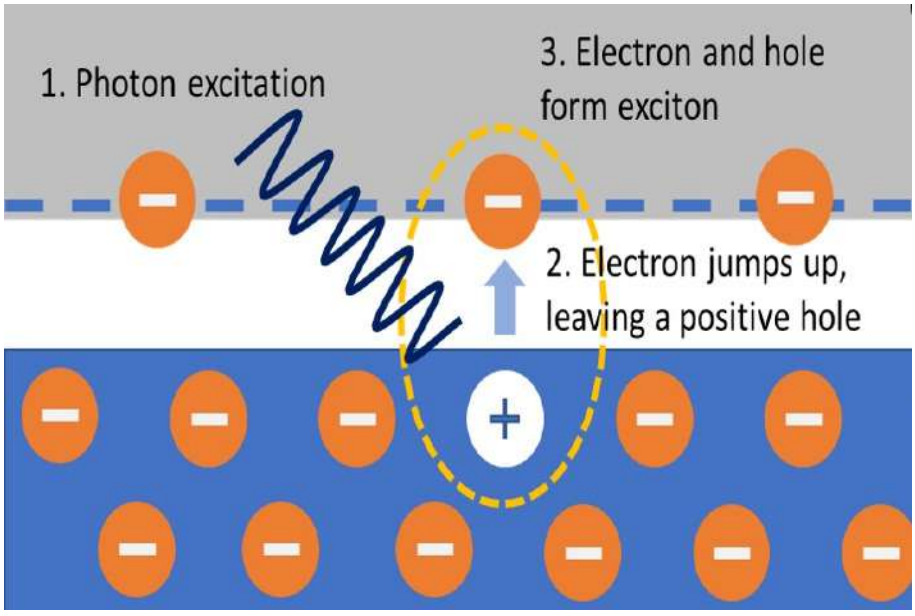


Figure 1.2: Schematic of an exciton formation.

The pseudomomentum carried by an exciton corresponds to the vector sum of the electron momentum , the hole momentum and their relative momentum. The pseudomomentum allows the exciton to move throughout the

crystal while the relative part determines its internal structure. In a perfect crystal an exciton has a uniform motion.

For an excitonic system, in a medium with dielectric constant $\varepsilon$ , the Bohr radius is given by:

$$a^{3D} = \frac{h^2\varepsilon}{e^2}\left(\frac{1}{m_e} + \frac{1}{m_h}\right) \tag{1.22}$$

$$a^{2D} = \frac{1}{2}a^{3D} = \frac{h^2\varepsilon}{2\mu e^2} \tag{1.23}$$

According to the size of exciton Bohr radius, one can distinguish:

*** Wannier exciton**

Here, the Bohr radius is larger and it extends over a number of lattice sites. Therefore, the corresponding exciton has a lower binding energy and is delocalized over a number of lattice sites. Both the hole and the electron are mobile. The underlying lattice of atoms is considered as a background field where holes and electrons exist as free particles, and the exciton is seen like an electron and a hole in orbit each other in this medium. The Wannier-Mott exciton is analogous to the hydrogen or positronium with the difference that the binding energy of the former is several orders of magnitude less than the positronium binding energy due to the rescaling of the Coulomb interaction.

*** Frenkel exciton**

The Bohr radius of a Frenkel exciton is smaller. An exciton is strongly bound and usually localized on one site. The hole and the electron don't move independently. The exciton motion is seen as hopping of both the hole and the electron from one atom to another. If an electron is excited from a valence shell of an atom into an excited state of a nearby atom. The Coulomb repulsion of the electron on the valence electrons of the new atom will be teed to push one of them into the hole left in the valence shell of the original atom when the electron was excited. This effectively causes the hole in the valence shell to follow the excited electron. One could say that the excited electron (negative charge) attracts the hole (positive charge) in the valence band,

taking it along to the new atom [62]. The Frenkel excitons are present most commonly in polymers, molecular crystals, and biological molecules and they are very important to explain energy transfer. Here, they find application in organic solar cells. They are also present in inorganic materials like alkali halides and noble gas crystals.

*** Hamiltonian of exciton**

An excitonic system is related to the Hamiltonian of its different particles, one gets:

$$H_{ex} = H_e + H_h + H_{e-h} \tag{1.24}$$

$H_e$ and $H_h$ represent respectively the Hamiltonian of electron and hole while $H_{e-h}$ corresponds to the interaction between them. The latest equation can be on the form:

$$H_{ex} = \frac{p_e^2}{2m_e} + \frac{p_h^2}{2m_h} - \frac{e^2}{\varepsilon|r_e - r_h|} \tag{1.25}$$

$\vec{p}_h = (p_{hx}, p_{hy}, p_{hz})$ and $m_h$ represent respectively the momentum vector and mass of hole, $r_e$ ($r_h$) is the electron (hole) coordinate and $e$ the electric charge.

### 1.2.2 Exciton-polaron

In solid state physics, phonons are very important because they represent the intrinsic characters of the solid and they are involved in the majority of excitonic mechanisms. For instance, in a crystal, the exciton formation from an excited pair of electron-hole or vice versa isn't possible without the involvement of phonons for the momentum and energy conservations. Exciton-polaron is a many-body quasiparticle formed when the electron-hole pair (exciton) interacts with optical or acoustic phonons via coupling to the deformation potentials. An exciton and its accompanying lattice distortion can be modeled as a dressed particle called exciton-polaron with an effective mass and a self-energy.

Thus, the crucial and additional aspect for this quasiparticle is the interaction between exciton and phonon. When the basis atoms have unequal charges, in ionic crystals of alkali halides for example, a mobile particle can

polarize the electric field around it. This polarization produces a displacement of ions in the lattice and then the lattice will vibrate in a frequency of resonance with the one of the polarization field. Usually, the vibrations frequency is in the range of optical phonon frequencies and such a polarization leads a strong coupling between carrier and phonons in polar crystals. This interplay is of large range meaning that even if the carrier-ion distance is relatively large there still have a polarization effect.

Moreover, in nonpolar crystals and semiconductors, the dilations related to phonons (lattice waves) can give rise to several localized deformations of the site. Usually, such dilations result in a drop of the bands energy and may be expressed in terms of an effective potential or deformation potential, which stands for the interaction of carrier-phonon [63].

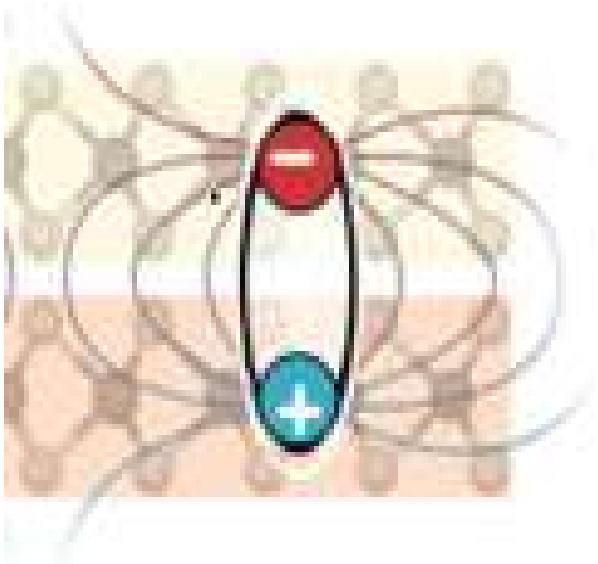

Figure 1.3: Representation of an exciton-polaron.

For excitonic polaron, the Hamiltonian of the composed system is as follows [64]:

$$H_{ex-pol} = H_{ex} + H_{ph} + H_{ex-ph} \tag{1.26}$$

$H_{ex-ph}$ corresponds to the Hamiltonian of exciton-phonon interaction and it can be written as:

$$H_{ex-ph} = \sum_{K,q,s} \Xi^{s}(q) C^{\dagger}_{K+q} C_K \left( b^{\dagger}_{-q,s} + b_{q,s} \right) \tag{1.27}$$

$\Xi^s(q)$ is the exciton-phonon coupling function while $K$ stands for the exciton wave vector and $s = ac/op$ for the phonon mode.

### 1.2.3 Overview on exciton-polaron

Exciton-polaron strongly modifies the optical spectra and generally in solid state systems its modeling by the use of standard techniques is a difficult task due to the absence of a unified and simple scheme which remains valid for a large range of the exciton-phonon couplings .

The exciton-polaron formation has been examined in materials for various configurations. The theory of 3D exciton-polaron has been well developed and the quasiparticle behaviour depends on its strength of interplay with phonons. The interaction between exciton and phonon plays an crucial role in the intrinsic and optical transport properties in materials. The energy and the effective mass are strongly related to the coupling strength of exciton-phonon. In 2018, Shree [65] underlined that compared to quantum well structures the exciton-phonon coupling is much stronger in 2D TMDCs . The importance of the interactions of exciton-phonon is also seen via the presence of a multitude of Raman features in the photoluminescence excitation experiments.

In 2021, Li et al. [66] studied $MoSe_2$ single layer at room temperature and revealed that the exciton-phonon coupling plays an important role in the determination optoelectronic properties of TMDCs. They used 2D microspectroscopy to evaluate the exciton-phonon coupling and detected the beating signals as a function of waiting time induced by the coupling between optical phonons and A-excitons. This technique gives a unique tool of measurement the coupling constant in other systems of heterogeneous semiconductors, with a spatial resolution of 260 nm and provides relevant parameters for the enhancement of optoelectronic devices. Moreover, in 2022 Antonius [67] investigated the theory of exciton-phonon coupling taking into account electron hole correlations in 2D materials with strong electron-hole interplay generally. Resulting from the exciton-phonon interplay, they derived a practical expression for the phonon induced term in the self energy of exciton, highlighted the temperature influence on the optical transition energies and

the increase in lifetime .

It appears that the formation of this quasiparticle is very linked to the exciton, the phonon and their interaction which is also useful in relaxation processes.

## 1.3 Phenomenon of relaxation

Here, we give some mechanisms that help to explain the phenomenon of relaxation, in a general frame and afterwards for the exciton interacting with phonons.

### 1.3.1 Generality

The easiest way to study carrier dynamics in quantum structures consists of generating a large number of carriers in the sample and observing their energy distribution as well as their evolution over time. For this, we can create a large number of electrons (and or holes) with excess energy, by optical (laser), electrical (direct voltage) or thermal excitations. After an extremely fast thermalization time between the carriers (a few hundred femtoseconds), the carriers will be distributed among the different available energy levels of the system, according to the relative importance of the various relaxation mechanisms.

The optical properties vary according to the materials used and the size of the structures. The energy relaxation mechanisms considered are generally governed by the principle of minimization the system energy taking into account the Pauli exclusion principle and the interactions between particles or quasiparticles. Relaxation of carrier energy in quantum structures can be done as follows [68]:
- interlevel relaxation, from excited states to states of lesser energy.
- electron-hole or excitonic recombination. It may involve carriers in different quantum states of the system when the selection rules are respected.

Note that the relaxation scheme can be much more complex depending

on the conditions of the problem. These processes can be radiative (emission of a photon), or non-radiative (transfer of excess energy to another carrier, to lattice vibrations or to a defect in the crystal). The electron excited by the absorption of photons or by another excitation is in interaction with a large number of other particles, which will lead to a rather efficient relaxation of the energy that it has stored. The processes differ depending on the interaction considered.

*** Radiative recombinaison**

The electron first interacts with the hole it left in the valence band (see possibly at high excitation density with holes corresponding to other excited electrons). To this interaction correspond the processes of radiative relaxation : by emitting a photon, the electron recombines with the hole. It is a perfectly symmetrical process to the one of linear absorption. Note that the radiative processes are slow, typically nanoseconds, sometimes more and rarely less. They only become important when the other relaxation processes have been unplugged.

*** Electron-electron interaction : collision**

An excited electron interacts with other electrons in the system. In a model of independent electrons, we can treat this interaction with a model of collision : an electron of conduction for example can in a collision with another electron of the system transmit all or part of its energy to it. In the case of metals, this problem (which is obviously important from the point of view of transport theories electronics) is treated using the Fermi liquid theory. Let's just say that the possibility for an electron above the Fermi level to excite other electrons depends on the phase space accessible to itself and to the electron it excites. In the final state of the collision, the latter being limited by the Pauli exclusion principle.

So far, we have considered only individual collision processes. Among the mechanisms of electronic energy losses, it is also necessary to take into account collective processes. We speak of loss of energy by excitation of plas-

mons. The concept of plasmon of a gas of free electrons (Drude model) is well known: it is the central element of the optical properties of metals. The existence of characteristic energy loss peaks corresponding to the energy of these plasmons is a well-known result in electronic energy loss spectroscopy, whether in metals or insulators.

*** Electron-phonon interaction**

The electrons are obviously in interaction with the ions of the network, but it is obviously necessary to specify that this interaction is taken into account in the band structure of the material. The vibrations of the lattice imply deviations from these equilibrium positions and then a modification of the interplay with electrons. The perturbative treatment of this interplay leads to the notion of electron-phonon interaction.

Network vibrations can be seen as a set of harmonic oscillators. The phonons are the vibration quanta corresponding to these oscillators. Like electrons, these phonons have a band structure (dispersion relation $\omega(q)$). Depending on the type and number of atoms per cell, we obtains two categories of branches corresponding to acoustic phonons and optical phonons, these last only in the case where there are two different atoms per cell. we can consider that the acoustic phonons represent the overall dilation oscillations of the lattice, the optical phonons represent the dipole oscillations of different atoms with respect to each other.

Using this representation, the interaction of lattice vibrations and the electron can be viewed as a collision between the phonon and the electron, during which the phonon is emitted or absorbed . We have :
- the annihilation of a $k$-state electron and a phonon with wave vector $q$ ; the creation of a $(k+q)$-state electron.
- the annihilation of a $(k+q)$-state electron ; the creation of a phonon with wave vector $q$ and a $k$-state electron.

Phonons carry an important moment. In a three-body collision (electron-photon-phonon), the absorption of a photon provides a large energy but little momentum, whereas the absorption (or emission) of a phonon involves little

of energy but a large moment transfer. This opens up the possibility of indirect transitions.

Let us point out, concerning the electron-phonon collision rate, that it depends on the effective ions lattice-electrons interaction. This means taking into account the screening of this interaction by the other charges of the lattice. From this point of view, metals and insulators differ profoundly. Screening by other conduction electrons is strong in metals whereas it is almost non-existent in insulators. This explains why the electron-phonon collision rate is much greater in the latter.

Finally, an electron undergoes a collision with a probability per unit time $1/\tau$. This probability does not depend on the position and the speed of the electron. The time $\tau$ is called *relaxation time*. This implies that an electron propagates on average for a time $\tau$ before its next collision and has spread an average of $\tau$ time since its last collision.

### 1.3.2 Case of polaron

Given that the separation energy between the GS and the first excited state is of the order of a few tens of meV, the first theoretical studies [53, 69, 70] predicted that energy relaxation was affected by the bottleneck phonon phenomenon. However, a finite relaxation time is measured by experiments pump-probe [71, 72]. The nature of this relaxation was first explained by Li [73] taking into account the intrinsic instability of LO-phonons. Others models [74, 75] were subsequently proposed but only allow the relaxation of polarons in a narrow energy window around that of the LO-phonons.

In the literature two models were available to describe the polaron relaxation:

- Li [73] were the first to consider carrier relaxation induced by LO-phonon instability. In his model, a phonon damping rate was phenomenologically incorporated into the time-dependent Schrodinger equation for the electron-LO-phonon system. From there, they derived a lifetime formula for polarons dependent on two parameters: the coupling strength of electron-LO-phonon and the rate of damping. This model was used taking these parameters as

adjustable to account for measurements of the increase in polaron lifetime with their energy in the range of 40 to 52 meV. However, this model does not explain the case of more energetic polarons.

- Verzelen [74] and Jacak [75] applied the Fermi's golden rule on polaron states assuming that the anharmonic mechanism highlighted by Bogani and Vallée for massive LO-phonons was the only one possible. This hypothesis leads to the existence of a narrow relaxation energy window: only polarons whose energy is between 35 and 44 meV can decay. This model therefore did not make it possible to interpret experiments where a much wider range of energy could be probed.

For the weak coupling, the relaxation of carrier in response to atomic motions alters only their frequencies. The carrier threrfore lowers the GS energy of the interacting system by a modest amount which vanishes as atomic vibrations are suppressed. For the strong coupling, much higher energy shifts appears and the carrier is self trapped: linked in the potential well generated by carrier induced shifts of atoms equilibrium positions. When the self trapped electron energy highly exceeds the characteristic energy of phonon then a stable and strong coupling polaron is formmed. Carrier induced the reduction of atomic vibrational frequencies then contribes to an energy of strong coupling polaron. For small polaron hopping, it implies local accumulation and dissipation of the atomic vibrations energy . In particular, the elemental thermally assisted small polaron hop starts as the atomic vibrations magnitudes increase while the self trapped carrier occupies its initial site and finishes when the vibrational energy is dissipated to neighboring atoms after the electronic transfers to its final site. Then, the hopping process implies vibrational dispersion. Only early studies of small polaron hopping addressed explicitly the actual inter-site transfer of an electronic carrier. They ignored the mechanisms ruling the local accumulation and subsequent dispersion of vibrational energy.

Instead, the local vibrational energies were assumed to keep their equilibrium distribution. In the non adiabatic limit, this process is justified since the possibility of an electronic transfer in response to atoms assuming favorable configurations is arbitrarily low. As such, the dispersion related

transfers of atomic vibrational energies are always fast enough to establish equilibrium prior to an electronic carrier transfer between sites. However, as noticed earlier, the small polaron hopping is typically adiabatic. In this case, the inter-site transfer of an electronic charge appears in less than a vibrational period whereas the dissipation and accrual of vibrational energy is much smaller. The small polaron hopping is then affected by the transport of vibrational energy. After a hop, the vibrations energy is lost away from the concerned sites. In a 3D vibrations system, following a jump with the energy of activation $E_A$, the sites energy falls to $K_BT/2$ after a time $\tau \approx (1/\Delta\omega)(2E_A/K_BT)^{2/3}$ , where $\omega$ stands for the frequencies dispersion which characterizes the phonons affected by the jump. Generally, this time of relaxation will overcome that governing the vibrations of atoms: $\omega\tau \gg 1$, where $\omega \gg \Delta\omega$ and $E_A \gg K_BT$ . Thus, the relaxation from one jump may not be completed before vibrations establish another adiabatic hop and the jump will then be correlated.

The coherent motion of large polaron also produces an absorption similar to the Drude absorption of conventional electronic carriers. Distinctively, a great mass of large polaron causes it to be only very poorly scattered by ambient phonons which reflect off its softened atomic vibrations. As such, a motion of large polaron is characterized by a long time of relaxation that limits its Drude-like contribution below the characteristic frequency of phonons. Then, there is a pseudogap in the absorption spectrum of large-polaron between the onset of its broad high-frequency photoionization band and its very low frequency Drude-like absorption. This pseudogap opens with decreasing temperature as the phonon scattering is gradually suppressed. The transport of large polaron depends critically on the modes of phonon implyed in the construction of potential well in which its electronic charge is self trapped. These modes are weakened locally by relaxation of the large polaron self trapped electronic charge to their atom vibratory displacements. A large polaron's local weakening of these vibrational modes impedes passage of the solid's indigenous phonons through it. This regional phonon softening is the origin of the scattering between a large polaron and ambient phonons. The scattering dynamics between a phonons and a large polaron depends on the speed with which the vibrations energy can be transported through a solid.

This phonon transport feature is ruled by their vibrational dispersion. Two examples illustrate contrasting limits : the acoustic phonons have significant dispersion with the speed of their longitudinal branches being just that of sound whereas the optical phonons are often considered as Einstein oscillators that possess no vibrational dispersion. Then, the large polaron great mass causes it to move slower than the acoustic phonons it scatters, and the Einstein oscillators move slowly than a large polaron.

### 1.3.3 Case of excitons

For excitons, the phenomenon of relaxation appears through two mechanisms : the multiple excitons generation and the exciton reconbinaition.

*** Multiple excitons generation**

Carriers multiplication is the mechanism wherein a single photon absorption leads to the excitation of many electrons that jump towards the conduction band. Theoretically for a conventional solar cell, a photon is able to excite only one electron across the semiconductor band gap and any excess energy of that photon is lost as heat. In a structure with carriers multiplication, the greater is the photons energy and on average more there are excitations across the band gap. In this case, the solar cell can produce more useful work in principle.

In organic materials, when a molecule is excited, electrons can access unoccupied upper orbitals and depending on the different possible configurations, a multitude of excited states are formed. The excited electron (conduction band) coupled with its corresponding hole (valence band) form an exciton. The carriers multiplication can be viewed as creating several excitons and its effect may enhance considerably the energy conversion efficiency of solar cells. However, one difficulty in the energy extraction may be the short lifetime of multiple excitons.

The quantum mechanical origin of multiple excitons generation is still under debate and some possibilities are suggested [76]:

- *Impact ionization.*

An exciton with high energy is excited by light and it irreversibly decays into a continuum of multiexciton states available at this energy. This model only requires the density of multiexciton states to be high and the exciton-multiexciton Coulomb coupling being quite small.

- *Coherent superposition of exciton and multiexciton states.*

This model is the first suggested but oversimplified since it didn't take into consideration the high density of multiexciton states. The light excites an exciton which coherently can turn into multiexciton and return to exciton many times. The mechanism requires the decay rate through phonons to be much lower than the exciton-multiexciton Coulomb coupling (it is not the case usually). Finally the excitation will decay through phonons to a smaller energy of exciton or multiexciton, as function of which decay is faster.

All these models can be treated by the same mathematical technique (density matrix) that can behave differently as function of the set of initial parameters : density of states, coupling strength and decay rates. Multiple excitons generation was detected in semiconducting single walled carbon nanotubes upon absorption of single photon [77] and in graphene [78].

*** Exciton recombinaton**

The generation of excitons is balanced by the process of disappearance called "recombination". Note that this recombination process can be quantified. Recombination is *direct* when the electron goes directly from BC to BV (band to band). Recombination can be *indirect* : the electron passes from the BC to an energy level of an impurity acting as a recombination center and located in the forbidden band, then it will be re-emitted towards the BV. This step can also be described as the capture by the recombinant center of a BV hole.

The recombination is *radiative* if the recombination energy is released in the form of photon emission. The luminescence of organic materials is due to the radiative recombination of excitons. Otherwise, we speak of *non-*

*radiative recombination* and we distinguish two main processes:
- Recombination by Auger effect : the recombining partners energy is transferred to a neighboring particle which becomes hot. This mechanism finds its analogue in the process of de-excitation of atoms.
- Phononic recombination : the partners energy is transferred to the network in the form of phonons.

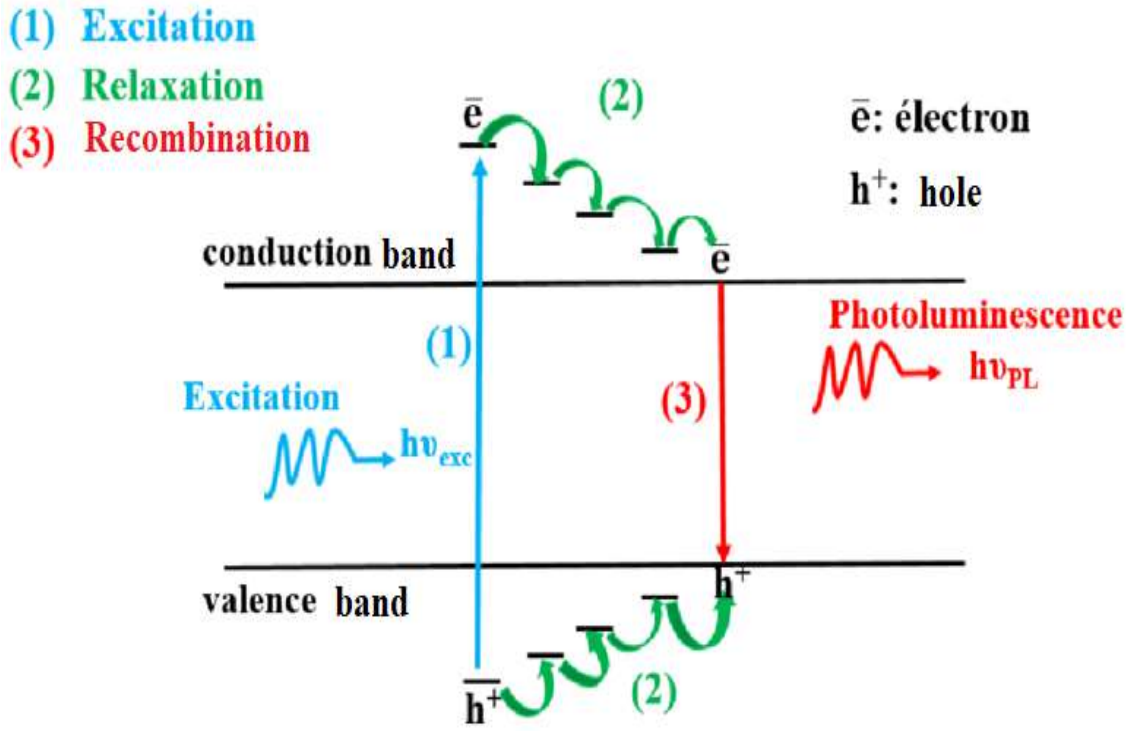


Figure 1.4: Exciton recombination process.

Really, the processes that govern the recombination are complex. Once formed, excitons can be subjected to various mechanisms :
- radiative de-excitation towards the GS
- interaction with another exciton
- vibrational de-excitation towards the GS
- interaction with a charge carrier
- dissociation
- interaction with a chemical impurity.

Due to these different mechanisms of relaxation, particles are in mouvement and that can lead to the conduction.

## 1.4 Generality on conductivity

The conductivity can be seen as the ability for a material to allow the electricity and heat to pass through it. From this point of view we distinguish different types of conductors. Both the electrons motion and the energy transfer between them governe the transport properties.

Heat transfer is an exchange of energy between two bodies caused by their temperature difference. There are two main forms of heat transfers: conduction and radiation transfers. We can thus distinguish : electrical conduction which refers to the transitions of thermally excited electrons; thermal conduction which is related to heat transfers ; the Seebeck effect which deals with the movement of hot carriers and the optical conduction resulting from the absorption of radiations.

### 1.4.1 Types of conductors

Naturally, the majority of materials falls into the category of conductors or insulators. A particular group of materials is intermediate between these two categories : there are semiconductors.

*** Insulators**

In these materials, electrons are linked very strongly to the atoms (molecules) making impossible to transfer charges from one site to another. An insulator (quartz, glass and plastic) has a high value of resistance and don't allow an electric current. In fact, as pointed Fig. 1.5 (a), electrons in BV are separated from the BC by a large gap called forbidden gap which is superior or equal to 6 eV.

*** Conductors**

Here, electrons are linked very loosely and so-called free electrons. These particles are free to move through the material and respond to nearby negative and positive charges. A conductor has a low value of resistance and

allows well the electric current. This is due to the fact that the BV overlaps the BC seen Fig. 1.5 (c). Metals $(Al, Pt, Cu, Ag)$ are generally good conductors.

### * Semiconductors

In a semiconductor at zero temperature, all the covalent bonds in the crystal are satisfied. The electrons completely fill the accessible energy bands of the BV and the conduction band is empty. The forbidden band which separates these two bands is called gap. There is a small gap between the valence and the conduction bands $E_g < 5eV$ in semiconductors. It is illustrated by Fig. 1.5 (b). With the increase in temperature or other excitations, electrons will have enough energy to move into the conduction band. Some examples of semiconductors are given in Table 1.1.

| Materials | $Si$ | $Ge$ | $GaAs$ | $ZnS$ |
|---|---|---|---|---|
| $E_g(eV)$ | 1.17 | 0.744 | 1.52 | 3.91 |

Table 1.1: Gap energy of some semiconductors at T=0K.

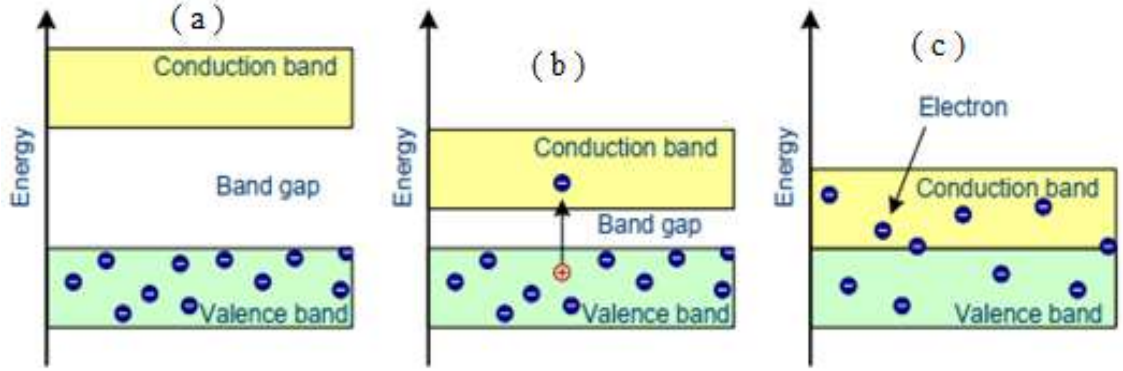


Figure 1.5: Band model for (a) insulator, (b) semiconductor and (c) conductor.

### - Intrinsic semiconductor

An intrinsic semiconductor is a pure semiconductor, that is to say in which there are very few impurities. At T=0K, all the covalent bonds of a crystal are satisfied. When the temperature is increased, electrons are detached of certain bonds and can move in the crystal. Electrons from the top of the valence band can be thermally excited into states at the bottom of the

conduction band (intrinsic ionization) : states of the conduction band are then populated by electrons leaving behind holes in the valence band. Under the action of electric or magnetic fields, the holes react like mobile charge carriers possessing a positive charge +e.

In an intrinsic semiconductor, the contribution of conduction band electrons comes only from the valence band. If we call $n$ the density of electrons and $p$ that of holes then $n = p = n_0$ and depending on the temperature $T$ we have:

$$n(T) = p(T) = n_0 e^{-E_g/2k_BT} \tag{1.28}$$

The variation in temperature of the density of charge carriers is therefore dominated by the exponential factor.

- **Extrinsic semiconductor**

In order to increase the intensity of the current and therefore the number of charge carriers in this interband process, one can voluntarily introduce impurities (substrate, atoms of different nature) capable of providing additional electrons or holes to the system: it is doping. A N-type semiconductor is a semiconductor doped with so-called donor impurities that provide additional electrons to the system. On the other hand, a P-type semiconductor is a semiconductor doped with so-called acceptor impurities which bring additional holes to the system. If $n_D$ is the density of donors and $n_A$ that of acceptors, then at equilibrium we have :

$$n + n_A = p + n_D \tag{1.29}$$

In short, semiconductors are materials whose conductivity is intermediate between that of insulators and conductors. It varies over several orders of magnitude under the effect of :

-temperature

-lighting

-presence of impurities (doping)

-others external perturbations (fileds).

The study of conductivity as a function of these parameters provides access

to the essential physical properties of materials.

### 1.4.2 Electrical conductivity

The electrical conductivity describes the ability of charge carriers to run through the material. Indeed, a valence bond can be broken if sufficient thermal or light energy is provided : one or more previous electrons involved in these bonds are thus torn off. This amounts, in the model of energy bands, to passing this or these electrons from the BV to a state located in the BC (at a level depending on their energy contribution). The electron is free since it no longer participates in a crystalline bond and can participate in electrical conduction. It behaves like a quasi-free particle in the semiconductor because it undergoes the influence of the lattice there. It is therefore a free "polaron" quasiparticle to which we now associate an effective mass different from that of the free electron. At the same time as an electron that has become free appears in the BC, an empty box appears in the BV. This empty place called "hole" is assigned a positive charge $+e$ whose displacement will be opposite to that of the electron during the application of an electric field.

When a conductor is subjected to the action of an electric field $\vec{E}$, a current flux density vector $\vec{j}$ is observed locally and it obeys the relation :

$$\vec{j} = \sigma_{el}\vec{E} \tag{1.30}$$

$\sigma_{el}$ being the electrical conductivity in unit of $S.m^{-1}$. Thus, it appears as the proportionality coefficient between the density of current and the field.

### 1.4.3 Thermal conductivity and Seebeck effect

Here, the interest is the ability to conduct or transfer heat in a material. We distingish two processes : the thermal conduction and the Seebeck effect.

#### * Thermal conductivity

The thermal conduction (or thermal diffusion) is a mode of energy transfer that takes place on a microscopic scale. For non metallic solids, the energy

transfer between two zones of different temperatures is done by the exchange of vibrational energy between the lattice atoms. For metals, the thermal energy is transported by conducting electrons that make the transfer more efficient. Heat conduction is faster over small distances and slower over high distances.

The study of conduction comes under the thermodynamics of non equilibrium phenomena. To understand the problem, consider two solids at two different temperatures, which are brought into contact at the instant $t = 0$. The heat can then be exchanged by conduction at the contact surface, but also inside the bodies. We assume that the set of two body does not exchange energy with the outside. As soon as the two bodies are brought into contact, the system is no longer in equilibrium. It evolves towards a state of equilibrium characterized by a uniform temperature. The time required to reach equilibrium or relaxation time is denoted by $\tau$.

Let us consider a surface situated in a material medium, oriented by a choice of direction for its normal. Let $\delta Q$ be the amount of heat passing through this surface in the direction of the normal between the times $t$ and $t + dt$. The heat flux is :

$$\Phi(t) = \frac{\delta Q}{dt} \tag{1.31}$$

This definition is analogous to that of charge flux in electromagnetism. The heat flux is measured in watts and it is therefore a thermal power. It measures the rate at which heat transfer occurs through a surface.

As in electromagnetism, we define a heat flux density vector ($\vec{\varrho}$), which represents at any point in space the direction of the heat transfer. For an infinitesimal surface $dS$ oriented, the elementary flow through this surface is written :

$$d\Phi = \vec{\varrho}.\vec{n}dS \tag{1.32}$$

Consider a thick plate ($e_d$) whose two faces are maintained at different temperatures. Let $\Phi$ be the heat flow crossing a portion of the plate area $S$. When the temperatures are stationary, the relationship between the heat

flux, the temperature difference and the thickness of the plate is written :

$$d\Phi = S\kappa\frac{T_1 - T_2}{e_d} \tag{1.33}$$

The flux per unit area is therefore proportional to the temperature variation and inversely proportional to the thickness of the plate. The coefficient $\kappa$ expressed in $Wm^{-1}K^{-1}$ is the thermal conductivity and it depends on the plate material. This last relation is the *Fourier's law* . To write it more generally, consider a temperature $T(x;t)$ depending only on a rectilinear space variable. If we take the temperature difference between $x$ and $x + dx$, we can write :

$$\varrho(x,t) = -\kappa\frac{T(x,t) - T(x)}{dx} = -\kappa\frac{\partial T}{\partial x} \tag{1.34}$$

A linear relationship is thus obtained between the flux density and the partial derivative of the temperature with respect to $x$. This relation is generalized using the gradient operator:

$$\vec{\varrho} = -\kappa(g\vec{r}adT) \tag{1.35}$$

The negative signe reflects the orientation of the thermal flux from high to low temperatures.

### * Seebeck effect

The Seebeck effect is at the crossroads between electrical and thermal conductions. As a material at the temperature $T$ is subject to a temperature difference $\Delta T$ respecting the condition $\Delta T \ll T$ , this generates a difference of potential $\Delta V$ called Seebeck voltage due to the hot carriers motion and therefore a current occurs. If the $\Delta V$ measurement shows no difficulty, that of $\Delta T$ is more delicate by a point of experimental view. The use of different types of sensor pairs for measuring $\Delta T$ have been described in the literature : resistors, diodes and thermocouples. However, thermocouples are the most used because they allow to measure not only $\Delta T$ but also $\Delta V$ in the sample. There are several methods to measure the Seebeck coefficient and the most common is the differential method [79, 80].

A thermocouple made up of two conductors A and B of different types, whose junctions are at temperatures $T_a$ and $T_b$ delivers an electromotrice force $V$ which depends on the one hand of the nature of A and B, and on the other hand of the temperatures of the two junctions. Globally, the temperature of one of the junctions is fixed, known and serves as a reference ($T_a = T_{ref}$), while the other junction is placed in the medium of which one seeks to measure the temperature.

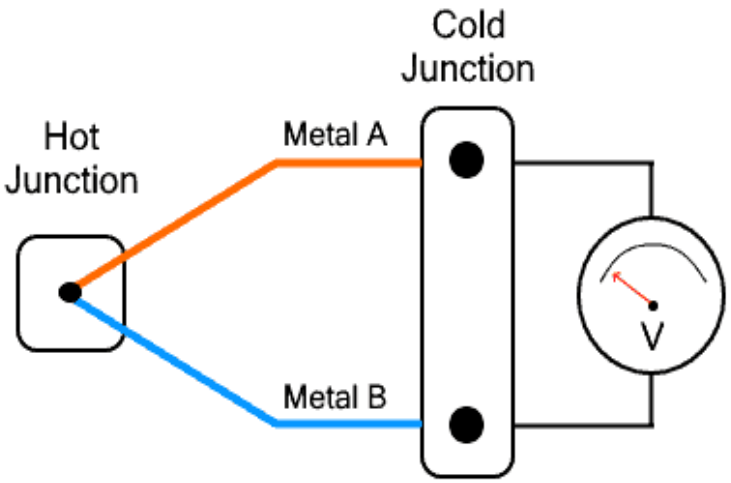


Figure 1.6: A thermocouple used for Seebeck coefficient measurement.

Moreover, in thermal conduction, when a conductor is placed between two different temperatures, we locally observe a heat flux density $\vec{\varrho}$ proportional to the temperature difference via its gradient such that:

$$\vec{\varrho} = -\kappa_0(\vec{\nabla}T) \tag{1.36}$$

In the presence of both an electric field and a temperature gradient, there will therefore be a possible influence of the electric field on the heat flow and a possible influence of the temperature gradient on the electric current. These effects remain linear and we can always write the following general relations :

$$\vec{\varrho} = -\kappa_0(\vec{\nabla}T) + M\vec{E} \tag{1.37}$$

$$\vec{j} = \sigma_{el}\vec{E} - L(\vec{\nabla}T) \tag{1.38}$$

Where $\kappa_0$ being the thermal conductivity of the material at zero electric field, $M$ and $L$ are kinetic coefficients theoretically linked.

In the absence of current ($\vec{j} = 0$), we can write Eq (1.38):

$$\vec{E} = \vartheta(\vec{\nabla}T) \tag{1.39}$$

with $\vartheta = L/\sigma_{el}$ the thermoelectric power. This leads to:

$$dV = -\vartheta dT \tag{1.40}$$

Considering respectively $\vartheta_a$ and $\vartheta_a$ for the conductors A and B, one gets:

$$\Delta V = (\vartheta_a - \vartheta_b)\Delta T \tag{1.41}$$

Thus, the Seebeck coefficient $S^b$ is measured in unit of $V.K^{-1}$ as :

$$S^b_{ab} = (\vartheta_a - \vartheta_b) = \frac{\Delta V}{\Delta T} \tag{1.42}$$

From this definition of the Seebeck coefficient follows the principle of its differential measurement.

At low temperature, it is easy to stick thermocouples (with conductive glues) or to braze them directly on the sample. The choice between thermocouples and resistors to measure $\Delta T$ is essentially determined by the use or not of a magnetic field. Generally, the Seebeck coefficient of thermocouples are very dependent on the applied magnetic field contrary to resistors whose resistance is almost independent of the field. The choice is guided by their sensitivity at low temperature, their mechanical properties (flexible-rigid) and their price. At high temperature, the use of thermocouple is almost exclusive and the contact sample-thermocouple is most often made by pressure because gluing is impossible.

One can notice that for a material, these conductive properties are linked by the figure of merit ($ZT$) which determines the efficiency of a thermoelectric material for a given temperature difference.

$$ZT = \frac{\sigma_{el}(S^b)^2}{\kappa}T \tag{1.43}$$

The higher $ZT$, the more efficient is the material for convert heat into electricity. At room temperature, high-performance materials reach a value of $ZT = 2.8$. From Eq.(1.43), $ZT$ tells us about two performance conditions for thermoelectric materials: good electrical conductivity and low thermal conductivity.

### 1.4.4 Optical conductivity

The optical conductivity is the property of material that expresses the link between the induced current density in the material and the induced electric field magnitude for arbitrary frequencies. It is a linear response function that generalizes the electrical conductivity usually considered in slowly variation of electric fields. In insulators, the optical conductivity is always finite in some frequency ranges above the optical gap whereas the static electrical conductivity tends to vanish.

In a simplest case, the optical conductivity is represented as a complex values scalar fonction of frequency only. In this point of view, the scalar optical conductivity $\sigma(\omega)$ , the electric current density and the electric field are related by the equation [81]:

$$J(\omega) = \sigma(\omega)E(\omega) \tag{1.44}$$

The optical conductivity unit is $\Omega^{-1}cm^{-1}$ and it is most often measured in optical frequency intervals through the reflectivity of polished samples under incidence or using variable incidence angles [82]. High precision is possible using optical transmission experiments for samples which can be splited into thin slices. To fully obtain the electronic properties of the interested material, such measurements are coupled with other methods working in various frequency ranges (microwave frequencies or in the static limit).

## 1.5 TMDC materials and their applications

This section focuses on the material we have studied. We present the structure of TMDC, give some of their applications and several works done

in this frame.

### 1.5.1 Structure of TMDCs

TMDCs have the chemical formula $MX_2$ in which $M$ is a transition metal and $X$ is a chalcogen. A TMDC structure consists on a $M$ atoms lattice sandwiched between two layers of $X$ atoms. In the bulk, these layers are stacked. When we speak of 1L TMDC, we mean the set of these three composed layers. As pointed Figure 1.7, in the periodic table the groups 4, 5, 6, 7, 9, 10 are the most usually combine with chalcogens to constitute TMDCs . For bonding orbitals with two $X$ atoms, each $M$ atom provides four valence electrons and the remaining electrons occupy the $d$-levels. As function of the subdivision of $d$-levels and the remaining valence electrons number, TMDC compounds can be insulators ($HfS_2$), semiconductors ($MoS_2, WS_2$), semimetals ($WTe_2$) and metals ($NbS_2, VSe_2$).

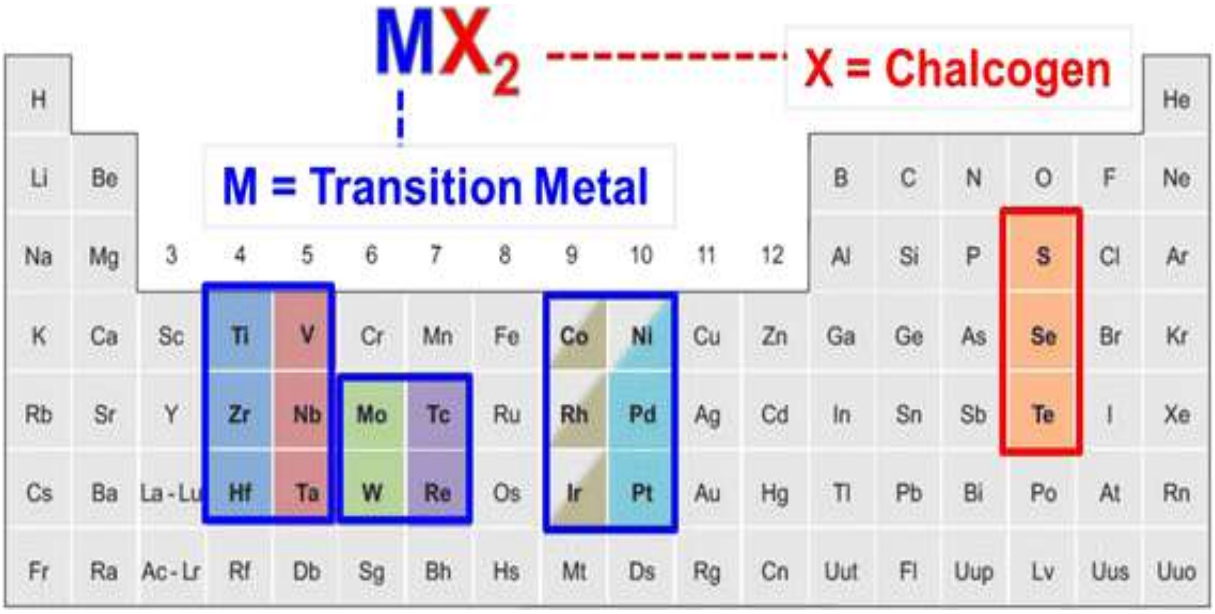


Figure 1.7: The periodic table of chemical elements.

$MX_2$ are semiconductors characterized by a band of indirect forbidden energy of 0.788 - 0.917 eV and direct transitions of 1,393 - 1,679 eV. Their electronic band structures indicate that at the point at the top of the BV corresponds to the $d_{z^2}$ states of the partially hybridized metal at the $p_z$ states of the chalcogen, the bottom of the BC being related to the states of $d_{xy}$ and $d_{x^2-y^2}$ of the metal with a low degree of $p$ chalcogen hybridization. Direct

transitions at point $K$ are associated with Wannier excitons with binding energies of the order of 50-100 meV.

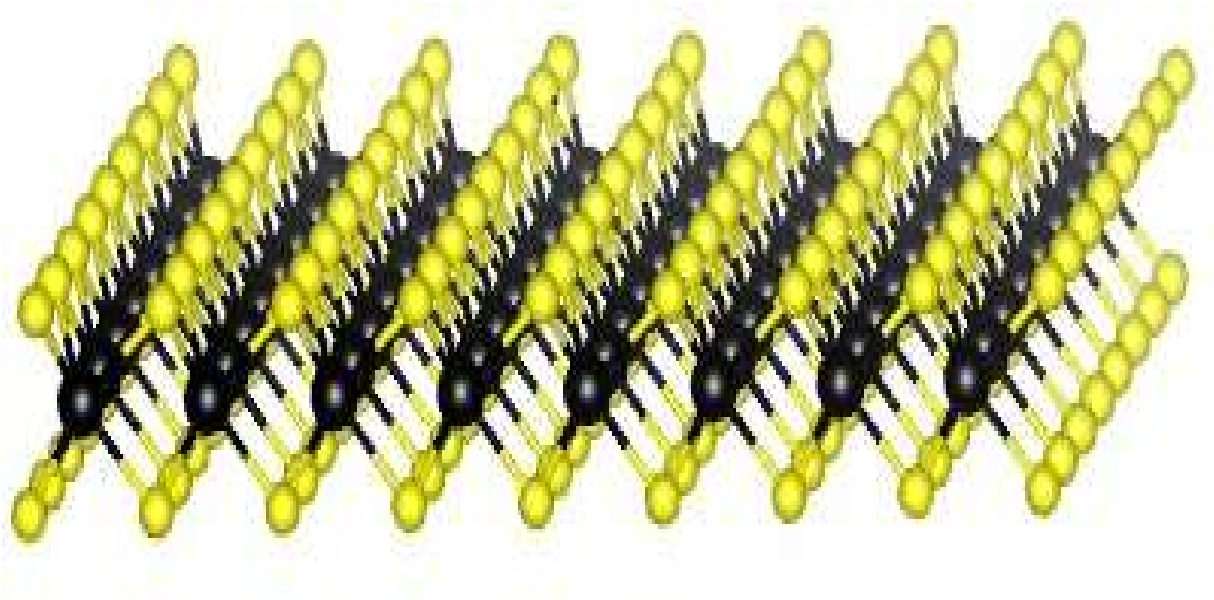

Figure 1.8: Arrangement of a monolayer TMDC: black spheres represent the transition metal ($M$) atoms and yellow ones the chalcogen ($X$) atoms.

The notion of gap or bandgap is related to the representation of semiconductors. The behavior of semiconductors is described by the theory of bands. The energy band structure defines the possible energy states that an electron can take in a crystal as function of a wave vector. In the phase diagram, the energy is represented according to the direction with the highest symmetry. It is divided into valence band, band gap and conduction band. The energy difference (distance) between the bottom of the conduction band and the top of the valence band is called gap energy (band gap):

$$E_g = E_c(K_0) - E_v(0) \tag{1.45}$$

In the phase diagram, one can distinguish the indirect gap and the direct gap. In the optoelectronic point of view, materials behave differently according to these gaps. For direct gap materials, the charge carriers can migrate from one band to another by a simple exchange of a photon whose momentum is insignifiant at this energy level. However, for indirect gap materials, the charge carriers have to interact with both a phonon and a photon in order to modify their wave vectors and it makes the transition much less

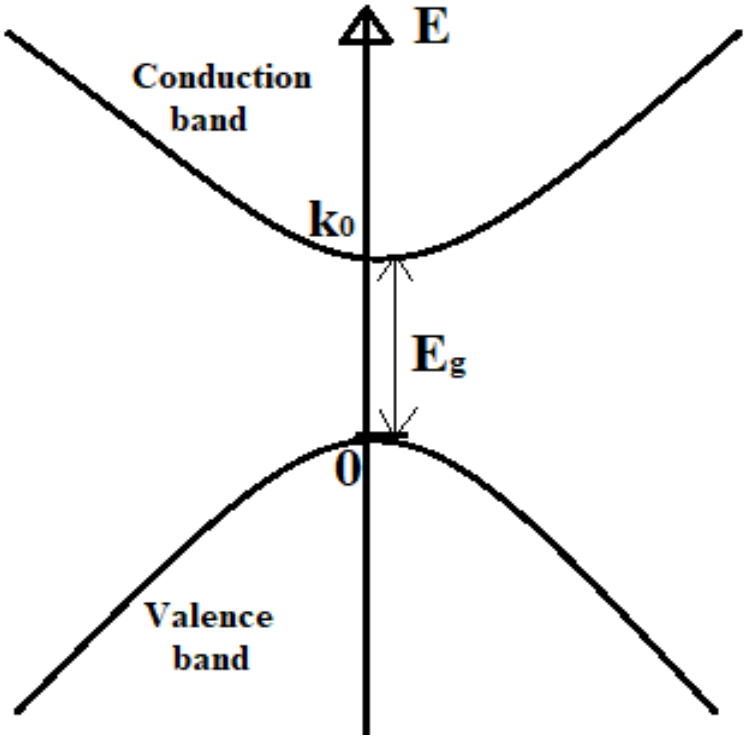


Figure 1.9: Schematic of band gap energy.

likely. In 2017, Xiao et al. [83] altered various polar substrates and found that the modulated amplitude of the band gap is in range of 100 and 500 mev. They showed that carriers highly bound with optical phonons (long wavelength modes) and provide the dominant contributions to the band gap modulation. By changing the internal distance of TMDC-substrate and the nature of polar substrates one can tun the band gap on a large scale.

Concerning the fabrication, lamellar TMDC crystals have weak interlayer forces of van der Waal and great intralayer covalent bonds. To obtain a thinner material, one can impart a shearing force to the bulk crystal for overcoming the Van der Waals strengths within the lattice. By repeating this process one can further exfoliate the lamellar flakes and allow the separation of 1L nanosheets eventually [84]. The manners to affect the mechanism can be splitted into some types: Micromechanical exfoliations consisting of introduce a peeling strength to isolate layers, a separation induced by shear or by compressive delamination. Exfoliation is a liquid medium generally operating by exposing it to strengths generated within a cavitation field or applying a vibrational energy to the crystal. Chemical exfoliation and intercalation work basing on the insertion of a small molecule or atom within the inter-

layer space of the bulk TMDC, before the forced expansion of the intercalate separates the crystals. Finally, the thinning methods don't require the sheets separation but rather the destructive elimination of undesirable layers from a bulk crystal to produce a 1L or multilayered nanosheets. Above is presented the fabrication of TMDC nanosheets by *top-down exfoliation* methods.

Beside, we also have the fabrication by *Bottom-up* methods. Bottom-up syntheses consist on the TMDC formation by the reaction of chalcogen and metal containing precursors. In TMDC production, these reactions have become increasingly popular and can be made in the liquid, solid and gaseous phase. In most cases, the goal is to form reactive $nX_2$ and $M^{n+}$ ions that will directly react to constitute the wanted material. Typically the chemistry is well-known and robust, there exists a large number of possible precursors. The difficulty and the novelty rest on the control of reaction kinetics and the improvement in understanding of the energetics. The gas-phase synthesis of 2D TMDCs is a promising research framework due to their inherent compatibility and scalability with existing technologies. Nanosheets grow in the solid and liquid-phase which involve the decomposition of a precursor mixture by either the injection into a hot liquid or the thermal decomposition within a solution [85]. It should be noted that molybdenum and tungsten disulfides exist in nature on the form of minerals called molybdenite and tungstenite.

### 1.5.2 Applications

In both large molecules and molecular lattices, excitons play important roles such as carrying energy, transmitting informations and activating some chemical reactions. Recently, excitons in 1L TMDCs have grown very rapidly due to their electronic and optical propertiess [86, 87]. TMDCs are viewed as one of the most interesting 2D materials due to their various applications. They became particularly promising due to their characteristics of semiconductor with a high stability and a large flexibility [14, 15], their electronic and optical properties which indicate applications in fabrication of electronic devices [17, 18, 88], spintronics [89], preparation of qubit [16], transistors, photovoltaics, optoelectronics, molecular sensing and photodetectors [20, 21], in valleytronic effects [22], in photoluminescence experiments [23]. They are good candidate for conductivity and have high optical absorption coefficient

and mobility.

**** Field-effect transistors***

It is over the past 10 years that the TMDC electrical properties were first used for field-effect transistors and precisely after the paper on graphene [90] that 1L TMDC semiconductor was investigated in field-effect transistors [91]. In graphene, the field-effect mobility is found to be at least 3 orders of magnitude greater than in 1L $MoS_2$. The interest of 1L TMDC semiconductor for this application is renewed in 2011 when large on/off ratios and low sub-threshold swings, top-gated 1L $MoS_2$ field-effect transistors with moderate mobilities were demonstrated at room temperature [92]. The ultrathin top gate dielectric and 2D channel coupled with a large band gap ($> 1$ eV) have allowed superior gate control, thus enabling large switching ratios and small off currents. This work also found that the carrier mobility increases in the presence of the top dielectric.

**** Digital electronic devices***

The digital electronic requires the reliable creation, storage and reading of distinct voltage states. we have two states in Boolean logic corresponding to false 0 or true 1. Digital electronic circuits are comprised of large assemblies of logic gates which are electronic implementations of the Boolean logic functions. Transistors are fundamental components of modern digital electronics since each logic gate usually consists of several transistors. The metal-oxide-semiconductor field-effect transistor is used as basic component for most digital electronic circuits. The two Boolean voltage states can be achieved by having two distinct states of conductance in a metal-oxide-semiconductor field-effect transistor separated by multiple orders of magnitude. At room temperature this high on/off current ratio requirement is easily reached in semiconductor materials with band gaps larger than $\sim 1$ eV. Unlike in gapless graphene, semiconductors TMDC with their substantial band gaps suggest that high on/off current ratios can be achieved, and thus digital electronics based on TMDCs is possible.

### * *Junctions and heterostructures*

In addition to circuits and devices based on individual TMDC semiconductor materials, TMDC materials present opportunities for unique device geometries based on heterostructures amd junctions. Such heterojunction devices was widely developed for crystalline semiconductors for high frequency applications. These semiconductor heterostructures have grown historically by epitaxial crystal growth methods and the range of possible heterojunctions is limited to those materials having closely matched lattice parameters. In revenge, since the van der Waals bond between TMDCs is relatively weak it weakens this constraint and then suggests a large range of possible junctions and heterostructures [93].

### * *Optoelectronics*

1L TMDC semiconductors with direct band gaps in the visible domain of the electromagnetic spectrum, strong photoluminescence and large exciton binding energies, are good candidates for applications in optoelectronic. Many classes of optoelectronic devices have been developed from ultrathin TMDCs semiconductors including photovoltaics, photodetectors and light emitting devices.

When incident photons (with energy greater than the band gap) are applied on a semiconductor, they lead to the reation of free carriers or excitons depending on the binding energy of exciton in that semiconductor. A photocurrent is generated from a built-in or applied electric field which separates bound excitons. Photodiodes and phototransistors are the two main categories of semiconductor-based photodetectors that exist. First studies on ultrathin $MoS_2$-based phototransistors have measured the photocurrent under global illumination by photons having energies superior than the 1.9 eV band gap. Also, the phototransistors have been extended to chemical vapor deposition grown few layer $WS_2$ [94]. Later, studies on the dependence of wavelength have suggested that the photocurrent roughly follows the absorption spectrum. This leads to speculation of carrier separation and interband absorption as most important mechanisms of photocurrent generation.

Photovoltaic cells are one of the most widespread P-N junctions applications. A great mobility semiconductor having a direct band gap close to 1.3 eV is sought for high performance junction photovoltaics. Here, 1L TMDC semiconductors are well placed both in terms of mobility and direct band gap values, making them suitable candidates for photovoltaic applications. Calculations on a Schottky junction solar cell (a stack of graphene-$MoS_2$) suggest a maximum power conversion performance of 1 percent whereas a type-II heterojunction between $WS_2/MoS_2$ is 1.5 percent. In experiments, an asymmetric metal-semiconductor-metal Schottky junction on a flake of few-layer $MoS_2$ resulted in working photovoltaic devices with 1 percent power conversion efficiency, whereas split-gated P-N junctions on 1L $WSe_2$ reached a power conversion efficiency of 0.5 percent.

**** Sensing application***

An electronic sensor exploits the variations of the electrical properties of the constituent materials during the interaction with an analyte. When a bulk material in a field effect transistor channel interacts with an analyte, the device capacitance or the material resistance usually undergoes relatively small changes because the interaction is limited to the surface. But, in atomically thin nanomaterials, the surface to volume ratio is near to unity and therefore the electrical properties are considerably perturbed by an analyte adsorption even submonolayer. This strategy is greatly exploited in carbon nanomaterials and should be also apply to ultrathin TMDC semiconductors. Studies of sensor enhancement based on TMDCs are relatively limited even if the domain of semiconductors TMDC-based electronic devices has increased rapidly. Precisely, reset-ability and selectivity issues need much more attention. Although the efficiency degradation of TMDC devices due to the interaction of adsorbate is reversible when these devices are subjected to the vacuum conditions, the reset-ability of TMDC-based sensors is susceptible to be greater than that of organic semiconductors in which this degradation is irreversible. Sensing applications are explored by several authors [95, 96].

TMDCs have also attracted interest by their fascinating properties rang-

ing from metal, semimetal, semiconductor to superconductor. The electrical control of their physical properties is significantly important for electronic devices. For example, investigate how the electrical manipulation of optical and electric dependences can improve the properties of these 2D materials.

### 1.5.3 Overview on TMDCs

Many authors have explored the polaron energy, the exciton-polaron energy and other properties in TMDCs, among them we can quote :

Thilagam [97] examined the mechanism of excitons generated through the process of LO-phonon-assisted scattering after the optical excitation of 1L TMDCs. The time of exciton formation is determined as a function of the carrier densities for some Frohlich coupling constants, the exciton wavevector, the energy of LO-phonon, the binding energy of exciton in the layered structure and the lattice temperature. In fact, for 1L $MoS_2$ at carrier temperatures inferior to 300K and charge density of $5.10^{11} cm^{-2}$, she obtained ultrafast exciton formation times on the sub-picosecond time scale. Her results show that excitons are formed faster in 1L selenide-based dichalcogenides ($WSe_2$ and $MoSe_2$) than in 1L sulfide-based dichalcogenides ($WS_2$ and $MoS_2$). TMDCs have appeared as promising compounds in which excitons form as stable quasiparticles with high binding energies and thus significantly influence the optical mechanisms of 1L TMDCs. The excitons dynamics in TMDCs have been widely studied over the last years both in terms of theory and applications. Also, it is recently that the excitons formation from free carriers has been measured.

Shahnazaryan et al. [98] have theoretically studied the Coulomb interaction between excitons in 1L TMDCs. Their results quantitatively describe the exciton-electron and exciton-exciton scattering in TMDCs, and are interessant for the design of perspective nonlinear optical devices based on 1L TMDCs. They have computed the exciton-electron interplay in 1L TMDCs, relevant for systems with an excess of free electrons. This interplay is characterized by the dominant attractive contribution of the exchange component enhancing with the exciton principal quantum number. Their results give a basis for the quantitative description of nonlinear effects in TMDC systems

and are useful for the creation of corresponding nonlinear optoelectronic devices.

Berman et al. [99] have studied the formation of superfluidity of dipolar excitons in double layer heterostructures formed by two TMDCs atomically thin layers. The dipolar excitons binding energy depends on the hole and electron reduced masses, the TMDC material polarizability and the interlayer separation between the two monolayers. Since the effective masses of holes and electrons are different for the same 1L TMDC, the exciton binding energy is higher for dipolar excitons with electrons in $MoS_2$ and $MoSe_2$, holes in $WS_2$ and $WSe_2$ than for dipolar excitons with electrons in $WS_2$ and $WSe_2$, holes in $MoS_2$ and $MoSe_2$. Moreover, it is found that when the hole and electron reduced masses increase then decreases the dipolar excitons binding energy.

Also, the magneto-optical mechanisms of 1L TMDCs have stimulated some opportunities for applications in which a comprehensive insight of the magnetic field action affecting the excitons is needed [100, 101]. Indeed, excitons in 1L TMDCs subjected to a magnetic field show interesting electronic and optical characteristics due to the excitons high binding energy [102, 103, 104, 105]. It is shown that the application of an external magnetic field to a 1L TMDC gives an experimental understanding of the excitons characteristics, such as their spatial extent [106].

## Conclusion

In this chapter, we have given an overview on polaron, exciton-polaron and TMDCs. These concepts are integrated in order to better understand the behavior of particles in structures. We have also presented a generality on the phenomena of relaxation and conductivity. To date, many methods and theories have emerged to evaluate the properties of systems in physics.

CHAPTER 2

# THEORY AND METHODS

## Introduction

In this chapter, we explain the theory and methods used in the thesis to derive the different properties. It consists of the 2D theory necessary to obtain the exciton-polaron energy ; the relaxation time approximation approach to derive the relaxation time, the electrical conductivity and Seebeck coefficient of a material ; the Fermi's golden rule used for the lifetime and optical absorption coefficient ; and the Kubo formula for optical conductivity.

## 2.1 2D theory

Here, 2D comes from the fact that the quasiparticle moves in the $xy$-plane representing the material layer. The 2D theory is convenient for the study of two-dimensional materials.

### 2.1.1 LLP variational method

Let us consider the Hamiltonian of Eq.(1.12). The total momentum operator for the polaron reads:

$$P = \sum_q \hbar q b_q^\dagger b_q + p \tag{2.1}$$

where $p = -i\hbar\nabla$ is the electron momentum. We use the following relation:

$$\Phi = \hat{S}_1 \Phi_2, \tag{2.2}$$

The wave function $\Phi$ satisfies the equation:

$$H\Phi = E_{pol}\Phi \tag{2.3}$$

The first transformation $S_1$ of LLP is defined as [107]:

$$S_1 = \exp\left\{\frac{i}{\hbar}\left(p - \sum_q \hbar q b_q^\dagger b_q\right) r\right\} \tag{2.4}$$

We apply the latest transformation on the electron momentum operator as:

$$S_1^{-1} p S_1 = p - \sum_q \hbar q b_q^\dagger b_q \tag{2.5}$$

$$S_1^{-1} p^2 S_1 = \left(p - \sum_q \hbar q b_q^\dagger b_q\right)^2 \tag{2.6}$$

and on the phonon operators as:

$$S_1^{-1} b_q S_1 = b_q e^{-iqr} \tag{2.7}$$

$$S_1^{-1} b_q^\dagger b_q S_1 = S_1^{-1} b_q^\dagger S_1 S_1^{-1} b_q S_1 = b_q^\dagger e^{iqr} b_q e^{-iqr} = b_q^\dagger b_q \tag{2.8}$$

$$S_1^{-1}\left(V_q b_q e^{iqr} + V_q^* b_q^\dagger e^{-iqr}\right) S_1 = V_q b_q + V_q^* b_q^\dagger \tag{2.9}$$

According to Eq. (1.12), the first transformed Hamiltonian is obtained as:

$$\tilde{H}_1 = S_1^{-1} H S_1 = \frac{\left(p - \sum_q \hbar q b_q^\dagger b_q\right)^2}{2m_e} + \sum_q \hbar\omega_{LO} b_q^\dagger b_q + \sum_q \left(V_q b_q + V_q^* b_q^\dagger\right) \tag{2.10}$$

From the Fröhlich perturbation analysis, in the intermediate coupling regime the virtual phonons number is not small. It follows that one cannot apply the perturbation theory to the Hamiltonian $\hat{H}$. Nevertheless, by the displacement canonical transformation one can remove the essential part of the interaction term from the $\hat{H}$. LLP proposed further a variational approach

of calculation. The trial wave function is taken as:

$$\Phi_2 = S_2 \left|0\right\rangle . \tag{2.11}$$

where $|0\rangle$ is the unperturbed Hamiltonian eigenstate with no phonons (vacuum state). Specifically $|0\rangle$ is defined by:

$$b_q|0\rangle = 0 \tag{2.12}$$

$$\langle 0\|0\rangle = 1 \tag{2.13}$$

The second LLP transformation is given by:

$$S_2 = exp\left\{ \sum_q \left( b_q^\dagger f_q - b_q f_q^* \right) \right\} \tag{2.14}$$

where $f_q$ is a variational function which is determined by minimizing of the GS energy. The significance of Eq. (2.14) is that it dresses the electron with the virtual phonon field, which describes the polarization. The unitary transformation $S_2$ is applied on the operators as:

$$S_2^{-1} b_q S_2 = b_q + f_q \tag{2.15}$$

$$S_2^{-1} b_q^\dagger S_2 = b_q^\dagger + f_q^* \tag{2.16}$$

The GS energy is calculated by:

$$E_{pol} = \langle \Phi | \, H \, | \Phi \rangle = \langle 0 | \, S_2^{-1} \tilde{H} S_2 \, | 0 \rangle . \tag{2.17}$$

In virtue of Eqs.(2.15) and (2.16), we obtain:

$$\begin{aligned} S_2^{-1}\tilde{H}S_2 &= \frac{\left[P-\sum_q \hbar q\left(b_q^\dagger+f_q^*\right)\left(b_q+f_q\right)\right]^2}{2m_e} \\ &+\sum_q \hbar\omega_{LO}\left(b_q^\dagger+f_q^*\right)\left(b_q+f_q\right) \\ &+\sum_q \left[V_q\left(b_q+f_q\right)+V_q^*\left(b_q^\dagger+f_q^*\right)\right] \end{aligned} \tag{2.18}$$

$$\begin{aligned} S_2^{-1}\tilde{H}S_2 &= \frac{\left[P-\sum_q \hbar q b_q^\dagger b_q-\sum_q \hbar q\left|f_q\right|^2-\sum_k \hbar q\left(b_q^\dagger f_q+b_q f_q^*\right)\right]^2}{2m_e} \\ &+\sum_q \hbar\omega_{LO}\left(b_q^\dagger b_q+b_q^\dagger f_q+b_q f_q^*+\left|f_q\right|^2\right) \\ &+\sum_q \left[V_q\left(b_q+f_q\right)+V_q^*\left(b_q^\dagger+f_q^*\right)\right] \\ &= H_0+H_1, \end{aligned} \tag{2.19}$$

where

$$\begin{aligned} H_0 &= \frac{\left[P-\sum_q \hbar q b_q^\dagger b_q\right]^2+\left[\sum_q \hbar q\left|f_q\right|^2\right]^2}{2m_e}+\sum_q\left(V_q f_q+V_q^* f_q^*\right)+\sum_q \hbar\omega_{LO} b_q^\dagger b_q \\ &+\sum_q \left|f_q\right|^2\left\{\hbar\omega_{LO}-\frac{\hbar q.P}{m_e}+\frac{\hbar^2 q^2}{2m_e}\right\}+\frac{\hbar^2}{m_e}\sum_q q b_q^\dagger b_q.\sum_{q'} q'\left|f_q\right|^2 \\ &+\sum_q b_q\left\{V_q+f_q^*\left[\hbar\omega_{LO}-\frac{\hbar q.P}{m_e}+\frac{\hbar^2 q^2}{2m_e}+\frac{\hbar^2 q}{m_e}.\sum_{q'} q'\left|f_q\right|^2\right]\right\} \\ &+\sum_q b_q^\dagger\left\{V_q^*+f_q\left[\hbar\omega_{LO}-\frac{\hbar q.P}{m_e}+\frac{\hbar^2 q^2}{2m_e}+\frac{\hbar^2 q}{m_e}.\sum_{q'} q'\left|f_q\right|^2\right]\right\} \end{aligned}$$

$$\begin{aligned} H_1 &= \sum_{q,q'} \frac{\hbar^2 q.q'}{2m_e} \left\{ b_q b_{q'} f_q^* f_{q'}^* + 2b_q^\dagger b_{q'} f_q f_q^* + b_q^\dagger b_{q'}^\dagger f_q f_{q'} \right\} \\ &+ \sum_{q,q'} \frac{\hbar^2 q.q'}{2m_e} \left\{ b_q^\dagger b_q b_{q'} f_{q'}^* + b_{q'}^\dagger b_q^\dagger b_q f_{q'} \right\}. \end{aligned} \tag{2.20}$$

Using Eqs. (2.12) and (2.13), we obtain from Eq. (2.17) that:

$$\begin{aligned} E_{pol} &= \frac{P^2 + \left[\sum_q \hbar q |f_q|^2\right]^2}{2m_e} + \sum_q \left(V_q f_q + V_q^* f_q^*\right) \\ &+ \sum_q |f_q|^2 \left\{ \hbar\omega_{LO} - \frac{\hbar q.P}{m_e} + \frac{\hbar^2 q^2}{2m_e} \right\} \end{aligned} \tag{2.21}$$

We minimize Eq. (2.21) by checking the $f$-functions such that:

$$\frac{\partial E_{pol}}{\partial f_q} = \frac{\partial E_{pol}}{\partial f_q^*} = 0. \tag{2.22}$$

This leads to:

$$f_q^* = -\frac{V_q}{\hbar\omega_{LO} - \frac{\hbar q.P}{m_e}(1-\varrho) + \frac{\hbar^2 q^2}{2m_e}} \tag{2.23}$$

$$f_q = -\frac{V_q^*}{\hbar\omega_{LO} - \frac{\hbar q.P}{m_e}(1-\varrho) + \frac{\hbar^2 q^2}{2m_e}} \tag{2.24}$$

Where $\varrho$ is a fraction ($\varrho < 1$) verifying:

$$\varrho P = \sum_q |f_q|^2 \hbar q \tag{2.25}$$

As the variational parameters are well defined, one can easily determine the GS energy from Eq. (2.21).

### 2.1.2 Hamiltonian of 2D exciton-polaron

The Hamiltonian of 2D exciton-polaron has the same form of Eq. (1.26):

$$\hat{H}^{2D} = \hat{H}_{ex}^{2D} + \hat{H}_{ph} + \hat{H}_{ex-ph}^{2D} \tag{2.26}$$

In the ideal 2D case, $\hat{H}_{ex}^{2D}$ represents the exciton Hamiltonian in the $xy$-plane appearing as:

$$\hat{H}_{ex}^{2D} = \frac{\left(P_{e,x}^2 + P_{e,y}^2\right)}{2m_e^*} + \frac{\left(P_{h,x}^2 + P_{h,y}^2\right)}{2m_h^*} - \frac{e^2}{\varepsilon|\rho_e - \rho_h|} \tag{2.27}$$

$\rho_e$ ($\rho_h$) is the electron (hole) coordinate in the $xy$-plane. The last term of Eq. (2.26) is the in-plane interaction term, given by [108]:

$$\hat{H}_{ex-ph}^{2D} = \sum_{K_\parallel, q_\parallel} \Xi^s(q_\parallel) C_{K_\parallel + q_\parallel}^\dagger C_{K_\parallel} \left(b_{q_\parallel} + b_{-q_\parallel}^\dagger\right) \tag{2.28}$$

Where $C_{K_\parallel}^\dagger (C_{K_\parallel})$ denotes the creation (annihilation) operator of an exciton and $K_\parallel$ its in-plane wave vector. The 2D coupling function due to deformation potential appears as:

$$\Xi^s(q_\parallel) = \sqrt{\frac{\hbar q_\parallel}{2\eta u S_{2D}}} \left[\frac{D_c^s}{(1+b_e^2)^{\frac{3}{2}}} - \frac{D_v^s}{(1+b_h^2)^{\frac{3}{2}}}\right] \tag{2.29}$$

$S_{2D}$ represents the area of the layer plane, $\eta$ denotes the area mass density and $u$ is the sound velocity. $D_c^s$ and $D_v^s$ are respectively the deformation potential constant for electron-phonon interaction inside conduction band and the corresponding expression for hole in the valence band.

The coupling function is approximated for $b_e, b_h \ll 1$ as:

$$\Xi^s(q_\parallel) = \sqrt{\frac{\hbar q_\parallel}{2\eta u S_{2D}}} \left(D_c^s - D_v^s\right) \tag{2.30}$$

Let consider the in-plane relative coordinate:

$$\rho = \rho_e - \rho_h \tag{2.31}$$

and the center of mass:

$$R = \frac{m_e^*}{M^*}\rho_e + \frac{m_h^*}{M^*}\rho_h \tag{2.32}$$

We establish:

$$\begin{cases} \nabla_{\rho_e} &= \frac{m_e^*}{M^*}\nabla_R + \nabla_\rho \\ \nabla_{\rho_h} &= \frac{m_h^*}{M^*}\nabla_R - \nabla_\rho \end{cases} \tag{2.33}$$

Then Eq. (2.27) becomes:

$$\hat{H}_{ex}^{2D} = \frac{-\hbar^2}{2m_e^*}\nabla_{\rho_e}^2 - \frac{\hbar^2}{2m_h^*}\nabla_{\rho_h}^2 - \frac{e^2}{\varepsilon\rho} \tag{2.34}$$

Thus

$$\hat{H}_{ex}^{2D} = \frac{-\hbar^2}{2M^*}\nabla_R^2 + \left(-\frac{\hbar^2}{2\mu^*}\nabla_\rho^2 - \frac{e^2}{\varepsilon\rho}\right) = \hat{H}_R + \hat{H}_\rho \tag{2.35}$$

$\mu^*$ is the effective reduced mass of exciton $1/\mu^* = (1/m_e^*) + (1/m_h^*)$ and $M^* = (m_e^* + m_h^*)$ its effective mass.
The task is to write the exciton Hamiltonian in second quantization, this means to check the exciton eigen energy on the form:

$$\hat{H}_{ex}^{2D} = \sum_{K_\parallel} E_{ex} C_{K_\parallel}^\dagger C_{K_\parallel} \tag{2.36}$$

This leads to the Schrödinger equation:

$$\hat{H}_{ex}^{2D}\Psi^{2D} = E_{ex}\Psi^{2D} \tag{2.37}$$

The 2D exciton wave function [109] is chosen as:

$$\Psi^{2D} = \varphi(R)\phi_{1s}(\rho) = exp(iK_\parallel.R)\sqrt{\frac{2}{\pi}}\frac{1}{a}exp\left(-\frac{\rho}{a}\right) \tag{2.38}$$

$a$ being a variational parameter. For the center of mass, we solve:

$$\frac{-\hbar^2}{2M^*}\nabla_R^2\varphi(R) = E_{K_\parallel}\varphi(R) \tag{2.39}$$

We have:

$$\frac{\partial\varphi(R)}{\partial R^2} = (iK_\parallel)^2\varphi(R) \tag{2.40}$$

Thus:

$$E_{K_\parallel} \approx E_g + \frac{\hbar^2 K_\parallel^2}{2M^*} \tag{2.41}$$

Also, for the relative coordinate, we have:

$$\langle\phi_{1s}|H_\rho|\phi_{1s}\rangle = -\frac{\hbar^2}{2\mu^*}\langle\phi_{1s}|\nabla_\rho^2|\phi_{1s}\rangle - \frac{e^2}{\varepsilon}\left\langle\phi_{1s}|\frac{1}{\rho}|\phi_{1s}\right\rangle \tag{2.42}$$

This leads to:

$$\begin{aligned}\langle\phi_{1s}|H_\rho|\phi_{1s}\rangle &= -\tfrac{\hbar^2}{2\mu^*}\left\langle\phi_{1s}|\tfrac{1}{\rho}\tfrac{\partial}{\partial\rho}\left(\rho\tfrac{\partial}{\partial\rho}\right)|\phi_{1s}\right\rangle - \tfrac{e^2}{\varepsilon}\left\langle\phi_{1s}|\tfrac{1}{\rho}|\phi_{1s}\right\rangle \\ &= -\tfrac{\hbar^2}{2\mu^* a^2}\langle\phi_{1s}||\phi_{1s}\rangle + \left(\tfrac{\hbar^2}{2\mu^* a} - \tfrac{e^2}{\varepsilon}\right)\left\langle\phi_{1s}|\tfrac{1}{\rho}|\phi_{1s}\right\rangle\end{aligned} \tag{2.43}$$

The second term vanishes according to Eq. (1.23) and we have :

$$\langle\phi_{1s}|H_\rho|\phi_{1s}\rangle = -\frac{\hbar^2}{2\mu^* a^2} = E_b^{2D} \tag{2.44}$$

$E_b$ is the exciton binding energy. According to Eqs. (2.41) and (2.44), the energy of 2D exciton is:

$$E_{ex} = E_{K_\parallel} - E_b^{2D} \tag{2.45}$$

Ultimately, the Hamiltonian for the 2D exciton-polaron reads:

$$\hat{H}^{2D} = \sum_{K_\parallel} E_{ex} C_{K_\parallel}^\dagger C_{K_\parallel} + \sum_q \hbar\omega_0 b_q^\dagger b_q + \sum_{K_\parallel, q_\parallel} \Xi^s(q_\parallel) C_{K_\parallel+q_\parallel}^\dagger C_{K_\parallel}\left(b_{q_\parallel} + b_{-q_\parallel}^\dagger\right) \tag{2.46}$$

We obtain a Hamiltonian which quantifies the exciton motion, depends on the different operators of creation and annihilation suitable for energies calculations.

### 2.1.3 GS energy of 2D exciton-polaron.

We can rewrite the latest Hamiltonian of 2D exciton-polaron as:

$$\hat{H}^{2D} = \hat{H}_0 + \hat{H}_{ex-ph}^{2D} \tag{2.47}$$

Where

$$\hat{H}_0 = \hat{H}_{ex}^{2D} + \hat{H}_{ph} \tag{2.48}$$

We use the following unitary transformation [27] to diagonalize the Hamiltonian:

$$U_{ex} = e^{iS} \tag{2.49}$$

With

$$S = \sum_{K_\parallel, q_\parallel} C^{\dagger}_{K_\parallel + q_\parallel} C_{K_\parallel} \left[ f^{*}_{ex}(K_\parallel, q_\parallel) b^{\dagger}_{-q_\parallel} + f_{ex}(K_\parallel, q_\parallel) b_{q_\parallel} \right] \tag{2.50}$$

Where the $f$-functions are variational parameters.

A series expansion of the transformed Hamiltonian gives:

$$\begin{aligned}
\hat{H}^T &= U^{-1}_{ex} \hat{H}^{2D} U_{ex} \\
&= U^{-1}_{ex} \hat{H}_0 U_{ex} + U^{-1}_{ex} \hat{H}^{2D}_{ex-ph} U_{ex} \\
&= \hat{H}_0 + i\left[S, \hat{H}_0\right] + i\left[S, \tfrac{i}{2}\left[S, \hat{H}_0\right]\right] + \hat{H}^{2D}_{ex-ph} + i\left[S, \hat{H}^{2D}_{ex-ph}\right] + \\
&\quad i\left[S, \tfrac{i}{2}\left[S, \hat{H}^{2D}_{ex-ph}\right]\right] \\
&= \hat{H}_0 + \left(i\left[S, \hat{H}_0\right] + \hat{H}^{2D}_{ex-ph}\right) + \left(\left[iS, \tfrac{i}{2}\left[S, \hat{H}_0\right]\right] + \left[iS, \hat{H}^{2D}_{ex-ph}\right]\right) + \\
&\quad i\left[S, \tfrac{i}{2}\left[S, \hat{H}^{2D}_{ex-ph}\right]\right] \\
&= \hat{H}_0 + \left(i\left[S, \hat{H}_0\right] + \hat{H}^{2D}_{ex-ph}\right) + \left(\left[iS, \tfrac{i}{2}\left[S, \hat{H}_0\right] + \hat{H}^{2D}_{ex-ph}\right]\right) + ... \\
&= \hat{H}_0 + \left(i\left[S, \hat{H}_0\right] + \hat{H}^{2D}_{ex-ph}\right) + i\left(\left[\tfrac{i}{2}\left[\hat{H}_0, S\right] + \hat{H}^{2D}_{ex-ph}, S\right]\right) + ...
\end{aligned} \tag{2.51}$$

The perturbation theory of second order permit to have:

$$\left[S, \hat{H}_0\right] = \hat{H}^{2D}_{ex-ph} \tag{2.52}$$

Let us evaluate the commutator:

$$\begin{aligned}
\left[S,\hat{H}_0\right] &= \left[\sum_{K'} E_{ex}(K')C^{\dagger}_{K'}C_{K'} + \sum_{q}\hbar\omega_0 b^{\dagger}_{q}b_{q}, \sum_{K,q_{\parallel}} C_{K+q_{\parallel}}C_{K}\left(f^{*}_{ex}b^{\dagger}_{-q_{\parallel}} + f_{ex}b_{q_{\parallel}}\right)\right] \\
&= \sum_{K'}\sum_{K,q_{\parallel}} E_{ex}(K')C^{\dagger}_{K'}C_{K}\left(f^{*}_{ex}b^{\dagger}_{-q_{\parallel}} + f_{ex}b_{q_{\parallel}}\right)\delta_{K',K+q_{\parallel}} + \\
&\quad \sum_{K'}\sum_{K,q_{\parallel}} E_{ex}(K')C^{\dagger}_{K+q_{\parallel}}C_{K'}\left(f^{*}_{ex}b^{\dagger}_{-q_{\parallel}} + f_{ex}b_{q_{\parallel}}\right)(-1)\delta_{K',K} + \\
&\quad \sum_{q}\sum_{K,q_{\parallel}} \hbar\omega_0 C^{\dagger}_{K+q_{\parallel}}C_{K}b_{q}f_{ex}(-1)\delta_{(q,q_{\parallel})} + \sum_{q}\sum_{K,q_{\parallel}} \hbar\omega_0 C^{\dagger}_{K+q_{\parallel}}C_{K}b^{\dagger}_{q}f^{*}_{ex}(1)\delta_{(q,-q_{\parallel})} \\
&= \sum_{K,q_{\parallel}} E_{ex}(K+q_{\parallel})C^{\dagger}_{K+q_{\parallel}}C_{K}\left(f^{*}_{ex}b^{\dagger}_{-q_{\parallel}} + f_{ex}b_{q_{\parallel}}\right)\delta_{K',K+q_{\parallel}} \\
&\quad - \sum_{K,q_{\parallel}} E_{ex}(K)C^{\dagger}_{K+q_{\parallel}}C_{K'}\left(f^{*}_{ex}b^{\dagger}_{-q_{\parallel}} + f_{ex}b_{q_{\parallel}}\right)(-1)\delta_{K',K} \\
&\quad - \sum_{K,q_{\parallel}} \hbar\omega_0 C^{\dagger}_{K+q_{\parallel}}C_{K}b_{q_{\parallel}}f_{ex} + \sum_{K,q_{\parallel}} \hbar\omega_0 C^{\dagger}_{K+q_{\parallel}}C_{K}b^{\dagger}_{-q_{\parallel}}f^{*}_{ex} \\
&= \sum_{K,q_{\parallel}} C^{\dagger}_{K+q_{\parallel}}C_{K}b^{\dagger}_{-q_{\parallel}}f^{*}_{ex}\left[E_{ex}(K+q_{\parallel}) - E_{ex}(K) + \hbar\omega_0\right] \\
&\quad \sum_{K,q_{\parallel}} C^{\dagger}_{K+q_{\parallel}}C_{K}b_{q_{\parallel}}f_{ex}\left[E_{ex}(K+q_{\parallel}) - E_{ex}(K) - \hbar\omega_0\right]
\end{aligned} \tag{2.53}$$

Also Eq. (2.28) is written as:

$$\hat{H}^{2D}_{ex-ph} = \sum_{K_{\parallel},q_{\parallel}} \Xi^{s}(q_{\parallel})C^{\dagger}_{K_{\parallel}+q_{\parallel}}C_{K_{\parallel}}b^{\dagger}_{-q_{\parallel}} + \sum_{K_{\parallel},q_{\parallel}} \Xi^{s}(q_{\parallel})C^{\dagger}_{K_{\parallel}+q_{\parallel}}C_{K_{\parallel}}b_{q_{\parallel}} \tag{2.54}$$

By identification between Eqs. (2.53) and (2.54), according to Eq. (2.52) we have:

$$f^{*}_{ex}\left[E_{ex}(K_{\parallel}+q_{\parallel}) - E_{ex}(K_{\parallel}) + \hbar\omega_0\right] = \Xi^{s}(q_{\parallel}) \tag{2.55}$$

and

$$f_{ex}\left[E_{ex}(K_{\parallel}+q_{\parallel}) - E_{ex}(K_{\parallel}) - \hbar\omega_0\right] = \Xi^{s}(q_{\parallel}) \tag{2.56}$$

Then we obtain the $f$-functions as :

$$f^{*}_{ex} = \frac{\Xi^{s}(q_{\parallel})}{E_{ex}(K_{\parallel}+q_{\parallel}) - E_{ex}(K_{\parallel}) + \hbar\omega_0} \tag{2.57}$$

$$f_{ex} = \frac{\Xi^{s}(q_{\parallel})}{E_{ex}(K_{\parallel}+q_{\parallel}) - E_{ex}(K_{\parallel}) - \hbar\omega_0} \tag{2.58}$$

Since Eq. (2.50) is completely defined, we directly apply the transformation to operators as follows:

$$\begin{aligned} U_{ex}^{-1} C_{K_\parallel}^\dagger U_{ex} &= C_{K_\parallel}^\dagger + \left[ C_{K_\parallel}^\dagger, i \sum_{K_\parallel, q_\parallel} C_{K_\parallel+q_\parallel}^\dagger C_{K_\parallel} (f_{ex}^* b_{-q_\parallel}^\dagger + f_{ex} b_{q_\parallel}) \right] \\ &= C_{K_\parallel}^\dagger - i \sum_{K_\parallel, q_\parallel} C_{K_\parallel+q_\parallel}^\dagger (f_{ex}^* b_{-q_\parallel}^\dagger + f_{ex} b_{q_\parallel}) \end{aligned} \tag{2.59}$$

$$\begin{aligned} U_{ex}^{-1} C_{K_\parallel} U_{ex} &= C_{K_\parallel} + \left[ C_{K_\parallel}, i \sum_{K_\parallel, q_\parallel} C_{K_\parallel+q_\parallel}^\dagger C_{K_\parallel} (f_{ex}^* b_{-q_\parallel}^\dagger + f_{ex} b_{q_\parallel}) \right] \\ &= C_{K_\parallel} \end{aligned} \tag{2.60}$$

$$\begin{aligned} U_{ex}^{-1} b_q^\dagger U_{ex} &= b_q^\dagger + \left[ b_q^\dagger, i \sum_{K_\parallel, q_\parallel} C_{K_\parallel+q_\parallel}^\dagger C_{K_\parallel} (f_{ex}^* b_{-q_\parallel}^\dagger + f_{ex} b_{q_\parallel}) \right] \\ &= b_q^\dagger \end{aligned} \tag{2.61}$$

$$\begin{aligned} U_{ex}^{-1} b_q U_{ex} &= b_q + \left[ b_q, i \sum_{K_\parallel, q_\parallel} C_{K_\parallel+q_\parallel}^\dagger C_{K_\parallel} (f_{ex}^* b_{-q_\parallel}^\dagger + f_{ex} b_{q_\parallel}) \right] \\ &= b_q \end{aligned} \tag{2.62}$$

$$\begin{aligned} U_{ex}^{-1} b_{q_\parallel} U_{ex} &= b_{q_\parallel} + \left[ b_{q_\parallel}, i \sum_{K_\parallel, q_\parallel} C_{K_\parallel+q_\parallel}^\dagger C_{K_\parallel} (f_{ex}^* b_{-q_\parallel}^\dagger + f_{ex} b_{q_\parallel}) \right] \\ &= b_{q_\parallel} + i \sum_{K_\parallel, q_\parallel} C_{K_\parallel+q_\parallel}^\dagger C_{K_\parallel} f_{ex}^* \end{aligned} \tag{2.63}$$

$$\begin{aligned} U_{ex}^{-1} b_{-q_\parallel}^\dagger U_{ex} &= b_{-q_\parallel}^\dagger + \left[ b_{-q_\parallel}^\dagger, i \sum_{K_\parallel, q_\parallel} C_{K_\parallel+q_\parallel}^\dagger C_{K_\parallel} (f_{ex}^* b_{-q_\parallel}^\dagger + f_{ex} b_{q_\parallel}) \right] \\ &= b_{-q_\parallel}^\dagger - i \sum_{K_\parallel, q_\parallel} C_{K_\parallel+q_\parallel}^\dagger C_{K_\parallel} f_{ex} \end{aligned} \tag{2.64}$$

$$\begin{aligned} U_{ex}^{-1} C_{K_\parallel+q_\parallel}^\dagger U_{ex} &= C_{K_\parallel+q_\parallel}^\dagger + \left[ C_{K_\parallel+q_\parallel}^\dagger, i \sum_{K_\parallel, q_\parallel} C_{K_\parallel+q_\parallel}^\dagger C_{K_\parallel} (f_{ex}^* b_{-q_\parallel}^\dagger + f_{ex} b_{q_\parallel}) \right] \\ &= C_{K_\parallel+q_\parallel}^\dagger \end{aligned} \tag{2.65}$$

Then with respect to Eq. (2.46), we evaluate the transformed Hamiltonian in the approximative diagonalized form:

$$\hat{H}^T = U_{ex}^{-1} \hat{H}^{2D} U_{ex} \approx \hat{H}_{ex}^{2D} + \hat{H}_{ph} + \hat{H}_{ex-ph}^{T2D} \tag{2.66}$$

With

$$\hat{H}^{T2D}_{ex-ph} = \sum_{K_\parallel, K'_\parallel, q_\parallel} \left[ \frac{1}{E_{ex}(K_\parallel+q_\parallel)-E_{ex}(K_\parallel)+\hbar\omega_0} - \frac{1}{E_{ex}(K_\parallel+q_\parallel)-E_{ex}(K_\parallel)-\hbar\omega_0} \right] \times |\Xi^i(q_\parallel)|^2 C^\dagger_{K_\parallel+q_\parallel} C_{K_\parallel} C^\dagger_{K'_\parallel+q_\parallel} C_{K'_\parallel} \tag{2.67}$$

The GS energy of the exciton-polaron is calculated at low thermalized phonon occupation as:

$$E^0_{ex-pol} = \left\langle \Psi_0 | \hat{H}^T | \Psi_0 \right\rangle \tag{2.68}$$

With GS wave function taken as:

$$|\Psi_0\rangle = |K_\parallel, n(q)\rangle = C^\dagger_{K_\parallel} |0\rangle_k |0\rangle_{ph} \tag{2.69}$$

Also

$$C_{K_\parallel} |0\rangle_k = 0 \tag{2.70}$$

$$b_q |0\rangle_{ph} = 0 \tag{2.71}$$

Let us separate the energy calculation into three parts and evaluate them as follows:

$$E_{01} = \langle 0,0 | \hat{H}^{2D}_{ex} | 0,0 \rangle = \sum_{K_\parallel} E_{ex} \langle 0,0 | C_{K_\parallel} C^\dagger_{K_\parallel} C_{K_\parallel} C^\dagger_{K_\parallel} | 0,0 \rangle = E_{ex} \tag{2.72}$$

$$E_{02} = \langle 0,0 | C_{K_\parallel} \hat{H}_{ph} C^\dagger_{K_\parallel} | 0,0 \rangle = \sum_q \hbar\omega_0 \langle 0 | b^\dagger_q b_q | 0 \rangle \langle 0 | C_{K_\parallel} C^\dagger_{K_\parallel} | 0 \rangle = 0 \tag{2.73}$$

$$\begin{aligned} E_{03} &= \langle 0,0 | \hat{H}^{T2D}_{ex-ph} | 0,0 \rangle \\ &= \langle 0,0 | \sum_{K_\parallel, q_\parallel} \Xi^s(q_\parallel) \left[ f^*_{ex} - f_{ex} \right] C_{K_\parallel} C^\dagger_{K_\parallel+q_\parallel} C_{K_\parallel} C^\dagger_{K_\parallel+q_\parallel} C_{K_\parallel} C^\dagger_{K_\parallel} | 0,0 \rangle \\ &= \sum_{K_\parallel, q_\parallel} \Xi^s(q_\parallel) \left[ f^*_{ex} - f_{ex} \right] \langle 0 | | 0 \rangle \langle 0 | C_{K_\parallel} C^\dagger_{K_\parallel} C_{K_\parallel} C^\dagger_{K_\parallel} B_{K_\parallel} B^\dagger_{K_\parallel} | 0 \rangle \\ &= \sum_{q_\parallel} \Xi^s(q_\parallel) \left[ f^*_{ex} - f_{ex} \right] \\ &= -\sum_{q_\parallel} \Xi^s(q_\parallel) \left[ f_{ex} - f^*_{ex} \right] \end{aligned} \tag{2.74}$$

Therefore, we have:

$$E^0_{ex-pol} = E_{ex} - \sum_{q_\parallel} |\Xi^s(q_\parallel)|^2 \left[\frac{1}{E_{ex}(K_\parallel+q_\parallel)-E_{ex}(K_\parallel)-\hbar\omega_0} - \frac{1}{E_{ex}(K_\parallel+q_\parallel)-E_{ex}(K_\parallel)+\hbar\omega_0}\right] \tag{2.75}$$

Let us evaluate the summation:

$$I_{ex}(K_\parallel) = \sum_{q_\parallel} |\Xi^s(q_\parallel)|^2 \left[\frac{1}{E_{ex}(K_\parallel+q_\parallel)-E_{ex}(K_\parallel)-\hbar\omega_0} - \frac{1}{E_{ex}(K_\parallel+q_\parallel)-E_{ex}(K_\parallel)+\hbar\omega_0}\right] \tag{2.76}$$

According to Eqs. (2.45) and (2.41), converting the summation into an integration, we have:

$$I_{ex}(K_\parallel) = \frac{S_{2D}}{(2\pi)^2}\int_0^\infty dq_\parallel \int_0^{2\pi} d\theta |\Xi^s(q_\parallel)|^2 \left[\frac{1}{\frac{\hbar^2}{2M^*}q_\parallel^2+\frac{\hbar^2}{M^*}K_\parallel.q_\parallel-\hbar\omega_0} - \frac{1}{\frac{\hbar^2}{2M^*}q_\parallel^2+\frac{\hbar^2}{M^*}K_\parallel.q_\parallel+\hbar\omega_0}\right] \tag{2.77}$$

$$I_{ex}(K_\parallel) = \frac{S_{2D}}{(2\pi)^2}\int_0^\infty dq_\parallel \int_0^{2\pi} d\theta |\Xi^s(q_\parallel)|^2 \left[\frac{1}{\frac{\hbar^2}{2M^*}q_\parallel^2+\frac{\hbar^2}{M^*}kq_\parallel\cos\theta-\hbar\omega_0} - \frac{1}{\frac{\hbar^2}{2M^*}q_\parallel^2+\frac{\hbar^2}{M^*}kq_\parallel\cos\theta+\hbar\omega_0}\right] \tag{2.78}$$

With respect to Eq. (2.30), we can rewrite the integration in the form:

$$I^{ex}(K_\parallel) = \frac{\hbar(D_c^s-D_v^s)^2}{2\eta u(2\pi)^2}\int_0^\infty dq_\parallel \int_0^{2\pi} d\theta q_\parallel^2 \left[\frac{1}{u_1+v\cos\theta} - \frac{1}{u_2+v\cos\theta}\right] \tag{2.79}$$

Where

$$u_1 = \frac{\hbar^2}{2M^*}q_\parallel^2 - \hbar\omega_0; \tag{2.80}$$

$$u_2 = \frac{\hbar^2}{2M^*}q_\parallel^2 + \hbar\omega_0 \tag{2.81}$$

$$v = \frac{\hbar^2}{M^*}kq_\parallel \tag{2.82}$$

Integrating over $\theta$ we obtain:

$$I^{ex}(K_\parallel) = \frac{\hbar(D_c^s-D_v^s)^2}{2\eta u(2\pi)^2}\int_0^\infty dq_\parallel q_\parallel^2 \left[\frac{1}{\sqrt{u_1^2-v^2}} - \frac{1}{\sqrt{u_2^2-v^2}}\right] \tag{2.83}$$

Let us take :

$$T_1 = \frac{(u_1 - v)}{(u_1 + v)} = 1 - \frac{2\hbar^2 kq/M^*}{\frac{\hbar q}{M^*}\left(\frac{q}{2} + k\right) - \hbar\omega_0} \tag{2.84}$$

and

$$T_2 = (u_2 + v) = \frac{\hbar q}{M^*}\left(\frac{q}{2} + k\right) + \hbar\omega_0 \tag{2.85}$$

Then we have:

$$\begin{aligned} I^{ex}(K_\parallel) &= \frac{\hbar(D_c^s - D_v^s)^2}{2\eta u(2\pi)^2}\int_0^\infty dq_\parallel q_\parallel^2 \times \\ &\left[\frac{\sqrt{T_1}}{\frac{\hbar q}{M^*}\left(\frac{q}{2} - k\right) - \hbar\omega_0} - \left(\frac{\hbar q}{M^*}\left(\frac{q}{2} + k\right) + \hbar\omega_0\right)^{-1}\left(1 - \frac{2\hbar^2 kq/M^*}{T_2}\right)^{-1/2}\right] \end{aligned} \tag{2.86}$$

For small wave vector $K_\parallel << q_\parallel$ and using the relation :

$$(1 + \epsilon)^n \approx 1 + n\epsilon + (n\epsilon)^2 \tag{2.87}$$

This integration (2.86) is split into two parts as:

$$I^{ex}(k) \approx G_{ex1} + G_{ex2}(k) \tag{2.88}$$

With

$$G_{ex1} = \frac{\hbar(D_c^s - D_v^s)^2}{2\eta u(2\pi)}\int_0^\infty dq_\parallel \left[\frac{q_\parallel^2}{\frac{\hbar^2 q_\parallel^2}{2M^*} - \hbar\omega_0} - \frac{q_\parallel^2}{\frac{\hbar^2 q_\parallel^2}{2M^*} + \hbar\omega_0}\right] \tag{2.89}$$

$$G_{ex2}(K_\parallel) = \frac{\hbar(D_c^s - D_v^s)^2}{2\eta u(2\pi)}\left(\frac{\hbar^2 k}{M^*}\right)^2\int_0^\infty dq_\parallel \left[\frac{q_\parallel^4}{\left(\frac{\hbar^2 q_\parallel^2}{2M^*} - \hbar\omega_0\right)^3} - \frac{q_\parallel^4}{\left(\frac{\hbar^2 q_\parallel^2}{2M^*} + \hbar\omega_0\right)^3}\right] \tag{2.90}$$

Integrating over $q_\parallel$, one gets:

$$G_{ex1} = \frac{\pi\sqrt{\hbar\omega_0}(D_c^s - D_v^s)^2}{\sqrt{2}\hbar^2\eta u}\left(m_e^* + m_h^*\right)^{3/2} \tag{2.91}$$

and

$$\begin{aligned} G_{ex2}(K_\parallel) &= \left(\frac{\hbar^2 K_\parallel^2}{2M^*}\right)\frac{3\pi(D_c^s - D_v^s)^2}{4\sqrt{2}\hbar^2\eta u}\frac{\left(m_e^* + m_h^*\right)^{3/2}}{\sqrt{\hbar\omega_0}} \\ &= \left(\frac{\hbar^2 K_\parallel^2}{2M^*}\right)\widetilde{G}_{ex2} \end{aligned} \tag{2.92}$$

The final expression of the GS energy of the exciton-polaron is obtained by substituting Eqs. (2.88) and (2.45) into Eq. (2.75). It gives:

$$E^0_{ex-pol} = E_g + \left(\frac{\hbar^2 K_\parallel^2}{2M^*}\right)\left(1 - \widetilde{G}_{ex2}\right) - E_b - G_{ex1} \tag{2.93}$$

For the first excited state, we use the wave function:

$$|\Psi_1\rangle = C^\dagger_{K_\parallel}|1\rangle_k|0\rangle_{ph} \tag{2.94}$$

Such that

$$E^1_{ex-pol}\langle\Psi_1|\hat{H}^T|\Psi_1\rangle \tag{2.95}$$

Thus, the first excited state energy is :

$$E^1_{ex-pol} = 4E_g + 4\left(\frac{\hbar^2 K_\parallel^2}{2M^*}\right)\left(1 - 2\widetilde{G}_{ex2}\right) - 4E_b - 8G_{ex1} \tag{2.96}$$

## 2.2 Fermi's golden rule

In quantum physics, Fermi's golden rule is a formula that describes the transition rate from one energy eigenstate of the system to another in a continuum, as a result of a weak perturbation. This probability of a transition per unit time is proportional to the coupling strength between the initial and final states of the system.

### 2.2.1 Lifetime of polaron.

The polaron lifetime is given using the golden principle rule [110]. It is defined as:

$$\frac{\hbar}{\tau_p} = 2\pi \sum_q |\langle n_{q'}|\langle\psi|H_{e-ph}|\psi\rangle|n_q\rangle|^2 \delta\left(E_{q'} - E_q\right) \tag{2.97}$$

$H_{e-ph}$ represents the electron-phonon Hamiltonian and $|\psi\rangle$ the system wave function. Where:

$$n_{q'} = n_q - 1 \tag{2.98}$$

Taking into account Eqs. (1.11) and (1.12), we have:

$$\begin{aligned}\frac{\hbar}{\tau_p} &= 2\pi \sum_q \left|\langle n_q - 1| \langle\psi| V_q e^{iq.r} \left[b_q + b_q^\dagger\right] |\psi\rangle |n_q\rangle\right|^2 \\ &= 2\pi \left\{ \sum_q \left|\langle n_q - 1| \langle\psi| V_q e^{iq.r} b_q |\psi\rangle |n_q\rangle + \langle n_q - 1| \langle\psi| V_q^* e^{-iq.r} b_q^\dagger |\psi\rangle |n_q\rangle\right|^2 \right\} \\ &= 2\pi \left\{ \sum_q \left|\langle\psi| V_q e^{iq.r} |\psi\rangle \langle n_q - 1| b_q |n_q\rangle + \langle\psi| V_q^* e^{-iq.r} |\psi\rangle \langle n_q - 1| b_q^\dagger |n_q\rangle\right|^2 \right\} \end{aligned} \tag{2.99}$$

Also

$$b_q |n_q\rangle = \sqrt{n_q} |n_q - 1\rangle \tag{2.100}$$

$$b_q^\dagger |n_q\rangle = \sqrt{n_q + 1} |n_q + 1\rangle \tag{2.101}$$

Substituting these previous relations in Eq. (2.99), we get:

$$\begin{aligned}\frac{\hbar}{\tau_p} &= 2\pi \sum_q \left|\langle\psi| V_q e^{iq.r} |\psi\rangle \sqrt{n_q} \langle n_q - 1| |n_q - 1\rangle\right|^2 \\ &= 2\pi \sum_q \left|\langle\psi| V_q e^{iq.r} |\psi\rangle \sqrt{n_q}\right|^2 \\ &= 2\pi \sum_q \bar{n}_q |V_q|^2 \left|\langle\psi| e^{iq.r} |\psi\rangle\right|^2 \\ &= 2\pi \sum_q \bar{n}_q |V_q|^2 \langle\psi| \left|e^{iq.r}\right|^2 |\psi\rangle \\ &= 2\pi \bar{n}_q \frac{\hbar^2 \omega_{Lo}^2}{V} 4\pi\alpha R_v \sum_q \frac{1}{q^2} \langle\psi| \left|e^{iq.r}\right|^2 |\psi\rangle \end{aligned} \tag{2.102}$$

Where $\bar{n}_q$ is the mean number of phonons. Since $\left|e^{iq.r}\right|^2 = 1$, then transforming the sum into integral, we have:

$$\frac{\hbar}{\tau_p} = 2\pi \bar{n}_q \frac{\hbar^2 \omega_0^2}{V} 4\pi\alpha R_v \frac{V}{8\pi^3} \int \frac{d^3q}{q^2} \tag{2.103}$$

Thus

$$\frac{\hbar}{\tau_p} = \bar{n}_q \frac{\hbar^2 \omega_0^2}{\pi} \alpha R_v \int \frac{d^3q}{q^2} \tag{2.104}$$

The expression of the polaron lifetime is then obtained by solving the integral of Eq. (2.104)

### 2.2.2 Lifetime of exciton polaron.

The lifetime of exciton-polaron [111] is also determined from the golden rule:

$$\frac{\hbar}{\tau_{ex}} = 2\pi \sum_{q} |\langle n_{q'}, K|H^{2D}_{ex-ph}|K, n_q\rangle|^2 \delta\left[E^0_{ex-pol}(K) - E^0_{ex-pol}(K+q) + \hbar\omega_0\right] \tag{2.105}$$

For the ground state, we have:

$$\frac{\hbar}{\tau_{ex}} = 2\pi \sum_{q} |\langle n_q - 1|\langle 0|C_K H^{2D}_{ex-ph} C^{\dagger}_K|0\rangle|n_q\rangle|^2 \delta\left[g(q)\right] \tag{2.106}$$

$g$ is a function taken as:

$$g(q) = E^0_{ex-pol}(K) - E^0_{ex-pol}(K+q) + \hbar\omega_0 \tag{2.107}$$

According to Eq. (2.93), the latest gives:

$$g(q) = \frac{\hbar^2(1-\tilde{G}_{ex2})}{2M^*}\left(-q^2 - 2K.q + \frac{2M^*\hbar\omega_0}{\hbar^2(1-\tilde{G}_{ex2})}\right) \tag{2.108}$$

Let use the following relation:

$$\delta\left[g(q)\right] = \sum_{i} \frac{\delta(q-q_i)}{|g'(q_i)|} \tag{2.109}$$

Where $q_i$ are the roofs of the $g$-fonction and we have:

$$\delta\left[g(q)\right] = \frac{M^*}{\hbar^2(1-\tilde{G}_{ex2})} \frac{\delta(q-q_1) + \delta(q-q_2)}{\sqrt{K^2 cos^2\theta + 2M^*\hbar\omega_0/\hbar^2(1-\tilde{G}_{ex2})}} \tag{2.110}$$

Where

$$\begin{cases} q_1 &= -K\cos\theta + \sqrt{K^2\cos^2\theta + 2M\hbar\omega_0/\hbar^2(1-\tilde{G}_{ex2})} \\ q_2 &= -K\cos\theta - \sqrt{K^2\cos^2\theta + 2M\hbar\omega_0/\hbar^2(1-\tilde{G}_{ex2})} \end{cases} \tag{2.111}$$

After averaging with respect to Eqs. (2.28) and (2.110), the lifetime of exciton polaron gives:

$$\frac{\hbar}{\tau_{ex}} = \frac{2\pi M^*}{\hbar^2(1-\tilde{G}_{ex2})}\sum_q \bar{n}_q \left(\Xi^s(q)\right)^2 \frac{\delta(q-q_1)+\delta(q-q_2)}{\sqrt{K^2 cos^2\theta + 2M^*\hbar\omega_0/\hbar^2(1-\tilde{G}_{ex2})}} \tag{2.112}$$

The mean number of phonon in the GS is taken from the quantum statistic as:

$$\bar{n}_q = \left[\beta E^0_{ex-pol} - 1\right]^{-1} \tag{2.113}$$

$\beta$ being the inverse of temperature.

It follows that the calculation of this property depends on the calculation of the sum which is directly related to the expression of exciton-phonon coupling function and the dimensionality of the material as pointed Eq. (2.103).

### 2.2.3 Optical absorption coefficient.

Here we consider a polaron interaction with light of frequency ($\Omega$). The total Hamiltonian takes the form:

$$H_{tot} = H_{pol} + V \tag{2.114}$$

The second term describes the interaction of the electron-phonon with light and is linked to the electric field induces by the photon ($E_i$) as:

$$V = -\frac{e}{m_e\Omega}E_i.p \tag{2.115}$$

The absorption coefficient ($\Gamma_p$) for absorption of light by free polaron is proportional to the probability $P(\Omega)$ that a photon is absorbed by this polaron

in its ground state [112]. We have:

$$\Gamma_p = \frac{\Omega}{\varepsilon_0 cn(2E_i^2)} P(\Omega) \tag{2.116}$$

$\varepsilon_0$ is the permittivity of vacuum, $c$ is the light velocity, $n$ is the refractive index of the structure in which the polaron moves. The incident light is viewed as a perturbation and the transition probability is taken from the Fermi golden rule [113]:

$$P(\Omega) = 2\pi \sum_f \langle \Phi_0|V|f\rangle\langle f|V|\Phi_0\rangle \delta(E_0 + \Omega - E_f) \tag{2.117}$$

$|\Phi_0\rangle$ and $|f\rangle$ are respectively the GS and the possible final state with energies $E_0$ and $E_f$. The representation of the $\delta$-function is:

$$\delta(x) = \frac{1}{\pi} Re \int_{-\infty}^{0} dt exp[-i(x + i\varepsilon)t] \tag{2.118}$$

Thus

$$\begin{aligned} P(\Omega) &= 2Re \sum_f \int_{-\infty}^{0} dt \langle \Phi_0|V|f\rangle\langle f|V|\Phi_0\rangle exp[-i(\Omega + i\varepsilon + E_0 - E_f)t] \\ &= 2Re \sum_f \int_{-\infty}^{0} dt exp[-i(\Omega + i\varepsilon)t] \langle \Phi_0|V|f\rangle\langle f|e^{iHt} V e^{-iHt}|\Phi_0\rangle \end{aligned} \tag{2.119}$$

Using the fact that:

$$\sum_f |f\rangle\langle f| = 1 \tag{2.120}$$

and the notations:

$$e^{iHt} V e^{-iHt} = V(t) \tag{2.121}$$

$$\frac{dV(t)}{dt} = i[H, V(t)] \tag{2.122}$$

We have :

$$P(\Omega) = 2Re \int_{-\infty}^{0} dt exp[-i(\Omega + i\varepsilon)t] \langle \Phi_0|V(0)V(t)|\Phi_0\rangle \tag{2.123}$$

Denoting

$$R(\Omega) = \int_{-\infty}^{0} dt exp[-i(\Omega + i\varepsilon)t]\langle\Phi_0|V(0)V(t)|\Phi_0\rangle \tag{2.124}$$

Eq. (2.123) is reduced to:

$$P(\Omega) = 2ReR(\Omega) \tag{2.125}$$

Substituting Eq. (2.115) in Eq. (2.124) we find that:

$$R(\Omega) = \left(\frac{e}{m\Omega}\right)^2 \int_{-\infty}^{0} dt e^{(-i(\Omega+i\varepsilon)t)}\langle\Phi_0|(E_i.p(0))(E_i.p(t))|\Phi_0\rangle \tag{2.126}$$

and then

$$P(\Omega) = 2\left(\frac{e}{m\Omega}\right)^2 Re \int_{-\infty}^{0} dt e^{(-i(\Omega+i\varepsilon)t)}\langle\Phi_0|(E_i.p(0))(E_i.p(t))|\Phi_0\rangle \tag{2.127}$$

It is convenient to apply the first LLP transformation (2.4) which eliminates the electron operators from the polaron Hamiltonian.

$$\mathcal{H} = S_1^{-1} H_{pol} S_1 = \mathcal{H}_0 + \mathcal{H}_1 : \tag{2.128}$$

$$\mathcal{H}_0 = \frac{P^2}{2m} + \sum_q \left(\omega_{LO} + \frac{q^2}{2m} - \frac{q.P}{m}\right) b_q^\dagger b_q + \sum_q (V_q b_q + V_q^* b_q^\dagger) \tag{2.129}$$

$$\mathcal{H}_1 = \frac{1}{2m}\sum_q q.q' b_q^\dagger b_{q'}^\dagger b_q b_{q'} \tag{2.130}$$

Here $\mathcal{H}_0$ can be exactly diagonalized to obtain the self-energy $E_{pol} = -\alpha\hbar\omega_{LO}$ while $\mathcal{H}_1$ contains the correlation effects between the phonons.

In the LLP approximation, the explicit form of the matrix element in (2.126) is:

$$\langle\Phi_0|(E_i.p(0))(E_i.p(t))|\Phi_0\rangle = \langle 0|S_2^{-1}S_1^{-1}E_i.pS_1S_1^{-1}E_i.p(t)S_1S_2|0\rangle \tag{2.131}$$

The application of $\hat{S}_1$ gives:

$$S_1^{-1}p(t)S_1 = S_1^{-1}e^{iHt}p(t)e^{-iHt}S_1 = S_1^{-1}e^{iHt}S_1S_1^{-1}pS_1S_1^{-1}e^{-iHt}S_1 \quad (2.132)$$

Using $\mathcal{H} = S_1^{-1}HS_1$, we arrive at $S_1^{-1}e^{iHt}S_1 = e^{iHt}$. Furthur we recall $S_1^{-1}pS_1 = P - \sum_q \hbar q b_q^\dagger b_q + p$, where $P = 0$ . This results in

$$S_1^{-1}p(t)S_1 = e^{i\mathcal{H}t}pe^{-i\mathcal{H}t} = -\sum_q \hbar q e^{i\mathcal{H}t}b_q^\dagger b_q e^{-i\mathcal{H}t} = -\sum_q \hbar q b_q^\dagger(t)b_q(t) \quad (2.133)$$

Then Eq. (2.131) takes the from:

$$\langle\Phi_0|(E_i.p(0))(E_i.p(t))|\Phi_0\rangle = \left\langle 0 \left| S_2^{-1}\left(\sum_q E_i.qb_q^\dagger b_q\right)\left(\sum_q E_i.qb_q^\dagger(t)b_q(t)\right)S_2 \right| 0 \right\rangle \quad (2.134)$$

The calculation of the matrix element (2.134) proceeds as follows:
$\langle\Phi_0|(E_i.p(0))(E_i.p(t))|\Phi_0\rangle =$

$$\begin{aligned}
&= \left\langle 0 \left| S_2^{-1}\left(\sum_q E_i.qb_q^\dagger b_q\right)\left(\sum_q E_i.qb_q^\dagger(t)b_q(t)\right)S_2 \right| 0 \right\rangle \\
&= \left\langle 0 \left| S_2^{-1}\left(\sum_q E_i.qb_q^\dagger b_q\right)S_2S_2^{-1}e^{i\mathcal{H}t}S_2S_2^{-1}\left(\sum_q E_i.qb_q^\dagger(t)b_q(t)\right)S_2S_2^{-1}e^{i\mathcal{H}t}S_2 \right| 0 \right\rangle \\
&= \left\langle 0 \left| S_2^{-1}\left(\sum_q E_i.qb_q^\dagger b_q\right)S_2e^{iS_2^{-1}\mathcal{H}S_2t}S_2^{-1}\left(\sum_q E_i.qb_q^\dagger(t)b_q(t)\right)S_2e^{-iS_2^{-1}\mathcal{H}S_2t} \right| 0 \right\rangle
\end{aligned} \quad (2.135)$$

We compute

$$S_2^{-1}\mathcal{H}S_2 = H_0 + H_1 \quad (2.136)$$

with

$$H_0 = S_2^{-1}\mathcal{H}_0S_2 = S_2^{-1}\left[\sum_q\left(\omega_{LO} + \frac{q^2}{2m}\right)b_q^\dagger b_q + \sum_q(V_qb_q + V_q^*b_q^\dagger)\right]S_2 \quad (2.137)$$

Further, we use $S_2^{-1} b_q S_2 = b_q + f_q$:

$$\begin{aligned} H_0 &= \sum_q \left(\omega_{LO} + \tfrac{q^2}{2m}\right) b_q^\dagger b_q + \sum_q \left(\omega_{LO} + \tfrac{q^2}{2m}\right) |f_q| + \\ &\quad \sum_q \left(\omega_{LO} + \tfrac{q^2}{2m}\right) \left(b_q^\dagger f_q + b_q f_q^\dagger\right) + \sum_q \left[V_q(b_q + f_q) + V_q^\dagger (b_q^\dagger + f_q^*)\right] \\ &= \sum_q \left(\omega_{LO} + \tfrac{q^2}{2m}\right) b_q^\dagger b_q + \sum_q \frac{|V_q|^2}{\left(\omega_{LO} + \frac{q^2}{2m}\right)} - 2\sum_q \frac{|V_q|^2}{\left(\omega_{LO} + \frac{q^2}{2m}\right)} \\ &= \sum_q \left(\omega_{LO} + \tfrac{q^2}{2m}\right) b_q^\dagger b_q - \sum_q \frac{|V_q|^2}{\left(\omega_{LO} + \frac{q^2}{2m}\right)} \end{aligned} \tag{2.138}$$

Analytically, the last term can be computed :

$$\begin{aligned} \sum_q \frac{|V_q|^2}{\omega_{LO} + \frac{q^2}{2m}} &= \frac{V}{(2\pi)^3} \int d^3q \left(\frac{\omega_{LO}}{q}\right)^2 \frac{4\pi\alpha}{V} \left(\frac{1}{2m\omega_{LO}}\right)^{\frac{1}{2}} \frac{|V_q|^2}{\omega_{LO} + \frac{q^2}{2m}} \\ &= \frac{\alpha\omega_{LO}}{2\pi^2} 4\pi \int_0^\infty dq \left(\frac{1}{2m\omega_{LO}} \frac{1}{1 + \frac{Q^2}{2m\omega_{LO}}}\right)^{\frac{1}{2}} \\ &= \frac{2\alpha\omega_{LO}}{\pi} \int_0^\infty dq \frac{1}{1+\varsigma^2} = \frac{2\alpha\omega_{LO}}{\pi} \arctan\varsigma|_0^\infty = \alpha\omega_{LO} \end{aligned} \tag{2.139}$$

$$H_0 = -\alpha\omega_{LO} + \sum_q \left(\omega_{LO} + \frac{q^2}{2m}\right) b_q^\dagger b_q \tag{2.140}$$

The term $H_1 = S_2^{-1} \mathcal{H}_1 S_2$ will be neglected. Neglecting $H_1$, consistent with the LLP description, introduces no error in order $\alpha$. Therefore (2.135) becomes:

$$\left\langle 0 \left| \begin{array}{c} \sum_q E_i.q \left(b_q^\dagger b_q + f_q b_q^\dagger + f_q^* b_q + f_q f_q^*\right) e^{iH_0 t} \\ \sum_q E_i.q \left(b_q^\dagger b_q + f_q b_q^\dagger + f_q^* b_q + f_q f_q^*\right) e^{-iH_0 t} \end{array} \right| 0 \right\rangle \tag{2.141}$$

For $P = 0$ there is no privileged direction and $\sum_q E_i.q f_q f_q^* = 0$, the latest equation reduces to:

$$\left\langle 0 \left| \sum_q E_i.q f_q^* b_q e^{iH_0 t} \sum_q E_i.q f_q b_q^\dagger e^{-iH_0 t} \right| 0 \right\rangle \tag{2.142}$$

From the equation of motion for $b_q^\dagger$:

$$\frac{db_q^\dagger(t)}{dt} = i\left[H_0, b_q^\dagger\right] = i\left(\omega_{LO} + \frac{q^2}{2m}\right) b_q^\dagger \tag{2.143}$$

It is easy now to calculate

$$e^{iH_0 t} b_q^\dagger e^{-iH_0 t} = b_q^\dagger \exp\left[i\left(\omega_{LO} + \frac{q^2}{2m}\right) t\right] \tag{2.144}$$

Thus, Eq. (2.131) becomes :

$$\langle\Phi_0|(E_i.p(0))(E_i.p(t))|\Phi_0\rangle = \sum_q (E_i.q)^2 f_q^* f_q \exp\left[i\left(\omega_{LO} + \tfrac{q^2}{2m}\right) t\right] + O(\alpha^2) \tag{2.145}$$

and the transition probability (2.127) then gives :

$$\begin{aligned} P(\Omega) &= 2Re\tfrac{e^2}{m^2\Omega^2} \sum_q (E_i.q)^2 f_q^* f_q \int_{-\infty}^0 dt \exp\left[-i\left(\Omega + i\varepsilon - \omega_{LO} - \tfrac{q^2}{2m}\right) t\right] \\ &= 2\pi\tfrac{e^2}{m^2\Omega^2} \sum_q (E_i.q)^2 |f_q|^2 \delta\left(\Omega - \omega_{LO} - \tfrac{q^2}{2m}\right) \end{aligned} \tag{2.146}$$

Using the functions (2.23) and (2.24) for $P = 0$, we obtain:

$$\begin{aligned} P(\Omega) &= \tfrac{2\pi e^2}{m^2\Omega^2} \sum_q \tfrac{(E_i.q)^2}{\left(\omega_{LO} + \frac{q^2}{2m}\right)} |V_q|^2 \delta\left(\Omega - \omega_{LO} - \tfrac{q^2}{2m}\right) \\ &= \tfrac{2\pi e^2}{m^2\Omega^2} \tfrac{V}{(2\pi)^3} \int d^3q \left(\tfrac{\omega_{LO}}{q}\right)^2 \tfrac{4\pi\alpha}{V} \left(\tfrac{1}{2m\omega_{LO}}\right)^{\frac{1}{2}} \\ &\quad \times \tfrac{(E_i.q)^2}{\left(\omega_{LO} + \frac{q^2}{2m}\right)^2} \delta\left(\Omega - \omega_{LO} - \tfrac{q^2}{2m}\right) \\ &= \tfrac{e^2\alpha E_i^2}{m^2\Omega^2\pi} \int_{-1}^1 dx x^2 \int_0^\infty dq \left(\tfrac{1}{2m\omega_{LO}}\right)^{\frac{1}{2}} \\ &\quad \times \frac{\frac{q^2}{2m\omega_{LO}}}{\left(1 + \frac{q^2}{2m\omega_{LO}}\right)^2} \tfrac{1}{\omega_{LO}} \delta\left(\tfrac{\Omega}{\omega_{LO}} - 1 - \tfrac{q^2}{2m\omega_{LO}}\right) \\ &= \tfrac{8e^2\alpha E_i^2}{3m\Omega^2} \int_0^\infty d\varsigma \tfrac{\varsigma^2}{(1+\varsigma)^2} \delta\left(\tfrac{\Omega}{\omega_{LO}} - 1 - \varsigma^2\right) \\ &= \tfrac{4e^2\alpha E_i^2}{3m\Omega^2} \Theta\left(\tfrac{\Omega}{\omega_{LO}} - 1\right) \frac{\sqrt{\frac{\Omega}{\omega_{LO}} - 1}}{\left(\frac{\Omega}{\omega_{LO}}\right)^2} \\ &= \tfrac{4e^2\alpha E_i^2 \omega_{LO}^2}{3m\Omega^4} \Theta\left(\tfrac{\Omega}{\omega_{LO}} - 1\right) \sqrt{\tfrac{\Omega}{\omega_{LO}} - 1} \end{aligned} \tag{2.147}$$

where:

$$\Theta\left(\frac{\Omega}{\omega_{LO}}-1\right)=\begin{cases}1 & if \quad \frac{\Omega}{\omega_{LO}}>1\\ 0 & if \quad \frac{\Omega}{\omega_{LO}}<1\end{cases} \tag{2.148}$$

The final expresson of the absorption coefficient is obtained by substituting the latest relation of the transiton probability in Eq. (2.116). It takes the form:

$$\Gamma_p(\Omega)=\frac{1}{\varepsilon_0 cn}\frac{2e^2\alpha\omega_{LO}^2}{3m\Omega^3}\Theta\left(\frac{\Omega}{\omega_{LO}}-1\right)\sqrt{\frac{\Omega}{\omega_{LO}}-1} \tag{2.149}$$

There is absorption of the light for $\Omega/\omega_{LO} \geq 1$. Then the optical absorption is possible when the photon energy is equal or exceeds the LO-phonon energy for the polaron case. Also, from the final expression, it is seen that the absorption coefficient doesn't depend of the electric field induced by the light ($E_i$).

## 2.3 Relaxation time approximation

In physics, the word relaxation usually means the return of a perturbed system into equilibrium. It is important to consider the RTA before the general theory when one studies the structure of a non-equilibrium state. The relaxation time $\tau(r,k)$ is introduced in the manner that the collision probability during the time $dt$ for a particle at phase space point $(r,k)$ in band $n$ is equal to $dt/\tau$ . If particles have the equilibrium distribution $f_n^0(r,k)$ with local temperature $T(r)$ the collisions do not affect the form of the distribution function. This approximation assumes the thermodynamic equilibrium corresponding to a local temperature is maintained through the scattering and that the information on the non-equilibrium state is completely lost due to the scattering processes. This specifies the distribution function of particles scattered near point $r$ between $t$ and $t+dt$. Let denote this distribution function $df_n(r,k,t)$ and the non-equilibrium one $f_n(r,k,t)$. Thus, $df_n$ can be found by considering an arbitrary form of $f_n$. This leads to the following expression :

$$df_n(r,k,t)=\frac{dt}{\tau_n(r,k)}f_n^0(r,k) \tag{2.150}$$

Moreover, the system will move out of the equilibrium if an external force is applied and when this force is removed, the system returns to the equi-

librium due to scattering events caused by the collision term. In RTA and according to the Boltzman equation, the form of the collision term should be :

$$\left(\frac{\partial f(k)}{\partial t}\right)_{collision} = \frac{f_0(k) - f(k)}{\tau(k)} \tag{2.151}$$

Here $f_0$ is the Fermi's distribution. This form of the collision term makes sure that the probability density function will return to the Fermi's function when all forces are suppressed. In the case of particles uniformly distributed in space $\nabla_r f = 0$ with no external forces, we have:

$$\frac{\partial f(k)}{\partial t} = \frac{f_0(k) - f(k)}{\tau(k)} \tag{2.152}$$

with the solution:

$$f(k,t) = (f(k,0) - f_0(k))\, e^{-t/\tau(k)} + f_0(k) \tag{2.153}$$

This solution describes a system starting in some initial non-equilibrium probability density function $f(k,0)$ and returns to its equilibrium in a relaxation time $\tau(k)$. Some $k$-states decay fater than others and each relaxation process can be studied via a relaxation time.

### 2.3.1 Relaxation time of exciton-polaron

From the RTA, the exciton-polaron relaxation time ($\tau$ ) can be written in the form [31]:

$$\begin{aligned}\frac{1}{\tau} \;=\; & \frac{2\pi}{\hbar}\sum_q |\Xi(q)|^2 \left\{ \left[n_B + f\left(E^0_{ex-pol}(K+q)\right)\right] \times \right. \\ & \delta\left(E^0_{ex-pol}(K) - E^0_{ex-pol}(K+q) + \hbar\omega_0\right) \\ & \left. + \left[1 + n_B - f\left(E^0_{ex-pol}(K+q)\right)\right] \delta\left(E^0_{ex-pol}(K) - E^0_{ex-pol}(K+q) - \hbar\omega_0\right) \right\}\end{aligned} \tag{2.154}$$

One can see the two terms of Eq. (2.154) are attributed respectively to electron and hole contributions on the exciton-polaron relaxation time. $n_B$ is the Bose-Einstein function and $f(E^0_{ex-pol}(K+q))$ is the Fermi-Dirac distribution with the Fermi energy ($E_F$) which is related to the carriers concentration

($c_{ex}$). There are given as follows:

$$n_B = \left\{exp\left[\beta E^0_{ex-pol}(K)\right] - 1\right\}^{-1} \tag{2.155}$$

$$f(E^0_{ex-pol}(K+q)) = \left\{1 + exp\beta\left[E^0_{ex-pol}(K+q) - E_F\right]\right\}^{-1} \tag{2.156}$$

$$E_F = \frac{\hbar^2}{2M}\left(3\pi^2 c_{ex}\right)^{\frac{2}{3}} \text{ in 3D} \tag{2.157}$$

$$E_F = \frac{\hbar^2\pi}{M} c_{ex} \text{ in 2D} \tag{2.158}$$

$\beta$ denotes the inverse of the temperature. Let taken the functions:

$$g(q) = E^0_{ex-pol}(K) - E^0_{ex-pol}(K+q) + \hbar\omega_0 \tag{2.159}$$

$$h(q) = E^0_{ex-pol}(K) - E^0_{ex-pol}(K+q) - \hbar\omega_0 \tag{2.160}$$

We also consider Eq. (2.93) and we establish:

$$\delta\left(g(q)\right) = \frac{M}{\hbar^2(1-\tilde{G}_{ex2})} \frac{\delta(q-q_1) + \delta(q-q_2)}{\sqrt{K^2\cos^2\theta + 2M\hbar\omega_0/\hbar^2(1-\tilde{G}_{ex2})}} \tag{2.161}$$

And

$$\delta\left(h(q)\right) = \frac{M}{\hbar^2(1-\tilde{G}_{ex2})} \frac{\delta(q-q_3) + \delta(q-q_4)}{\sqrt{K^2\cos^2\theta - 2M\hbar\omega_0/\hbar^2(1-\tilde{G}_{ex2})}} \tag{2.162}$$

with $q_1, q_2$ and $q_3, q_4$ the roots of the $g$ and $h$ -functions respectively:

$$\begin{cases} q_1 &= -K\cos\theta + \sqrt{K^2\cos^2\theta + 2M\hbar\omega_0/\hbar^2(1-\tilde{G}_{ex2})} \\ q_2 &= -K\cos\theta - \sqrt{K^2\cos^2\theta + 2M\hbar\omega_0/\hbar^2(1-\tilde{G}_{ex2})} \end{cases} \tag{2.163}$$

$$\begin{cases} q_3 &= -K\cos\theta + \sqrt{K^2\cos^2\theta - 2M\hbar\omega_0/\hbar^2(1-\tilde{G}_{ex2})} \\ q_4 &= -K\cos\theta - \sqrt{K^2\cos^2\theta - 2M\hbar\omega_0/\hbar^2(1-\tilde{G}_{ex2})} \end{cases} \tag{2.164}$$

Therefore, Eq. (2.154) gives:

$$\begin{aligned}\frac{1}{\tau} &= \frac{2\pi M}{\hbar^3(1-\tilde{G}_{ex2})}\sum_q |\Xi^s(q)|^2\times \\ &\left\{\left[n_B + f\left(E^0_{ex-pol}(K+q)\right)\right]\frac{\delta(q-q_1)+\delta(q-q_2)}{\sqrt{K^2cos^2\theta - 2M\hbar\omega_0/\hbar^2(1-\tilde{G}_{ex2})}}\right. \\ &\left.+\left[1+n_B - f\left(E^0_{ex-pol}(K+q)\right)\right]\frac{\delta(q-q_3)+\delta(q-q_4)}{\sqrt{K^2cos^2\theta - 2M\hbar\omega_0/\hbar^2(1-\tilde{G}_{ex2})}}\right\}\end{aligned} \tag{2.165}$$

The evaluation of the sum over $q$ leads to the relaxation time of exciton polaron in the corresponding material.

### 2.3.2 Electrical conductivity

Among others, the parameters that testify to the electrical conductivity in a material are the carrier mobility and the current density.

#### * Mobility of carriers

In absence of the electric field, the free carriers have a movement resembling chip jumps characterized by changes in direction called "Brownian movement". Atoms, impurities and lattice defects are all obstacles for carriers to collide with each other. When an electric field $\vec{E}$ is applied to a semiconductor, each carrier undergoes an electrostatic force $\vec{F_{el}} = e_\alpha \vec{E}$ (with $e_\alpha = -e$ for electron and $+e$ for hole) and a viscous type frictional force $(-f\vec{v})$ which describes the effect of collisions. Its acceleration is written as $\vec{a} = \vec{F_{el}}/m$:

$$\vec{a} = \frac{e_\alpha}{m}\vec{E} - \frac{f}{m}\vec{v} \tag{2.166}$$

$$\vec{a} = \frac{e_\alpha}{m}\vec{E} - \frac{1}{\tau}\vec{v} \tag{2.167}$$

where $m$ is the carrier mass, $\vec{v}$ its drift speed and $f = m/\tau$ reflects viscous type friction. In steady state, $\vec{a} = \vec{0}$ we have:

$$\vec{v} = \frac{e_\alpha \tau}{m}\vec{E} = \mu\vec{E} \tag{2.168}$$

This makes it possible to express the speed of electron entrainment:

$$\vec{v_e} = -\frac{e\tau}{m_e}\vec{E} = \mu_e\vec{E} \tag{2.169}$$

and that of the holes:

$$\vec{v_h} = \frac{e\tau}{m_h}\vec{E} = \mu_h\vec{E} \tag{2.170}$$

The mobility ($\mu$) of the carriers is defined as the coefficient of proportionality between the speed and the electric field, which gives for electrons and holes:

$$\mu_e = -\frac{e\tau}{m_e} < 0 \tag{2.171}$$

$$\mu_h = \frac{e\tau}{m_h} > 0 \tag{2.172}$$

We obtain a negative mobility for the electrons. Many works prefer to consider mobility in absolute value.

Generally, three mechanisms influence mobility :

- Coulomb collisions: the ionic impurities and generally all the charged centers hinder the path of the carriers.
- Collisions with the lattice: the atoms of the crystal lattice which vibrate around their average position (phonons) are obstacles for the carriers.
- Collisions on the surface roughness: the dimensions of a semiconductor component not being infinite, carriers sometimes hit the surface and are all the more hampered in their movement as this surface is of poor quality.

The mobility of the carriers is constant as long as the electric field is weak. This means that the speed of electrons and holes remains proportional to the electric field but this proportionality disappears when the electric field becomes too high. The carriers acquire a certain kinetic energy which increases with the electric field and which they yield to the network during shocks. For strong electric fields, the energy to be released becomes too high and the carriers retain part of it after the shocks: this is called the phenomenon of hot carriers because then carriers are no longer in thermal equilibrium with the network. Thus, the speed does not remain proportional

to the electric field and the mobility becomes a function of the network temperature and the carrier temperature. We get for the electrons:

$$\mu_e = \mu_{0e}\sqrt{\frac{T_{network}}{T_e}} \tag{2.173}$$

This relation shows that the mobility decreases when the temperature of the carriers increases. $\mu_{0e}$ represents the mobility of electrons at low electric field. A similar relation is established for holes.

*** Current density**

The current density ($\vec{j}$) is defined as the flow of charges that pass per unit area. It is therefore equal to the speed of the charges ($\vec{v}$) multiplied by the concentration of charges ($c$). For the electrons this gives:

$$\vec{j_e} = -ec\vec{v_e} \tag{2.174}$$

By replacing the speed of the electron by its expression as a function of the mobility and the field (see Eq. 2.168), we find the expression for the current density of the electrons. By following the same reasoning, we also obtain the current density of the holes:

$$\vec{j_e} = -ec\mu_e\vec{E} = \sigma_e\vec{E} \tag{2.175}$$

$$\vec{j_h} = ec\mu_h\vec{E} = \sigma_h\vec{E} \tag{2.176}$$

The electrical conductivity $\sigma$ represents the coefficient of proportionality between the current density and the electric field. According to Eq. (2.171), we have:

$$\sigma_e = -ec\mu_e = \frac{e^2c\tau}{m_e} > 0 \tag{2.177}$$

Similarly, for the holes:

$$\sigma_h = ec\mu_h = \frac{e^2c\tau}{m_h} > 0 \tag{2.178}$$

In the case of conduction by electrons and holes, the total current density is written as:

$$\vec{J} = \vec{j_e} + \vec{j_h} = (\sigma_e + \sigma_h)\vec{E} \tag{2.179}$$

The total electrical conductivity then reads:

$$\sigma_{el} = \sigma_e + \sigma_h \tag{2.180}$$

Thus, both electron and hole contribute to the total electrical conductivity.

When the material is also subjected to a static magnetic field $\vec{B}$ along the $z-$ axis then there is *Hall effect* and *a magnetoresistance*. Indeed, there appears an additional magnetic force $\vec{F}_B = e_\alpha \vec{v} \wedge \vec{B}$. In agreement with Eq. (2.167) and assuming that all carriers have the same speed then in steady state, we have:

$$\frac{e_\alpha}{m}(\vec{E} + \vec{v} \wedge \vec{B}) - \frac{1}{\tau}\vec{v} = \vec{0} \tag{2.181}$$

We replace the expression of the speed as a function of the current density $\vec{v} = \vec{j}/ce_\alpha$ and we establish:

$$\vec{E} = \frac{m}{ce_\alpha^2 \tau}\vec{j} - \frac{1}{ce_\alpha}\vec{j} \wedge \vec{B} \tag{2.182}$$

This equation can be put on the form:

$$\vec{E} = R_{el}\vec{j} \tag{2.183}$$

with the resistivity $R_{el}$ defined by:

$$R_{el} = \frac{1}{\sigma_{el}} \tag{2.184}$$

*** Calcultation using RTA**

The electrical conductivity based on the RTA is given by [114] :

$$\sigma_{el} = e^2 \int \Lambda(E) \left(-\frac{\partial f}{\partial E}\right) dE \tag{2.185}$$

where $\Lambda(E)$ is the transport function taken as:

$$\Lambda(E) = \frac{1}{S_{2D}} \sum_{K} \nu_g^2 \tau \delta \left[ E - E^0_{ex-pol}(K) \right] \tag{2.186}$$

$\tau$ is the relaxation time evaluated by (2.165) and $\nu_g$ corresponds to the group velocity [115] defined as:

$$\nu_g = \frac{1}{\hbar} \frac{\partial E^0_{ex-pol}}{\partial K} = \frac{\hbar K}{M} (1 - \tilde{G}_{ex2}) \tag{2.187}$$

Here we also use Eq. (2.109) to transform the Dirac function of Eq. (2.186) into a suitable form for integration:

$$\delta \left( E - E^0_{ex-pol} \right) = \frac{M}{\hbar^2 (1 - \tilde{G}_{ex2}) K_0} \left\{ \delta(K + K_0) + \delta(K - K_0) \right\} \tag{2.188}$$

with

$$K_0(E) = \left( \frac{2Md}{\hbar^2 (1 - \tilde{G}_{ex2})} \right)^{1/2} \tag{2.189}$$

$$d = E + G_{ex1} + E_b - E_g \tag{2.190}$$

Thus, $\Lambda$ is determined by transforming the summation of Eq. (2.186) into an integration. This leads to:

$$\Lambda(E) = \frac{(1 - \tilde{G}_{ex2})}{2\pi M K_0} \int dK \left\{ K^3 \tau(K) \delta(K + K_0) + K^3 \tau(K) \delta(K - K_0) \right\} \tag{2.191}$$

Integrating over $K$, one gets:

$$\Lambda(E) = \frac{(1 - \tilde{G}_{ex2})}{2\pi M} K_0^2 \left\{ \tau(K_0) - \tau(-K_0) \right\} \tag{2.192}$$

Since the transport function is well determined, the calculation of the electrical conductivity with this method remains the integration of Eq. (2.185).

### 2.3.3 Seebeck coefficient

This coefficient estimates the current generated by the motion of hot particles in the system. In the absence of an electric current (important condition), when a material is subject to a temperature gradient ($\vec{gradT}$), the electric field ($\vec{E}$) which grows in the material is given by the equation:

$$\vec{E} = S^b(\vec{\nabla}T) \tag{2.193}$$

where $S^b$ is the Seebeck's coefficient. Using the relation $\vec{E} = -\vec{gradV}$ , we obtain:

$$S^b = -\frac{dV}{dT} \tag{2.194}$$

The Seebeck coefficient [116] is linked to the electrical conductivity in the relalaxation time approximation by the following relation:

$$S^b = -\frac{e}{\sigma_{el}} \int \Lambda(E) \left(-\frac{\partial f}{\partial E}\right) \frac{E - E_F}{T} dE \tag{2.195}$$

It can be split into a simple expression with respect to Eq. (2.185) as:

$$S^b = -\frac{\beta}{e}\frac{C_1}{C_2} \tag{2.196}$$

where

$$C_1 = \int \Lambda(E) \left(-\frac{\partial f}{\partial E}\right) (E - E_F) dE \tag{2.197}$$

$$C_2 = \int \Lambda(E) \left(-\frac{\partial f}{\partial E}\right) dE \tag{2.198}$$

Thus, the Seebeck coefficient can be easily evaluated because $\Lambda(E)$ is well determined by Eq. (2.192).

## 2.4 Kubo formula for optical conductivity

In the linear response theory, the Kubo formula [112] expresses the optical conductivity as a current-current correlation function :

$$\sigma(\omega) = i\frac{Ne^2}{Vm\omega} + \frac{1}{Vh\omega}\int_0^\infty e^{i\omega t}\langle[J_x(t), J_x(0)]\rangle dt. \tag{2.199}$$

$V$ represents the system volume and $J$ is the current operator which is linked to the charge carrier momentum operators :

$$J = \sum_{\alpha=1}^{N} \frac{e_\alpha}{m_\alpha} p_\alpha. \tag{2.200}$$

where $e_\alpha$ is the electric charge ($-e$ for electron, $+e$ for hole) and $P = \sum_\alpha p_\alpha$ corresponds to the total momentum operator. At zero temperature, the real part of the optical conductivy follows :

$$Re\sigma_{(\omega)} = \frac{1}{Vh\omega}\frac{e^2}{m^2} Re\left\{\int_0^\infty e^{i\omega t}\langle[P_x(t), P_x(0)]\rangle dt\right\}. \tag{2.201}$$

In (2.201), we integrate twice by parts over $t$ as follows:

$$\begin{aligned}
& \int_0^\infty dt\langle[P_x(t),P_x]\rangle e^{i\omega t-\delta t} \\
= & \tfrac{1}{i\omega-\delta}\left\{\langle[P_x(t),P_x]\rangle e^{i\omega t-\delta t}|_{t=0}^{\infty}-\int_0^\infty dt\left\langle\left[\tfrac{d}{dt}P_x(t),P_x\right]\right\rangle e^{i\omega t-\delta t}\right\} \\
= & -\tfrac{1}{i\omega-\delta}\int_0^\infty dt\left\langle\left[\tfrac{d}{dt}\left(e^{\frac{it}{\hbar}H}P_xe^{-\frac{it}{\hbar}H}\right),P_x\right]\right\rangle e^{i\omega t-\delta t} \\
= & -\tfrac{1}{i\omega-\delta}\int_0^\infty dt\left\langle\left[\left(e^{\frac{it}{\hbar}H}\tfrac{i}{\hbar}[H,P_x]e^{-\frac{it}{\hbar}H}\right),P_x\right]\right\rangle e^{i\omega t-\delta t} \\
= & -\tfrac{1}{i\omega-\delta}\int_0^\infty dt\left\langle\left[\tfrac{i}{\hbar}[H,P_x],e^{-\frac{it}{\hbar}H}P_xe^{\frac{it}{\hbar}H}\right]\right\rangle e^{i\omega t-\delta t} \\
= & -\tfrac{1}{i\omega-\delta}\int_0^\infty dt\left\langle\left[F_x(0),e^{-\frac{it}{\hbar}H}P_xe^{\frac{it}{\hbar}H}\right]\right\rangle e^{i\omega t-\delta t} \\
= & -\left(\tfrac{1}{i\omega-\delta}\right)^2\left\{\left\langle\left[F_x(0),e^{-\frac{it}{\hbar}H}P_xe^{\frac{it}{\hbar}H}\right]\right\rangle e^{i\omega t-\delta t}|_{t=0}^{\infty}\right. \\
& \left.\int_0^\infty dt\left\langle\left[F_x(0),\tfrac{d}{dt}e^{-\frac{it}{\hbar}H}P_xe^{\frac{it}{\hbar}H}\right]\right\rangle e^{i\omega t-\delta t}\right\} \\
= & -\left(\tfrac{1}{i\omega-\delta}\right)^2\left\{-\langle[F_x,P_x]\rangle+\int_0^\infty dt\left\langle\left[F_x(0),e^{-\frac{it}{\hbar}H}\left(\tfrac{i}{\hbar}[H,P_x]\right)e^{\frac{it}{\hbar}H}\right]\right\rangle e^{i\omega t-\delta t}\right\} \\
= & -\left(\tfrac{1}{i\omega-\delta}\right)^2\left\{-\langle[F_x,P_x]\rangle+\int_0^\infty dt\left\langle\left[F_x(0),e^{-\frac{it}{\hbar}H}F_x(0)e^{\frac{it}{\hbar}H}\right]\right\rangle e^{i\omega t-\delta t}\right\} \\
= & -\left(\tfrac{1}{i\omega-\delta}\right)^2\left\{-\langle[F_x,P_x]\rangle+\int_0^\infty dt\left\langle\left[e^{\frac{it}{\hbar}H}F_x(0)e^{-\frac{it}{\hbar}H},F_x(0)\right]\right\rangle e^{i\omega t-\delta t}\right\} \\
= & \tfrac{1}{(\omega+i\delta)^2}\left\{-\langle[F_x,P_x]\rangle+\int_0^\infty dt\,\langle[F_x(t),F_x(0)]\rangle\,e^{i\omega t-\delta t}\right\}
\end{aligned} \tag{2.202}$$

with $F\equiv\frac{i}{\hbar}[H,P]$ the force operator applied to the electron center of mass. Both $F_x$ and $P_x$ are hermitian operators and the average $\langle[F_x,P_x]\rangle$ is imaginary. For $\omega\neq 0$, this term does not contribute into $Re\sigma(\omega)$. Hence, by these integrations the real part of the optical conductivity of the many-polaron system is given through a force-force correlation function :

$$Re\sigma_{(\omega)}=\frac{1}{V\hbar\omega^3}\frac{e^2}{m^2}Re\left\{\int_0^\infty e^{i\omega t}\langle[F_x(t),F_x(0)]\rangle dt\right\}. \tag{2.203}$$

For the polaron case, the force operator is evaluated as:

$$F_x=\frac{i}{\hbar}[H_{pol},P_x]=\frac{i}{\hbar}[H_e+H_{ph}+H_{e-ph},P_x]. \tag{2.204}$$

Further, we use the commutators:

$$[H_e,P_x]=0 \tag{2.205}$$

$$[\rho_q,P_x]=-\hbar q_x\rho_q \text{ with } \rho_q=e^{iq.r} \tag{2.206}$$

Hence

$$\begin{aligned}[H_{e-ph}, P_x] &= \sum_q \left(V_q b_q[\rho_q, P_x] + V_q^* b_q^\dagger[\rho_{-q}, P_x]\right) \\ &= -\hbar \sum_q q_x \left(V_q b_q \rho_q - V_q^* b_q^\dagger \rho_{-q}\right), \end{aligned} \tag{2.207}$$

It appears that the commutator of the Hamiltonian with the total momentum operator leads to the expression of the force :

$$F = -i \sum_q q \left(V_q b_q \rho_q - V_q^* b_q^\dagger \rho_{-q}\right). \tag{2.208}$$

Therefore it is important to use the force-force correlation function since the product $F_x(t)F_x(0)$ is proportional to $|V_q|^2$ which characterizes the amplitude of the carrier-phonon interplay. By substituting (2.208) into (2.203), the real part of the optical conductivity becomes :

$$\begin{aligned} Re\sigma(\omega) &= \tfrac{1}{V\hbar\omega^3}\tfrac{e^2}{m^2} Re \int_0^\infty dt e^{i\omega t - \delta t} \sum_{q,q'} q_x q'_x \\ &\quad \times \langle [[V_q b_q(t) + V_{-q}^* b_{-q}^\dagger(t)]\rho_q(t), (V_{-q'} b_{-q'} + V_{q'}^* b_{q'}^\dagger)\rho_{-q'}]\rangle. \end{aligned} \tag{2.209}$$

Up to this point, no approximations other than linear response theory have been made.

For the latest equation, we use the polaron wave function $|\Psi_0\rangle = U|\phi_{ph}\rangle|\phi_e\rangle$ , $U$ being a unitary transformation as LLP one. Eq. (2.209) is then trans-

formed to the approximate one:

$$\begin{aligned}
Re\sigma(\omega) &= \tfrac{1}{V\hbar\omega^3}\tfrac{e^2}{m^2} Re\int_0^\infty dt e^{i\omega t-\delta t}\sum_{q,q'} q_x q'_x \\
&\times\left\langle \phi_e\left|\left\langle \phi_{ph}\right| U^{-1}\left[\begin{array}{c} e^{\frac{it}{\hbar}H}[V_q b_q + V^*_{-q} b^\dagger_{-q}]\rho_q e^{-\frac{it}{\hbar}H}, \\ (V_{-q'} b_{-q'} + V^*_{q'} b^\dagger_{q'})\rho_{-q'} \end{array}\right] U\left|\phi_{ph}\right\rangle\right|\phi_e\right\rangle \\
&= \tfrac{1}{V\hbar\omega^3}\tfrac{e^2}{m^2} Re\int_0^\infty dt e^{i\omega t-\delta t}\sum_{q,q'} q_x q'_x \\
&\times\left\langle \phi_e\left|\left\langle \phi_{ph}\right|\left[\begin{array}{c} e^{\frac{it}{\hbar}\tilde{H}}U^{-1}[V_q b_q + V^*_{-q} b^\dagger_{-q}]U\rho_q e^{-\frac{it}{\hbar}\tilde{H}}, \\ U^{-1}(V_{-q'} b_{-q'} + V^*_{q'} b^\dagger_{q'})U^{-1}\rho_{-q'} \end{array}\right]\right|\phi_{ph}\right\rangle\right|\phi_e\right\rangle \\
&= \tfrac{1}{V\hbar\omega^3}\tfrac{e^2}{m^2} Re\int_0^\infty dt e^{i\omega t-\delta t}\sum_{q,q'} q_x q'_x \\
&\times\left\langle \phi_e\left|\left\langle \phi_{ph}\right|\left[e^{\frac{it}{\hbar}\tilde{H}}(V_q(b_q - f^*_q\rho_{-q}) + V^*_{-q}(b^\dagger_{-q} - f_{-q}\rho_{-q}))\rho_q e^{-\frac{it}{\hbar}\tilde{H}},\right.\right.\right. \\
&\left.\left.\left.(V_{-q'}(b_{-q'} - f^*_{-q'}\rho_{q'}) + V^*_{q'}(b^\dagger_{q'} - f_{q'}\rho_{q'}))\rho_{-q'}\right]\right|\phi_{ph}\right\rangle\right|\phi_e\right\rangle .
\end{aligned} \tag{2.210}$$

So, we have arrived at the expression

$$\begin{aligned}
Re\sigma(\omega) &= \tfrac{1}{V\hbar\omega^3}\tfrac{e^2}{m^2} Re\int_0^\infty dt e^{i\omega t-\delta t}\sum_{q,q'} q_x q'_x \\
&\times\left\langle \phi_e\left|\left\langle \phi_{ph}\right|\left[e^{\frac{it}{\hbar}\tilde{H}}(V_q(b_q - f^*_q\rho_{-q}) + V^*_{-q}(b^\dagger_{-q} - f_{-q}\rho_{-q}))\rho_q e^{-\frac{it}{\hbar}\tilde{H}},\right.\right.\right. \\
&\left.\left.\left.(V_{-q'}(b_{-q'} - f^*_{-q'}\rho_{q'}) + V^*_{q'}(b^\dagger_{q'} - f_{q'}\rho_{q'}))\rho_{-q'}\right]\right|\phi_{ph}\right\rangle\right|\phi_e\right\rangle .
\end{aligned} \tag{2.211}$$

Recall that $\rho_q\rho_{-q} = \rho_{-q}\rho_q$ and $V_q f^*_q = V_{-q} f^*_{-q}$, after the summation over $q$ the terms proportional to $\rho_{-q}\rho_q$ vanish. Thus, we have :

$$\begin{aligned}
Re\sigma(\omega) &= \tfrac{1}{V\hbar\omega^3}\tfrac{e^2}{m^2} Re\int_0^\infty dt e^{i\omega t-\delta t}\sum_{q,q'} q_x q'_x \\
&\times\left\langle \phi_e\left|\left\langle \phi_{ph}\right|\left[e^{\frac{it}{\hbar}\tilde{H}}(V_q b_q + V^*_{-q} b^\dagger_{-q})\rho_q e^{-\frac{it}{\hbar}\tilde{H}},\right.\right.\right. \\
&\left.\left.\left.(V_{-q'} b_{-q'} + V^*_{q'} b^\dagger_{q'})\rho_{-q'}\right]\right|\phi_{ph}\right\rangle\right|\phi_e\right\rangle .
\end{aligned} \tag{2.212}$$

The optical conductivity (2.212) then takes the form:

$$\begin{aligned} Re\sigma(\omega) &= -\frac{2e^2}{V\hbar m^2\omega^3} Im \int_0^\infty dt e^{i\omega t-\delta t} \sum_q q_x^2 |V_q|^2 \\ &\times Im\left[e^{-i\omega_{LO}t}\left\langle \phi_e \left| e^{i\tilde{H}_e t/\hbar}\rho_q e^{-i\tilde{H}_e t/\hbar}\rho_{-q}\right| \phi_e\right\rangle\right] \end{aligned} \tag{2.213}$$

Considering an isotropic polaron system, $q_x^2$ in 3D can be written as $\frac{1}{3}(q_x^2+q_y^2+q_z^2)=\frac{1}{3}q^2$, what provides the expression :

$$Re\sigma_{3D}(\omega) = -\frac{2}{3V\hbar\omega^3}\frac{e^2}{m^2}\sum_q q^2|V_q|^2 Im\int_0^\infty dt e^{i\omega t-\delta t} Im\left[e^{-i\omega_{LO}t}F(q,t)\right], \tag{2.214}$$

with the correlation function :

$$F(q,t) = \left\langle \phi_e \left| e^{\frac{it}{\hbar}\tilde{H}_e}\rho_q e^{-\frac{it}{\hbar}\tilde{H}_e}\rho_{-q}\right| \phi_e\right\rangle \tag{2.215}$$

A similar derivation for the case of 2D gives :

$$Re\sigma_{2D}(\omega) = -\frac{1}{A\hbar\omega^3}\frac{e^2}{m^2}\sum_q q^2|V_q|^2 Im\int_0^\infty dt e^{i\omega t-\delta t} Im\left[e^{-i\omega_{LO}t}F(q,t)\right], \tag{2.216}$$

where $A$ is the surface of the 2D system.

We can show that, as far as $|\phi_e\rangle$ is the ground state, the integral $\int_{-\infty}^{\infty} dt e^{i\omega t-\delta|t|}F(q,-t)$ for positive $\omega$ is equal to zero. Let $\left\{\left|\psi_{el}^{(n)}\right\rangle\right\}$ being the total basis set of the eigenfunctions of the Hamiltonian $\tilde{H}_e$. Using these functions we expand $F(q,t)$:

$$\begin{aligned} F(q,t) &= \sum_n \left\langle \phi_e \left| e^{\frac{it}{\hbar}\tilde{H}_e}\rho_q e^{-\frac{it}{\hbar}\tilde{H}_e}\right| \phi_e^{(n)}\right\rangle \left\langle \phi_e^{(n)} \left|\rho_{-q}\right| \phi_e^{(0)}\right\rangle \\ &= \sum_n \left|\left\langle \phi_e^{(n)} \left|\rho_{-q}\right| \phi_e^{(0)}\right\rangle\right|^2 e^{\frac{it}{\hbar}(\tilde{E}_0-\tilde{E}_m)}, \end{aligned} \tag{2.217}$$

$$\begin{aligned}\int_{-\infty}^{\infty} dt e^{i\omega t-\delta|t|}F(q,-t) &= \sum_n \left|\left\langle \phi_e^{(n)}\left|\rho_{-q}\right|\phi_e^{(0)}\right\rangle\right|^2 \int_{-\infty}^{\infty} dt e^{i\omega t+\frac{i}{\hbar}(\tilde{E}_n-\tilde{E}_0)t-\delta|t|} \\ &= \sum_n \left|\left\langle \phi_e^{(n)}\left|\rho_{-q}\right|\phi_e^{(0)}\right\rangle\right|^2 2\pi\delta\left(\omega+\tfrac{\tilde{E}_n-\tilde{E}_0}{\hbar}\right)=0,\end{aligned} \tag{2.218}$$

because $\omega > 0$, $\omega + \frac{\tilde{E}_n-\tilde{E}_0}{\hbar}$ is never equal to zero.

Rewriting Eq. (2.213) with the dynamic structure factor of the electron gas, one gets :

$$Re\sigma_{3D}(\omega) = \frac{1}{6V\hbar\omega^3}\frac{e^2}{m^2}\sum_q q^2|V_q|^2\int_{-\infty}^{\infty} dt e^{i(\omega-\omega_{LO})t-\delta|t|}F(q,t). \tag{2.219}$$

$$Re\sigma_{2D}(\omega) = \frac{1}{4A\hbar\omega^3}\frac{e^2}{m^2}\sum_q q^2|V_q|^2\int_{-\infty}^{\infty} dt e^{i(\omega-\omega_{LO})t-\delta|t|}F(q,t). \tag{2.220}$$

Eqs. (2.219) and (2.220) give the expression of the real part of the optical conductivity respectively in 3D and 2D. The imaginary part can be obtained by a same process.

## Conclusion

In this second chapter, we have shown the theory and methods which we intend to use for the evaluation of the system energy, the relaxation time, the electrical conductivity, the Seebeck coefficient, the optical conductivity and the optical absorption coefficient. These properties will be investigate in TMDCs compounds to obtain our results.

CHAPTER 3

# RESULTS AND DISCUSSIONS

## Introduction

Now that the various methods are explained, let present and comment our different results. This chapter is organized as follows : at first, we look at the dynamics of exciton-polaron under a magnetic barrier and an electric field. We describe our exciton-polaron system in a TMDC, derive its corresponding energy and the Tsallis entropy necessary to understand the system. In addition, we investigate the exciton-polaron formation and relaxation in TMDCs. The third part is devoted to the electrical properties in TMDC materials through electrical conductivity and Seebeck coefficient. At the end, we explore the optical properties by investigating the optical conductivity and the optical absorption coefficient in TMDCs. For each part, the analytical result is provided followed by the numerical results and discussion. The influence of both magnetic barrier and electric field is highlighted for each property. The selected materials are $MoSe_2$, $MoS_2$, $WSe_2$ and $WS_2$.

## 3.1 Dynamics of exciton-polaron in TMDCs under magnetic barrier and electric field

The system is taken as an exciton under the influence of a magnetic barrier and an electric field, and interacting with LO-phonons in a 1L TMDC. The considered Hamiltonian is written as:

$$\hat{H} = \frac{\left(\vec{P}_e + e\vec{A}_e\right)^2}{2m_e^*} - eE_{el}y_e + \frac{\left(\vec{P}_h - e\vec{A}_h\right)^2}{2m_h^*} + eE_{el}y_h - \frac{e^2}{\varepsilon|\vec{\rho}_e - \vec{\rho}_h|} + \hat{H}_{ph} + \hat{H}_{ex-ph}^{2D} \tag{3.1}$$

The field of the magnetic barrier is given by [117] $\vec{B} = (0, 0, B_z)$ with $B_z(x) = B_0 l_B[\delta(x) - \delta(x - L)]$ and the width of the barrier is denoted by $L$ taken at $150nm$. The standard magnetic field $B_0$ of this barrier is related to the magnetic length $l_B$ by $B_0 = \hbar/(el_B^2)$. From the Dirac delta function, the magnetic strength can also take the form:

$$B_z(x) = \begin{cases} B_0 l_B, & if \quad x = 0 \\ -B_0 l_B, & if \quad x = L \\ 0, & otherwise \end{cases} \tag{3.2}$$

Such magnetic barrier can be constructed as showed by Ghosh et al. [118]. Figure 3.1 illustrates the present case where two long narrow magnetic stripes are placed perpendicular to the TMDC layer respectively at $x = 0$ (with $B_0 l_B$) and $x = L$ (with $-B_0 l_B$). The magnetic vector potential $\vec{A} = (0, A_y, 0)$ is given by:

$$A_y(x) = B_0 l_B[\Theta(x) - \Theta(x - L)] = \begin{cases} A, & 0 < x < L \\ 0, & otherwise \end{cases} \tag{3.3}$$

where $A = \hbar/(el_B)$ and $\Theta$ is the Heaviside function.

The LO-phonon Hamiltonian appears as :

$$\hat{H}_{ph} = \sum_q \hbar\omega_0 b_q^\dagger b_q \tag{3.4}$$

The term of exciton-phonon interaction is given by Eq. (2.28):

$$\hat{H}_{ex-ph}^{2D} = \sum_{K,q} \Xi^{op}(q) C_{K+q}^\dagger C_K \left(b_q + b_{-q}^\dagger\right) \tag{3.5}$$

where $C_K^{\dagger}(C_K)$ denotes the creation (annihilation) operator of an exciton.

Notice that to simplify, in the following, we will use $q$ and $K$ to mean the 2D wave vectors respectively for phonon and exciton.

The exciton-LO phonon coupling function is given by:

$$\Xi^{op}(q) = (D_c^{op} - D_v^{op}) \sqrt{\frac{\hbar q}{2\eta u S_{2D}}} \tag{3.6}$$

$S_{2D}$ represents the area of the TMDC layer, $\eta$ denotes the area mass density and $u$ is the sound velocity. The deformation potential constant is $D_c^{op}(D_v^{op})$ for electron (hole) -LO phonon coupling at some critical points $(K, K')$ inside the conduction (valence) band.

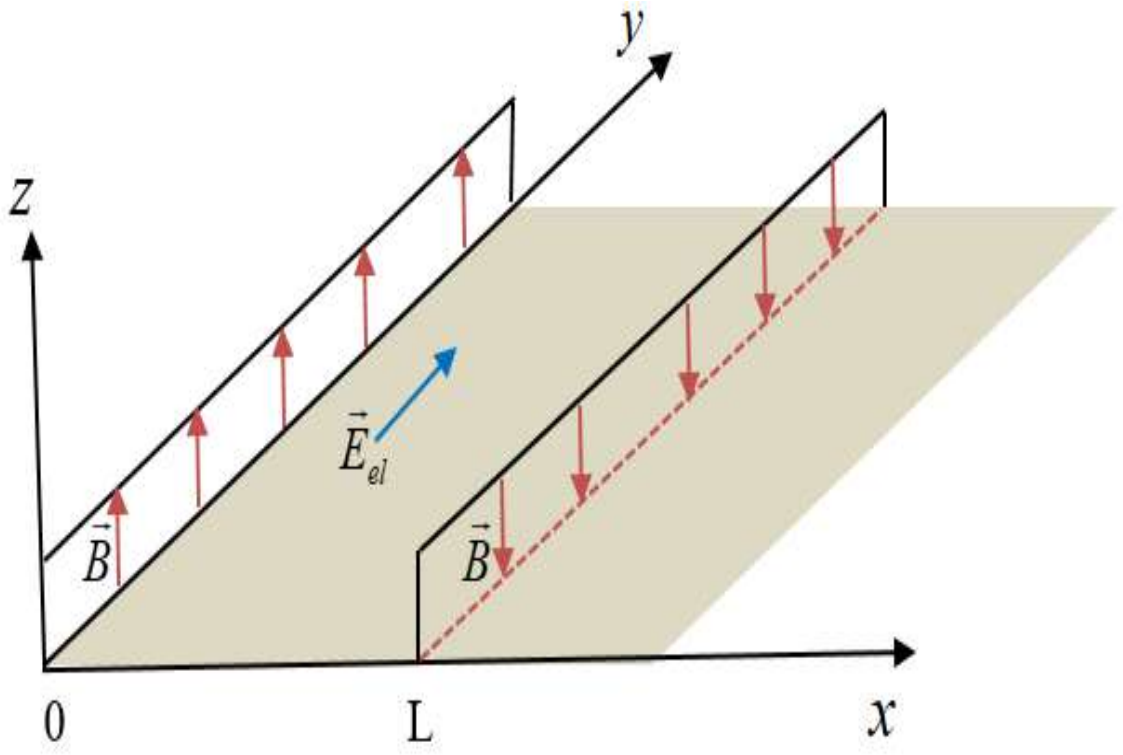


Figure 3.1: Schematic of the considered structure: a magnetic barrier bounded by two long narrow magnetic stripes ( red arrows) placed perpendicular to the 1L TMDC (light brown) and under an electric field $E_{el}$ (blue arrow).

The data of the selected TMDCs are presented in Table 3.1. The effective masses $m_e^*$ and $m_h^*$ are in unit of free electron mass $(m_0)$ whereas the LO-phonon energy $\hbar\omega_0$, the deformation potential constant $D_c^{op}\,(D_v^{op})$, the

binding energy $E_b$ and the gap energy $E_g$ are in unit of $eV$.

| Materials | $m_e^*$ | $m_h^*$ | $\hbar\omega_0$ | $D_c^{op}$ | $D_v^{op}$ | $E_b$ | $E_g$ |
|---|---|---|---|---|---|---|---|
| $MoSe_2$ | 0.64 | 0.71 | 0.0365 | 5.2 | 4.9 | 0.174 | 1.56 |
| $WSe_2$ | 0.39 | 0.51 | 0.0291 | 2.3 | 3.1 | 0.231 | 1.65 |
| $WS_2$ | 0.31 | 0.42 | 0.0435 | 3.1 | 2.3 | 0.19 | 2.10 |
| $MoS_2$ | 0.51 | 0.58 | 0.0443 | 5.8 | 4.6 | 0.313 | 1.87 |

Table 3.1: Parameters of each TMDC compound taken from [27, 83].

### 3.1.1 Energy of exciton-polaron

In order to obtain the exciton-polaron energy, we transformation the following electronic part of the Hamiltonian:

$$\hat{H}_{ex}^{2D} = \frac{\left(\vec{P}_e + e\vec{A}_e\right)^2}{2m_e^*} - eE_{el}y_e + \frac{\left(\vec{P}_h - e\vec{A}_h\right)^2}{2m_h^*} + eE_{el}y_h - \frac{e^2}{\varepsilon|\vec{\rho}_e - \vec{\rho}_h|} \quad (3.7)$$

As in chapter 2, let rewrite the latest Hamiltonian in the second quantification (2.36) but with the eigen energy for the 2D exciton denoted by ($\lambda$). For that, since we are in the presence of magnetic field, we use [119]:

$$\Psi^{2D} = e^{iK^*.R}\sqrt{\frac{2}{\pi}}\frac{1}{a}e^{-\rho/a} \text{ with } K^* = K - \frac{e}{\hbar}A \quad (3.8)$$

Processing as for Eq.(2.45), the exciton eigen energy is obtained as:

$$\lambda(K, B, E_{el}) = E_g + \frac{\hbar^2 K^2}{2M^*} - E_b + \xi_B - \xi_{el} \quad (3.9)$$

$\xi_B$ and $\xi_{el}$ represent respectively the electric and magnetic parameters appearing as:

$$\xi_{el} = 2eaE_{el}/\pi \quad (3.10)$$

$$\xi_B = \frac{\hbar^2}{l_B^2}\left(\frac{1}{2M^*} + \frac{1}{2\mu^*}\right) \quad (3.11)$$

The $f_{ex}$-functions depending of the fields appear as:

$$f_{ex}^* = \frac{\Xi^{op}(q)}{\lambda(K+q, l_B, E_{el}) - \lambda(K, l_B, E_{el}) + \hbar\omega_0} \quad (3.12)$$

$$f_{ex} = \frac{\Xi^{op}(q)}{\lambda(K+q, l_B, E_{el}) - \lambda(K, l_B, E_{el}) - \hbar\omega_0} \tag{3.13}$$

Then the transformed Hamiltonian of the interaction part becomes:

$$\begin{aligned} \hat{H}^{T2D}_{ex-ph} &= \sum_{K,K',q} |\Xi^{op}(q)|^2 \left( \frac{1}{\lambda(K+q,l_B,E_{el}) - \lambda(K,l_B,E_{el}) + \hbar\omega_0} \right. \\ &\left. - \frac{1}{\lambda(K+q,l_B,E_{el}) - \lambda(K,l_B,E_{el}) - \hbar\omega_0} \right) C^{\dagger}_{K+q} C_K C^{\dagger}_{K'+q} C_{K'} \end{aligned} \tag{3.14}$$

Also, we use the wave function $|\Psi_0\rangle$ to average the transformed Hamiltonian and obtain the GS energy of exciton-polaron:

$$E^0_{ex-pol}(K, B, E_{el}) = E_g + \left( \frac{\hbar^2 K^2}{2M^*} \right) \left( 1 - \tilde{G}_{ex2} \right) - E_b - G_{ex1} + \xi_B - \xi_{el} \tag{3.15}$$

The same way as for Eq. (2.96), we establish the expression of the first excited state energy as:

$$E^1_{ex-pol}(K, B, E_{el}) = 4E_g + 4 \left( \frac{\hbar^2 K^2}{2M} \right) \left( 1 - 2\tilde{G}_{ex2} \right) - 4E_b - 8G_{ex1} + 4\xi_B - 4\xi_{el} \tag{3.16}$$

From the latest, one can see that the energy and the motion of exciton-polaron are modified by the magnetic barrier and the electric field through $\xi_{el}$ and $\xi_B$ respectively.

### 3.1.2 Tsallis entropy

In physics, the entropy is a property which estimates the disorder in a system and the Tsallis entropy [120, 121] is given by:

$$S_j = \frac{1 - \sum_{i=1} P_i^j}{j - 1} \tag{3.17}$$

The parameter $j \in \Re$ is the entropy degree and $P_i$ are the probabilities satisfying:

$$\sum_{i=1} P_i^j = 1 \tag{3.18}$$

Let denote by $P_1$ and $P_2$ the probabilities for the GS and the first excited state. That leads to:

$$S_j = \frac{1 - P_1^j - P_2^j}{j - 1} \tag{3.19}$$

with

$$P_1^j = \frac{\left[1 - \beta(1-j)E^0_{ex-pol}\right]^{\frac{1}{1-j}}}{Z_j} \tag{3.20}$$

$$P_2^j = \frac{\left[1 - \beta(1-j)E^1_{ex-pol}\right]^{\frac{1}{1-j}}}{Z_j} \tag{3.21}$$

And the partition function is taken as:

$$Z_j = \left[1 - \beta(1-j)E^0_{ex-pol}\right]^{\frac{1}{1-j}} + \left[1 - \beta(1-j)E^1_{ex-pol}\right]^{\frac{1}{1-j}} \tag{3.22}$$

Since the energies $E^0_{ex-pol}$ and $E^1_{ex-pol}$ are well known from Eqs. (3.15) and (3.16), then we can evaluate this entropy property.

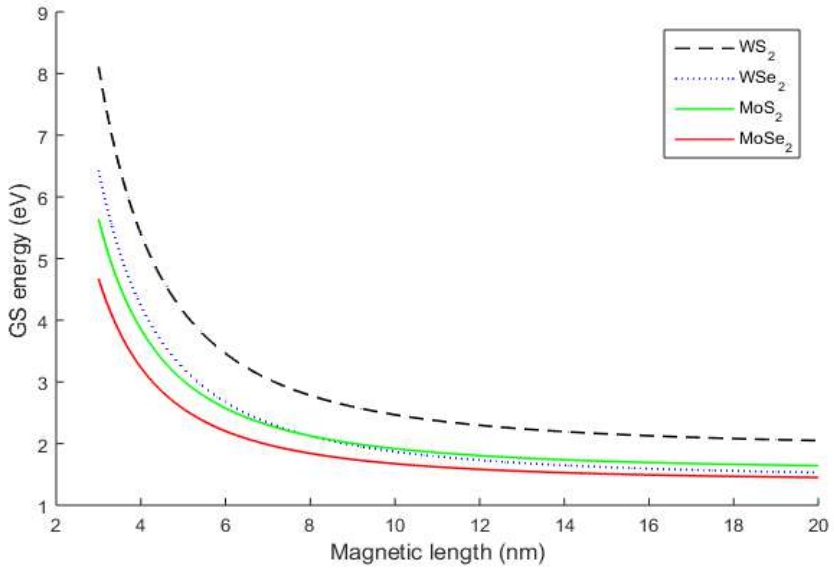


Figure 3.2: GS energy of exciton-polaron as function of the magnetic length for $E_{el} = 0$.

Figure 3.2 displays the GS energy of an exciton-polaron versus the magnetic length ($l_B$) for different 1L TMDCs. $WS_2$ has the highest GS energy. As we can see from this figure, the exciton-polaron GS energy is very sensitive to the applied magnetic field in all considered 2D materials. The variation of magnetic field in the increasing direction enhances the GS energy of the

system. Therefore, since the magnetic length is a function of $1/B$ , the exciton-polaron interaction becomes stronger as well as the magnetic length reduces and inversely. It is seen that the GS energy drops with the expansion of $l_B$ and there is a shift between the monolayers. The magnetic field plays an interesting role on the energy of an exciton-polaron in TMDCs. Due to magnetic barrier, the interaction between particles is strengthened and the exciton-polaron is more confined in TMDCs. This result is in accordance with what was found by Myoung et al [117]. The authors have proved that magnetic gate is suitable for use as base elements for one-electron tunneling systems or spin-polarized devices. In fact, the decrease in the length scale enhances the barrier height and the exciton-polaron is well confined in the ground state. This assumption is found spectacularly in systems like TMDCs where the electronic structure changes abruptly when they are stripped down from few to a single atomic layer [122].

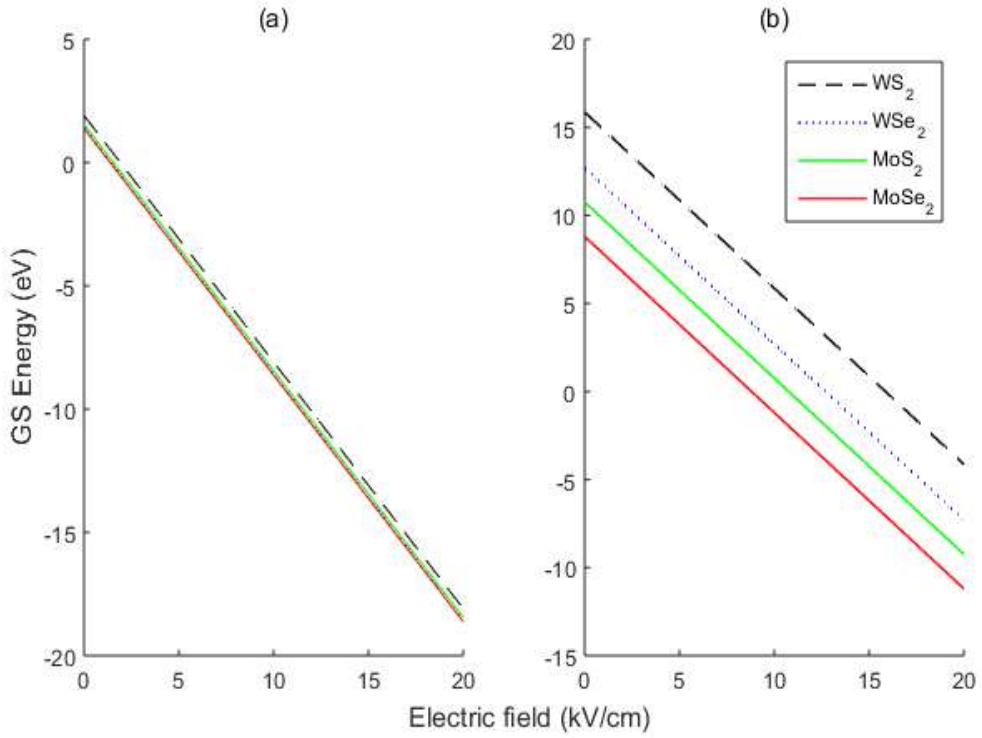


Figure 3.3: GS energy of exciton-polaron as function of the electric field for (a) $\xi_B = 0$ and (b) $l_B = 2nm$.

Figure 3.3 plots the GS energy of the exciton-polaron as a function of the electric field respectively for $(a)$ very high magnetic length and $(b)$ weak magnetic length. In both case, we observe a monotonic form of the curves.

It follows that the electric field reduces the ground state energy. In fact, the presence of the electric field decreases the binding energy of the exciton-polaron since the electron and hole move differently in the electric field. Also, Oukerroum et al [123] shows that the electric field tends to move the electron and hole densities in the opposite directions thus the overlap of the electron and hole wavefunctions.

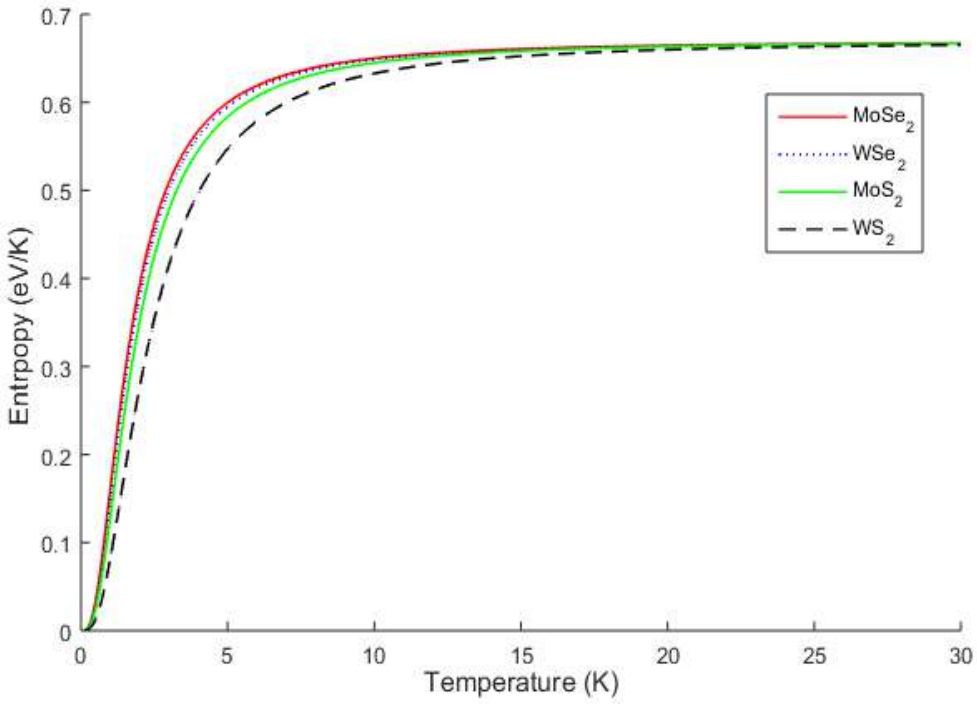


Figure 3.4: Entropy versus temperature for $j = 1.1$ in the absence of fields.

In Figure 3.4, we have plotted the entropy of an exciton-polaron versus temperature for some 1L TMDCs. $MoSe_2$ has the highest entropy. The figure shows the increase of entropy with temperature : it expands up to $T = 25K$ and then remains constant. The entropy starts from zero and increases until reaches the thermodynamic equilibrium which confirms the principle of the third law of thermodynamic, it is in accordance with physics laws and the work of [124]. The explanation of the increasing entropy can also be due to the fact that phonons cause random fluctuations of energy from each local state. These fluctuations break the coherence of the excitonic states and lead to a process of relaxation at the origin of various phenomena like decoherence. Then, as a result, the system is decoherent for $T < 25K$, coherent for $T > 25K$.

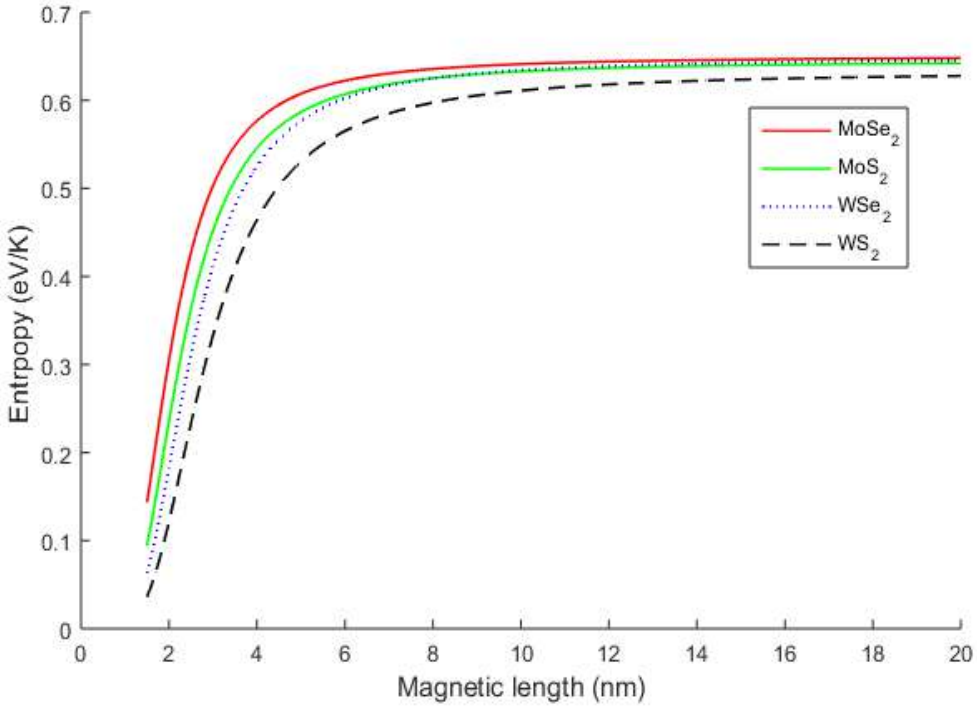


Figure 3.5: Entropy as function of the magnetic length for $j = 1.1$ , $T = 10K$ and $E_{el} = 0$.

We observe in Figure 3.5 that the entropy increases and reaches an equilibrium state with the enhancement of magnetic length ($l_B$). The higher the magnetic length, the higher the disorder until a certain period and then, coherence can be restored in the system. It can be seen that the magnetic barrier modifies the entropy behavior. One can see that the entropy of the system is very sensitive to the monolayers TMDCs, the magnetic length and the temperature. We find that the magnetic barrier controls the system disorder and it is in accordance with the result obtained by Fobasso et al [125].

Then it is possible to control the information of the system. This means that it is possible to encode quantum information on the high-frequency vibrations of exciton-polaron in quantum communication protocol. It is well recognized that an accumulation of entropy signifies the deficiency of informations within the system and therefor the variation of the magnetic length plays an essential role in the coherence control of systems [106, 126].

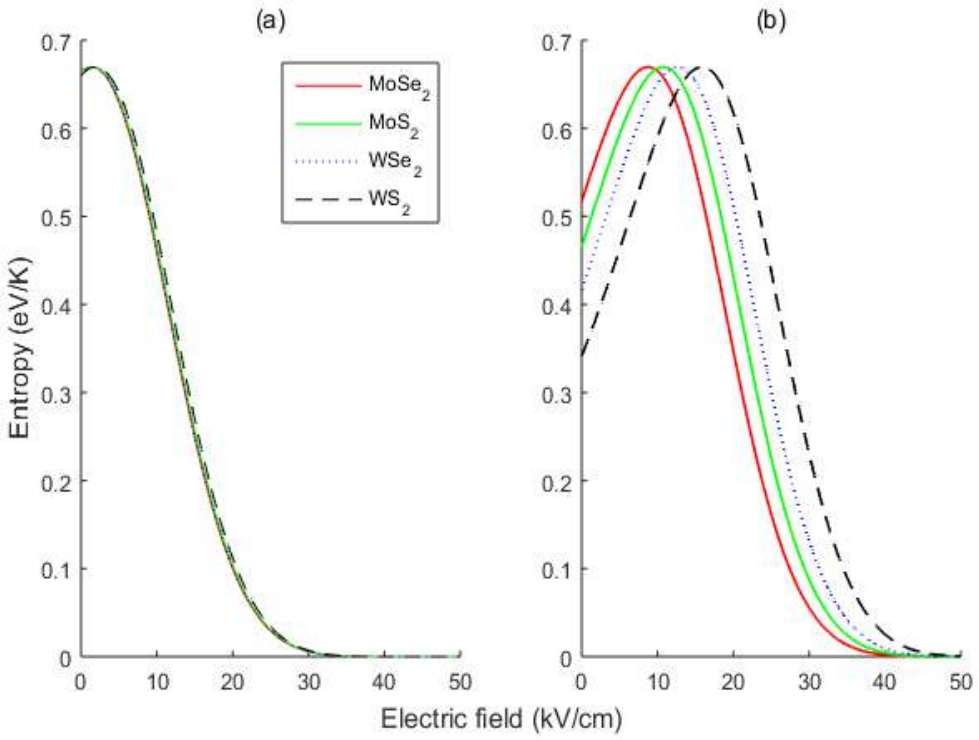


Figure 3.6: Entropy versus electric field for $j = 1.1$ , $T = 20K$ , (a) $\xi_B = 0$ and (b) $l_B = 2nm$.

Figure 3.6 presents the entropy variation as function of the electric field for $(a)$ very high magnetic length and $(b)$ weak value of the magnetic length. Figure $(a)$ shows the decrease of this property when enhances the electric field. In fact, the disorder due to the temperature that perturbs the exciton-polaron motion is reduced by the presence of the electric field which directs the particles movement. This is in agreement with the work of Khordad et al [127].

In figure $(b)$, we first observe the increase of the entropy until the peak demonstrating the dominance of the magnetic barrier effect in this range. Beyond the peak, the electric field overpasses and then causes the regression of the entropy. The result indicates that the electric field can be used to stabilise the disorder in the system.

## 3.2 Formation and relaxation of exciton-polaron under the magnetic barrier and electric field in TMDCs

The formation of polaronic systems is linked to the interaction with phonons and the fact that the time of optical phonons is approximately constant and finite in materials. The presence of both electric and magnetic fields perturbs the excitonic states and the behavior of the system. This perturbation of states leads to the relaxation of the system which later returns to the equilibrium, thus the necessity of evaluate the relaxation time.

### 3.2.1 Lifetime of exciton-polaron

Let us consider Eq.(2.112):

$$\frac{\hbar}{\tau_{ex}} = \frac{2\pi M^*}{\hbar^2(1-\tilde{G}_{ex2})} \sum_q \bar{n}_q \left(\Xi^{op}(q)\right)^2 \frac{\delta(q-q_1)+\delta(q-q_2)}{\sqrt{K^2 cos^2\theta + 2M^*\hbar\omega_0/\hbar^2(1-\tilde{G}_{ex2})}} \tag{3.23}$$

Notice that $\Xi^{op}(q)$ is defined by Eq. (3.6) for the case of TMDC. Then the lifetime of exciton-polaron becomes:

$$\frac{\hbar}{\tau_{ex}} = \frac{\pi M^* \left(D_c^{op} - D_v^{op}\right)^2}{\eta u(1-\tilde{G}_{ex2})S_{2D}} \sum_q \bar{n}_q q \frac{\delta(q-q_1)+\delta(q-q_2)}{\sqrt{K^2 cos^2\theta + 2M^*\hbar\omega_0/\hbar^2(1-\tilde{G}_{ex2})}} \tag{3.24}$$

Converting the summation into an integration, one gets:

$$\frac{\hbar}{\tau_{ex}} = \frac{\pi M^* \left(D_c^{op} - D_v^{op}\right)^2}{\eta u\hbar(1-\tilde{G}_{ex2})S_{2D}} \frac{S_{2D}}{(2\pi)^2} \bar{n} \int_0^{2\pi} d\theta \int_0^{\infty} dq q^2 \frac{\delta(q-q_1)+\delta(q-q_2)}{\sqrt{K^2 cos^2\theta + 2M^*\hbar\omega_0/\hbar^2(1-\tilde{G}_{ex2})}} \tag{3.25}$$

The integration over $q$ gives:

$$\frac{1}{\tau_{ex}} = \frac{M^* \left(D_c^{op} - D_v^{op}\right)^2}{4\pi\eta u\hbar^2(1-\tilde{G}_{ex2})} \bar{n} \int_0^{2\pi} d\theta \frac{q_1^2+q_2^2}{\sqrt{K^2 cos^2\theta + 2M^*\hbar\omega_0/\hbar^2(1-\tilde{G}_{ex2})}} \tag{3.26}$$

Thus, the expression of exciton-polaron lifetime according to Eq. (2.163) is:

$$\frac{1}{\tau_{ex}} = \frac{M^* \left(D_c^{op} - D_v^{op}\right)^2}{\pi\eta u\hbar^2(1-\tilde{G}_{ex2})}\bar{n}\int_0^{2\pi} d\theta \frac{K^2 cos^2\theta + M^*\hbar\omega_0/\hbar^2(1-\tilde{G}_{ex2})}{\sqrt{K^2 cos^2\theta + 2M^*\hbar\omega_0/\hbar^2(1-\tilde{G}_{ex2})}} \tag{3.27}$$

### 3.2.2 Relaxation time of exciton-polaron

From Eq. (2.165), and with respect to Eq. (3.6) the relaxation time of exciton-polaron in TMDC is written as:

$$\begin{aligned}\frac{1}{\tau} &= \frac{\pi M(D_c^{op}-D_v^{op})^2}{\eta u\hbar^2(1-\tilde{G}_{ex2})S_{2D}}\sum_q q\left\{\left[n_B + f\left(E^0_{ex-pol}(K+q)\right)\right]\frac{\delta(q-q_1)+\delta(q-q_2)}{\sqrt{K^2cos^2\theta - 2M\hbar\omega_0/\hbar^2(1-\tilde{G}_{ex2})}}\right. \\ &\left. + \left[1 + n_B - f\left(E^0_{ex-pol}(K+q)\right)\right]\frac{\delta(q-q_3)+\delta(q-q_4)}{\sqrt{K^2cos^2\theta - 2M\hbar\omega_0/\hbar^2(1-\tilde{G}_{ex2})}}\right\}\end{aligned} \tag{3.28}$$

In the previous equation, we transform the summation into integration and we integrate over $q$. This leads to:

$$\begin{aligned}\frac{1}{\tau} &= \frac{M^*(D_c^{op}-D_v^{op})^2}{\pi\eta u\hbar^2(1-G_{ex2})}K\left\{\left[n_B + f\left(E^0_{ex-pol}(K) + \hbar\omega_0\right)\right]I^+\right. \\ &\left. + \left[1 + n_B - f\left(E^0_{ex-pol}(K) - \hbar\omega_0\right)\right]I^-\right\}\end{aligned} \tag{3.29}$$

where:

$$I^+ = \int_0^{2\pi} d\theta \frac{cos^2\theta + \dfrac{M\hbar\omega_0}{\hbar^2K^2(1-\tilde{G}_{ex2})}}{\sqrt{cos^2\theta + \dfrac{2M\hbar\omega_0}{\hbar^2K^2(1-\tilde{G}_{ex2})}}} \tag{3.30}$$

$$I^- = \int_0^{2\pi} d\theta \frac{cos^2\theta - \dfrac{M\hbar\omega_0}{\hbar^2K^2(1-\tilde{G}_{ex2})}}{\sqrt{cos^2\theta - \dfrac{2M\hbar\omega_0}{\hbar^2K^2(1-\tilde{G}_{ex2})}}} \tag{3.31}$$

We see that $I^+$ and $I^-$ can be written as function of the elliptic integrals of the first kind $F_1$ and the second kind $F_2$:

$$I^+ = \frac{4}{A_2}\left\{(A_1-1)F_1\left(\pi/2, A_2\right) + F_2\left(\pi/2, A_2\right)\right\} \tag{3.32}$$

$$I^{-} = 4\left\{(B_1 - 1)F_1\left(\pi/2, 1/B_2\right) + F_2\left(\pi/2, 1/B_2\right)\right\} \tag{3.33}$$

with

$$A_1 = \frac{\hbar^2K^2(1-\tilde{G}_{ex2}) + M\hbar\omega_0}{\hbar^2K^2(1-\tilde{G}_{ex2}) + 2M\hbar\omega_0} \; ; \; A_2^2 = \frac{\hbar^2K^2(1-\tilde{G}_{ex2})}{\hbar^2K^2(1-\tilde{G}_{ex2}) + 2M\hbar\omega_0} \tag{3.34}$$

$$B_1 = \frac{\hbar^2K^2(1-\tilde{G}_{ex2}) - M\hbar\omega_0}{\hbar^2K^2(1-\tilde{G}_{ex2})} \; ; \; B_2^2 = \frac{\hbar^2K^2(1-\tilde{G}_{ex2})}{\hbar^2K^2(1-\tilde{G}_{ex2}) - 2M\hbar\omega_0} \tag{3.35}$$

Then we obtain the solution of each integral as:

$$I^{+} \approx \pi\left[\frac{\sqrt{\hbar^2K^2(1-\tilde{G}_{ex2}) + 2M\hbar\omega_0}}{\hbar K\sqrt{1-\tilde{G}_{ex2}}} + \frac{\hbar^3K^3(1-\tilde{G}_{ex2})^{3/2} + M\hbar\omega_0\hbar K\sqrt{1-\tilde{G}_{ex2}}}{2\left(\hbar^2K^2(1-\tilde{G}_{ex2}) + 2M\hbar\omega_0\right)^{3/2}}\right] \tag{3.36}$$

$$I^{-} \approx \pi\left[\frac{2\hbar^2K^2(1-\tilde{G}_{ex2}) - 2M\hbar\omega_0}{\hbar^2K^2(1-\tilde{G}_{ex2})} + \frac{2(M\hbar\omega_0)^2 - M\hbar\omega_0\hbar^2K^2(1-\tilde{G}_{ex2})}{2\hbar^4K^4(1-\tilde{G}_{ex2})^2}\right] \tag{3.37}$$

Therefore, the relaxation time of exciton-polaron is obtained since $I^{+}$ and $I^{-}$ are determined analytically according to equation (3.29).

We present in Figure 3.7 the exciton-polaron lifetime versus the temperature for various 1L TMDC materials. Among the selected TMDCs, $MoSe_2$ is the best that favors the exciton-polaron existence. We observe the decrease of lifetime with temperature. In fact, the enhancement of temperature raises the lattice thermal vibrations and the disorder that weaken the interaction between phonons and particles. Then, the probability that the electron (hole) absorbs a phonon can be probably lower. It is in accordance with the results of [128, 129].

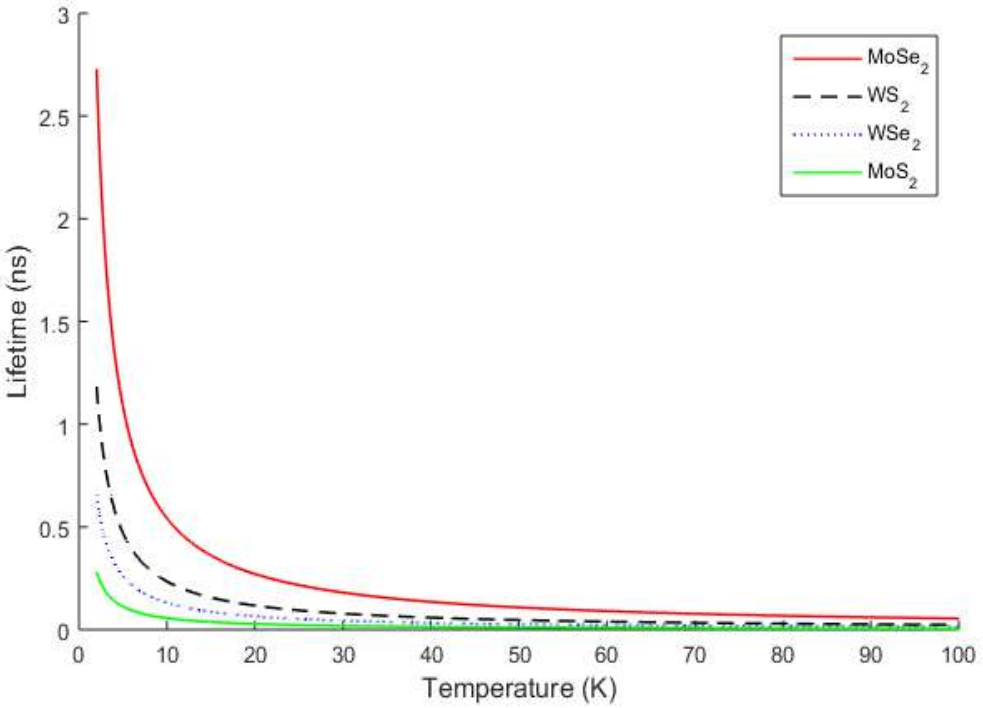


Figure 3.7: Lifetime of exciton-polaron as function of the temperature for selected TMDCs in the absence of fields.

It is seen that the highest value of lifetime is observed near absolute zero of temperature and it becomes zero for higher temperature values. This explains the death of the exciton-polaron. Thus, high temperature values are damaging for the formation of exciton-polaron. For lifetime, the coherence is observed at $T > 25K$ (as for entropy) and the system is not granted to the exciton-polaron. We suspect the existence of either an exciton or polarons according to the results of Sun et al [130] since the lifetime of the system vanishes. Also, our results are closed to the experiments [131, 132] where excitonic lifetime is 0.02-0.16 ns at room temperature for $MoSe_2$ and $WSe_2$ monolayers.

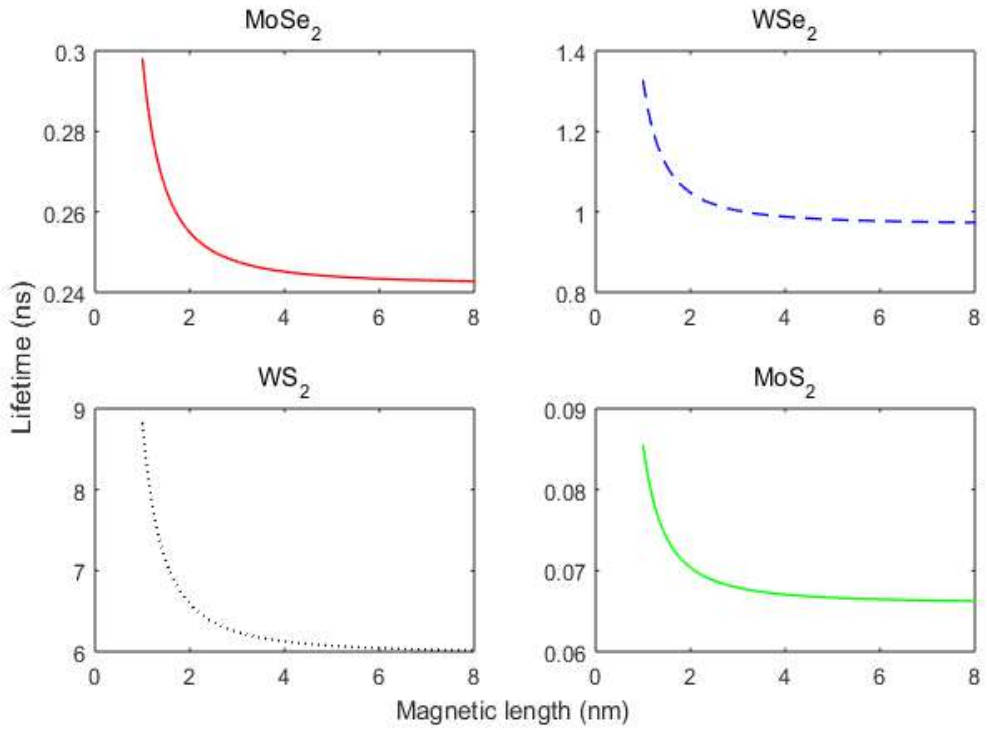


Figure 3.8: Lifetime of exciton-polaron as function of the length scale ($l_B$) of the magnetic barrier for $T = 2K$ and $E_{el} = 0$.

Figure 3.8 presents the exciton-polaron lifetime as function of the magnetic length for the four TMDCs. It is observed that the exciton-polaron lifetime decreases with the increase of the length scale. This is in agreement with [133]. This can be explained through the confinement of exciton motion. In the presence of magnetic field, the distance between particles is reduced, the binding energy is enhanced and electron (hole) better interacts with the structure. This interaction is reduced when enhances the magnetic length and then the existence of exciton-polaron becomes weak in the barrier. We can confirm that the change in exciton-polaron can alter the interplay effects with phonons, thus affects the decay time. The monolayer TMDC with long decay time is $WS_2$. It is seen that at low magnetic length, the exciton-polaron has a long decay time and great energy, this result is in agreement with [134, 113]. These characteristics make the TMDC sheets a robust system for performing indirect exciton-polaron condensation in space.

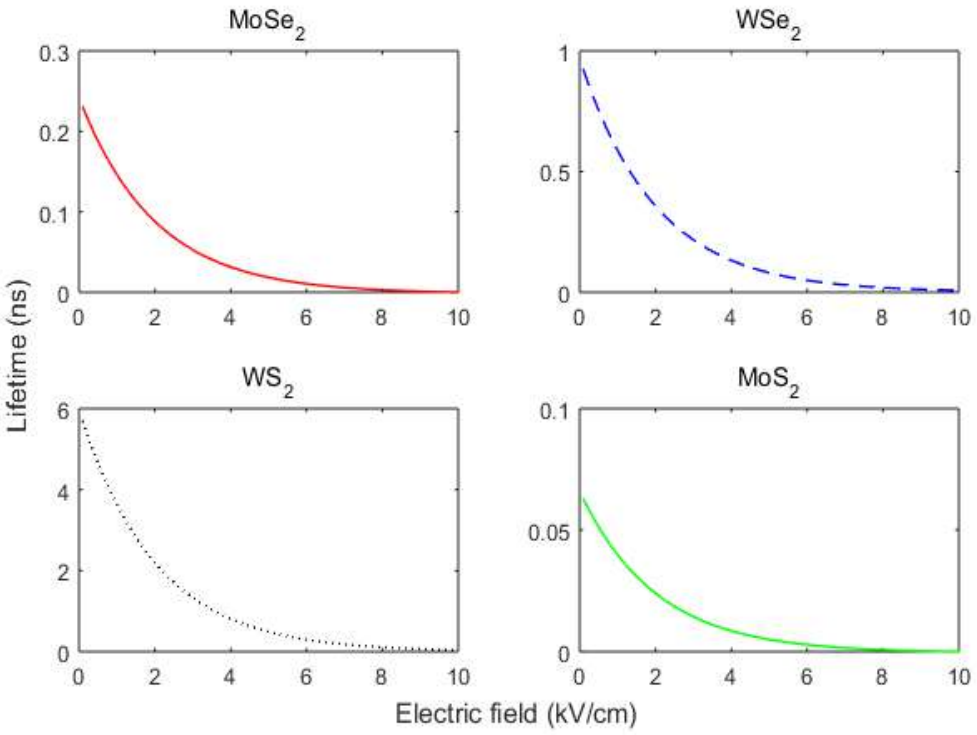


Figure 3.9: Exciton-polaron lifetime versus electric field for $T = 2K$ and $\xi_B = 0$.

Figure 3.9 presents the evolution of the lifetime of exciton-polaron versus the electric field. We observe the highest value of the lifetime at zero electric field and as the electric field increases it falls. One can say that in the presence of the external electric field, electron and hole are directed in opposite directions and then disadvantages the exciton formation. Thus, the excitonic effect is reduced by the electric field and it can dissociate the exciton-polaron for high strengths. Moreover, the results demonstrate that the TMDC in which the exciton-polaron has high energy also has a long decay time.

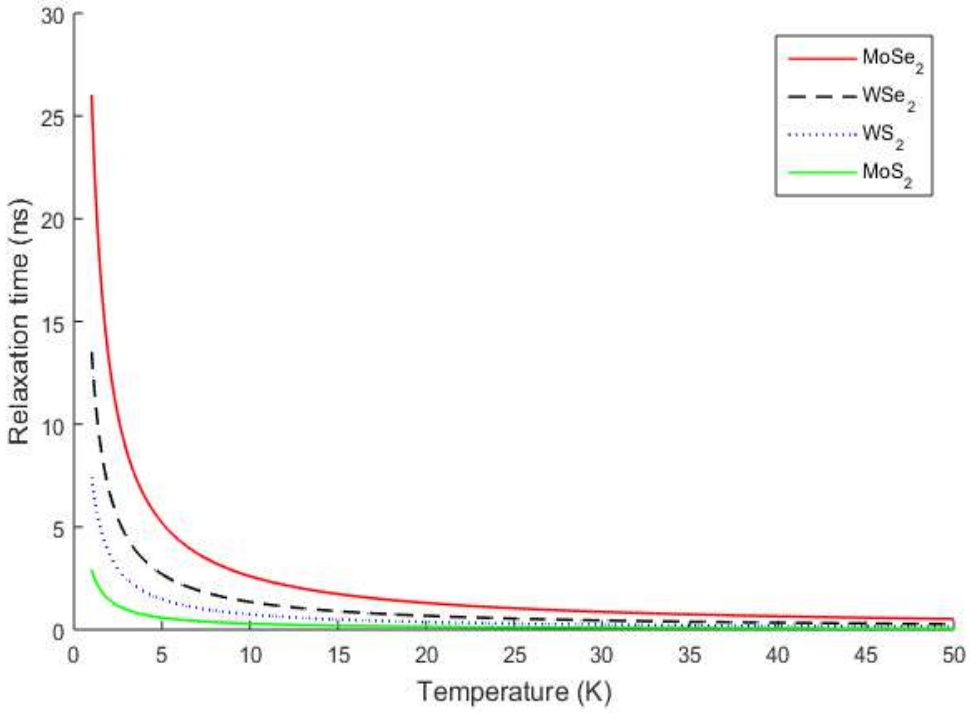


Figure 3.10: Relaxation time of exciton-polaron versus temperature out of the fields and for $c_{ex} = 10^{12} cm^{-2}$.

Figure 3.10 presents the temperature dependence on the relaxation time. The lowest relaxtion time is observed in $MoS_2$ and the highest in $MoSe_2$. The greatest amplitudes are observed for lower temperatures and it decreases when the temperature is increased. In fact, the increase of temperature perturbs the electron (hole) distribution and increases the diffusion coefficient in the excitonic network of TMDC. This leads to the appearance of loss power in the system and then the decrease of the exciton-polaron relaxation time. For high temperatures ($T > 25K$), the relaxation time becomes constant and the system reaches the thermal equilibrium. The relaxation of exciton-polaron is related to the process of dressing with phonon: more the carriers interact with the structure and less they relax. One can say that due to temperature, the exciton interacts with more phonons and then it takes few time to reach the equilibrium. The result agrees with the works of Glazov [135] and Maidannyk et al [5].

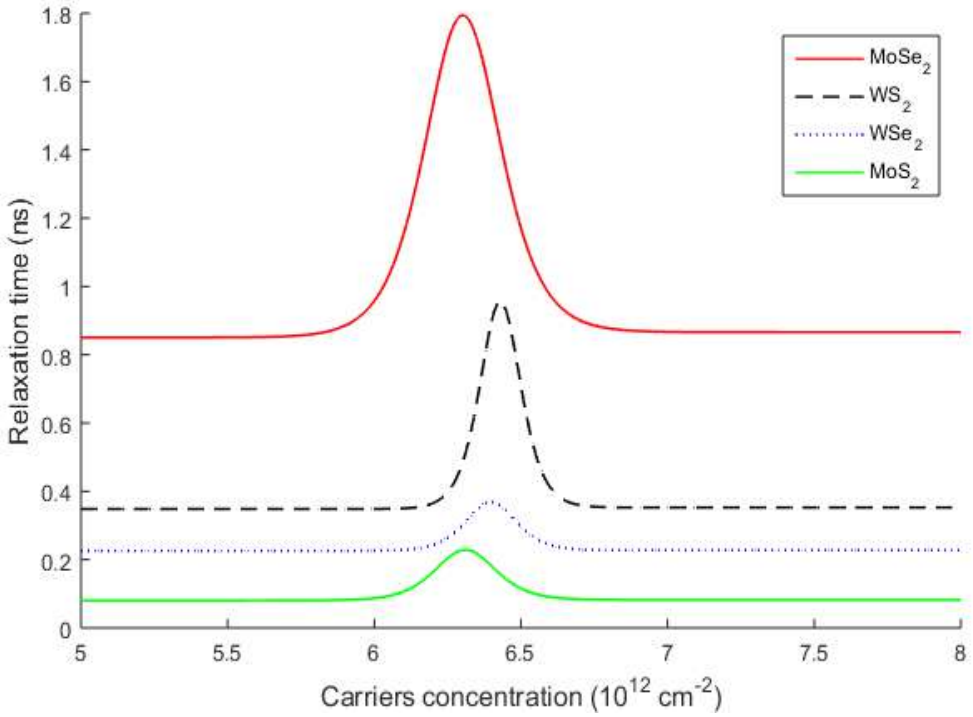


Figure 3.11: Relaxation time of exciton-polaron versus the carriers concentration for $T = 25K$.

Figure 3.11 shows the influence of carriers concentration on the exciton-polaron relaxation. It is seen that due to the increase of the carriers concentration, the relaxation time doesn't have a monotonic behavior. This influence is observed only for concentrations around a critical value corresponding to the peak. The increase of the carrier concentration means the increase of electrons and holes number in the structure. It is seen that at a low fixed temperature there is a corresponding critical value of carrier concentration. Up to this value, the particles interact with phonons that lead to their cooling, contributing then to the increase of the relaxation time. However, above this critical value it is higher concentrations, the collisions between carriers can enhance the heat in the material and then decreases the relaxation time as seen for the previous figures. The latest is in agreement with the study of Huang et al [136]. Also, $MoS_2$ has the lowest peak appearing at lowest critical value.

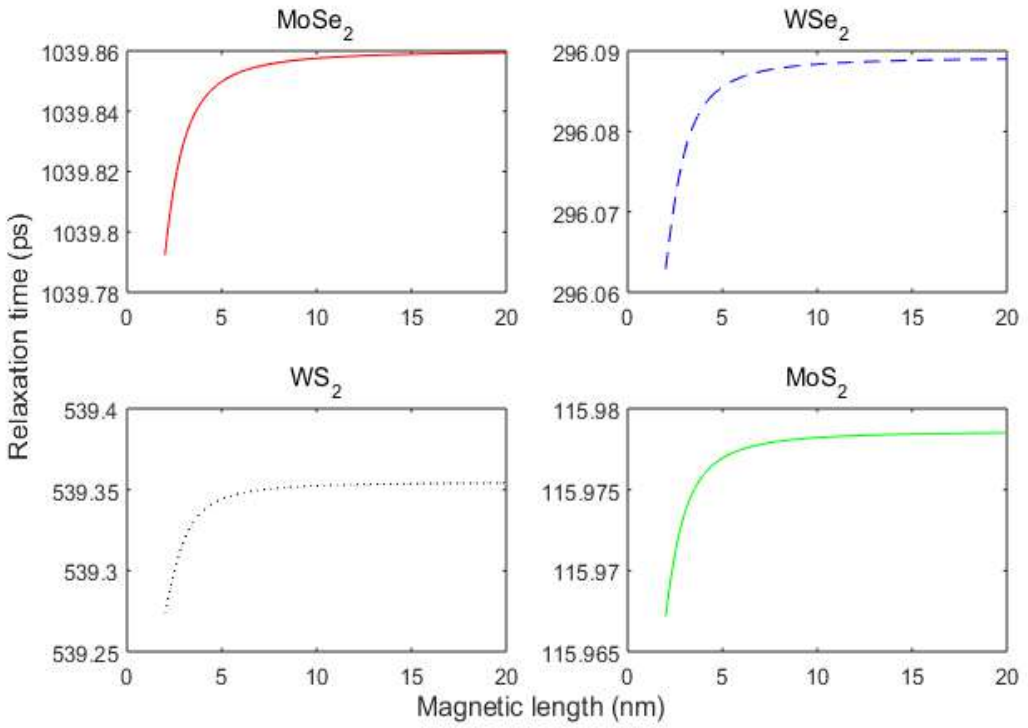


Figure 3.12: Relaxation time of exciton-polaron versus the magnetic length for $T = 25K$ , $c_{ex} = 10^{12}cm^{-2}$ and $E_{el} = 0$.

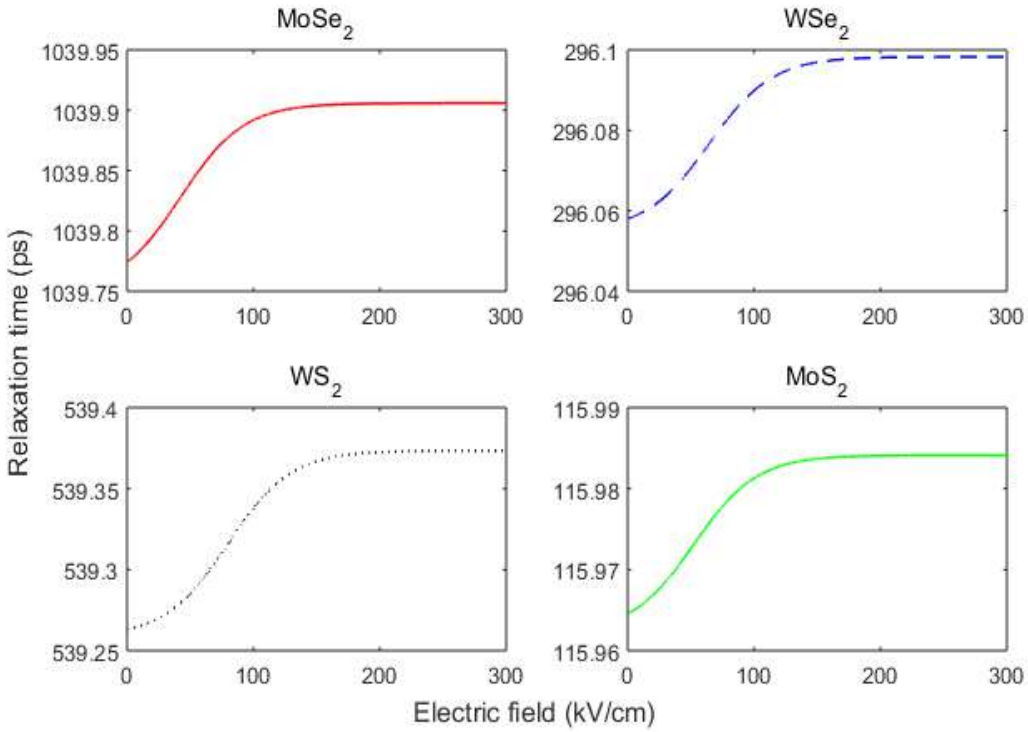


Figure 3.13: Relaxation time of exciton-polaron versus the electric field for $T = 25K$ , $c_{ex} = 10^{12}cm^{-2}$ and $l_B = 2nm$.

Figures 3.12 and 3.13 show the relaxation time of the exciton-polaron as

a function of the magnetic length ($l_B$) and the electric field respectively. The result indicates that the relaxation time increases as the magnetic length and electric parameter increase, and it saturates for high values of these parameters. The relaxation of exciton-polaron is related to the process of phonons absorption-emission in TMDCs. This process is influenced by the interaction with phonons: as less the exciton interacts in the structure it more relaxes. The presence of a magnetic field induces good confinement for electrons and holes that favors the Coulomb's interaction since it reduces the interparticle distance [32]. Therefore, since the magnetic length is inversely proportional to the magnetic field, increasing it has the effect of an opposition to the reduction of electron-hole distance and then reduces the exciton binding energy. This justifying the increase of the relaxation time observed in Figure 3.12 and it adheres with [137]. Also, it is observed that the saturation occurs at $l_B = 15nm$ meaning that the exciton-polaron reaches its maximum relaxation time and one can say that the phenomenon of relaxation is sensitive to low values of the magnetic length.

Moreover, as the electric field is applied, it delocalizes the hole and electron toward different directions. This generates the decrease of exciton binding energy contributing to the reduction of particle interactions and can lead to exciton dissociation [39]. Therefore, the electron and hole are more relaxed in presence of an external electric field and the exciton-polaron relaxation time enhances as shown in Figure 3.13.

## 3.3 Electrical properties in TMDCs within the magnetic barrier and electric field

It has been known that the temperature, the magnetic barrier and the electric field modify the dynamic and the formation of quasiparticles. In this part, we are interested on the properties that characterize the motion of the charge carriers responsible of the current in TMDC materials. We focus on the electrical conductivity and the Seebeck coefficient.

### 3.3.1 Electrical conductivity in TMDCs

Let us recall the formula of the electrical conductivity given by Eq.(2.185):

$$\sigma_{el} = e^2 \int \Lambda(E) \left(-\frac{\partial f}{\partial E}\right) dE \tag{3.38}$$

Also, the transport function $\Lambda$ is taken as Eq.(2.192) :

$$\Lambda(E) = \frac{(1-\tilde{G}_{ex2})}{2\pi M} K_0^2 \left\{\tau(K_0) - \tau(-K_0)\right\} \tag{3.39}$$

where $K_0(E)$ is defined by Eq. (2.189) but with the parameter $(d)$ appearing as:

$$d = E + E_b + G_{ex1} - E_g - \xi_B + \xi_{el} \tag{3.40}$$

It is observed that parameter $d$ contains the fields information. Therefore, substituting the latest relations in Eq.(3.38), the electrical conductivity reads:

$$\sigma_{el} = \frac{32\eta u \hbar^4 (1-G_{ex2})^3}{\pi M^3 (D_c^{op} - D_v^{op})^4} \beta e^2 \int_0^\infty dE \frac{(d-\hbar\omega_0)\sqrt{d}}{\nu^2 - \aleph^2} f(E) \tag{3.41}$$

with the parameters $\nu$ and $\aleph$ respectively obtained as:

$$\begin{aligned} \nu &= \left[n_B + f(E+\hbar\omega_0)\right] \left(\frac{8d^2+9\hbar\omega_0 d+4(\hbar\omega_0)^2}{(d+\hbar\omega_0)^{1/2}}\right) \\ &\quad +2\left[1+n_B - f(E-\hbar\omega_0)\right] \left(\frac{5d-\hbar\omega_0}{\sqrt{d-\hbar\omega_0}}\right) \end{aligned} \tag{3.42}$$

and

$$\aleph = 4\left[1+n_B - f(E-\hbar\omega_0)\right] \left(\frac{\hbar\omega_0 - d}{\sqrt{d}}\right) \tag{3.43}$$

### 3.3.2 Seebeck coefficient in TMDCs

Since the electrical conductivity depends on temperature, it is convenient to calculate the Seebeck coefficient which evaluates the electric current generated by a gradient of temperature. From chapter 2, the Seebeck coefficient can take the form of Eq.(2.196):

$$S^b = -\frac{\beta}{e}\frac{C_1}{C_2} \tag{3.44}$$

with $C_1$ and $C_2$ obtained taking into account Eqs.(2.197), (2.198) and (3.39) as:

$$C_1 = \int_0^{\infty} dE \frac{(d - \hbar\omega_0)\sqrt{d}}{\nu^2 - \aleph^2} f(E)(E - E_F) \tag{3.45}$$

$$C_2 = \int_0^{\infty} dE \frac{(d - \hbar\omega_0)\sqrt{d}}{\nu^2 - \aleph^2} f(E) \tag{3.46}$$

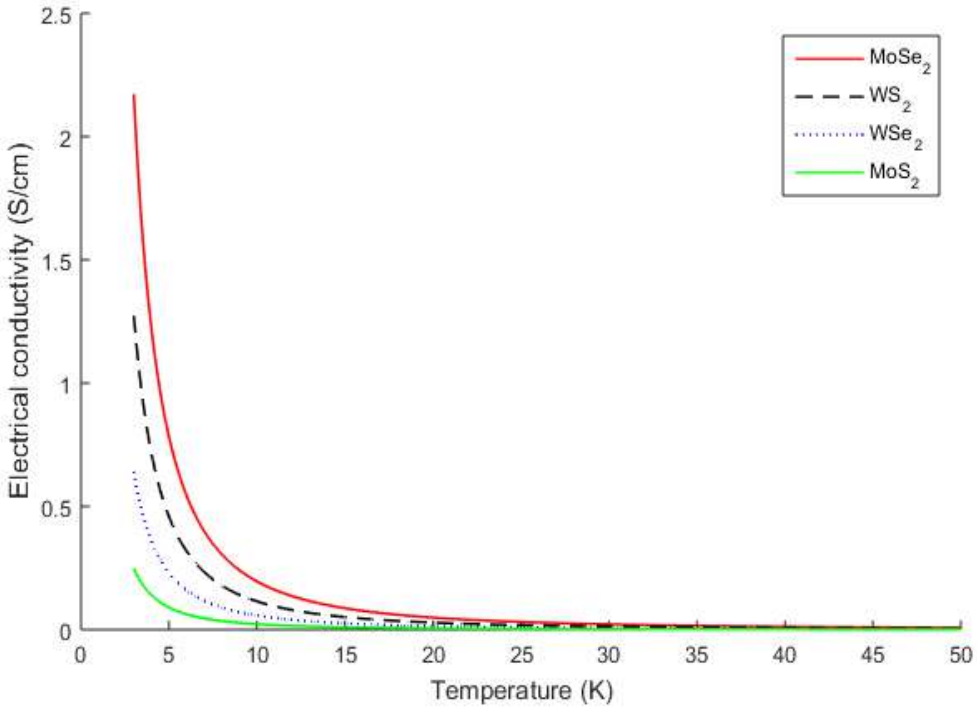


Figure 3.14: Electrical conductivity versus temperature for $c_{ex} = 10^{12} cm^{-2}$ , $\xi_B = 0$ and $E_{el} = 0$.

Figure 3.14 plots the electrical conductivity as function of the temperature for four materials. Among the selected materials, $MoSe_2$ shows the highest amplitude for this property. It is seen that the electrical conductivity of TMDCs decreases when increases the temperature. In fact, when raises the temperature in the medium, that enhances the lattice vibrations, modifies the particles direction and therefore reduces the electron (hole) motion. The enhancement of temperature creates a disorder that perturbs the electronic transitions. This is in agreement with the work of Xu et al [138]. At very low temperature, it is highest conductivities in TMDCs whereas at high temperatures it is lower conductivity, it becomes constant and can vanishes. The curve presents two ranges of temperature: $T < 20K$, a drop of conductivity is observed and it can be related to the appearance of conductor-semiconductor

phase transition. $T > 20K$, we observe a slowly decreasing of conductivity which characterize a metallic behaviour. This joins the work of Meziane et al [139].

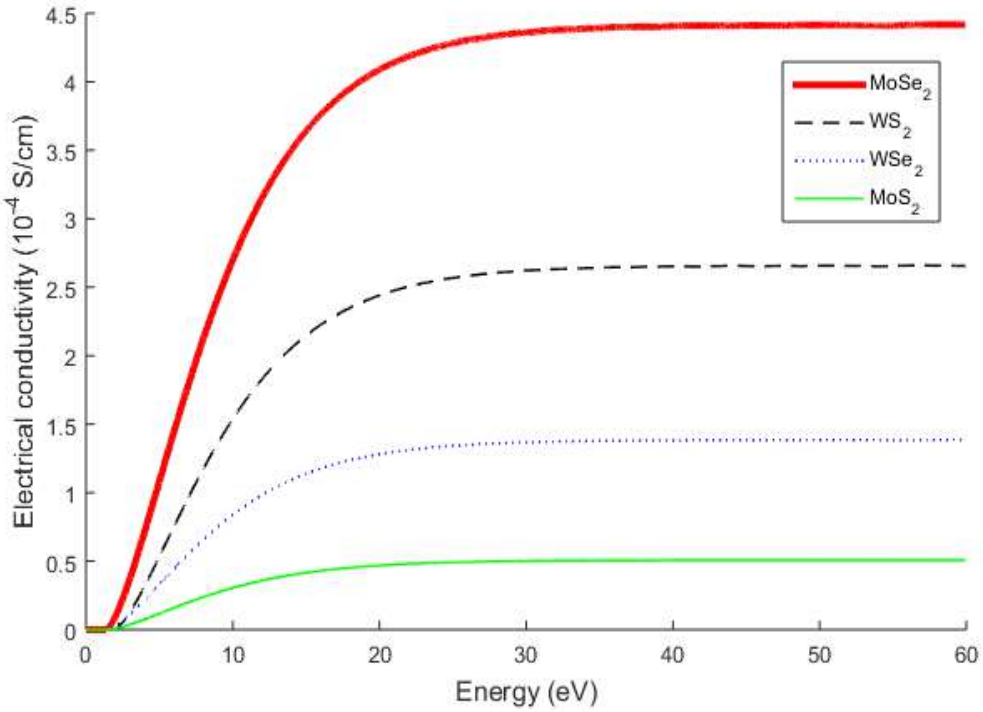


Figure 3.15: Electrical conductivity versus energy of exciton-polaron for $T = 5K$ , $c_{ex} = 10^{12}cm^{-2}$ , $\xi_B = 0$ and $E_{el} = 0$.

Figure 3.15 displays the electrical conductivity versus the system energy for four materials. It is observed that the electrical conductivity is an increasing function of the energy. This is explained by the fact that particles in the valence band need to be energetic for transition toward the conduction band. Seen Eqs.(3.41), (3.40) and this figure, the conductivity appears when the energy of the system reaches to the gap energy and it increases to a maximum then becomes constant. Since there is a gap between valence and conduction bands in TMDCs, the electron with energy lower than the gap energy remains in the valence band and the more it gains in energy the more its possibility of reaching the conduction band enhances.

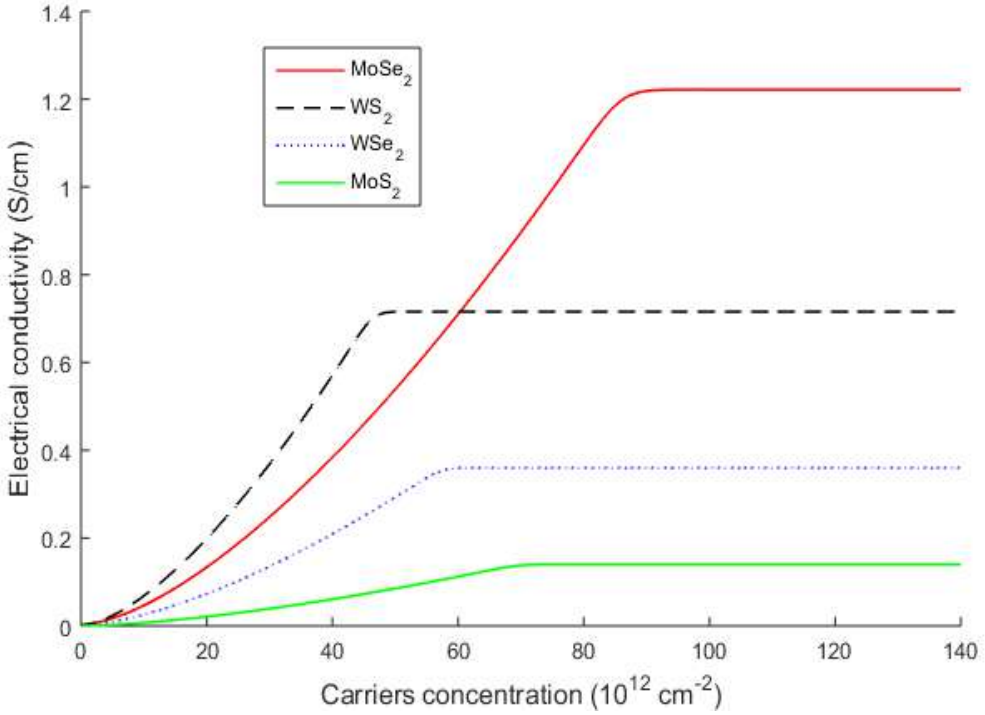


Figure 3.16: Electrical conductivity as function of the concentration of charge carriers for $T = 5K$ , $c_{ex} = 10^{12} cm^{-2}$ , $\xi_B = 0$ and $E_{el} = 0$.

Figure 3.16 shows that the electrical conductivity increases when enhances charge carriers concentration. In fact, as the number of carriers increases, the particles move gradually toward the conduction band up to the Fermi energy and then saturation occurs meaning that the conduction band is full. The number of particles increases the transitions, the more the energy of particles increases and it becomes easy to move toward the conduction band. $MoSe_2$ is the most interesting for electrical conductivity and is due to the fact that it has the lowest gap energy. This result is in accordance with the works [140] and [31]. Moreover, as was pointed Seung-il [33], it is seen from different TMDCs that the greater the relaxation time and the higher the electrical conductivity. Therefore, when the exciton-polaron lasts before reaching equilibrium that favors the electronic jumps in the material.

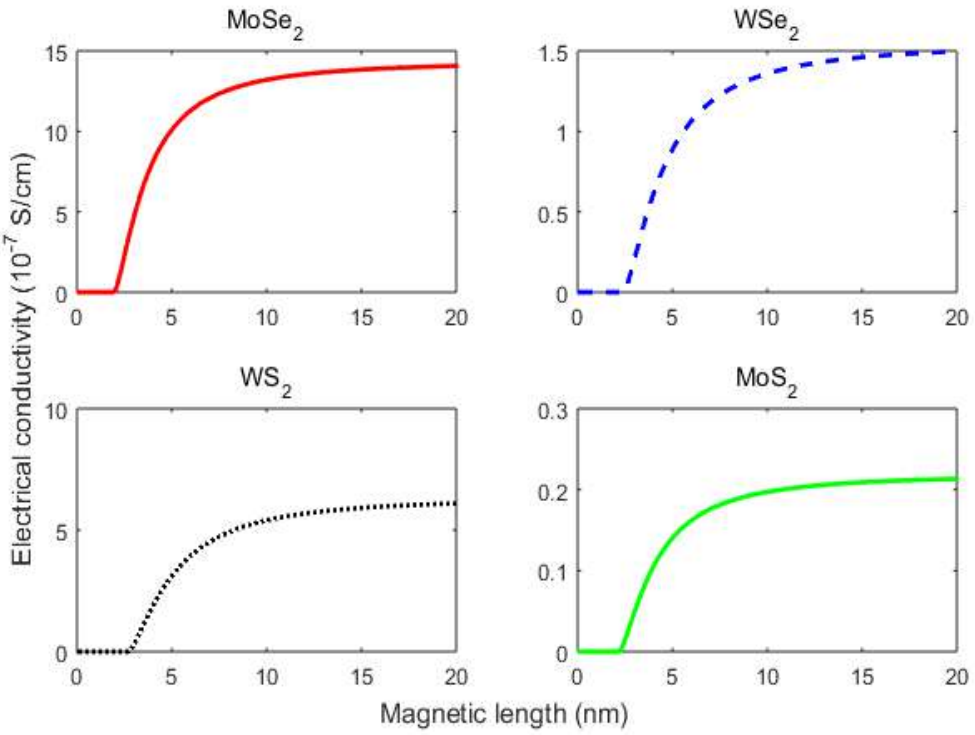


Figure 3.17: Electrical conductivity versus the magnetic length for $T = 25K$ , $c_{ex} = 10^{12}cm^{-2}$ and $E_{el} = 0$.

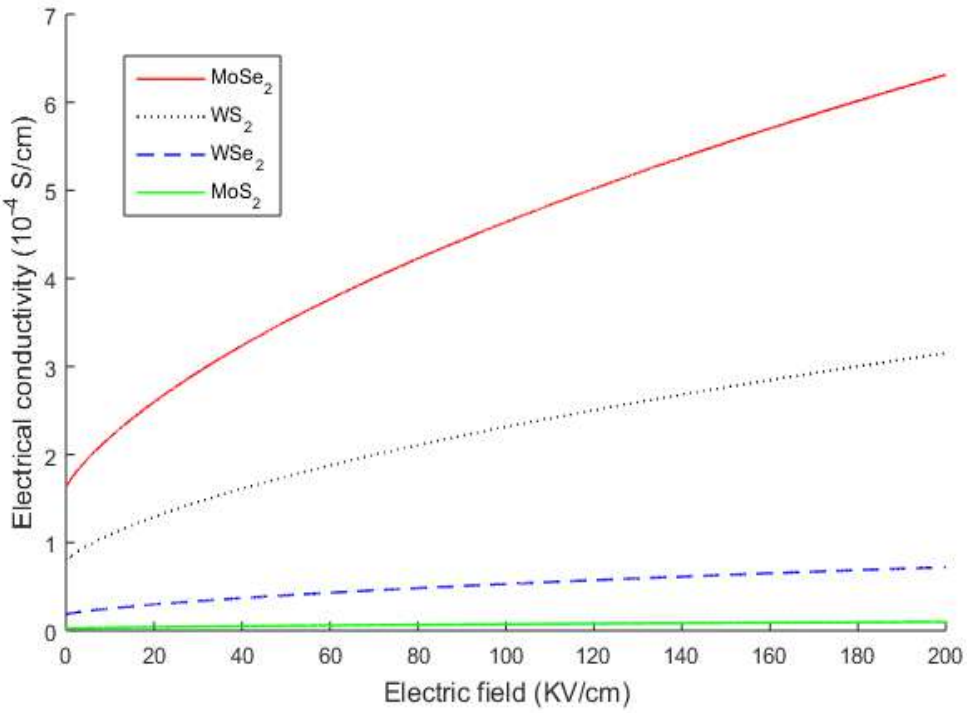


Figure 3.18: Electrical conductivity versus the electric field for $T = 25K$ , $c_{ex} = 10^{12}cm^{-2}$ and $\xi_B = 0$.

Figures 3.17 and 3.18 present the electrical conductivity for TMDCs as

a function of the magnetic length and electric field respectively. One can see from Equation (3.41) that, the electrical conductivity is proportional to $\sqrt{d}$ and we have $\sqrt{d} = \sqrt{E + E_b + G_{ex1} - E_g}$ when the fields are zero. Then, in absence of any field, the electrical conductivity appears when the system energy overpasses the band gap energy, so that the electron can transit toward the conduction band.

Now from Figure 3.17, it follows that there is no electrical conductivity for low values of the magnetic length. This result indicates that at very high magnetic strength, there is no electrical conductivity in TMDCs. Moreover, the system energy should be greater than the band gap and the magnetic parameter since the electrical conductivity becomes proportional to $\sqrt{E + E_b + G_{ex1} - E_g - \xi_B}$ according to Eq.(3.40). As the magnetic length increases, it favors the attenuation of the magnetic strength, and the electrical conductivity becomes possible. This occurs when the magnetic length reaches a value around $2.5nm$ and from this value the electrical conductivity increases as the magnetic length increases. This enhancement of the electrical conductivity is in accordance with [138, 141]. Also, applying the magnetic field along the $z$-direction induces the confinement and carriers concentration in the $xy$-plane. Then, as $l_B$ increases, electron and hole interactions with phonons grow because the particles motion increases. In [107] it is shown that the polaron motion is fast with higher magnetic barrier lengths.

When the electric field is applied as shown in Figure 3.18, the electrical conductivity increases when the electric parameter increases. The electric parameter enhances the system energy and then facilitates the electronic transitions (the term $\sqrt{E + E_b + G_{ex1} - E_g + \xi_{el}}$ into Eq. 3.40). In the same way, in [39] it is demonstrated that the exciton energy level decreases with the electric field increase. In addition, the applied electric field induces an electric force responsible of the increase of electron motion in TMDCs and it agrees with Nguepnang et al [142]. Among the selected TMDCs, $MoSe_2$ has the greatest amplitude and its electrical conductivity begins at a low value ($l_B \approx 2nm$) meaning that it is a suitable TMDC for studies in high magnetic fields. This can be due to its lowest band gap energy which favors the electronic transition between valence and conduction bands.

This result of $MoSe_2$, also suggested by Figures 3.12 and 3.13, fits with [33] which showed that the electrical conductivity rises when the relaxation time increases.

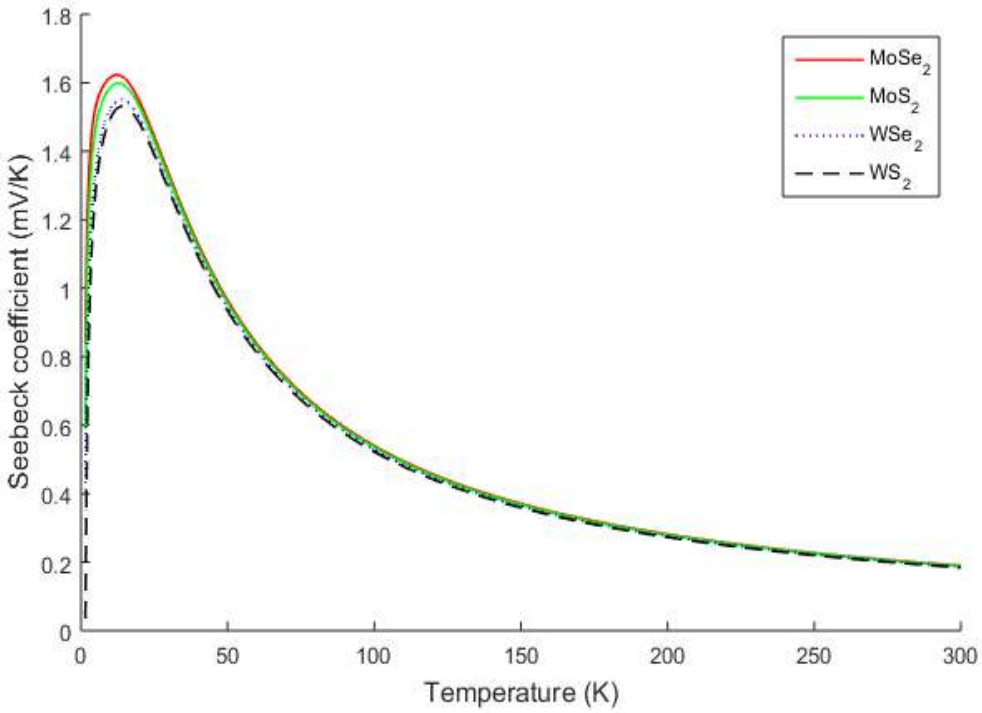


Figure 3.19: Seebeck coefficient versus temperature for $c_{ex} = 10^{12} cm^{-2}$ , $\xi_B = 0$ and $E_{el} = 0$.

Figure 3.19 plots the Seebeck coefficient as function of the temperature for various 1L TMDCs. $MoSe_2$ also has the highest magnitude of Seebeck coefficient and it adheres with the works of Qin et al [30] and Ge et al [31]. It is seen that the Seebeck coefficient of TMDCs behaves differently at low temperature and high temperature. At very low temperature, the Seebeck coefficient approaches zero meaning that the change of temperature is too weak and not sensitive for the material. It increases to a maximum when enhances temperature and the peak is observed at temperature close to $15K$. The low change of temperature ($T < 15K$) creates the movement of hot particles, inducing a voltage and then appears the Seebeck effect. This induction is attenuated in high temperatures range because particles are very hot and favor a collision motion in the structure. High temperatures ($T > 15K$) act in the system as a perturbation which favors the disorder and then reduce the Seebeck voltage. Therefore, TMDCs generate an electric current when they are subject of temperature least than $15K$ but this current is dominated

by the thermal disorder due to high temperatures. The result agrees with the works of Selvaggi [143] and Ashraf et al [144].

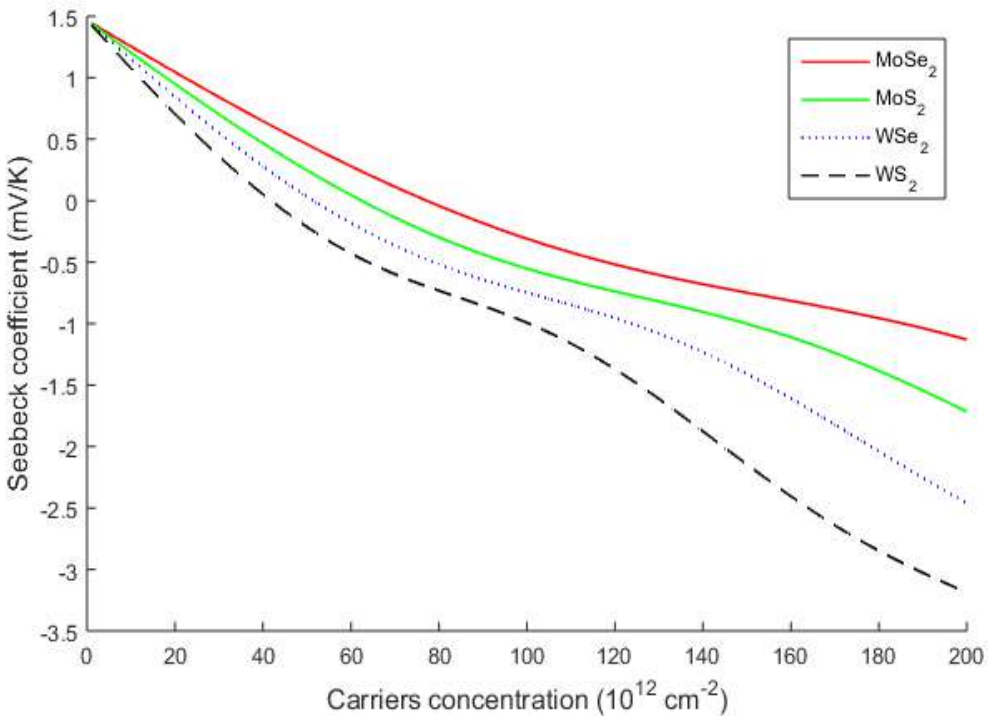


Figure 3.20: Seebeck coefficient as function of the charge carriers concentration for $T = 100K$ , $\xi_B = 0$ and $E_{el} = 0$.

Figure 3.20 plots the Seebeck coefficient versus the carrier concentration for various 1L TMDCs. It is shown that the Seebeck coefficient is a decreasing function of the carrier concentration. In the case of exciton-polaron, we observe negative and positive values of the Seebeck coefficient which refer to the presence of electron and hole respectively in the system. The result indicates the dominance of the electrons in this thermoelectric property when enhances the carriers concentration. In fact, the Seebeck effect implies the creation of a low electric field and the electron charge favors an electric force opposite to the field in direction. Then more the structure is concentrated in electrons and the stronger is the opposition to the appearance of the current induced by the temperature change; this explains the decrease observed on the curves.

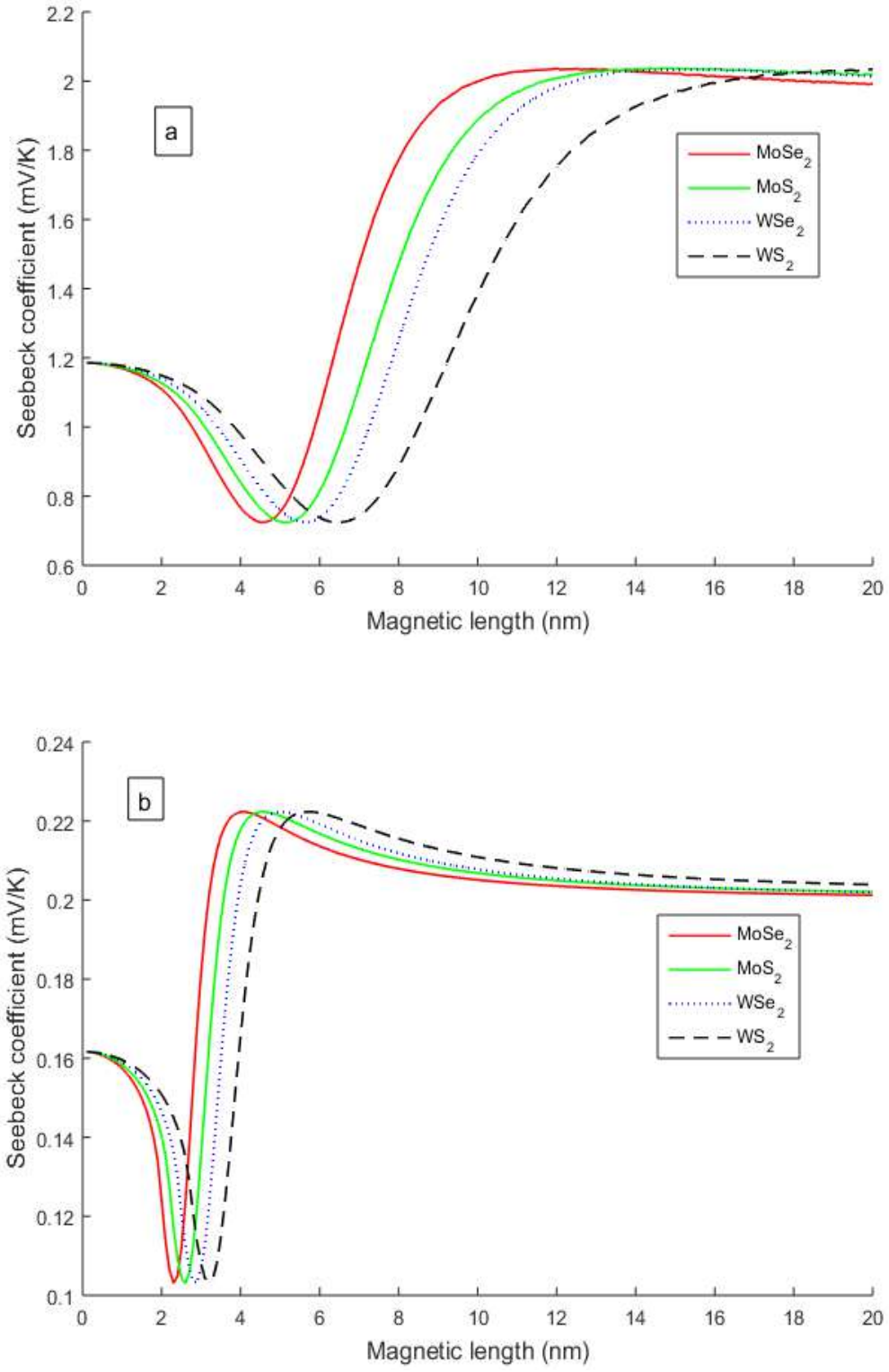


Figure 3.21: Seebeck coefficient versus the magnetic length for $c_{ex} = 10^{12} cm^{-2}$ , $E_{el} = 0$ , (a) $T = 5K$ and (b) $T = 150K$.

The Seebeck coefficient as a function of the magnetic length for low and high temperatures and diverse TMDCs, is presented in Figures 3.21 $(a)$ and $(b)$ respectively. It is observed that the curves don't present monotonic

shapes. The Seebeck coefficient falls up to a critical value of the magnetic length, and above this value it increases. In fact, as the temperature changes in TMDCs, it generates excitations and increases the motion of particles. This leads to the appearance of a voltage responsible of the Seebeck effect. At a fixed temperature and for low values of the magnetic length, which means high magnetic field, the magnetic influence dominates. Then electron (hole) is more confined than subjected to thermal perturbation and it explains the decrease of this property.

In the opposite way, above the critical value of the magnetic length, which means low magnetic field, the temperature effect dominates and enhances the Seebeck coefficient. It is in agreement with the results of [141, 145]. Also, the result shows that the magnetic effect is less significant in high temperature range since one can observe the regression of the critical values range (from $5-7nm$ in Figure 3.21 $(a)$ to $2.5-3.5nm$ in Figure 3.21 $(b)$ and the reduction of the Seebeck coefficient values regarding Figure 3.21 $(a)$ and Figure 3.21 $(b)$. In addition, for very high values of the magnetic length $l_B > 18nm$ in Figure 3.21 $(a)$ and $l_B > 10nm$ in Figure 3.21 $(b)$, the Seebeck coefficient becomes constant and the magnetic barrier doesn't more influence this property. At $T = 5K$, the highest amplitude is obtained for $WS_2$ at low magnetic length and for $MoSe_2$ at high magnetic length.

Figure 3.22 presents the evolution of the Seebeck coefficient in the presence of the external electric field. Without the magnetic influence as pointed Figure 3.22 $(a)$, the result shows the highest amplitudes of the coefficient at zero electric field and it decreases gradually as the field increases. It is in agreement with [146]. Thus, the Seebeck effect as a thermoelectric power property, is favored by the absence of the electric field. In this case, when the temperature changes, the electron (hole) moves directed only by the temperature gradient from the hot source to the cold one's and then it generates the Seebeck voltage.

In the presence of the electric field, the particles motion is governed by the field. As the strength of the electric field increases, the electric force enhances and overcomes the effect of the temperature gradient. This explains the decrease of the Seebeck coefficient curves.

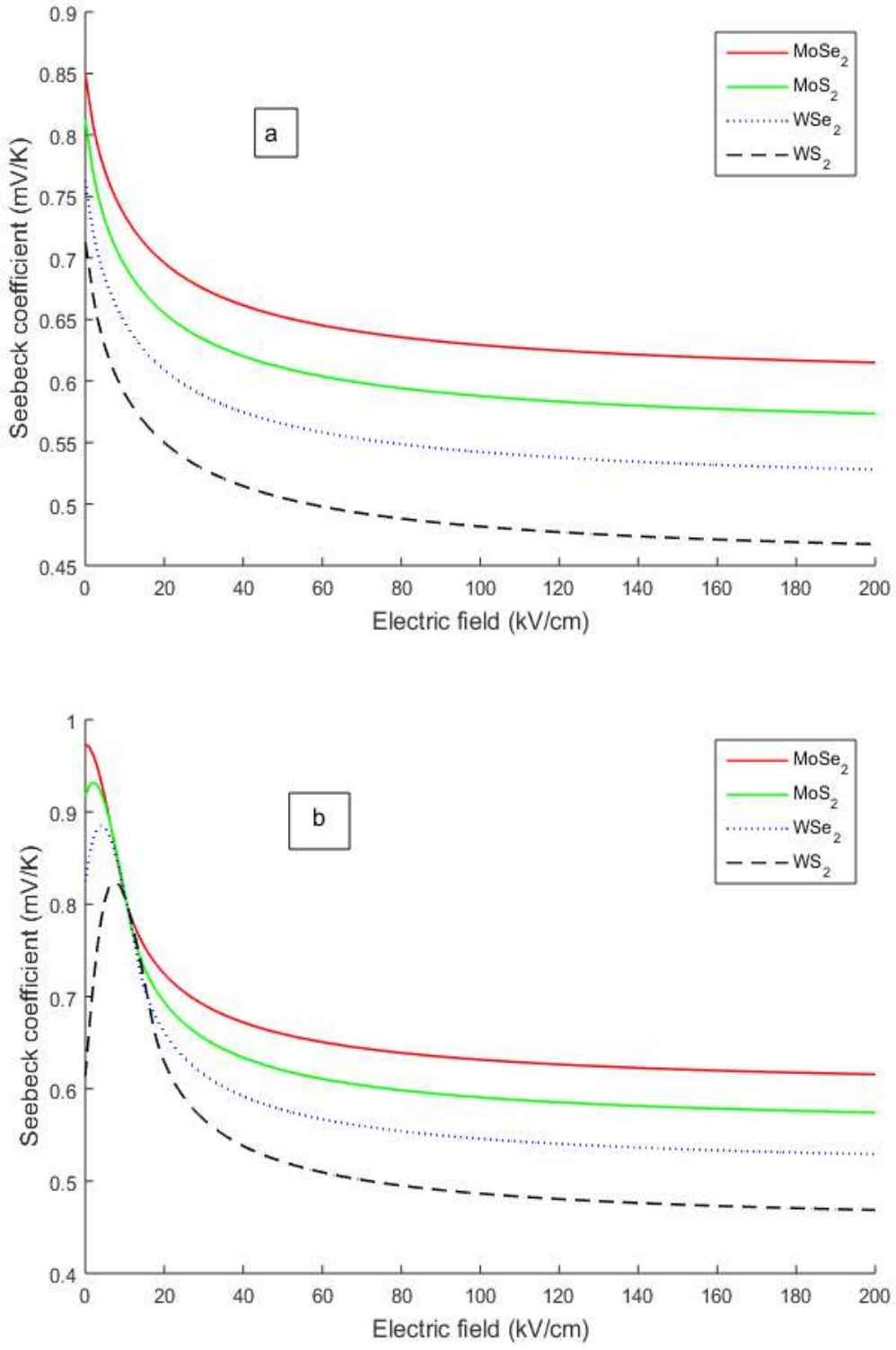


Figure 3.22: Seebeck coefficient versus the electric field for $T = 25K$ , $c_{ex} = 10^{12}cm^{-2}$ , (a) $\xi_B = 0$ and (b) $l_B = 5nm$.

Figure 3.22 $(b)$ shows the challenge between magnetic field and electric fields. The increase characterizes the dimonance of magnetic effect whereas

the decrease indicates the dominance of the electric field. One can say that the electric field opposes the magnetic field in the Seebeck coefficient.

## 3.4 Optical properties in TMDCs subject to the magnetic barrier and electric field

In an excitonic system, the excited electron can transit via an absorption or emission process. This motion of the electron (and its corresponding hole) can be responsible of the conductivity in the material and can be due to the absorption of an external energy (light) evaluated by the optical absorption coefficient. In this part, we are interested on the properties that characterize the optical response of the TMDC materials.

### 3.4.1 Optical conductivity

We use the Kubo formula of Eq. (2.199) as follows:

$$\sigma_{(\omega)} = i\frac{2e^2}{SM\omega} + \frac{1}{S\hbar\omega}\int_0^\infty dt e^{i\omega t}\langle[J(t), J(0)]\rangle \tag{3.47}$$

The current operator of a particle is defined as [147]:

$$j_{(\alpha)} = \frac{i}{\hbar}e_\alpha\left[H, r_\alpha\right] \tag{3.48}$$

with the index $\alpha = e, h$ used for electron or hole. Then, the total current operator reads:

$$J = e\left(\frac{P_h}{m_h} - \frac{P_e}{m_e}\right) \tag{3.49}$$

Therefore, $\sigma_{(\omega)}$ becomes:

$$\sigma_{(\omega)} = i\frac{2e^2}{SM\omega} + \frac{1}{S\hbar\omega}\int_0^\infty dt e^{i\omega t}\left\langle\frac{e^2}{m_h^2}[p_h(t), p_h(0)] + \frac{e^2}{m_e^2}[p_e(t), p_e(0)]\right\rangle \tag{3.50}$$

After integrating by parts, one gets:

$$\sigma_{(\omega)} = i\frac{2e^2}{SM\omega} - \frac{e^2}{S\hbar\omega^3}\int_0^\infty dt e^{i\omega t}\left\langle \frac{1}{m_e^2}[F_e(t), F_e(0)] + \frac{1}{m_h^2}[F_h(t), F_h(0)]\right\rangle \tag{3.51}$$

The force operator is defined as $F_\alpha(t) = (i/\hbar)\,[H, p_\alpha]$ with the linear momentum operator taking in the second quantization as $p_\alpha = \hbar K_\alpha C^\dagger_{K_\alpha} C_{K_\alpha}$. Thus

$$\begin{aligned} F_e(t) &= -i\left\{\left(\tfrac{e^2B^2}{2m_e} - eE_{el}\right) C^\dagger_{K_e}(t)C_{K_e}(t)\right. \\ &\left. + \sum_q q\Xi(q) C^\dagger_{K_e}(t)C_{K_e}(t)\left(b_q(t) + b^\dagger_{-q}(t)\right)\right\} \end{aligned} \tag{3.52}$$

$$\begin{aligned} F_h(t) &= -i\left\{\left(\tfrac{e^2B^2}{2m_h} + eE_{el}\right) C^\dagger_{K_h}(t)C_{K_h}(t)\right. \\ &\left. + \sum_q q\Xi(q) C^\dagger_{K+q}(t)C_{K}(t)\left(b_q(t) + b^\dagger_{-q}(t)\right)\right\} \end{aligned} \tag{3.53}$$

Also, the time dependence of the operators is given by:

$$b_q(t) = e^{-i\omega_0 t} b_q(0); b^\dagger_{-q}(t) = e^{i\omega_0 t} b^\dagger_{-q}(0) \tag{3.54}$$

and

$$C^\dagger_K(t)C_K(t) = e^{\frac{it}{\hbar}\lambda_K} C^\dagger_K(0) e^{\frac{-it}{\hbar}\lambda_K} C_K(0) \tag{3.55}$$

$$C^\dagger_{K+q}(t)C_K(t) = e^{\frac{it}{\hbar}\lambda_{K+q}} C^\dagger_{K+q}(0) e^{\frac{-it}{\hbar}\lambda_K} C_K(0) \tag{3.56}$$

Then Eq. (3.51) gives:

$$\begin{aligned} \sigma_{(\omega)} &= i\tfrac{2e^2}{SM\omega} + \tfrac{e^2}{S\hbar\omega^3}\tfrac{1}{\omega^2}\int_0^\infty dt e^{i\omega t}\left\langle \left\{ -\sum_q \left(\tfrac{e^2B^2(m_e^3+m_h^3)}{2m_e^3m_h^3} - \tfrac{eE_{el}(m_h^2-m_e^2)}{2m_e^2m_h^2}\right)\times\right. \right. \\ &\quad q\Xi(q) C^\dagger_{K+q}C_K\left(b_q + b^\dagger_{-q}\right) \\ &\quad + \sum_q \left(\tfrac{e^2B^2(m_e^3+m_h^3)}{2m_e^3m_h^3} - \tfrac{eE_{el}(m_h^2-m_e^2)}{2m_e^2m_h^2}\right) q\Xi(q) C^\dagger_{K+q}C_K\left(U(t)b_q + T(t)b^\dagger_{-q}\right) \\ &\quad \left.\left. + \tfrac{(m_h^2+m_e^2)}{m_e^2m_h^2}\sum_q q^2\Xi^2(q) C^\dagger_{K+q}C_K C^\dagger_{K+q}C_K\left[U(t) - T(t)\right]\right\}\right\rangle \end{aligned} \tag{3.57}$$

where

$$T(t) = exp\frac{it}{\hbar}\left(\lambda_{K+q} - \lambda_K + \hbar\omega_0\right) \tag{3.58}$$

$$U(t) = exp\frac{it}{\hbar}\left(\lambda_{K+q} - \lambda_K - \hbar\omega_0\right) \tag{3.59}$$

Let average with $U_{ex}|\Psi_0\rangle$. We first apply the unitary transformation and obtain:

$$\begin{aligned}
\sigma_{(\omega)} &= i\frac{2e^2}{SM\omega} + \frac{e^2}{S\hbar\omega^3}\frac{1}{\omega^2}\int_0^\infty dt e^{i\omega t}\left\langle\left\{-\sum_q\left(\frac{e^2B^2(m_e^3+m_h^3)}{2m_e^3m_h^3} - \frac{eE_{el}(m_h^2-m_e^2)}{2m_e^2m_h^2}\right)\times\right.\right. \\
&\quad q\Xi(q)C^\dagger_{K+q}C_K\left(b_q + b^\dagger_{-q} + iC^\dagger_{K+q}C_K(f^*_{ex} - f_{ex})\right) \\
&\quad +\sum_q\left(\frac{e^2B^2(m_e^3+m_h^3)}{2m_e^3m_h^3} - \frac{eE_{el}(m_h^2-m_e^2)}{2m_e^2m_h^2}\right)q\Xi(q)C^\dagger_{K+q}C_K\times \\
&\quad \left(U(t)b_q + T(t)b^\dagger_{-q} + iU(t)C^\dagger_{K+q}C_Kf^*_{ex} - iT(t)C^\dagger_{K+q}C_Kf_{ex}\right) \\
&\quad \left.\left.+\frac{(m_h^2+m_e^2)}{m_e^2m_h^2}\sum_q q^2\Xi^2(q)C^\dagger_{K+q}C_KC^\dagger_{K+q}C_K\left[U(t) - T(t)\right]\right\}\right\rangle
\end{aligned} \tag{3.60}$$

Using the GS wave function, we have:

$$\begin{aligned}
\sigma_{(\omega)} &= i\frac{2e^2}{SM\omega} + \frac{e^2}{S\hbar\omega^3}\frac{1}{\omega^2}\int_0^\infty dt e^{i\omega t}\times \\
&\quad \left\langle\left\{-\sum_q\left(\frac{e^2B^2(m_e^3+m_h^3)}{2m_e^3m_h^3} - \frac{eE_{el}(m_h^2-m_e^2)}{2m_e^2m_h^2}\right)q\Xi(q)(f^*_{ex} - f_{ex})\right.\right. \\
&\quad +i\sum_q\left(\frac{e^2B^2(m_e^3+m_h^3)}{2m_e^3m_h^3} - \frac{eE_{el}(m_h^2-m_e^2)}{2m_e^2m_h^2}\right)q\Xi(q)\left[U(t)f^*_{ex} - T(t)f_{ex}\right] \\
&\quad \left.\left.+\frac{(m_h^2+m_e^2)}{m_e^2m_h^2}\sum_q q^2\Xi^2(q)\left[U(t) - T(t)\right]\right\}\right\rangle
\end{aligned} \tag{3.61}$$

After integrating over $t$ , the imaginary part of the optical conductivity appears as:

$$\begin{aligned}
Im\left[\sigma_{(\omega)}\right] &= \frac{2e^2}{SM\omega} + \frac{\hbar e^2}{S\hbar\omega}\frac{(m_h^2+m_e^2)}{m_e^2m_h^2\omega^2}\sum_q q^2\Xi^2(q)\times \\
&\quad \left(\frac{1}{\lambda_{K+q} - \lambda_K + \hbar\omega - \hbar\omega_0} - \frac{1}{\lambda_{K+q} - \lambda_K + \hbar\omega + \hbar\omega_0}\right)
\end{aligned} \tag{3.62}$$

It is seen that the imaginary part represents the optical conductivity out of any field. For the present case, in which we investigate the effect of fields,

we will focus on the real part obtained as:

$$\begin{aligned} Re\left[\sigma_{(\omega)}\right] &= \frac{e^2}{S\hbar\omega}\frac{1}{\omega^2}\left\{\frac{1}{\omega}\sum_q\left(\frac{e^2B^2(m_e^3+m_h^3)}{2m_e^3m_h^3}-\frac{eE_{el}(m_h^2-m_e^2)}{2m_e^2m_h^2}\right)q\Xi(q)(f_{ex}^*-f_{ex})\right. \\ &+\hbar\sum_q\left(\frac{e^2B^2(m_e^3+m_h^3)}{2m_e^3m_h^3}-\frac{eE_{el}(m_h^2-m_e^2)}{2m_e^2m_h^2}\right)q\Xi(q)\times \\ &\left.\left(\frac{f_{ex}}{\lambda_{K+q}-\lambda_K+\hbar\omega+\hbar\omega_0}-\frac{f_{ex}^*}{\lambda_{K+q}-\lambda_K+\hbar\omega-\hbar\omega_0}\right)\right\} \end{aligned} \tag{3.63}$$

The final expression of the real part of optical conductivity is determined by replacing the summation into integration. We have:

$$Re\left[\sigma(\omega)\right]=\sigma_B(\omega)-\sigma_{el}(\omega) \tag{3.64}$$

where

$$\begin{aligned} \sigma_B(\omega) &= \frac{e^2(D_C^{op}-D_v^{op})^2}{16S\eta u\pi^2\hbar\omega}\frac{\hbar^3(m_e^3+m_h^3)}{m_e^3m_h^3\omega^2l_B^2}\int_0^\infty dq\int_0^{2\pi}d\theta q^3\times \\ &\left\{\frac{1/\omega}{\frac{\hbar^2q^2}{2M}+\frac{\hbar^2}{M}Kq\cos\theta-\hbar\omega_0}-\frac{1/\omega}{\frac{\hbar^2q^2}{2M}+\frac{\hbar^2}{M}Kq\cos\theta+\hbar\omega_0}\right. \\ &+\frac{\hbar}{\left(\frac{\hbar^2q^2}{2M}+\frac{\hbar^2}{M}Kq\cos\theta+\hbar\omega+\hbar\omega_0\right)\left(\frac{\hbar^2q^2}{2M}+\frac{\hbar^2}{M}Kq\cos\theta-\hbar\omega_0\right)} \\ &\left.-\frac{\hbar}{\left(\frac{\hbar^2q^2}{2M}+\frac{\hbar^2}{M}Kq\cos\theta+\hbar\omega-\hbar\omega_0\right)\left(\frac{\hbar^2q^2}{2M}+\frac{\hbar^2}{M}Kq\cos\theta+\hbar\omega_0\right)}\right\} \end{aligned} \tag{3.65}$$

and

$$\begin{aligned} \sigma_{el}(\omega) &= \frac{e^3(D_C^{op}-D_v^{op})^2}{16S\eta u\pi^2}\frac{(m_h^2-m_e^2)}{m_e^2m_h^2\omega^3}E_{el}\int_0^\infty dq\int_0^{2\pi}d\theta q^3\times \\ &\left\{\frac{1/\omega}{\frac{\hbar^2q^2}{2M}+\frac{\hbar^2}{M}Kq\cos\theta-\hbar\omega_0}-\frac{1/\omega}{\frac{\hbar^2q^2}{2M}+\frac{\hbar^2}{M}Kq\cos\theta+\hbar\omega_0}\right. \\ &+\frac{\hbar}{\left(\frac{\hbar^2q^2}{2M}+\frac{\hbar^2}{M}Kq\cos\theta+\hbar\omega+\hbar\omega_0\right)\left(\frac{\hbar^2q^2}{2M}+\frac{\hbar^2}{M}Kq\cos\theta-\hbar\omega_0\right)} \\ &\left.-\frac{\hbar}{\left(\frac{\hbar^2q^2}{2M}+\frac{\hbar^2}{M}Kq\cos\theta+\hbar\omega-\hbar\omega_0\right)\left(\frac{\hbar^2q^2}{2M}+\frac{\hbar^2}{M}Kq\cos\theta+\hbar\omega_0\right)}\right\} \end{aligned} \tag{3.66}$$

### 3.4.2 Optical absorption coefficient

As shown in chapter 2, we establish a similar relation as Eq.(2.126) for the case of exciton-polaron:

$$\begin{aligned} Re\left[R(\hbar\Omega)\right] &= \left(\tfrac{e}{\hbar\Omega}\right)^2 \int_{-\infty}^{0} dt e^{-it(i\varepsilon+\hbar\Omega)} \langle\Psi| E_i.\left\{\tfrac{p_e(0)}{m_e}+\tfrac{p_h(0)}{m_h}\right\}\times \\ & E_i.\left\{\tfrac{p_e(t)}{m_e}+\tfrac{p_h(t)}{m_h}\right\}|\Psi\rangle \end{aligned} \tag{3.67}$$

Now, let us apply the unitary transformation (2.49):

$$\begin{aligned} Re\left[R(\hbar\Omega)\right] &= \left(\tfrac{e}{\hbar\Omega}\right)^2 \int_{-\infty}^{0} dt e^{-it(i\varepsilon+\hbar\Omega)} \langle\Psi| E_i.U_{ex}^{-1}\left\{\tfrac{p_e(0)}{m_e}+\tfrac{p_h(0)}{m_h}\right\}U_{ex}\times \\ & E_i.U_{ex}^{-1}\left\{\tfrac{p_e(t)}{m_e}+\tfrac{p_h(t)}{m_h}\right\}U_{ex}|\Psi\rangle \end{aligned} \tag{3.68}$$

We have for $P=0$:

$$\begin{aligned} U_{ex}^{-1}pU_{ex} &= p + i\left[\sum_{K,q} C_{K+q}^{\dagger}C_K(f_{ex}^{*}b_{-q}^{\dagger}+f_{ex}b_q), P-\sum_q \hbar\omega_0 q b_q^{\dagger}b_q\right] \\ &= p - i\hbar\omega_0\sum_{K,q} qC_{K+q}^{\dagger}C_K(f_{ex}b_q - f_{ex}^{*}b_{-q}^{\dagger}) \end{aligned} \tag{3.69}$$

Therefore:

$$\begin{aligned} Re\left[R(\hbar\Omega)\right] &= \left(\tfrac{e}{\hbar\Omega}\right)^2 \int_{-\infty}^{0} dt e^{-it(i\varepsilon+\hbar\Omega)} \langle\Psi|\times \\ & E_i.\left\{\tfrac{p_e}{m_e}+\tfrac{p_h}{m_h}-\tfrac{i\hbar\omega_0}{\mu}\sum_{K,q} qC_{K+q}^{\dagger}C_K(f_{ex}b_q - f_{ex}^{*}b_{-q}^{\dagger})\right\}\times \\ & E_i.\left\{\tfrac{p_e(t)}{m_e}+\tfrac{p_h(t)}{m_h}-\tfrac{i\hbar\omega_0}{\mu}\sum_{K,q} qC_{K+q}^{\dagger}(t)C_K(t)(f_{ex}b_q(t) - f_{ex}^{*}b_{-q}^{\dagger}(t)\right\}|\Psi\rangle \end{aligned} \tag{3.70}$$

By using Eqs. (3.69), (3.54) and (3.55), we have:

$$\begin{aligned} Re[R(\hbar\Omega)] &= \left(\frac{e}{\hbar\Omega}\right)^2 \int_{-\infty}^{0} dt e^{-it(i\varepsilon+\hbar\Omega)} \left\{\frac{2\hbar^2E_i^2K^{*2}}{M^2} - \frac{\hbar^2E_i^2(m_e^2+m_h^2)}{m_e^2m_h^2a^2}\right. \\ & \left. + \frac{(\hbar\omega_0)^2}{\mu^2}\sum_q (E_i.q)^2 f_{ex}f_{ex}^{*}e^{-it(\lambda_K-\lambda_{K+q}-\hbar\omega_0)}\right\} \end{aligned} \tag{3.71}$$

We consider the energy ratio :

$$\chi = \frac{\hbar\Omega}{\hbar\omega_0} \tag{3.72}$$

The optical absorption coefficient reads:

$$\begin{aligned}\Gamma(\chi) &= \frac{\pi e^2}{cn\varepsilon_0\hbar(\hbar\omega_0)^2\chi}\left\{\frac{2\hbar^2K^{*2}}{M^2}-\frac{\hbar^2(m_e^2+m_h^2)}{m_e^2m_h^2a^2}\right\}\delta(\chi)\\ &+\frac{\pi e^2\omega_0}{cn\varepsilon_0\mu^2E_i^2\chi}\sum_q(E_i.q)^2f_{ex}f_{ex}^*\delta\left[-\frac{\hbar^2}{2M}(q^2+2kq\cos\theta)+\hbar\omega_0(\chi-1)\right]\end{aligned} \tag{3.73}$$

Transforming the summation into an integration, one gets:

$$\begin{aligned}\Gamma(\chi) &= \frac{\pi e^2}{cn\varepsilon_0\hbar(\hbar\omega_0)^2\chi}\left\{\frac{2\hbar^2}{M^2}\left(k^2+\frac{1}{l_B^2}\right)-\frac{\hbar^2(m_e^2+m_h^2)}{m_e^2m_h^2a^2}\right\}\delta(\chi)\\ &+\frac{M\hbar\omega_0e^2(D_c^{op}-D_v^{op})^2}{4\pi cn\varepsilon_0\eta\mu^2\hbar^2\mu^2\chi}\sin^2(\gamma)\int_0^{2\pi}d\theta\int_0^{\infty}dqq^4\frac{\delta\left[q^2+2kq\cos\theta-2M\hbar\omega_0(\chi-1)/\hbar^2\right]}{\frac{\hbar^4}{4M^2}(q^2+2kq\cos\theta)^2-(\hbar\omega_0)^2}\end{aligned} \tag{3.74}$$

$\gamma$ is the angle between the field induced by incident photon ($E_i$) and the normal of TMDC.

Let us take $q_0^2 = 2M\hbar\omega_0(\chi-1)/\hbar^2$ for $\chi > 1$. We first integrate over $q$ in Eq. (3.74), it gives:

$$\begin{aligned}\Gamma(\chi) &= \frac{e^2\sqrt{\pi}}{cn\varepsilon_0\hbar(\hbar\omega_0)^2}\left\{\frac{2\hbar^2}{M^2}\left(k^2+\frac{1}{l_B^2}\right)-\frac{\hbar^2(m_e^2+m_h^2)}{m_e^2m_h^2a^2}\right\}\frac{exp(-\chi^2/\alpha^2)}{|\alpha|\chi}\\ &+\frac{M\hbar\omega_0e^2(D_c^{op}-D_v^{op})^2}{8\pi cn\varepsilon_0\eta\mu\hbar\mu^2}\frac{\sin^2(\gamma)}{\chi}\int_0^{2\pi}\frac{d\theta}{\sqrt{\hbar^2k^2\cos^2\theta+2M\hbar\omega_0(\chi-1)}}\times\\ &\left\{\frac{q_5^4}{\frac{\hbar^4}{4M^2}(q_5^2+2kq_5\cos\theta)^2-(\hbar\omega_0)^2}+\frac{q_6^4}{\frac{\hbar^4}{4M^2}(q_6^2+2kq_6\cos\theta)^2-(\hbar\omega_0)^2}\right\}\end{aligned} \tag{3.75}$$

where

$$\begin{cases} q_5 &= -Kcos\theta+\frac{1}{\hbar}\sqrt{\hbar^2K^2\cos^2\theta+2M\hbar\omega_0(\chi-1)}\\ q_6 &= -Kcos\theta-\frac{1}{\hbar}\sqrt{\hbar^2K^2\cos^2\theta+2M\hbar\omega_0(\chi-1)}\end{cases} \tag{3.76}$$

This leads to:

$$\Gamma(\chi) = \frac{e^2\sqrt{\pi}}{cn\varepsilon_0\hbar(\hbar\omega_0)^2}\left\{\frac{2\hbar^2}{M^2}\left(k^2+\frac{1}{l_B^2}\right)-\frac{\hbar^2(m_e^2+m_h^2)}{m_e^2m_h^2a^2}\right\}\frac{exp(-\chi^2/\alpha^2)}{|\alpha|\chi}+\frac{Me^2(D_c^{op}-D_v^{op})^2}{8\pi cn\varepsilon_0\eta\mu\hbar(\hbar\omega_0)\mu^2}\times \frac{\sin^2(\gamma)}{\chi^2(\chi-2)}\int_0^{2\pi}d\theta\frac{16k^4\cos^4\theta+32M\hbar\omega_0(\chi-1)k^2\cos^2\theta/\hbar^2+4M^2(\hbar\omega_0)^2(\chi-1)^2/\hbar^4}{\sqrt{\hbar^2k^2\cos^2\theta+2M\hbar\omega_0(\chi-1)}} \tag{3.77}$$

The final expression of the absorption coefficient is obtained by integrating the previous equation over $\theta$ . It is proportional to the photon incidence, the photon frequency, the magnetic length and the TMDC parameters. Also, one can observe that the optical absorption coefficient does not depend of the electric field ($E_i$) induced by the incident light.

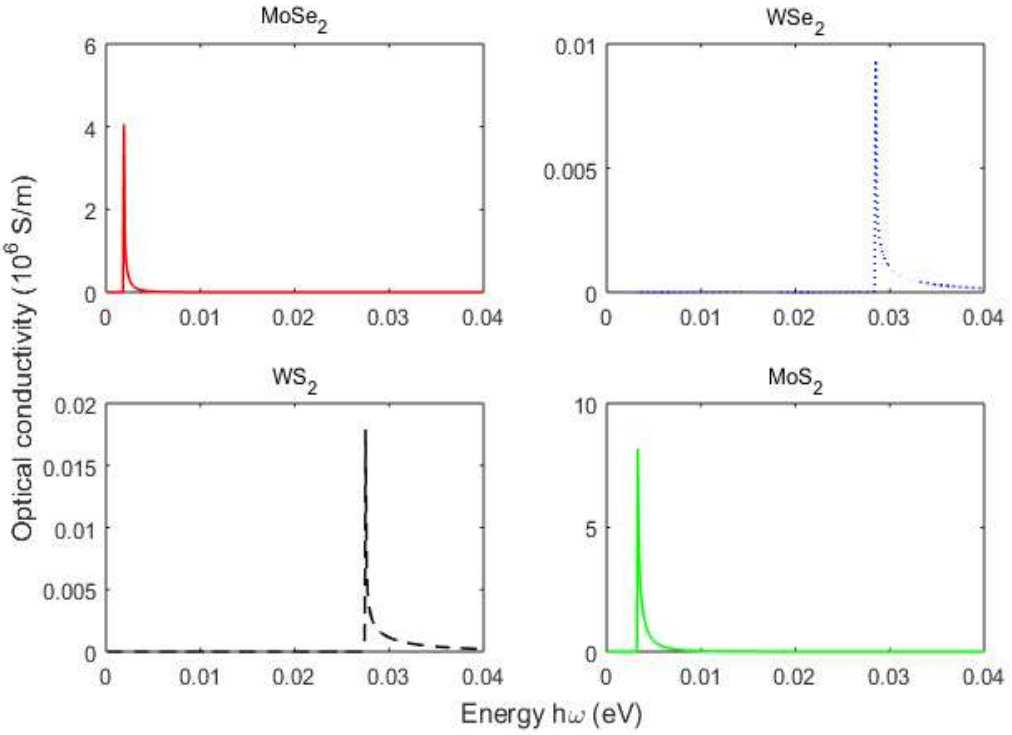


Figure 3.23: Imaginary part of the optical conductivity as function of the frequency for selected TMDCs.

Figure 3.23 presents the real part of optical conductivity as a function of the frequency for different monolayer TMDCs. The highest optical conductivity is obtained for $MoS_2$. It is shown that the conductivity appears when the system absorbs the phonon and this is observed by the appearance of the peak which characterizes the first relaxed excited state. From Eqs. (3.65) and (3.66), one can see that the optical conductivity is inversely proportional to the frequency and then it falls when the frequency is increased. This re-

sult is in accordance with that obtained by previous authors [116, 148]. It is noticed that this behavior is observed for all materials but the optical conductivity starts at a different value of frequency for each material showing the difference of vibration in these TMDCs. $MoS_2$ and $MoSe_2$ are interesting for optical conductivity because of their high magnitudes and it occurs at low frequencies.

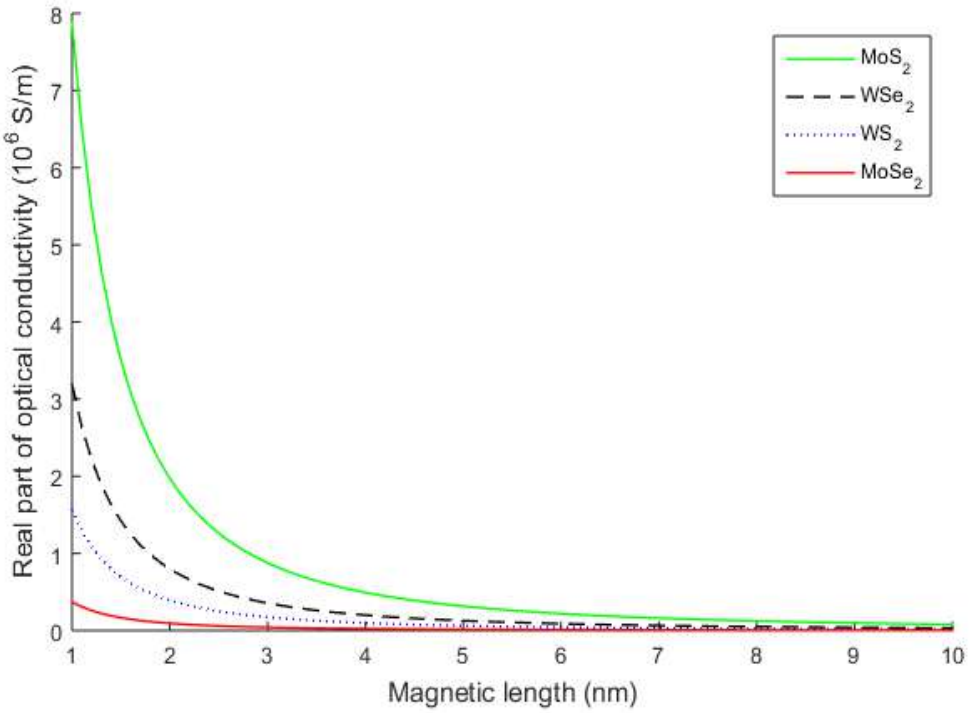


Figure 3.24: Optical conductivity real part as function of the magnetic length for $\hbar = 0.1eV$ and $E_{el} = 0$.

Moreover, the particles are well confined in the presence of the magnetic barrier favoring the growth of their energies. The increase of the magnetic length has the effect of reduce the exciton-polaron energy, then decreasing the optical conductivity as pointed in Figure 3.24.

Also, the presence of the electric field modifies the Coulomb force between electrons and holes reducing the exciton binding energy. In addition, according to Eq. (3.15) it is seen that the increase of the electric field leads to the decrease of the system energy. Therefore, the electric field doesn't favor the optical transitions. The negative sign in Figure 3.25 is justified by the dominance of the electric field effect against the magnetic barrier.

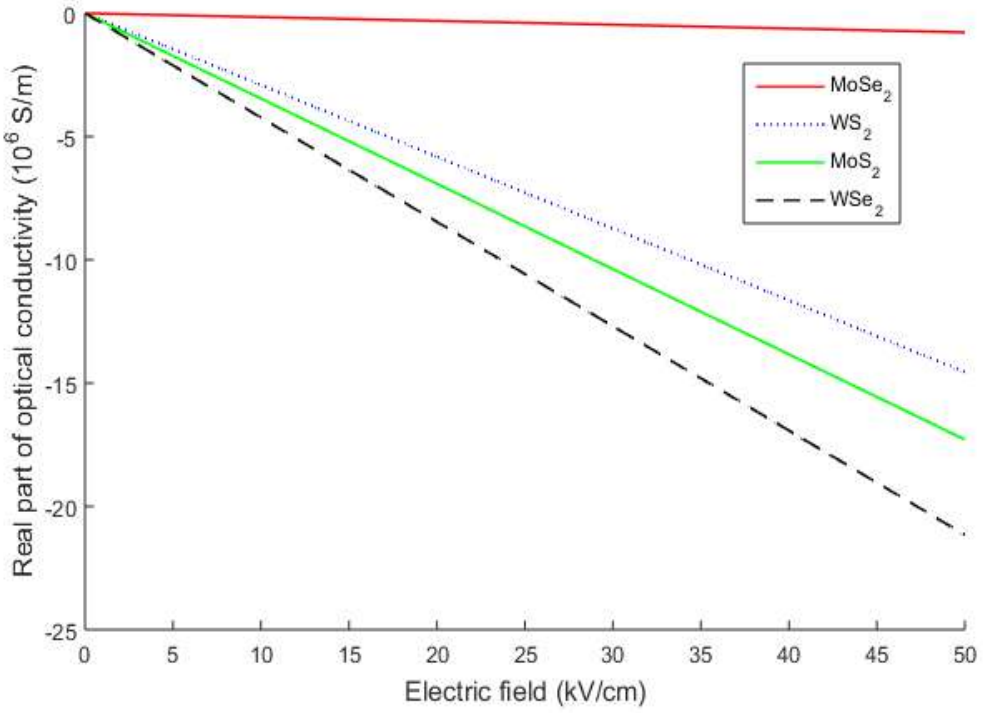


Figure 3.25: Optical conductivity real part as function of the electric field for $l_B = 2nm$ and $\hbar = 0.1eV$.

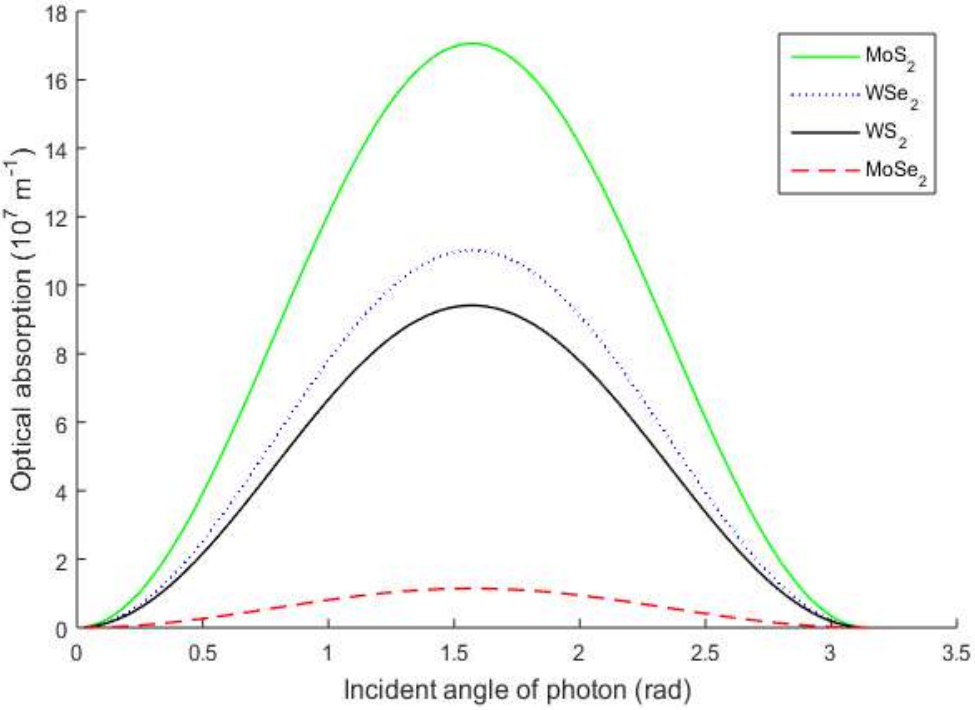


Figure 3.26: Optical absorption as function of the photon incidence angle for $\chi = 2.01$ , $l_B = 10nm$ and $E_{el} = 0$.

Figure 3.26 displays the behavior of the optical absorption coefficient as function of the photon incidence. The optical absorption coefficient is highest for $MoS_2$. It is observed that the peak of absorption appears at $\gamma = \pi/2$ corresponding to the incident photon in the plane. In fact, for this value of the angle, the total strength of the field induced by incident photon interactes with exciton-polaron in TMDC materials. Also, the lowest absorption of photon by exciton-polaron is obtained for incidence normal to the plane. The result indicates that as the angle varies from the normal to $\pi/2$, the stronger the interaction with photon and then increases the probability of absorbing photon.

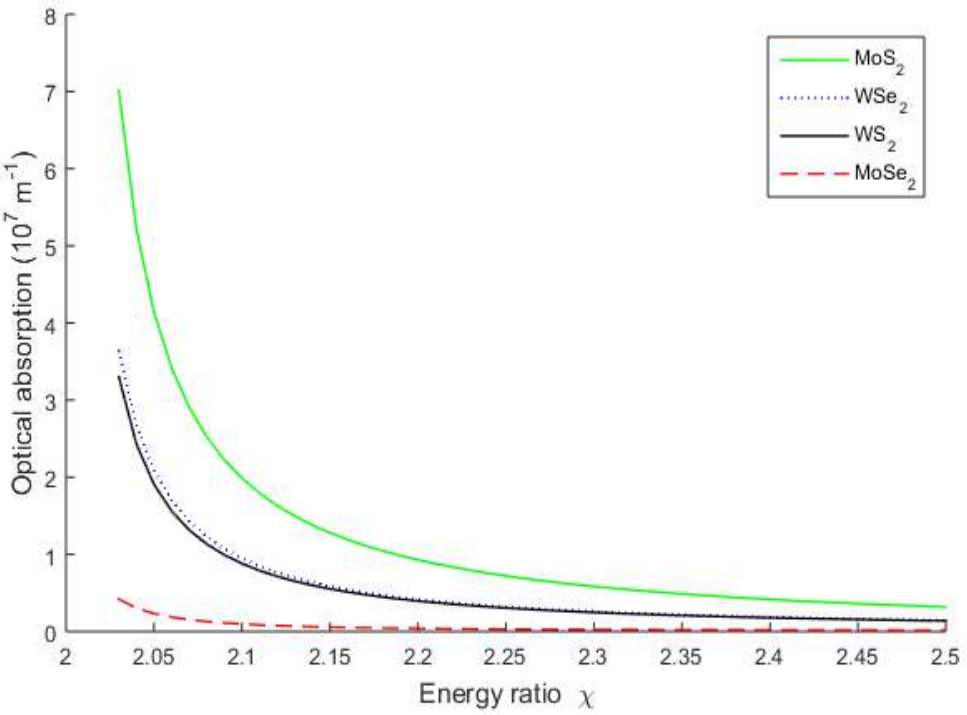


Figure 3.27: Optical absorption versus energy of incident photons for $l_B = 10nm$ and $\gamma = \pi/2$.

Figure 3.27 plots the optical absorption coefficient versus the energy of incident photon for different 1L TMDC materials. From Eq. (3.77), it is convenient to take $\chi > 1 - \left(\hbar^2 K^2 \cos^2\theta / 2M\hbar\omega_0\right)$ due to the presence of the square root. For $\chi < 2$ i.e $\hbar\Omega < 2\hbar\omega_0$ the exciton-polaron doesn't absorb. The absorption of light by exciton-polaron starts when the photon energy is more than twice phonon energy $\chi > 2$. Then, we observe a peak characterising the first relaxed excited state and a decrease when enhances

the photon energy. For the polaron, the absorption occurs when $\hbar\Omega = \hbar\omega_0$ as shown Li et al [113]. The exciton-polaron need more energy to absorb than polaron, this can be due to the presence here of hole-phonon and electron-phonon interactions. This is in agreement with the recent work of Kenfack et al [149] and the experimental one of Lengers et al [150]. Also, the coherence of the system is observed for $\chi > 2.5$.

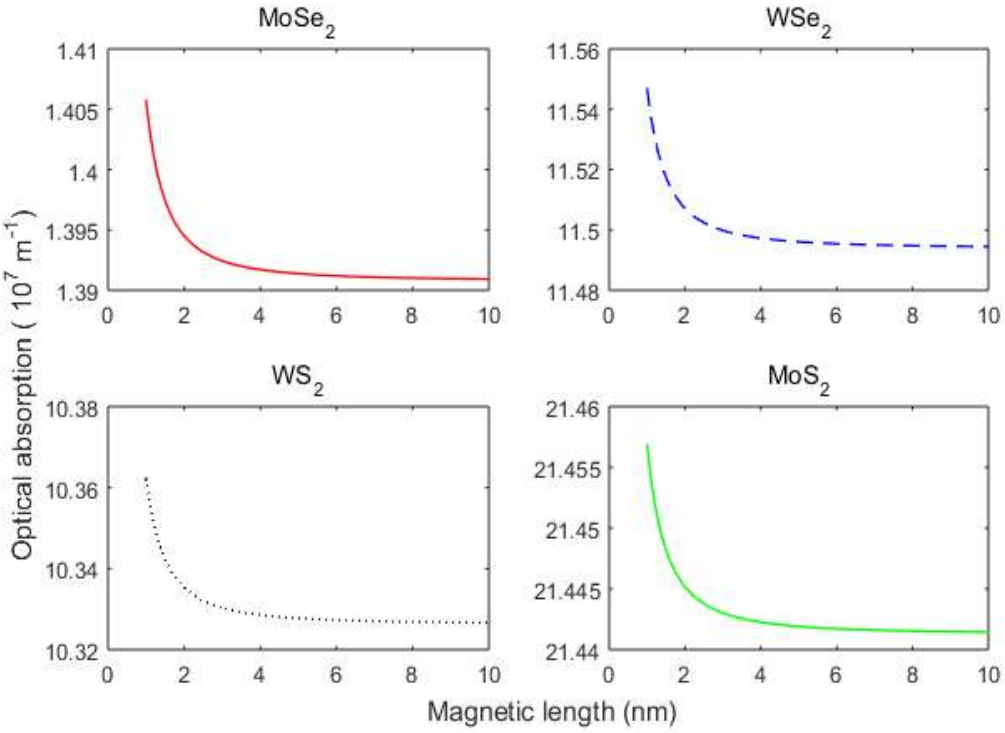


Figure 3.28: Optical absorption as function of the length scale ($l_B$) of the barrier for $\chi = 2.01$ and $\gamma = \pi/2$.

Figure 3.28 presents the reduction of the optical absorption with the increase of magnetic length since it is proportional to $1/(l_B^2)$ as shows Eq. (3.77). The spectra of absorption in 1Ls TMDCs exhibits strong signatures of the unusually pronounced exciton-polaron interference in such materials of short magnetic length. This good absorption at low magnetic length delivers a useful utility for quantifying absorption spectra in popular monolayers materials. This result is in agreement with existing theoretical explanations of optical devices that are focused mainly on basic excitonic resonances by using a simple Wannier scheme for correlated electron-hole couples [151, 152] or the Ab-initio Bethe-Salpeter equation [153, 154]. But in these works, the linear form of the excitonic resonance tends to be incorporated phenomenologically like a Lorentzian. As the source of line forms is diverse [155], some works are

dedicated to the description of the impact of excitonic phonon interaction [156]. Here, we add the influence of magnetic barrier on the spectra since the presence of magnetic field enhances the probability of absorbing the photon by exciton-polaron in the ground state. Thus, the results show that as the electron and hole need more phonon energy to absorb light, the absorption can be adjusted by the magnetic barrier.

## Conclusion

In this chapter, we have displayed analytical and numerical results of relaxation and conductive properties of exciton-polaron in four 1L TMDCs. We first describe the exciton-polaron system in TMDCs. Then, we have investigated some properties necessary to explore this topic. We have evaluated the energies (ground and first excited states), the entropy of the defined system, the lifetime and the relaxation time of exciton-polaron, the electrical conductivity, the Seebeck coefficient, the optical conductivity and the optical absorption coefficient. The influence of both magnetic and electric fields have been shown and a comparison is made among the selected compounds: $MoSe_2$, $MoS_2$, $WSe_2$ and $WS_2$.

# GENERAL CONCLUSION

In this thesis, we investigated the relaxation and conductivity of exciton-polaron in 1L TMDCs under a magnetic barrier and an electric field. This was done for four different TMDC compounds $MoSe_2$ , $WSe_2$ , $WS_2$ and $MoS_2$ for comparison. We showed the effect of the temperature, the magnetic field and the electric field on each property. In this way, we first explore the dynamic of exciton-polaron to understand the behavior of this quasiparticle. In addition, we look at the formation and the relaxation of exciton-polaron in the perturbed system. Moreover, we have evaluated the transport properties through electrical conductivity, Seebeck coefficient, optical conductivity and optical absorption coefficient.

Concerning the dynamic of exciton-polaron, we have quantified the 2D exciton energy to obtain suitable ground state and first excited state energies of exciton-polaron in TMDCs by combining the variational method and the 2D theory. This energy decreases as well as increases the magnetic length. Then the exciton-polaron is confined in the magnetic barrier with lower magnetic length. However, the interplay that links the electron-hole pair is weak as we apply electric field and therefore the electric field has the effect of reduce the energy of exciton-polaron. The highest energy is obtained for $WS_2$ and the lowest for $MoSe_2$. This favorable energy could have impact on other properties of the system. For the entropy, there is no entropy in the exciton-polaron system at zero temperature. It increases with the temperature and then the disorder increases as the temperature enhances in the material and there is loss of information in the system. From $T > 25K$ it remains constant and the thermodynamic equilibrium is reached for all TMDCs. Contrary to the energy, the highest entropy is observed in $MoSe_2$ and the lowest in $WS_2$. One can see that the more the system is confined or energetic and the less

there is disorder in the system. This justify the increases of the entropy with magnetic length and its decrease in electric field.

For the exciton-polaron formation, we showed that the greatest value of lifetime is observed at zero temperature and it decreases as increases the temperature in TMDCs. For high value of temperature, the lifetime vanishes and we suspect then the appearance of either exciton or polaron. Also, the exciton-polaron lifetime decreases when enhance the magnetic length and the electric field. It means that the quasiparticle has long lifetime in the magnetic barrier with low magnetic lengths and for weak electric fields. This condition adheres with the results on dynamics of exciton-polaron. $WS_2$ has the highest lifetime.

The relaxation time is a decreasing function of the temperature. One can say that due to temperature, the exciton interacts with more phonons and then it takes few time to reach the equilibrium. In addition, increasing the concentration of carriers leads to a cooling, opposes the previous effect of temperature and increases the relaxation time up to a critical value around $6,35.10^{12} cm^{-2}$ . However, the relaxation increases when increase the magnetic length and the electric field. In fact, the magnetic barrier influence on exciton-polaron is greater for low values of the magnetic length which is inversely proportional to magnetic field while electric field causes relaxation by perturbing the system.

For the electrical properties in TMDCs, we found that the electrical conductivity decreases when increase the temperature and it increases with the system's energy, the carriers concentration, the magnetic length of the barrier and the electric field. In fact, at low temperature $T < 25K$, the electronic transitions are possible but high temperatures (which also means high entropy) much act as a disturbance for these movements. Moreover, the electron to jump towards the conduction band needs energy to overcomes the band gap. This explains the increase of this property with the system energy, with electric field and magnetic barrier. In addition, as the concentration of carriers grows the electrons move gradually to the conduction band and the highest electrical conductivity is observed in $MoSe_2$.

The Seebeck coefficient increases as function of the temperature up to a peak and then it decreases. We observed that electrons highly contribute to this property seen the dominance of negative values. The magnetic dependence globally presents two ranges: low magnetic lengths $l_B < 2.5nm$ (great magnetic strength) in which the Seebeck coefficient decreases and high magnetic lengths $l_B > 2.5nm$ (weak magnetic strength) in which it increases. Then as the temperature is applied, it meets the particles bound in the 2D material and a challenge occurs. This explains the changes of the curve. However, the motion of hot carriers responsible of Seebeck coefficient is perturbed by the presence of the external electric field, then decreases the Seebeck coefficient. $MoSe_2$ presents the best performance for thermoelectric properties.

We show that the frequency dependence on optical conductivity is crucial to the study of materials. The optical conductivity begins at a value of the frequency characterized by a peak and then it decreases as the frequency enhances. In fact, as the frequency increases, we observed the peak of absorption in order for $MoSe_2$,$MoS_2$, $WS_2$ and $WSe_2$. Also, the optical conductivity decreases when increase the magnetic length and the electric field. In addition, the optical absorption coefficient is more important when photons reach with an incidence near to the TMDC surface. The absorption decreases with the increase of incident light energy. Nevertheless, the light absorption by exciton-polaron begins when the photon energy is more than twice phonon energy ($\hbar\Omega > 2\hbar\omega_0$). This is due to the presence of both electron and hole in the system. Since the system needs more energy for absorption, then the magnetic barrier can contribute to improve the process of absorption. Among the selected TMDCs, $MoS_2$ is the best for optical transport properties.

This thesis provides data able to improve the transport properties in 1L TMDCs and particular the conductivity. It highlights the environment influence on the relaxation and the conductivity. The temperature effect confers to this material a great capacity of thermoelectricity. The magnetic barrier and the external electric field can be used to adjust the TMDC performance. It is useful for the improvement of electronic, thermoelectric and optic de-

vices.

Nevertheless, there still have some ideas which we think can be the subject of future works:

* For this study, we have taken the width of the magnetic barrier $L = 150nm$. We can explore the effect of varying this parameter on the exciton-polaron properties.

* Investigate the influence of a substrate on our conductive properties.

* Study the Peltier effect in TMDCs.

# BIBLIOGRAPHY


[1] Geddo, and G. Iadonisi (1990), Polaronic effects on two-dimensionnal excitons, *Nuovo Cimento D*, **12**: 1641-1650.

[2] Y. J. C. Koteles (1988), Exterimental exciton binding energies in GaAs/$Ga_{1-x}Al_x$ as quantum wells as a function of well width, *Phys. Rev. B*, **37**: 6332

[3] V. Jankovic, and N. Vukmirovic (2015), Dynamics of exciton formation and relaxation in photoexcited semiconductors, *Phys. Rev. B*, **92**: 235208.

[4] S. Brem, M. Selig, G. Berghaeuser, and E. Malic (2018), Exciton relaxation cascade in two-dimensional transition metal dichalcogenides, *Scientific Reports*, **8**: 8238.

[5] V. A. Maidannyk, and Y. H. Roos (2016), Modification of the WLF model for characterization of the relaxation time temperature relationship in trehalose-whey protein isolate systems, *J. Food. Eng.*, **188**: 21-31.

[6] I. Singh , S. Madan , A. Kaur , J. Kumar , P. K. Bhatnagar , and P. C. Mathur (2014), Study of relaxation dynamics of photogenerated excitons in $CuInS_2$ quantum dots, *MRS Communications*, **4**: 1-5 .

[7] L. Foglia, S. Vempati , B. T. Bonkano, L. Gierster , M. Wolf , S. Sadofev , and J. Stahler (2019), Revealing the competing contributions of charge carriers, excitons and defects to the non-equilibrium optical properties of ZnO, *Struct Dyn*, **6** : 034501.

[8] A. O. El-Ballouli, E. Alarousu, A. Usman, J. Pan, O. M. Bakr, and O. F. Mohammed (2014), Real time observation of ultrafast intraband relax-

ation and exciton multiplication in PbS quantum dots, *ACS Photonics*, **1**: 285-292.

[9] H. Khoirunnisa, and M. A. Majidi (2018), Exploring excitonic signal in optical conductivity of ZnO through first order electron hole vertex correction, *International Conference on Theoretical and Applied Physics*, **1011**: 012073.

[10] R. W. Havener, Y. Liang , L. Brown , L. Yang , and J. Park (2014), Van Hove singularities and excitonic effects in the optical conductivity of twisted bilayer graphene, *Nano. Lett.* **14**: 3353-3357

[11] H. Haug, and S. W. Koch (1989), Semiconductor laser theory with many body effects, *Phys. Rev. A*, **39**: 1887.

[12] C. Ell , R. Blank , S. Benner , and H. Haug (1989), Simplified calculations of the optical spectra of two and three dimensional laser excited semiconductors, *J. Opt. Soc. Am. B*, **6**: 2006-2012.

[13] N. M. R. Peres, R. M. Ribeiro, and A. H. C. Neto( 2010), Excitonic effects in the optical conductivity of gated graphene, *Phys. Rev. Lett.*, **105**: 055501.

[14] A. Kormányos, V. Zolyomi, Drummond, N. Drummond, and G. Burkard (2014), Spin-orbit coupling, quantum dots, and qubits in monolayer transition metal dichalcogenides, *Phys. Rev. X*, **4**: 011034.

[15] Song, Xiang-Xiang, Liu, Di, Mosallanejad, Vahid, You, Jie, Han, Tian-Yi, Chen, Dian-Teng, Li, Hai-Ou, Cao, Gang, Xiao, Ming, Guo, Guang-Can, Guo, and Guoping (2015), A gate defined quantum dot on the two-dimensional transition metal dichalcogenide semiconductor $WSe_2$, *Nanoscale*, **7**: 16867-16873

[16] A. J. Pearce, and G. Burkard (2017), Electron spin relaxation in a transition metal dichalcogenide quantum dot, *2D Mater*, **4**: 025114.

[17] G. Fiori, F. Bonaccorso, G. Iannccone, T. Palacios, D. Neumaier, A. Seabaugh, S. K. Banerjee, and L. Colombo (2014), Electronics based on two-dimensional materials, *Nat. Nanotechnol.*, **9**: 768-779.

[18] M. Bernardi, C. Ataca, M. Palummo, and J. C. Grossman (2017), Optical and electronic properties of two-dimensional layered materials, *Nanophotonics*, **6**: 479.

[19] K. F. Mak, K. He , C. Lee , G. H. Lee , J. Hone , T. F. Heinz , and J. Shan (2013), Tightly bound trions in monolayer $MoS_2$, *Nat. Mater.* , **12**: 207- 211.

[20] D. Y. Qiu , T. Cao , and S. G. Louie (2015), Nonanalyticity, valley quantum phases, and lightlike, exciton dispersion in monolayer transition metal dichalcogenides: theory and first-principles calculations, *Phys. Rev. Lett.*, **115**: 176801.

[21] L. Yang , C. Xie , J. Jin , R. A. Nauman , C. Feng , P. Liu , and B. Xiang (2018), Properties, preparation and applications of low dimensional transition metal dichalcogenides, *Nanomaterials*, **8**: 463

[22] P. Dey, L. Yang , C. Robert, G. Wang, B. Urbaszek, X. Marie, and S. A. Crooker (2017), Gate controlled spin valley locking of resident carriers in $WSe_2$ monolayers, *Phys. Rev. Lett.*, **119**: 13.

[23] S. Ono, and T. Ogura (2018), Anomalous energy shift of laterally confined two dimensional excitons, *J. Appl. Phys.*, **124**: 034301.

[24] Akay D (2018), Trigonal warping and photo-induced effects on zone boundary phonon in monolayer graphene, *Superlattices and Microstructures*, **117**: 18-24.

[25] Akay D (2021), Manipulating electronic dynamics of 8-Pmmn borophene with surface optical phonons, *Semicond. Sci. Technol.*, **36** : 045001.

[26] B. S. Kandemir, and D. Akay (2018), Photoinduced dynamical band gap in graphene: the effects of electron-phonon and spin-orbit interaction, *Phys. Stat. Solidi. B*, **255**: 10 1800163.

[27] A. Thilagam (2015), Excitonic polarons in low dimensional transition metal dichalcogenides, *Physica B Condensed Matter*, **464**: 44-50.

[28] S. Yang , S. Tongay , Y. Li , Q. Yue , J-B. Xia , S-S. Li ,J. Li , and S-H. Wei (2014), Layer-dependent electrical and optoelectronic responses of $ReSe_2$ nanosheet transistors, *Nanoscale*, **6**: 7226-7231.

[29] R. S. Chen, C. C. Tang, W. C. Shen, and Y. S. Huang (2014), Thickness-dependent electrical conductivities and ohmic contacts in transition metal dichalcogenides multilayers, *Nanotechnology*, **25**: 415706.

[30] D. Qin, P. Yan, G. Ding, X. Ge, H. Song, and G. Gao (2018), Monolayer $PdSe_2$ a promising two-dimensional thermoelectric material, *Sci. Rep.*, **8**: 2764.

[31] Y. Ge, W. Wenhui, R. Yulu, and L. Yong (2020), Large thermoelectric power factor of high mobility transition metal dichalcogenides with 1T phase, *Phys. Rev. Res.*, **2**: 013134.

[32] M. Van der Donck, M. Zarenia, and F. M. Peeters (2018), Excitons, trions, and biexcitons in transition-metal dichalcogenides: Magnetic-field dependence, *Phys. Rev. B*, **97**: 195408 .

[33] N. Seung-il (2012), Electrical conductivity of quark matter at finite T under external magnetic field, *Phys. Rev. D*, **86**: 033014.

[34] A. Das, H. Mishra , and R. K. Mohapatra (2020), Magneto-Seebeck coefficient and Nernst coefficient of a hot and dense hadron gas, *Phys. Rev. D*, **102**: 014030.

[35] M. Tahir, P. Vasilopoulos, and F. M. Peeters (2015), Magneto-optical transport properties of monolayer phosphorene, *Phys. Rev. B*, **92**: 045420.

[36] S. Chaudhary, Christina Knapp, and G. Refael (2021), Anomalous exciton transport in response to a uniform in-plane electric field, *Phys. Rev. B*, **103**: 165119.

[37] A. Balocchi, Q. H. Duong, P. Renucci, B. Liu, C. Fontaine, T. Amand, D. Lagarde, and X. Marie (2011), Full electrical control of the electron spin relaxation in GaAs quantum wells, *Phys. Rev. Lett.*, **107**: 136604.

[38] E. Kasapoglu, H. Sari, M. Bursal, and I. Sokmen (2003), Exciton absorption in quantum-well wires under the electric field, *Physica E*, **16**: 237-243.

[39] E. M. Proupin, and C. T. Giner (2004), Electric-field and exciton structure in CdSe nanocrystals, *Phys. Rev. B*, **69**: 125336.

[40] I. E. Tamm (1930), Eine bemerkung zur diracschen theorie der lichterstroung und dispersion, *Phys. Z.*, **65**: 705-708.

[41] L. Landau (1933), On the motion of electrons in a crystal lattice, *Phys. Z. Sowjetunion*, **3**: 664-665.

[42] H. Fröhlich (1954), Electrons in lattice fields, *Advances in Physics*, **3**: 325-361.

[43] T. Holstein (1959), Studies of polaron motion: Part II, The small polaron, *Annals of physics*, **8**: 343-389.

[44] J. T. Devreese (1996), Polarons, *Encycl. Appl. Phys.*, **14**: 383-409.

[45] J. Sak (1972), Theory of surface polarons, *Physical Review B*, **6**: 3981.

[46] H. Y. Zhou, and S. W. Gu (1994), Strong coupling polaron in quantum well wire, *Solid state communications*, **91**: 725-729.

[47] S. D. Sarma, and B. Mason (1985), Optical phonon interaction effects in layered semiconductor structures, *Annals of Physics*, **163**: 78-119.

[48] H. Fröhlich (1937), Theory of electrical breakdown in ionic crystals, *Proceedings of the Royal Society of London. Series A-Mathematical and Physical Sciences*, **160**: 230-241.

[49] H. Fröhlich (1949), Theory of dielectrics, *Clarendon Press*, Oxford.

[50] T. Lee, F. Low, and D. Pines (1953), The motion of slow electrons in a polar crystal, *Physical Review B*, **90**: 297.

[51] S. I. Pekar (1954), Untersuchungen über die Elektronentheorie der Kristalle, Übers. aus dem Russichen von Helmut Vogel., Akademieverlag.

[52] W. Huybrechts (1976), Note on the ground-state energy of the feynman polaron model, *Journal of Physics C: Solid State Physics*, **9** : 211.

[53] U. Bockelmann, and G. Bastard (1990), Phonon scattering and energy relaxation in two, one and zero-dimensional electron gases, *Phys. Rev. B*, **42**: 8947.

[54] F. Comas, C. Trallero-Giner, and R. Riera (1989), LO-phonon confinement and polaron effect in a quantum well, *Physical Review B*, **39**: 5907.

[55] K. D. Zhu, and T. Kobayashi (1994), Magnetic field effects on strong-coupling polarons in quantum dots, *Physics Letters A*, **190**: 337-340.

[56] D. M. Larsen (1986), Perturbation theory for the two-dimensional polaron in a magnetic field, *Physical Review B*, **33**: 799.

[57] J. Devreese, E. Kartheuser, R. Ward, and A. Baldereschi (1973), Effect of internal excitations of polarons on magneto-optical absorption and cyclotron resonance in polar crystals, *physica status solidi (b)*, **59**: 629-640.

[58] J. Cibert, P. Petroff, G. Dolan, S. Pearton, A. Gossard, and J. English (1986), Optically detected carrier confinement to one and zero dimension in gaas quantum well wires and boxes, *Applied Physics Letters*, **49**: 1275-1277.

[59] A. Erçelebi, and R. Senger (1996), Ground-state description of quasi-one-dimensional polarons with arbitrary electron-phonon coupling strength, *Physical Review B*, **53**: 11008.

[60] R. Senger, and A. Erçelebi (1998), Q1d-polarons in rigid boundary cylindrical wires, *Turkish Journal of physics*, **22**: 169-180.

[61] G. Q. Hai, F. Peeters, and J. Devreese (1990), Polaron energy and effective mass in a quantum well, *Physical Review B*, **42**: 11063.

[62] S. W. Koch, M. Kira, G. Khitrova, and H. M. Gibbs (2006), Semiconductor excitons in new light, *Nat. Mater.*, **5**: 523-531.

[63] J. Bardeen, and W. Shockley (1950), Deformation potentials and mobilities in non-polar crystals, *Phys. Rev.*, **80**: 72.

[64] Singh (1994), Excitation energy transfer processes in condensed matter, New York Plenum.

[65] S. Shree, M. Semina, C. Robert, B. Han, T. Amand, A. Balocchi, M. Manca, E. Courtade, X. Marie, T. Taniguchi, K. Watanabe, M. M. Glazov, and B. Urbaszek (2018), Observation of exciton phonon coupling in $MoSe_2$ monolayers, *Phys. Rev. B*, **98**: 035302.

[66] D. Li, C. Trovatello, S. D. Conte, M. Nub, G. Soavi, G. Wang, A. C. Ferrari, G. Cerullo, amd T. Brixner (2021), Exiton phonon coupling strength in single layer $MoSe_2$ at room temperature, *Nature Communications*, **12**: 954.

[67] G. Antonius, and S. G. Louie (2022), Theory of exciton-phonon coupling, *Phys. Rev. B*, **105**: 085111.

[68] R. Heitz, M. Veit, N. N. Ledentsov, A. Hoffmann, D. Bimberg, V. M. Ustinov, P. S. Kopev, and Z. I. Alferov (1997), Energy relaxation by multiphonon processes in InAs/GaAs quantum dots, *Phys. Rev. B*, **56**: 10435.

[69] H. Benisty, C. M. Sotomayor-Torres, and C. Weisbuch (1991), Intrinsic mechanism for the poor luminescence properties of quantum-box systems, *Phys. Rev. B*, **44**: 10945 .

[70] T. Inoshita, and H. Sakaki (1992), Electron relaxation in a quantum dot : Significance of multiphonon processes, *Phys. Rev. B*, **46**: 7260.

[71] S. Sauvage, P. Boucaud, R. P. S. M. Lobo, F. Bras, G. Fishman, R. Prazeres, F. Glotin, J. M. Ortega, and J. M. Gerard (2002), Long polaron lifetime in InAs/GaAs self-assembled quantum dots, *Phys. Rev. Lett.*, **88**: 177402.

[72] E. A. Zibik, L. R. Wilson, R. P. Green, G. Bastard, R. Ferreira, P. J. Phillips, D. A. Carder, J. P. R. Wells, J. W. Cockburn, M. S. Skolnick, M. J. Steer, and M. Hopkinson (2004), Intraband relaxation via polaron decay in InAs self-assembled quantum dots, *Physical Review B*, **70**: 161305.

[73] X. Q. Li, H. Nakayama, and Y. Arakawa (1999), Phonon bottleneck in quantum dots : Role of lifetime of the confined optical phonons, *Phys. Rev. B*, **59**: 5069.

[74] O. Verzelen, R. Ferreira, and G. Bastard (2000), Polaron lifetime and energy relaxation in semiconductor quantum dots, *Phys. Rev. B*, **62**: R4809.

[75] L. Jacak, J. Krasnyj, D. Jacak, and P. Machnikowski (2002), Anharmonicity-induced polaron relaxation in GaAs/InAs quantum dots, *Phys. Rev. B*, **65**: 113305.

[76] D. Timmerman, I. Izeddin, P. Stallinga, I. N. Yassievich, and T. Gregorkiewicz (2008), Space-separated quantum cutting with silicon nanocrystals for photovoltaic applications, *Nature Photonics*, **2** : 105.

[77] S. Wang, M. Khafizov, X. Tu, M. Zheng, and T. D. Krauss (2010), Multiple exciton generation in single-walled carbon nanotubes, *Nano Letters.*, **10**: 23812386.

[78] K. J. Tielrooij, J. C. W. Song, S. A. Jensen, A. Centeno, A. Pesquera, E. Zurutuza, M. Bonn, L. F. Levitov, and F. H. L. Koppens (2013), Photoexcitation cascade and multiple hot-carrier generation in graphene, *Nature Physics*, **9**: 248-252.

[79] A. T. Burkov, A. I. Fedotov, and S. V. Novikov (2016), Methods and apparatus for measuring thermopower and electrical conductivity of thermoelectric materials at high temeratures, *Thermoelectrics for power generation - A look at trends in the technology*,**15**: 353-389.

[80] T. M. Tritt, and M. A. Subramanian (2006), Thermoelectric materials - phenomena and applications: a bird's eye view , *MRS Bulletin*, **31**: 188-198.

[81] P. D. Pietro (2013), Optical properties of Bismuth-based topological insulators, *Springer International Publishing*, ISBN 9783319019918 p. 64.

[82] H. N. Singh (2000), Handbook of advanced electronic and photonics materials and devices, *Elsevier Science*, **10**: p.66.

[83] Y. Xiao, Z. Q. Li, and Z. W. Wang (2017), Polaron effect on the bandgap modulation in monolayer transition metal dichalcogenides, *J. Phys. Condens. Matter*, **29**: 485001.

[84] D. Golberg (2011), Nanomaterials: Exfoliating the inorganics, *Nature Nanotechnology*, **6**: 200.

[85] J. Brent, N. Savjani, and P. O'Brien (2017), Synthetic approaches to two-dimensional transition metal dichalcogenide nanosheets, *Progress in Materials Science*, **89**: 411-478.

[86] S. Ayari, A. Smiri, A. Hichri, S. Jaziri, and T. Amand (2018), Radiative lifetime of localized excitons in transition-metal dichalcogenides, *Phys. Rev. B*, **98**: 205-430.

[87] J. V. Nguepnang, C. Kenfack-Sadem, A. Kenfack-Jiotsa, C. Guimapi, A. J. Fotue, and A. E. Merad (2021), Electron-phonon coupling contribution on the optical absorption and the dynamic of exciton-polaron in monolayer transition meta dichalcogenides, *Opt. Quant. Electron.*, **53**: 654.

[88] S. V. Mandyam, H. M. Kim, and M. Drndic (2020), Large area few-layer TMD film growths and applications, *J. Phys. Mater.*, **3**: 024008.

[89] H. G. Ji, P. S. Fernandez, U. Erkilic, and H. Ago (2021), Stacking orientation-dependent photoluminescence pathways in artificially stacked bilayer $WS_2$ nanosheets grown by chemical vapor deposition: implications for spintronics and valleytronics, *ACS Appl. Nano Mater.*, **4**: 3717-3724.

[90] K. S. Novoselov, A. K. Geim, S. Morozov, D. Jiang, Y. Zhang, S. Dubonos, I. Grigorieva, and A. Firsov (2004), Electric field effect in atomically thin carbon films, *Science*, **306**: 666-669.

[91] K. Novoselov, D. Jiang, F. Schedin, T. Booth, V. Khotkevich, S. Morozov, and A. Geim (2005), Two-Dimensional Atomic Crystals, *Proc. Natl. Acad. Sci. U.S.A.*, **102**: 10451-10453.

[92] B. Radisavljevic, A. Radenovic, J. Brivio, V. Giacometti, and A. Kis (2011), Single-layer $MoS_2$ transistors, *Nature Nanotechnology*, **6**: 147-150.

[93] I. V. Grigorieva, and A. K. Geim (2013), Van der Waals Heterostructures, *Nature*, **499**: 419-425.

[94] N. Perea-Lopez,A. L. Elias, A. Berkdemir, A. Castro-Beltran,H. R. Gutierrez, S. Feng, T. Hayashi, F. Lopez-Urias, S. Ghosh, et al. (2013),

Photosensor Device Based on Few Layered $WS_2$ Films, *Adv. Funct. Mater.*, **23**: 5511-5517.

[95] B. L. Li, J. Wang, H. L. Zou, S. Garaj, C. T. Lim, J. Xie, N. P. Li, and D. T. Leong (2016), Low-dimensional transition metal dichalcogenide nanostructures based sensors, *Advanced Functional Materials*, **26**: 7034-7056.

[96] J. Ping, Z. Fan, M. Sindoro, Y. Ying, and H. Zhang (2017), Recent advances in sensing applications for two dimemsional transition metal dichalcogenide nanosheets and their composites, *Advanced Functional Materials*, **27** : 1605817.

[97] Thilagam (2016), Exciton formation assisted by longitudinal optical phonons in monolayer transition metal dichalcogenides, *J. Appl. Phys.*, **120**: 124306.

[98] V. Shahnazaryan, I. Iorsh, I. A. Shelykh, and O. Kyriienko (2017), Exciton-exciton interaction in transition-metal dichalcogenide monolayers, *Phys. Rev. B*, **96**: 115409.

[99] O. L. Berman, and R. Y. Kezerashvili (2017), Superfluidity of dipolar excitons in a transition metal dichalcogenide double laye, *Phys. Rev. B*, **96**: 094502.

[100] N. D. Hien, C. V. Nguyen, N. N. Hieu, S. S. Kubakaddi, C. A. Duque, M. E. Mora-Ramos, L. Dinh, T. N. Bich, and H. V. Phuc (2020), Magneto-optical transport properties of monolayer transition metal dichalcogenides, *Phys. Rev. B*, **101**: 045424.

[101] C. V. Nguyen, N. N. Hieu, D. Muoi, C. A. Duque, E. Feddi, H. V. Nguyen, L. T. T. Phuong, B. D. Hoi, and H. V. Phuc (2018), Linear and nonlinear magneto-optical properties of monolayer $MoS_2$, *J. Appl. Phys.*, **123**: 034301.

[102] W. Liu, Z. Lin, S. Tian, Y. Huang, H. Xue, K. Zhu, C. Gu, Y. Yang, and J. Li (2021), Plasmonic effect on the magneto-optical property of monolayer WS2 studied by polarized-Raman spectroscopy, *Applied Sciences*, **11**: 1599.

[103] J. Forste, N. V. Tepliakov, S. Y. Kruchinin, J. Lindlau, V. Funk, M. Forg, K. Watanable, T. Taniguchi, A. S. Baimuratov, and A. Hogele (2020), Exciton g-factors in monolayer and bilayer $WSe_2$ from experiment and theory, *Nat. Communications*, **11**: 1-8.

[104] E. Jung, J. C. Park, Y. S. Seo, J. H. Kim, J. Hwang, and Y. H. Lee (2022), Unusually large exciton binding energy in multilayered 2H-$MoTe_2$, *Scientific reports*, **12**: 1-10.

[105] A. J. Chaves, R. M. Ribeiro, T. Frederico, and N. M. R. Peres (2017), Excitonic effects in the optical properties of 2D materials: an equation of motion approach, *2D Materials*, **4**: 025086.

[106] A. V. Stier, N. P. Wilson, K. A. Velizhanin, J. Kono, X. Xu, and S. Crooker (2018), Magneto-optics of exciton Rydberg states in a monolayer semiconductor, *Phys. Rev. Lett*, **120**: 057405.

[107] J. R. D. Djomou, S. C. Kenfack, A. J. Fotue, M. F. C. Fobasso, and L. C. Fai (2018), Contribution of bulk and surface phonons to the properties of polaron in a $Zn_{1-x}Cd_xSe - ZnSe$ heterojunction confined in a triangular potential, *Physica B: Condensed Matter*, **548**: 58-70.

[108] A. Thilagam, and J. Singh (1996), Excitonic polarons in quasi-two-dimensional structures, *Appl. Phys. A*, **62**: 445-450 .

[109] V. K. Kozin, V. A. Shabashow, A. V. Kavokin, and I. A. Shelykh (2021), Anomalous exciton Hall effect, *Phys. Rev. Lett.*, **126**: 036801.

[110] Z. Li (2018), The ground state lifetime of polaron in a two-dimensional quantum pseudodot system, *Indian J. Phys.*, **93**: 707-711.

[111] D. Kozawa, R. Kumar, A. Carvalho, K. K. Amara, W. Zhao, S. Wang, M. Toh, R. M. Ribeiro, A. H. Castro Neto, K. Matsuda, and G. Eda (2014), Photocarrier relaxation pathway in two dimensional semiconducting transition metal dichalcogenides, *Nature communication*, **5**: 4543.

[112] J. T. Devreese (2018), Frohlich polarons: lecture course including detailed theoretical derivations, 8th edition, Antwerpen, Belgium.

[113] P. F. Li, and Z. W. Wang (2018), Optical absorption of Frohlich polaron in monolayer transition metal dichalcogenides, *J. Appl. Phys.*, **123**: 204-308.

[114] G. Pizzi, D. Volja, B. Kozinsky, M. Fornari, and N. Marzari (2014), Boltzwann, a code for the evaluation of thermoelectric and electronic transport properties with a maximally localized Wannier functions basis, *Comput. Phys. Commun.*, **185**: 422-429.

[115] M. J. Tomczak, K. Haule , T. Miyake , A. Georges , and G. Kotliar (2010), Thermopower of correlated semiconductors: application to $FeAs_2$ and $FeSb_2$ , *Phys. Rev. B*, **82**: 085104.

[116] S. Huang, H. J. Liu, D. D. Fan, P. H. Jiang, J. H. Liang, G. H. Cao, R. Z. Liang, and J. Shi (2018), First principle study of the thermoelectric properties of the Zintl compound KSnSb, *J. Phys. Chem. C*, **122**: 4217-4223.

[117] N. Myoung, G. Ihm, and S. Lee (2010), Transport in armchair graphene nanoribbons modulated by magnetic barriers, *Physica E*, **42**: 2808-2811.

[118] S. Ghosh, and M. Sharma (2009), Electron optics with magnetic vector potential barriers in graphene, *J. Phys. Condens. Matter*, **21**: 292204.

[119] G. K. Cong, N. Timothy, and J. Kono (2018), Excitons in magnetic fields, *Encyclopedia of Modern Optics II*, **2**.

[120] R. Khordad, and H. R. R. Sedehi (2018), Study of non-extensive entropy of bound polaron in monolayer graphene, *Indian J. Phys.*, **92**: 979-984.

[121] C. Tsallis (1988), Possible generalization of Boltzmann-Gibbs statistics, *J. Stat. Phys.*, **52**: 479-487 .

[122] A. Splendiani, L. Sun, Y. Zhang, T. Li, J. Kim, C. Y. Chim, G. Galli, and F. Wang (2010), Emerging photoluminescence in monolayer $MoS_2$, *Nano Lett.*, **10**: 1271-1275, .

[123] A. Oukerroum, E. Feddi, J. B. Bailach, J. M. Pastor, F. Dujardin, and E. Assaid (2010), On the anomalous Stark effect in a thin disc-shaped quantum dot, *J. Phys.:Condens. Matter*, **22**: 375301.

[124] I. Niehues, R. Schmidt, M. Druppel, P. Marauhn, D. Christiansen, M. Selig, G. Berghauser, D. Wigger, R. Schneider, L. Braasch, R. Koch, A. Castellanos-Gomez, T. Kuhn, A. Knorr, E. Malic, M. Rohlfing, S. M. de Vasconcellos, and R. Bratschitsch (2018), Strain control of exciton phonon coupling in atomically thin semiconductors, *Nano. Lett.*, **18**: 1751-1757.

[125] M. F. C. Fobasso, A. J. Fotue, S. C. Kenfack, and L. C. Fai (2020), Thermal properties of magnetopolaron in GaAs delta potential under Rashba effect, *Physica E: Low dimensional Systems and Nanostructures*, **118**: 113-941 .

[126] A. A. Mitioglu, K. Galkowski, A. Surrente, L. Klopotowski, D. Dumcenco, A. Kis, D. K. Maude, and P. Plochocka (2016), Magnetoexcitons in large area CVD grown monolayer $MoS_2$ and $MoSe_2$ on sapphire, *Phys. Rev. B*, **93**: 165412.

[127] R. Khordad, H. R. R. Sedehi, and H. Bahramiyan (2018), Simultaneous effects of impurity and electric field on entropy behavior in double cone-like quantum dot, *Commun. Theor. Phys.*, **69**: 95-100.

[128] M. Tiotsop, A. J. Fotue, G. K. Fautso, S. C. Kenfack, E. Mainimo , H. B. Fotsin, and L. C. Fai (2016), Effect of temperature on lifetime and shannon entropy of magnetopolaron in RbCl triangular quantum dot, *Chinese Journal of Physics*, **54**: 795-801 .

[129] Z. X. Li, and J. L. Xiao (2011), Ground state lifetime of strong-coupled polaron in an asymmetric quantum dot, *J. At. Mol. Sci.*, **2**: 74-80.

[130] S. S. Sun (2013), Dynamics of exciton dissociation in donor-acceptor polymer heterojunctions, *J. Chem. Phys.*, **138**: 164905 .

[131] L. Yuanshuang, L. Huanglong, Q. Cuicui, H. Xiangmin, and D. Liu (2020), Layer-dependent signatures for exciton dynamics in monolayer and multilayer $WSe_2$ revealed by fluorescence lifetime imaging measurement, *Nano Reasearch.*, **13**: 661-666 .

[132] N. Zhonghui, S. Yongliang, S. Qin, W. Yuhan, J. Hongzhu, Z. Qijing, C. Yang, M. Yuze, S. Fengqi, and W. Xiaoyong (2019), Tailoring exciton

dynamics of monolayer transition metal dichalcogenides by interfacial electron-phonon coupling, *Communications Physics*, **2**: 103.

[133] Y. J. Zheng, Y. Chen, Y. L. Huang, P. K. Gogoi, M. Y. Li, L. J. Li, P. E. Trevisanutto, Q. Wang, S. J. Pennycook, A. T. S. Wee, and S. Y. Quek (2019), Point defects and localized excitons in 2D $WSe_2$, *ACS Nano*, **13**: 6050-6059.

[134] Q. H. Wang, K. Zadeh, K. Kourosh, C. Andras, N. J. Strano, and S. Michael (2012), Electronics and optoelectronics of two-dimensional transition metal dichalcogenides, *Nature Nanotechnology*, **7**: 699-712 .

[135] M. M. Glazov (2020), Quantum interference effect on exciton transport in monolayer semiconductors, *Phys. Rev. Lett.*, **124**: 166802.

[136] S. Huang, M. Sanderson, J. Tian, Q. Chen, F. Wang, and C. Zhang (2018), Hot carrier relaxation in three dimensional gapped Dirac semimetals, *J. Phys. D Appl. Phys.*, **51**: 015101.

[137] C. Meier, S. Lüttjohann, M. Offer, H. Wiggers, and A. Lorke (2009), Silicon Nanoparticles: Excitonic Fine Structure and Oscillator Strength, *Advances in Solid State Physics*, **48**: 79-90.

[138] H. Xu, J. Wei, H. Zhou, J. Feng, T. Xu, H. Du, C. He, Y. Huang, J. Zhang, Y. Liu, H. C. Wu, C. Gu, X. Wang, Y. Guang, H. Wei, Y. Peng, W. Jiang W, G. Yu, and X. Han (2020), High spin hall conductivity in large-area type II Dirac semimetal $PtTe_2$, *Adv. Mater.*, **32**: 2000513.

[139] S. Meziane, H. I. Faraoun, and C. Esling (2016), The layered transition metal dichalcogenides as materials for storage clean energy: ab initio investigations, *Int. J. Energy Power Eng.*, **10**: 1126539.

[140] D. Wickramaratne, F. Zahid, and R. K. Lake (2014), Electric and thermoelectric properties of few-layer TMDs, *J. Chem. Phys.*, **140**: 124710.

[141] A. Das, H. Mishra, and R. K. Mohapatra (2019), Electrical conductivity and Hall conductivity of a hot and dense hadron gas in a magnetic field: a relaxation time approach, *Phys. Rev. D*, **99**: 094031.

[142] J. V. Nguepnang, A. K. Teguimfouet, C. S. Kenfack, and A. J. Kenfack (2022), Polaron dynamic and decoherence in transition metal dichalcogenides under electric field, *Indian J. Phys.*, **96**: 2001-2010.

[143] J. P. Selvaggi (2019), Modeling the seebeck coefficient for organic materials with the Kubo-Greenwood integral and a Gaussian density of states, *Journal of Computational Electronics*, **18**: 473-481.

[144] S. Ashraf, V. Forsberg, C. G. Mattsson, and G. Thungström (2019), Thermoelectric properties of n-type molybdenum disulfide $MoS_2$ thin film by using a simple measurement method, *Materials*, **12**: 3521.

[145] B. Skinner, and L. Fu (2018), Large nonsaturating thermopower in a quantizing magnetic field, *Sci. Adv.*, **4**: eaat2621.

[146] J. Hong, C. Lee, J. S. Park, and J. H. Shim (2016), Control of valley degeneracy in $MoS_2$ by layer thickness and electric field and its effect on thermoelectric properties, *Phys. Rev. B,* **93**: 035445.

[147] M. Oliva-Leyva, and C. Wang (2017), Magneto-optical conductivity of anisotropic two-dimensional Dirac Weyl materials, *Annals of Physics*, **384**: 61-70.

[148] L. Glen, Goodvin, S. Andrey, Mishchenko, and M. Berciu (2011), Optical conductivity of the Holstein polaron, *Phys. Rev. Lett.*, **107**: 076403.

[149] C. Kenfack-Sadem, A. K. Teguimfouet, A. Kenfack Jiotsa, and R. M. K. Tsiaze (2021), Dynamics and decoherence of exciton polaron in monolayer transition metal dichalcogenides, *J. Electronic Materials*, **50**: 2911-2921.

[150] F. Lengers, T. Kuhn, and D. E. Reiter (2020), Theory of the absorption line shape in monolayer of transition metal dichalcogenides, *Phys. Rev. B*, **101**: 155-304.

[151] E. Malic, M. Selig, M. Feierabend, S. Brem, D. Christiansen, F. Wendler, A. Knorr, and G. Berghauser (2018), Dark excitons in transition metal dichalcogenides, *Phys. Rev. Materials*, **2**: 014002.

[152] L. Meckbach, T. Stroucken, and S. W. Koch (2018), Influence of the effective layer thickness on the ground state and excitonic properties of transition metal dichalcogenide systems, *Phys. Rev. B*, **97**: 035425.

[153] T. Deilmann, and K. S. Thygesen (2017), Dark excitations in monolayer transition metal dichalcogenides, *Phys. Rev. B*, **96**: 201113.

[154] M. Druppel, T. Deilmann, J. Noky, P. Marauhn, P. Kruger, and M. Rohlfing (2018), Electronic excitations in transition metal dichalcogenide monolayers from an LDA+GdW approach, *Phys. Rev. B*, **98**: 155433.

[155] G. Moody, C. Kavir Dass, K. Hao, C. Chen, L. Li, A. Singh, G. Tran, K. Clark, X. Xu, G. Berghauser, E. Malic, A. Knorr, and X. Li (2015), Intrinsic homogeneous linewidth and broadening mechanisms of excitons in monolayer transition metal dichalcogenides, *Nat. Commun.*, **6**: 8315.

[156] M. Selig, G. Berghauser, A. Raja, P. Nagler, C. Schuller, T. F. Heinz, T. Korn, A. Chernikov, E. Malic, and A. Knorr (2016), Excitonic linewidth and coherence lifetime in monolayer transition metal dichalcogenides, *Nat. Commun.*, **7**: 13279.

# LIST OF PUBLICATIONS

1- C. S. Kenfack, **A. K. Teguimfouet**, A. J. Kenfack, and R. M. K. Tsiaze (2021), Dynamics and decoherence of exciton polaron in monolayer transition metal dichalcogenides, *Journal of Electronic Materials*, 50: 2911-2921.

2- **A. K. Teguimfouet**, C. S. Kenfack, J. V. Nguepnang, A. J. Kenfack, and K. Bhattacharyya (2022), Relaxation and transport of excitonic polaron in monolayer transition metal dichalcogenides, *Iranian Journal of Science and Technology Transactions A: Science*, 46: 717-730.

3- **A. K. Teguimfouet**, C. S. Kenfack, A. J. Kenfack, F. C. M. Fobasso, M. El-Yadri, L. M. Perez, D. Laroze, and E. Feddi (2022), Magnetic barrier and temperature effects on optical and dynamic properties of exciton-polaron in monolayers transition metal dichalcogenides, *Physica E: Low-dimensional Systems and Nanostructures*, 144: 115448.

4- C. S. Kenfack, **A. K. Teguimfouet**, A. B. Moubissi, N. Cortes, F. C. M. Fobasso, M. Nasale, and A. J. Kenfack (2023), Magnetic barrier and electric field effects on exciton-polaron relaxation and transport properties in transition metal dichalcogenide monolayers, *Physical Review B*, 107: 075134.

**OTHERS**

5- J. V. Nguepnang, **A. K. Teguimfouet**, C. S. Kenfack, and A. J. Kenfack (2022), Polaron dynamic and decoherence in transition metal dichalcogenides under electric field, *Indian Journal of Physics*, 96: 2001-2010.

Journal of ELECTRONIC MATERIALS
https://doi.org/10.1007/s11664-021-08808-9


ORIGINAL RESEARCH ARTICLE

# Dynamics and Decoherence of Exciton Polaron in Monolayer Transition Metal Dichalcogenides

C. KENFACK-SADEM,[1,4,5] A. KITIO TEGUIMFOUET,[2] A. KENFACK-JIOTSA,[3] and R.M. KEUMO TSIAZE[2,4]

1.—Laboratory of Condensed Matter and Nanomaterials, Department of Physics, Faculty of Science, University of Dschang, P.O. Box 67, Dschang, Cameroon. 2.—Laboratory of Mechanic-Materials and Structures, Department of Physics, Faculty of Science, University of Yaounde I, P.O. Box 812, Yaoundé, Cameroon. 3.—Département de Physique, Ecole Normale Supérieure, Université de Yaoundé 1, BP 42, Yaoundé, Cameroun. 4.—International Chair in Mathematical Physics and Applications (ICMPA-UNESCO Chair), University of Abomey-Calavi, 072, P.O. Box 50, Cotonou, Republic of Benin. 5.—e-mail: kevinsadem@yahoo.fr

The dynamics and decoherence of excitonic polaron in a two-dimensional monolayer transition metal dichalcogenides (TMDCs) in quantum dot have been investigated using a variational method. We focused on confinement and temperature effects on dynamics properties and decoherence of exciton polaron, and found that the entropy increases with increasing temperature and dot radius. We observed that due to temperature the lifetime decreases and exciton or polaron can exits independently in the system. The high mobility of exciton-polaron decreases when enhancing the temperature and dot radius. We show that the optical absorption of photon starts when the photon energy is twice the phonon energy. Among the TMDCs studied, we observed the lowest entropy for $WS_2$, the longest lifetime for $MoSe_2$, the highest mobility for $MoS_2$ and the greatest absorption for $MoS_2$. We have also determined the ranges of decoherence for each property, and it appears that the increase in temperature, dot radius and photon energy does not favor decoherence. It is seen that, in the decoherence phase, the system has lower disorder, higher amplitude of lifetime, mobility and absorption.

**Key words:** Exciton polaron, Decoherence, Transition metal dichalcogenides, Quantum dot

## INTRODUCTION

Transition metal dichalcogenides (TMDCs) are one of the two-dimensional (2D) materials with a wide range of applications, such as electronic device manufacturing,[1] spintronics,[2] and qubit preparation.[3] A diversity of TMDC-based devices has been exhibited, including field effect transistors, heterostructure junctions[4] and photodetectors.[5] TMDCs compounds are formulated as $MX_2$ where M is the transition metal and X is a chalcogen element. In the structure, the M atoms are sandwiched between two layers of chalcogen atoms coupled to each other by van der Waals interactions. The layer can be subdivided into different layers and provide another sample of TMDCs materials.[6,7] For these materials, the electronic transition from indirect to direct band gap results in an enhancement of photoluminescence spectral peaks,[8,9] which are used for photoluminescence[10] and optoelectric[11] applications. The band gap can also be fitted in TMDCs such as $MoSe_2$, $WSe_2$, $WS_2$, $MoS_2$. The band gap changes depending on the polar substrates and the internal distance between the substrate and the monolayer TMDCs.[12]

An exciton–polaron arises when the electron and the hole interact with the acoustic or optical phonons due to lattice deformations. Both theoretical[13,14] and experimental[15,16] studies have been

(Received September 17, 2020; accepted February 5, 2021)

Published online: 09 March 2021

realized in 2D and three-dimensional excitonic state systems.[17,18] Interactions with phonons have been shown to contribute significantly to excitonic states. Semiconductor quantum dots (QDs) are used as basic building blocks for quantum information processing, in which the operations are strongly related to the presence of the coherence.[19] For such applications, it is necessary to understand decoherence in QDs with the exciton relaxation process.

The interaction of phonons with excitons in QDs has been found to control their decoherence at low temperatures,[20] and helps to understand their optical properties. An important source of decoherence of the QD exciton is the process of dressing with bulk phonons.[21] Experimental data indicate a dressing time of the confined exciton to be of the order of 1 picosecond and a decay time (of order of 100 picosecond) being shorter than the radiative recombination time ($\sim$ 1 ns) at absolute-zero temperature.[22] Also, there are theoretical[23,24] and experimental[25,26] studies on decay rates, called lifetime of quasi-particulate states. Electron–phonon scattering influences the lifetime of excited electronic states and hole states, especially for the former.[27,28] The evaluation of lifetime contributes to understanding the relaxation process of excitonic polaron in nanostructures. The decoherence effect due to exciton-phonon interaction in CdSe quantum dots has been studied and it has been seen that the scattering rate strongly depends on the confinement: it decreases with decreasing of dot radius.[29] Excitons enclosed in single-layer 2D QD TMDCs have been the subject of scientific interest. The dot radius should be comparable to the effective Bohr radius or a few tenths of an angstrom.[30] The type of confinement is therefore a determining factor in the study of decoherence in nanostructures.[31,32]

One of the theoretical difficulties of the polaron excitonic model is the fact that Hamiltonian operators are not always diagonally shaped. Sometimes, it may be necessary to employ diagonalization techniques to determine the proper eigenvalues of the Hamiltonian, the eigenfunctions of the system or other parameters.[33,34] Using a similar method, the mass and the energy displacements of the excitonic polaron at the ground state for some single-layer of TMDCs have been determined.[35] However, in order to explore the phenomenon of information loss, entropy is a useful parameter in this sense as it gives an idea of the behavior of the superposition state. Some studies have been carried out to derive entropy in small structures.[36,37] In addition, it has been demonstrated that TMDCs materials have possibility of high charge carrier mobility and precisely $MoSe_2$ has high-performance carrier transport.[38] When considering the longitudinal and surface optical (substrate-induced) phonon modes on the polaron in TMDCs, the behaviors of absorption are determined by the interplays between the strength of electron-optical phonon coupling and the energy of optical phonon.[39] It is clear that entropy, lifetime, mobility and optical absorption coefficients are significant properties necessary to adequately qualify a polaronic exciton system, despite the fact that little attention has been paid to these characteristics.

In this paper, we determine the excitonic polaron properties of common low-dimensional monolayer TMDCs materials. Firstly, we present the model and calculations in which analytical expressions of Tsallis entropy, lifetime, mobility and the optical absorption coefficient are derived. Secondly, in the numerical results and discussion, a comparison is made between the TMDCs materials, the temperature effect and the confinement influence evaluated for these parameters. Finally, we conclude by summarizing the results.

## MODEL AND CALCULATIONS

We consider an exciton moving in a lab representing a monolayer TMDC, interacting with longitudinal optical phonons in two dimensions.[35] Here, the particles are in a QD confinement and the Hamiltonian of the system is taken as:

$$\hat{H} = \hat{H}_{\mathrm{ex}}^{2D} + \hat{H}_r + \hat{H}_{\mathrm{ph}} + \hat{H}_{\mathrm{ex-ph}}^{2D} \tag{1}$$

In Eq. 1, the first term is the Hamiltonian of exciton given by:

$$\hat{H}_{\mathrm{ex}}^{2D} = \sum_K E^{\mathrm{ex}}(K)\, C_K^{+} C_K \tag{2}$$

where $C_K^{+}$ and $C_K$ denote the creation and annihilation operators of the exciton. $K$ is the exciton wave vector. $E^{\mathrm{ex}}$ is the exciton energy in the layered slab given explicitly by:

$$E^{\mathrm{ex}}(K) = E_{\mathrm{g}} + \frac{\hbar^2 K^2}{2M^*} \tag{3}$$

$E_{\mathrm{g}}$ and $M*$ are, respectively, the band gap in the monolayer TMDC and the effective mass of the exciton ($M* = m_e^* + m_h^*$).

The second term of (1) represents the Hamiltonian of the exciton along the $(x,y,z)$-direction:

$$\hat{H}_r = \frac{P_{\mathrm{e}}^2}{2m_e^*} + \frac{P_{\mathrm{h}}^2}{2m_h^*} - E_{\mathrm{b}} + U_{\mathrm{e}} + U_{\mathrm{h}} \tag{4}$$

where $P_e$ ($P_h$) is the electrons (holes) momentum and $E_b$ the binding energy of the exciton including the electron–hole Coulomb interaction. $U$ is the QD confining potential[30] taken as:

$$U_I = \begin{cases} 0 & \text{for } r_i \le R \\ \infty & \text{for } r_i > R \end{cases} \tag{5}$$

$r_I$ represents the position of the electron ($I = e$) and hole ($I = h$), and $R$ is the dot radius.

The phonon energy operator appears as:

$$\hat{H}_{\mathrm{ph}} = \sum_{q} \hbar\omega\, b_q^{+} b_q \tag{6}$$

where $b_q^{+}$ ($b_q$) is the phonon's creation (annihilation) operator with the wave vector $q$.

The last term of (1) gives the Hamiltonian of the exciton–phonon interaction by:

$$\hat{H}^{2D}_{\mathrm{ex-ph}} = \sum_{K,q_{//}} \Xi^{\mathrm{op}}(q_{//})\, C^{+}_{(K+q_{//})} C_K \left(b_{q_{//}} + b^{+}_{-q_{//}}\right) \tag{7}$$

where $q_{//}$ represents the component of the phonon wave vector in the $xy$ plane. The exciton–phonon coupling function is taken as:

$$\Xi^{\mathrm{op}}(q_{//}) = \sqrt{\frac{\hbar q_{//}}{2S\rho u}} \left[\frac{D_c^{\mathrm{op}}}{\left(1+b_e^2\right)^{3/2}} - \frac{D_v^{\mathrm{op}}}{\left(1+b_h^2\right)^{3/2}}\right] \tag{8}$$

with $S$, the surface area of the layer planes, $\rho$ being the area mass density and $u$ the sound velocity of the phonon mode. $D_c^{\mathrm{op}}$ and $D_v^{\mathrm{op}}$ denote, respectively, the deformation potential constant for electron–optical phonon interaction at the critical points $(K, K')$ in the conduction band and the corresponding expression for a hole in the valence band. We consider $b_e$ , $b_h << 1$ and then (8) becomes:

$$\Xi^{\mathrm{op}}(q_{//}) = \left(D_c^{\mathrm{op}} - D_v^{\mathrm{op}}\right)\sqrt{\frac{\hbar q_{//}}{2S\rho u}}. \tag{9}$$

Using the Lee Low Pines transformation:

$$U_{\mathrm{ex}} = \exp(iS) \tag{10}$$

where

$$S = \sum_{K,q_{//}} C^{+}_{K+q_{//}} C_K \left[f^{*}_{\mathrm{ex}}(K, q_{//}) b^{+}_{-q_{//}} + f_{\mathrm{ex}}(K, q_{//})\, b_{q_{//}}\right]. \tag{11}$$

The functions are determined as:

$$\begin{aligned} f^{*}_{\mathrm{ex}} &= \frac{\Xi^{\mathrm{op}}(q_{//})}{E^{\mathrm{ex}}_{(K+q_{//})} - E^{\mathrm{ex}}_{(K)} + \hbar\omega} \\ f_{\mathrm{ex}} &= \frac{\Xi^{\mathrm{op}}(q_{//})}{E^{\mathrm{ex}}_{(K+q_{//})} - E^{\mathrm{ex}}_{(K)} - \hbar\omega}. \end{aligned} \tag{12}$$

The transformed Hamiltonian obtained after the use of (10) is given as:

$$\hat{H}^{T} = U^{-1}_{\mathrm{ex}} \hat{H} U_{\mathrm{ex}} \approx \hat{H}^{2D}_{\mathrm{ex}} + \hat{H}_r + \hat{H}_{\mathrm{ph}} + \hat{H}^{T2D}_{\mathrm{ex-ph}} \tag{13}$$

where

$$\begin{aligned} \hat{H}^{T2D}_{\mathrm{ex-ph}} = \sum_{K,K',q_{//}} & \left|\Xi^{\mathrm{op}}(q_{//})\right|^2 \\ & \left[\frac{1}{E^{\mathrm{ex}}_{(K+q_{//})} - E^{\mathrm{ex}}_{(K)} + \hbar\omega} - \frac{1}{E^{\mathrm{ex}}_{(K+q_{//})} - E^{\mathrm{ex}}_{(K)} - \hbar\omega}\right] C^{+}_{(K+q_{//})} \\ & C_K C^{+}_{(K'+q_{//})} C_{K'} \end{aligned} \tag{14}$$

**Tsallis Entropy**

In physics, entropy is a property which estimates the disorder in a system,[40,41] and the Tsallis entropy[42] depending on a degree ($\alpha$) takes the form:

$$S_\alpha = \frac{1 - \sum_{i=1} P_I^{\alpha}}{\alpha - 1} \tag{15}$$

This leads to:

$$S_\alpha = \frac{1 - P_1^{\alpha} - P_2^{\alpha}}{\alpha - 1} \tag{16}$$

The probabilities are $P_1$ for the ground state and $P_2$ for the first excited state given by:

$$\begin{aligned} P_1 &= \frac{\left[1 - \beta(1-\alpha)E^0_{\mathrm{ex-pol}}\right]^{1/1-\alpha}}{Z_\alpha} \text{ and } P_2 \\ &= \frac{\left[1 - \beta(1-\alpha)E^1_{\mathrm{ex-pol}}\right]^{1/1-\alpha}}{Z_\alpha} \end{aligned} \tag{17}$$

The partition function is defined as:

$$\begin{aligned} Z_\alpha = & \left[1 - \beta(1-\alpha)E^0_{\mathrm{ex-pol}}\right]^{1/1-\alpha} \\ & + \left[1 - \beta(1-\alpha)E^1_{\mathrm{ex-pol}}\right]^{1/1-\alpha} \end{aligned} \tag{18}$$

where the parameter $\alpha \in \Re$ is the entropy degree and $\beta$ is the inverse of temperature. $E^0_{\mathrm{ex-pol}}$ and $E^1_{\mathrm{ex-pol}}$ are, respectively, the ground state and the first excited state energy of the excitonic polaron.

For the ground state, we have:

$$E^0_{\mathrm{ex-pol}} = \langle \Psi_0 | \hat{H}^{T} | \Psi_0 \rangle \tag{19}$$

with

$$|\Psi_0\rangle = |\varphi(r_e, r_h)\rangle |K, n(q)\rangle = |\varphi(r_e, r_h)\rangle C^{+}_K |0\rangle_k |0\rangle_{\mathrm{ph}} \tag{20}$$

where

$$\varphi(r_e, r_h) = \mathrm{Const} \cdot \sin\left(\frac{\pi r_e}{R}\right) \sin\left(\frac{\pi r_h}{R}\right) \tag{21}$$

$|0\rangle_k$ and $|0\rangle_{\rm ph}$ represent, respectively, the exciton's and phonon's vacuum states.

Thus

$$E^0_{\rm ex-pol} = \left(\frac{\hbar^2 k^2}{2M^*}\right)\left(1-\tilde{B}_{\rm ex2}\right) + E_{\rm g} + E_r^{\rm ex} - E_b - B_{\rm ex1} \tag{22}$$

where

$$E_r^{\rm ex} = \frac{\hbar^2\pi^2}{2m_e^* R^2} + \frac{\hbar^2\pi^2}{2m_h^* R^2} = \frac{\hbar^2\pi^2}{2\mu^* R^2} \tag{23}$$

$$\begin{aligned} B_{\rm ex1} &= \frac{\pi\sqrt{\hbar\omega}\left(D_c^{\rm op} - D_v^{\rm op}\right)^2}{\sqrt{2}\hbar^2\rho u}\left(m_e^* + m_h^*\right)^{3/2} \text{ and} \\ \tilde{B}_{\rm ex2} &= \frac{3\pi\left(D_c^{\rm op} - D_v^{\rm op}\right)^2}{4\sqrt{2}\hbar^2\rho u}\frac{\left(m_e^* + m_h^*\right)^{3/2}}{\sqrt{\hbar\omega}}. \end{aligned} \tag{24}$$

Now, for the first excited state, one obtains the energy:

$$E^1_{\rm ex-pol} = \langle\Psi_1|\hat{H}^T|\Psi_1\rangle \tag{25}$$

with

$$|\Psi_1\rangle = |\varphi(r_e, r_h)\rangle C_K^+|1\rangle_k|0\rangle_{\rm ph}. \tag{26}$$

According to Eq. 13, we have:

$$\begin{aligned} E^1_{\rm ex-pol} = 4\left(\frac{\hbar^2 k^2}{2M^*}\right)\left(1-2\tilde{B}_{\rm ex2}\right) + 4E_{\rm g} + 2E_r^{\rm ex} - 2E_b \\ - 8B_{\rm ex1}. \end{aligned} \tag{27}$$

Considering Eqs. 22 and 27, we obtain the entropy of the system.

## Lifetime

As in other materials, phonons have a finite duration in TMDCs, and then the excitonic polaron life is closely related to the time of electron (hole)–phonon interaction. The lifetime[43] ($\tau$) can be taken as:

$$\frac{\hbar}{\tau} = 2\pi\sum_q \left|\langle n_{q'}, K|H^{2D}_{\rm ex-ph}|K, n_q\rangle\right|^2 \delta\left[E_k - E_{k+q} + \hbar\omega\right]. \tag{28}$$

We consider:

$$n_{q'} = n_q - 1. \tag{29}$$

Then, for the ground state, we have:

$$\begin{aligned} \frac{\hbar}{\tau} =& 2\pi\sum_q \left|\langle n_q - 1|\langle 0|C_K H^{2D}_{\rm ex-ph} C_K^+|0\rangle|n_q\rangle\right|^2 \delta \\ & \left[\frac{\hbar^2}{2M}\left(q^2 + 2kq - \frac{2M\hbar\omega}{\hbar^2}\right)\right]. \end{aligned} \tag{30}$$

According to Eq. 7, and after averaging, we have:

$$\frac{\hbar}{\tau} = \frac{4\pi M}{\hbar^2} n_q \sum_q \left(\Xi^{\rm op}_{(q)}\right)^2 \delta\left[q^2 + 2kq - \frac{2M\hbar\omega}{\hbar^2}\right]. \tag{31}$$

The Dirac function is transformed, converting the summation into integration and, according to Eq. 9, we obtain:

$$\frac{1}{\tau} = \frac{M\left(D_c^{\rm op} - D_v^{\rm op}\right)^2}{2\rho u\sqrt{k^2 + 2M\hbar\omega}} n_q \int_0^\infty {\rm d}q_{//}\, q_{//}^2\left[\delta(q_{//} - q_1) + \delta(q_{//} - q_2)\right] \tag{32}$$

where

$$\begin{aligned} q_1 &= -k + \sqrt{k^2 + 2M\hbar\omega} \text{ and } q_2 \\ &= -k - \sqrt{k^2 + 2M\hbar\omega}. \end{aligned} \tag{33}$$

After integrating, we have:

$$\frac{1}{\tau} = \frac{2M\left(D_c^{\rm op} - D_v^{\rm op}\right)^2}{\rho u} n_q \frac{\left(k^2 + M\hbar\omega\right)}{\sqrt{k^2 + 2M\hbar\omega}}. \tag{34}$$

The temperature dependence is obtained taking the mean number of phonons according to the quantum statistics theory:

$$n_q = \left[\exp(\beta\hbar\omega) - 1\right]^{-1}. \tag{35}$$

## Mobility

The electron and hole interact with phonons in TMDCs and the mobility characterizes how quickly the exciton moves in these materials. Let us take the form of the mobility in the self-energy relaxation time approximation[38] as:

$$\mu_{\rm ex} = \frac{-e}{V}\int {\rm d}K \frac{\partial f_0}{\partial E^0_{\rm ex-pol}} v_K^2\, \tau_K \tag{36}$$

where $V$ is the volume of crystalline unit cell, $f_0$ is the Fermi–Dirac distribution function and $v_k$ the group velocity[44] given by:

$$f_0 = \left[1 + \exp\beta\left(E^0_{\rm ex-pol} - E_F\right)\right]^{-1} \tag{37}$$

$$v_K = \frac{1}{\hbar}\partial_K E^0_{\rm ex-pol} = \frac{\hbar\left(1-\tilde{B}_{\rm ex2}\right)}{M}K. \tag{38}$$

The Fermi energy is a function of the carrier concentration, as follows:

$$E_F = \frac{\hbar^2 \pi}{M} n_{\mathrm{ex}}. \tag{39}$$

After derivation over the energy, one obtains:

$$\mu_{\mathrm{ex}} = \frac{e}{V}\beta \int \mathrm{d}K \frac{\exp\beta\left(E^0_{\mathrm{ex-pol}} - E_F\right)}{\left[1+\exp\beta\left(E^0_{\mathrm{ex-pol}} - E_F\right)\right]^2} v_K^2\, \tau_K. \tag{40}$$

Considering Eq. 34, the integration over the exciton wave vector permits the obtaining of the expression of the mobility:

$$\mu_{\mathrm{ex}} = \frac{e\rho u\left(1-\tilde{B}_{\mathrm{ex2}}\right)^2}{4M^3\pi^2(D_c^{\mathrm{op}} - D_v^{\mathrm{op}})^2} \frac{\beta}{n_q} \int_0^\infty \mathrm{d}k\, \frac{k^4\sqrt{k^2+2M\hbar\omega}}{k^2+M\hbar\omega} \frac{\exp\left(\frac{\hbar^2\left(1-\tilde{B}_{\mathrm{ex2}}\right)\beta}{2M}k^2 - \eta\right)}{\left[1+\exp\left(\frac{\hbar^2\left(1-\tilde{B}_{\mathrm{ex2}}\right)\beta}{2M}k^2 - \eta\right)\right]^2} \tag{41}$$

where

$$\eta = \beta\left(E_F - E_r^{\mathrm{ex}} + E_b\right). \tag{42}$$

## Optical Absorption

Here, we are interested in the property of TMDCs to interact with an incident photon. Then, we consider an exciton–polaron which absorbs light, and this absorption depends on the possibility of absorbing the photon in the ground state. Thus, the optical absorption coefficient[45] ($\Gamma$) of the excitonic polaron is given by:

$$\Gamma(\hbar\Omega) = \frac{\Omega}{cn\varepsilon_0 2E^2} P(\hbar\Omega) \tag{43}$$

where $P(\hbar\Omega)$ gives the probability of absorbing photons and $\Omega$ stands for the frequency of light. $\varepsilon_0$ and $c$ represent, respectively, the permittivity of vacuum and the light velocity. $n$ characterizes the medium in which the exciton–polaron moves, and is the index of refraction; $E$ is the electric field intensity induced by the incident photon. The transition probability[39] is given by:

$$P(\hbar\Omega) = 2\pi \sum_f \langle\Psi_0|\, V\,|\Psi_f\rangle\langle\Psi_f|\, V\,|\Psi_0\rangle \delta\left(E_0 + \hbar\Omega - E_f\right) \tag{44}$$

$\Psi_0$ is the ground state wave function with energy $E_0$, $\Psi_f$ are the wave functions of all possible final states and $E_f$ their respective energies. $V$ is the time-dependent perturbation described by the electric dipole interaction $V = eE\cdot r$. Inserting the latter in Eq. 44, we rewrite Eq. 43 as:

$$\Gamma(\hbar\Omega) = \frac{\Omega}{cn\varepsilon_0 E^2}\left(\frac{e}{\hbar\Omega}\right)^2 \int_{-\infty}^{0} \mathrm{d}t\, e^{-it(I\varepsilon+\hbar\Omega)} \langle\Psi_0|E \cdot \left\{\frac{p_e(0)}{m_e} + \frac{p_h(0)}{m_h}\right\} E \cdot \left\{\frac{p_e(t)}{m_e} + \frac{p_h(t)}{m_h}\right\} |\Psi_0\rangle \tag{45}$$

It is convenient to apply the unitary transformation (10) to obtain:

$$\Gamma(\hbar\Omega) = \frac{\Omega}{cn\varepsilon_0 E^2}\left(\frac{e}{\hbar\Omega}\right)^2 \int_{-\infty}^{0} \mathrm{d}t\, e^{-it(I\varepsilon+\hbar\Omega)} \langle n(q), K|\, U_{\mathrm{ex}}^{-1} E \cdot \left\{\frac{p_e(0)}{m_e} + \frac{p_h(0)}{m_h}\right\} U_{\mathrm{ex}} U_{\mathrm{ex}}^{-1} E \cdot \left\{\frac{p_e(t)}{m_e} + \frac{p_h(t)}{m_h}\right\} U_{\mathrm{ex}} |K, n(q)\rangle. \tag{46}$$

For $P = 0$

$$U_{\mathrm{ex}}^{-1} E\cdot p(0) U_{\mathrm{ex}} = -\sum_q \hbar\omega E\cdot q \times \left[b_q^+ b_q + I\sum_{K,q_{//}} C^+_{K+q_{//}} C_K (f_{\mathrm{ex}} b_{q_{//}} - f^*_{\mathrm{ex}} b^+_{-q_{//}})\right]. \tag{47}$$

Thus:

$$\Gamma(\hbar\Omega) = \frac{\Omega}{cn\varepsilon_0 E^2}\left(\frac{e\hbar\omega}{\mu\hbar\Omega}\right)^2 \int_{-\infty}^{0} \mathrm{d}t\, e^{-it(I\varepsilon+\hbar\Omega)} \times \langle n(q), K| \sum_q (E\cdot q)^2 f_{\mathrm{ex}} f^*_{\mathrm{ex}} C^+_{K+q_{//}} C_K b_{q_{//}} C^+_{K'+q_{//}}(t) C_{K'}(t) b^+_{-q_{//}}(t) |K, n(q)\rangle. \tag{48}$$

From the relationship:

$$\frac{\mathrm{d}\,C(t)}{\mathrm{d}t} = I\left[H^T, C(t)\right]. \tag{49}$$

We establish:

$$C^+_{K'+q_{//}}(t)\, C_{K'}(t) = C^+_{K'+q_{//}}(0)\, C_{K'}(0)\, \exp\left[-it(E^{\mathrm{ex}}_{(K')} - E^{\mathrm{ex}}_{(K'+q_{//})})\right]. \tag{50}$$

And:

$$b^+_{-q_{//}}(t) = b^+_{-q_{//}}(0)\exp(it\hbar\omega). \tag{51}$$

Then, the absorption coefficient becomes:

$$\Gamma(\hbar\Omega) = \frac{\Omega}{cn\varepsilon_0 E^2}\left(\frac{e\hbar\omega}{\mu\hbar\Omega}\right)^2 \int_{-\infty}^{0} \mathrm{d}t\, e^{-it(I\varepsilon+\hbar\Omega)} \exp\left[-it(E^{\mathrm{ex}}_{(K')} - E^{\mathrm{ex}}_{(K'+q_{//})} + \hbar\omega)\right] \langle n(q)|\langle 0|C_K \sum_q (E\cdot q)^2 f_{\mathrm{ex}} f^*_{\mathrm{ex}} C^+_{K+q_{//}} C_K b_{q_{//}} C^+_{K'+q_{//}}(0)\, C_{K'}(0) b^+_{-q_{//}}(0)\, C^+_K|0\rangle|n(q)\rangle \tag{52}$$

After averaging, we have:

$$\Gamma(\hbar\Omega) = \frac{\pi\Omega}{cn\varepsilon_0 E^2}\left(\frac{e\hbar\omega}{\mu\hbar\Omega}\right)^2 \sum_q (E\cdot q)^2 f_{\mathrm{ex}} f^*_{\mathrm{ex}} \delta\left(\hbar\Omega + E^{\mathrm{ex}}_{(K)} - E^{\mathrm{ex}}_{K+q_{//}} - \hbar\omega\right). \tag{53}$$

Let us take:

$$\chi = \frac{\Omega}{\omega}. \tag{54}$$

According to Eqs. 3 and 12, converting summation into integration, one can obtain:

$$\Gamma(\chi) = \frac{\pi\omega e^2}{cn\varepsilon_0\mu^2 E^2\chi}\frac{s}{(2\pi)^2}\int_0^{2\pi}\mathrm{d}\theta\int_0^{\infty}\mathrm{d}q_{//}E^2 q_{//}^3\cos^2(\theta)\, \frac{\hbar(D_c^{\mathrm{op}} - D_v^{\mathrm{op}})^2}{2s\rho u}\, \frac{q_{//}\delta\left[-\frac{\hbar^2 q_{//}}{M*}\left(\frac{q_{//}}{2}+K\right) + \hbar\omega(\chi-1)\right]}{\left(\frac{\hbar^2 q_{//}}{M*}\left(\frac{q_{//}}{2}+K\right)\right)^2 - (\hbar\omega)^2}. \tag{55}$$

For small wave vectors, we obtain:

$$\Gamma(\chi) = \frac{\hbar\,\omega\, e^2(D_c^{op} - D_v^{op})^2}{8cn\varepsilon_0\rho u\mu^2\chi}\int_0^{\infty} dq_{//}\, \frac{q_{//}^4}{\left(\frac{\hbar^2 q_{//}^2}{2M*}\right)^2 - (\hbar\omega)^2}\delta \left[-\frac{\hbar^2 q_{//}^2}{2M*} + \hbar\omega(\chi-1)\right]. \tag{56}$$

We also take:

$$q_0^2 = \frac{2M*\hbar\omega(\chi-1)}{\hbar^2}. \tag{57}$$

Then:

$$\Gamma(\chi) = \frac{\sqrt{\hbar\omega}\, e^2(D_c^{\mathrm{op}} - D_v^{\mathrm{op}})^2(M*)^{9/2}}{2\sqrt{2}\hbar^5 cn\varepsilon_0\rho u\left(m_e^* m_h^*\right)^2}\frac{(\chi-1)^{3/2}}{\chi^2(\chi-2)}. \tag{58}$$

## NUMERICAL RESULTS AND DISCUSSION

The characteristics of each material that we have used for the calculations are given in Table I.

Figure 1 displays the excitonic polaron entropy as a function of the temperature for various monolayer TMDCs at $\alpha = 1.1$. It is shown that the entropy increases when enhancing the temperature. When thermal vibrations increase, the interatomic distance in the material increases and the band gap energy decreases. The probability of the excitonic polaron becomes small in the TMDCs and the transition from ground state to first excited state becomes faster. Then, the disorder increases and there is a loss of information in the system. This result is in accordance with the one in Refs. 37 and 46. The entropy becomes constant for $T = 25$ K. This behavior satisfies the third law of thermodynamics, and the result shows that the system is decoherent for $T < 25$ K and coherent for $T > 25$ K. For $T < 25$ K, it is also observed that the system is more decoherent in the $MoSe_2$ and more coherent in $WS_2$. For $T > 25$ K, the thermodynamics equilibrium is reached for all materials and then the system is coherent.

Figure 2 plots the excitonic polaron entropy versus the QD radius for various monolayer TMDCs. Figure 2a shows that the entropy increases when the dot radius is increased. This result indicates that, at low temperatures, the system is decoherent for $R < 6$ Å. For $R > 6$ Å the entropy becomes constant and then the system is coherent for each material. Fig. 2b indicates that the high temperatures act in the system to be coherent for all TMDCs materials. However, this is possible if $R > 2$ Å and for $R < 2$ Å it is decoherent at high temperatures. It is also seen that the entropy remains high for $MoSe_2$ whereas $MoS_2$ and $WSe_2$ are challenged: $WSe_2$ dominates when increasing the dot radius. In the absence of the confinement, it

**Table I. Parameters of monolayer TMDCs materials taken from Refs. 12 and 35**

| Material | $m_e$ | $m_h$ | $\hbar\omega$(eV) | $D_c^{\mathrm{op}}$(eV) | $D_v^{\mathrm{op}}$(eV) | $E_b$ (eV) | $E_g$ (eV) |
|---|---|---|---|---|---|---|---|
| $MoSe_2$ | 0.64 | 0.71 | 0.0365 | 5.2 | 4.9 | 0.174 | 1.56 |
| $WSe_2$ | 0.39 | 0.51 | 0.0291 | 2.3 | 3.1 | 0.231 | 1.65 |
| $WS_2$ | 0.31 | 0.42 | 0.0435 | 3.1 | 2.3 | 0.19 | 2.10 |
| $MoS_2$ | 0.51 | 0.58 | 0.0443 | 5.8 | 4.6 | 0.313 | 1.87 |

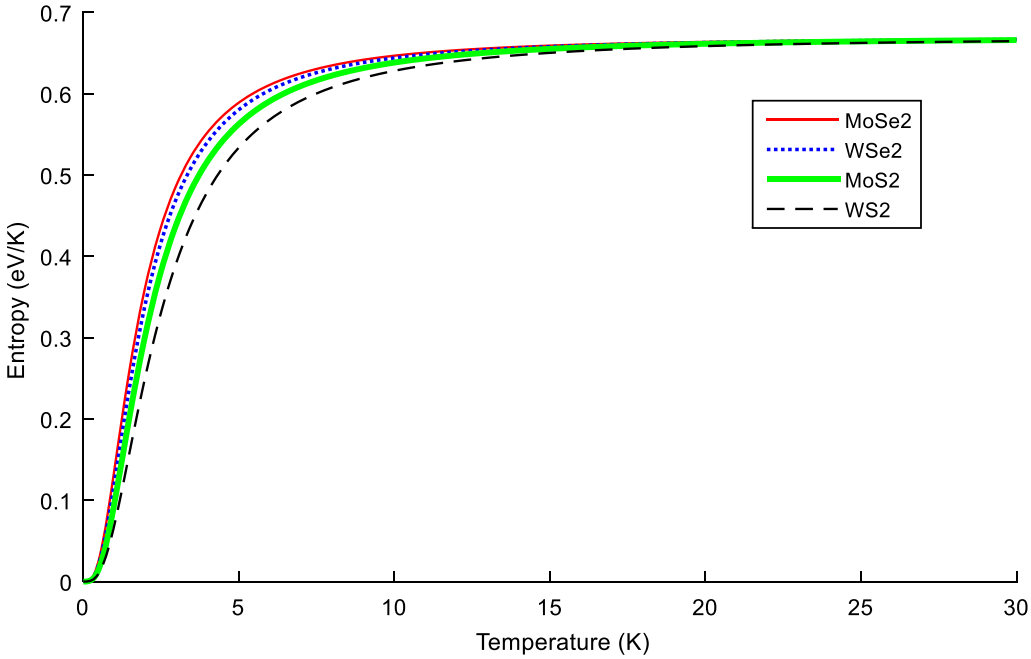


Fig. 1. Excitonic polaron entropy as a function of the temperature for various TMDCs at $\alpha = 1.1$.

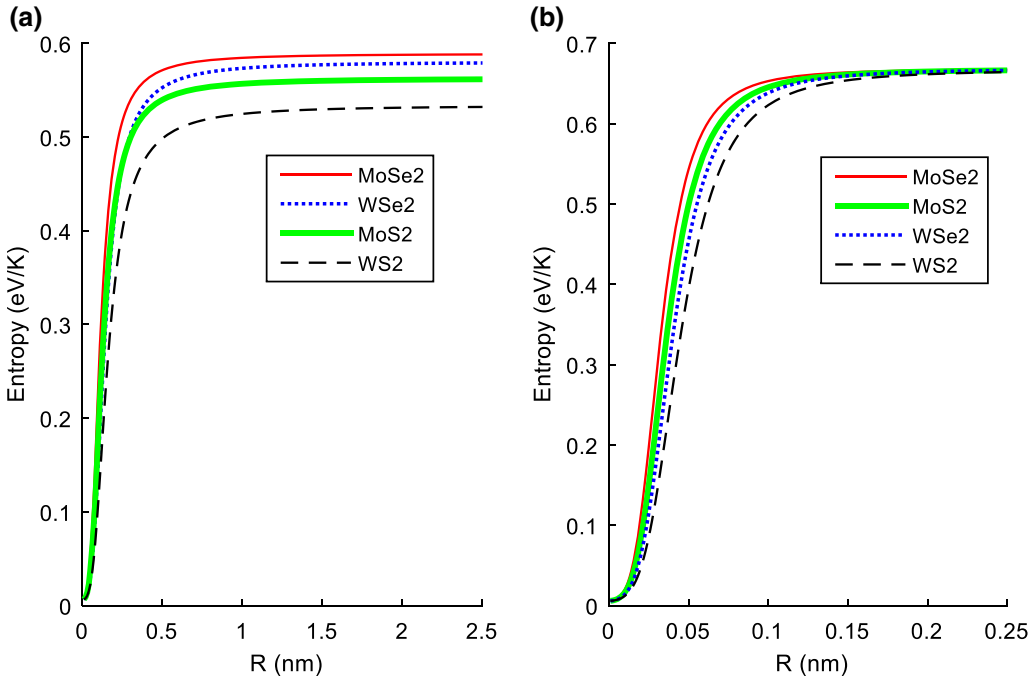


Fig. 2. Excitonic polaron entropy versus the QD radius for different TMDCs for $\alpha = 1.1$, (a) $T$ = 5 K and (b) $T$ = 50 K.

is observed that the entropy is non-zero due to the temperature effect.

We present in Fig. 3 the excitonic polaron lifetime versus the temperature for various monolayer TMDCs materials. We observe the decrease in the lifetime with increasing temperature. In fact, when the temperature increases, the lattice thermal vibrations is enhanced, and this increases the number of phonons interacting with the particles. Then, the probability that the electron (hole) absorbs a phonon can be probably larger. This is in accordance with the results of Refs. 23 and 24. The excitonic polaron lifetime is higher in $MoSe_2$. It is seen that the highest value of lifetime is observed near absolute zero of temperature and it becomes zero for higher temperature values. This explains the death of the excitonic polaron.

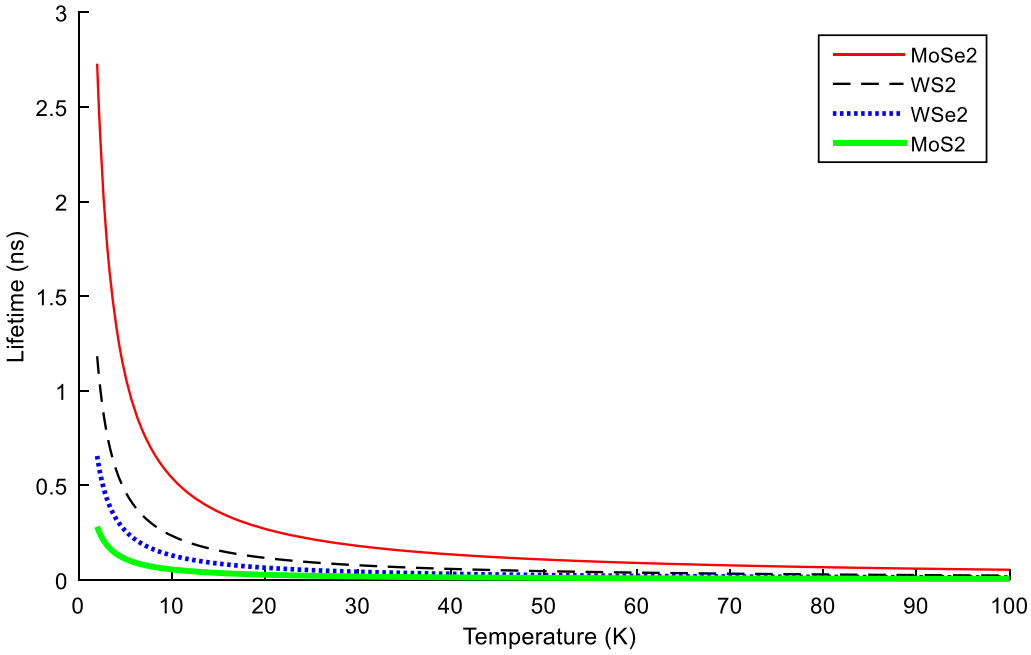


Fig. 3. Excitonic polaron lifetime versus the temperature for various TMDCs.

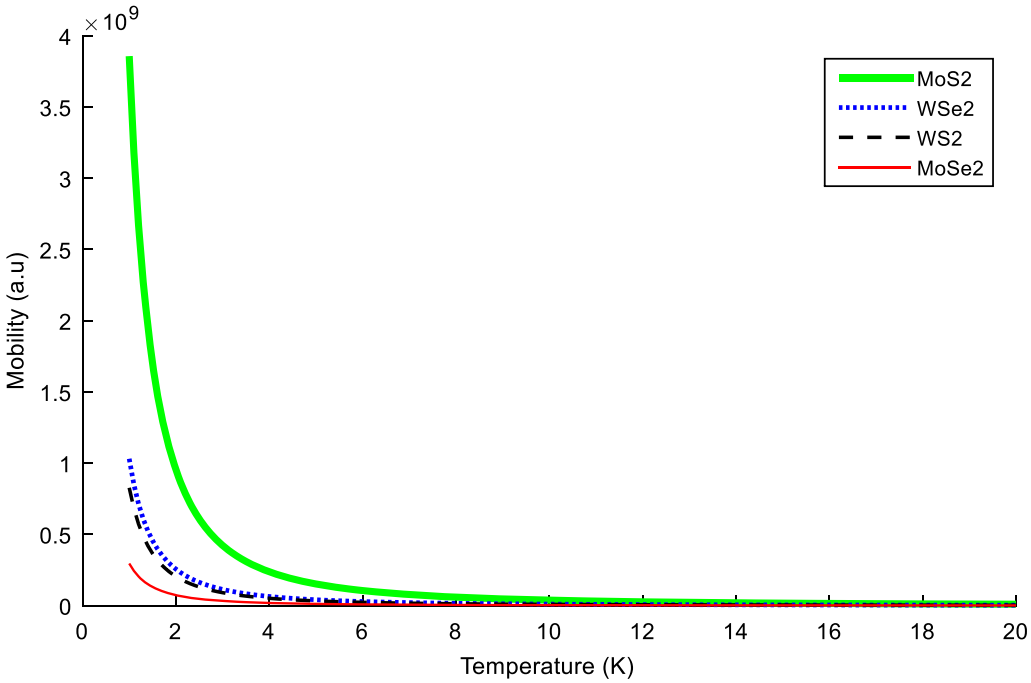


Fig. 4. Exciton-polaron mobility versus the temperature for various TMDCs for $n_{ex} = 2 \times 10^{12}$ cm$^{-2}$, $R$ = 1 Å.

Thus, high temperature values are damaging for the formation of exciton polaron. Among the selected TMDCs, $MoSe_2$ is the best that favors the exciton polaron existence. For lifetime, the coherence is observed at $T > 25$K (as for entropy) and the system is not granted to the excitonic polaron. We suspect the existence of either the exciton or polaron according to the results of Ref. 47 since the lifetime of the system vanishes. Also, our results are closed to the experimental one[48,49] where excitonic lifetime is $0.02 - 0.16$ ns at room temperature for $MoSe_2$ and $WSe_2$ monolayer.

In Fig. 4, we plot the exciton–polaron mobility versus the temperature for different monolayer TMDCs materials for $n_{ex} = 2 \times 10^{12}$ cm$^{-2}$, $R$ = 1 Å. One can see that the mobility of exciton–polaron decreases with increasing temperatures. This is in agreement with Ref. 50. The result shows that an

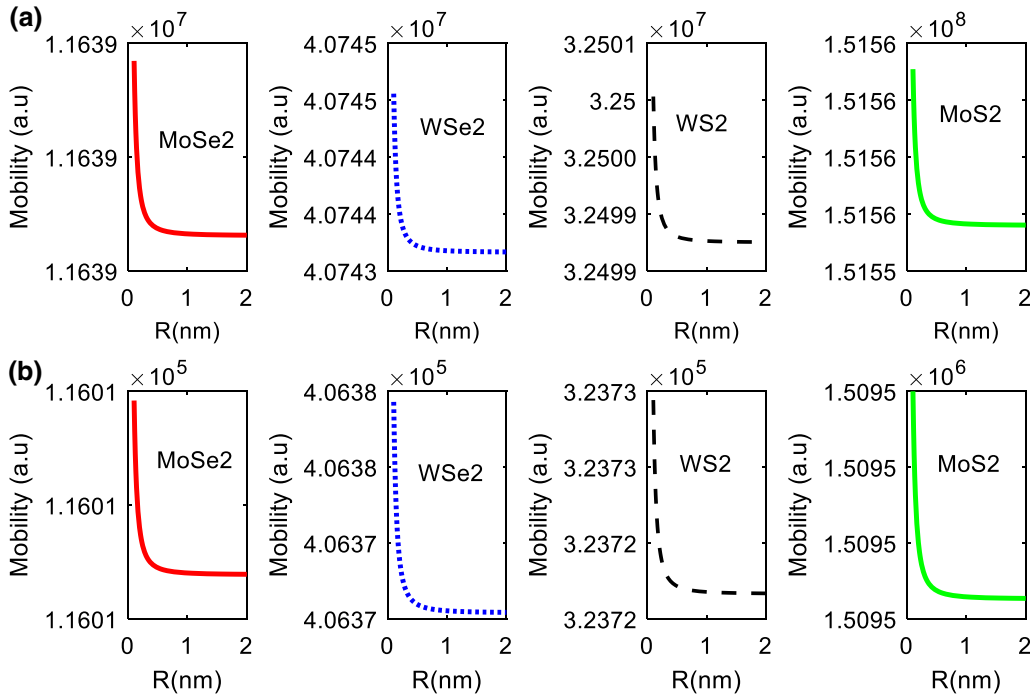


Fig. 5. Exciton–polaron mobility versus the QD radius for various TMDCs for $n_{ex} = 2 \times 10^{12}$ cm$^{-2}$, (a) $T = 5$ K and (b) $T = 50$ K.

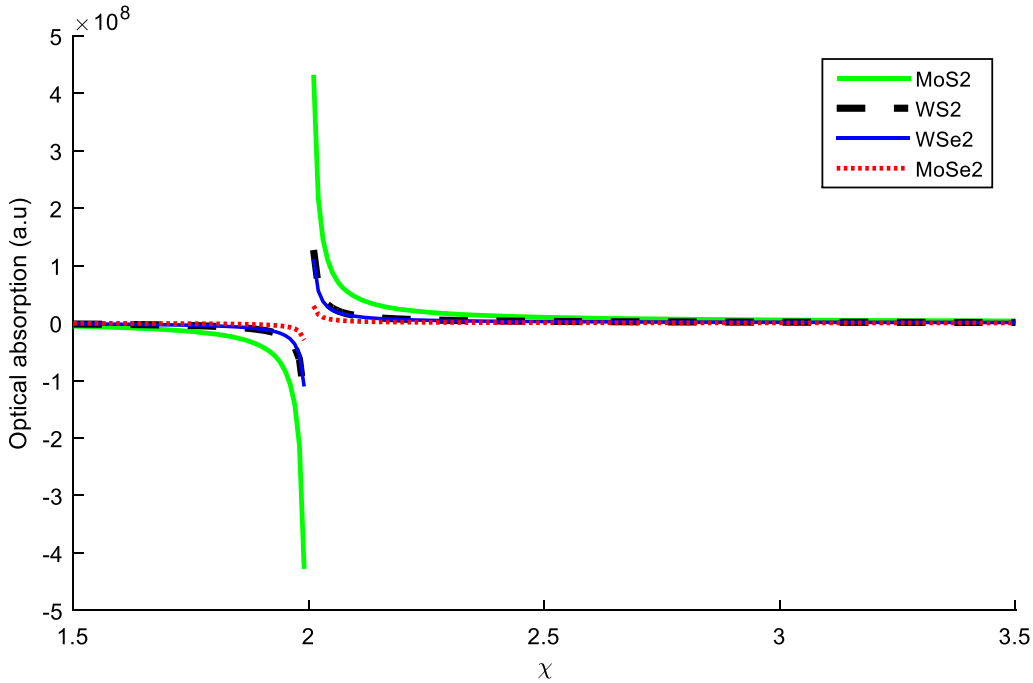


Fig. 6. Optical absorption coefficient versus the energy of incident photon for different TMDCs.

increase in temperature increases the entropy in the system and then reduces the mobility of the exciton–polaron. Also, for the mobility, the system is not coherent at low temperature $T < 25$ K and becomes coherent for $T > 25$ K. The highest mobility is obtained for $MoS_2$ and the lowest for $MoSe_2$.

Figure 5 displays the reduction of mobility with the quantum dot radius, respectively, at 5K and 50K. For a QD, the enhancement of the radius leads to a decrease in confined energy and then a reduction in the exciton-polaron mobility. The result indicates that at any temperature the system is decoherent for $R < 10$ Å, and coherent for $R > 10$ Å.

According to the amplitudes, we observe that the TMDCs materials have a high mobility, and it is

interesting for thermoelectric power factors, as shown by Ref. 38.

Figure 6 shows plots of the optical absorption coefficient versus the energy of incident photon for different monolayer TMDCs materials. We observe that the absorption starts at a peak characterizing the first relaxed excited state and decreases when enhancing the photon energy. For $\chi < 2$ ($\hbar\Omega < 2\hbar\omega$), the excitonic polaron does not absorb. The absorption starts when the photon energy is more than twice the one of phonons. Then, the exciton polaron needs more energy to absorb than the polaron. This can be due to the presence here of hole–phonon and electron–phonon interactions. This result is in accordance with the one of Ref. 39 for the case of the polaron and Ref. 51 for the positive energies. Also, the coherence of the system is observed for $\chi > 2.5$. The absorption of photon by exciton polaron is highest in $MoS_2$ and lowest in $MoSe_2$.

## CONCLUSION

The investigation of the Tsallis entropy, the mobility, the lifetime and the optical absorption coefficient of the excitonic polaron in quasi-2D TMDCs QDs has been made. We extend the study to four different monolayer TMDCs materials $MoSe_2$, $WSe_2$, $WS_2$, $MoS_2$ whose parameters are recorded in Table I. The entropy is an increasing function of temperature and dot radius for each TMDCs material. This indicates that either for $T < 25$ K and $R < 6$ Å or $T > 25$ K and $R < 2$ Å, the system losses its quantum properties and conserves them either for $T > 25$ K and $R > 2$ Å or $T < 25$ K and $R > 6$ Å. The high mobility of TMDCs is a decreasing function of temperature and radius for each TMDCs material. For this property the exciton–polaron is coherent for R> 10 Å and decoherent otherwise at all temperatures. The exciton–polaron lifetime falls with increasing temperature and vanishes at high temperatures. So the temperature and the quantum confinement are very important in nanostructures. Such parameters can show the way to adjust the material's properties and then control the electron (or hole) transitions. For TMDCs materials, the exciton–polaron is coherent at high temperature, but in a very short time, whereas it is not coherent at low temperature for a longer period of time. The absorption of photon by the exciton–polaron needs twice the phonon energy as a polaron and the system becomes coherent for $\chi > 2.5$. Recently, interlayer excitons in TMDCs have demonstrated good performances,[52] such as large exciton binding energy[53] and longer lifetime[54] at room temperature. It will be interesting to evaluated Tsallis entropy, mobility and optical absorption in such heterostructures.

## CONFLICT OF INTEREST

The authors declare that they have no conflict of interest.

## REFERENCES


1. A. Kormányos, V. Zolyomi, N. Drummond, and G. Burkard, *Phys. Rev. X* 4, 011034 (2014).
2. X.-X. Song, D. Liu, V. Mosallanejad, J. You, T.-Y. Han, D.-T. Chen, H.-O. Li, G. Cao, M. Xiao, G.-C. Guo, and G, *Nanoscale* 7, 40 (2015).
3. A.J. Pearce, and G. Burkard, *2D Mater.* 4, 025114 (2017).
4. T. Georgiou, R. Jalil, D.B. Belle, L. Britnel, V.R. Gorbachev, V.S. Morozov, Y.-J. Kim, A. Gholinia, J.S. Haigh, O. Makarovsky, and L. Eaves, *Nat. Nanotechnol.* 8, 2 (2013).
5. B. Radisavljevic, A. Radenovic, J. Brivio, V. Giacometti, and A. Kis, *Nat. Nanotechnol.* 6, 3 (2011).
6. J.H. Cho, J. Lee, Y. Xia, B. Kim, Y. He, M.J. Renn, T.P. Lodge, and C.D. Frisbie, *Nat. Mater.* 7, 11 (2008).
7. S. Mouri, Y. Miyauchi, and K. Matsuda, *Nano Lett.* 13, 5944 (2013).
8. K. Mak, C. Lee, J. Hone, J. Shan, and T.F. Heinz, *Phys. Rev. Lett.* 105, 136805 (2010).
9. K. Mak, K. He, C. Lee, G.H. Lee, J. Hone, T. Heinz, and J. Shan, *Nat. Mater.* 12, 207 (2013).
10. D. Christiansen, M. Selig, G. Berghauser, R. Schmidt, I. Niehues, R. Schneider, A. Arora, S. Michaelis, R. Bratschitseh, E. Mallic, and A. Knorr, *Phys. Rev. Lett.* 119, 187402 (2017).
11. P. Back, S. Zeytinoglu, A. Ijaz, M. Kroner, and A. Imamoglu, *Phys. Rev. Lett.* 120, 037401 (2018).
12. Y. Xiao, Z-Q. Li, and Z-W. Wang, *J. Phys. Condens. Matter.* 29, 485001 (2017).
13. M. Geddo and G. Iadonisi, *Nuovo Cimento D* 12, 1641–1650 (1990).
14. M.H. Degani, and O. Hipolito, *Phys. Rev. B* 35, 4507 (1987).
15. E.S. Koteles and J.Y. Chi, *Phys. Rev. B* 37, 6332 (1988).
16. J. Maan, G. Belle, A. Fasolino, M. Altarelli, and K. Ploog, *Phys. Rev. B* 30, 2253 (1984).
17. J.T. Devreese and F. Peeters, *Polarons and Excitons in Polar Semiconductors and Ionic Crystals* (Springer Science and Business Media, 2013).
18. J. Singh, *Excitation Energy Transfer Processes in Condensed Matter: Theory and Application* (Springer Science and Business Media, 2013).
19. E. Biolatti, R.C. Lotti, P. Zanardi, and F. Rossi, *Phys. Rev. Lett.* 85, 5647 (2000).
20. I. Favero, G. Cassabois, R. Ferreira, D. Darson, C. Voisin, J. Tianon, and C. Delalande, *Phys. Rev. B* 68, 233301 (2003).
21. B. Krummheuer, V.M. Axt, and T. Kuhn, *Phys. Rev. B* 65, 195313 (2002).
22. L. Jacak, P. Machnikowski, J. Krasnyj, and P. Zoller, *Eur. Phys. J. D*. https://doi.org/10.1140/epjd/e2003000202 (2003).
23. M. Tiotsop, A.J. Fotue, G.K. Fautso, S.C. Kenfack, E. Mainimo , H.B. Fotsin, and L.C. Fai, *Chin. J. Phys.* 54, 795–801 (2016).
24. Z. Li, *Indian J. Phys.* 93, 6 (2018).
25. S. Xu, J. Cao, C. Miller, D. Mantell, R.J. Miller, and Y. Gao, *Phys. Rev. Lett.* 76, 483 (1996).
26. Y. Bai, J. Olivier, G. Bullard, C. Liu, and M. Therien, *Proc. Natl. Acad. Sci USA* 115, 4 (2018).
27. T. Valla, J. Camacho, Z. Pan, A. Fedorov, A. Walters, C. Howard, and M. Ellerby, *Phys. Rev. Lett.* 102, 107007 (2009).
28. J. Park, S. Rosenblatt, Y. Yaish, V. Sazonova, H. Ustunel, S. Braig, T. Arias, P. Brouwer, and P. Mceuen, *Nano. Lett.* 4, 517 (2004).
29. K. Sellami, and S. Jaziri, *Phys. Stat. Sol. c* 3, 9 (2006).
30. S. Ono and S. Tomohiro, *J. Appl. Phys.* 124, 034301 (2018).
31. M. Tiotsop, A. Fotue, G. Fautso, S. Kenfack, H. Fotsin, and L. Fai, *Superlattices Microstruct.* 103, 70–77 (2017).
32. S. Kenfack, A. Fotue, F. Fobasso, G. Bawe, and L. Fai, *Superlattices Microstruct.* 111, 32–44 (2017).
33. D. Akay, *Superlattices Microstruct.* 117, 18–24 (2018).
34. B.S. Kandemir, and D. Akay, *Phys. Stat. Solidi. B* 225, 10 (2018).
35. A. Thilagam, *Physica B* 464, 44–50 (2015).
36. R. Khordad, *Contin. Much. Thermodyn.* 28, 947–956 (2016).

37. R. Khordad and H. R. Sedehi, *Indian. J. Phys.* 92, 979–984 (2018).
38. Y. Ge, W. Wenhui, Y. Ren, and Y. Liu, *Phys. Rev. Res.* 2, 013134 (2020).
39. P.-F. Li, and Z.-W. Wang, *J. Appl. Phys.* 123, 204308 (2018).
40. J.J. Hopfeld and A.V. Herz, *Proc. Natl. Acad. Sci. USA* 92, 6655–6662 (1995).
41. R. Khordad, and H.R. Sedehi, *Indian J. Phys.* 91, 7 (2017).
42. C. Tsallis, *J. Stat. Phys.* 52, 479–487 (1988).
43. D. Kozawa, R. Kumar, A. Carvalho, K. Amara, W. Zhao, S. Wang, M. Toh, R. Ribeiro, A.C. Neto, K. Matsuda, and G. Eda, *Nat. Commun.* 5, 4543 (2014).
44. M.J. Tomczak, K. Haule, T. Miyake, A. Georges, and G. Kotliar, *Phys. Rev. B* 82, 085104 (2010).
45. J. Devreese, W. Huybrechts, and L. Lemmes, *Phys. Stat. Sol. B* 48, 77 (1971).
46. R. Quinton, B. Tabibi, and F.J. Seo, *J. Nanosci. Nanotechnol.* 18, 3 (2018).
47. Z. Sun, and S. Stafstrom, *J. Chem. Phys.* 138, 64905 (2013).
48. L. Yuanshuang, L. Huanglong, Q. Cuicui, H. Xiangmin, and D. Liu, *Nano Res.* 13, 3 (2020).
49. N. Zhonghui, S. Yongliang, S. Qin, W. Yuhan, J. Hongzhu, Z. Qijing, C. Yang, M. Yuze, S. Fengqi, W. Xiaoyong, I. Turcu, W. Xinran, X. Yongbing, Y. Shi, J. Zhao, R. Zhang, and F. Wang, *Commun. Phys.* (2019). https://doi.org/10.1038/s420050190202.
50. M.F. Jearvist, *Phys. Rev. B* 96, 195202 (2017).
51. F. Lengers, T. Kuhn, and D.E. Reiter, *Phys. Rev. B* 101, 155304 (2020).
52. S. Lukman, L. Ding, L. Xi, Y. Tao, A.C. Riis-jensen, G. Zhang, Q.Y.S. Wu, M. Yang, S. Luo, C. Hsu, L. Yao, G. Liang, H. Liu, Y.-W. Zhang, K.S. Thygesen, Q.J. Wang, Y. Feng, and J. Teng, *Nat. Nanotechnol.* (2020). https://doi.org/10.1038/s41565-020-0717-2.
53. C. Hogni Kamban, and G. Thomas Pedersen, C. Hogni Kamban, and G. Thomas Pedersen, *Sci. Rep.* (2020). https://doi.org/10.1038/s41598-020-62431-y.
54. Z. Sun, J. Beaumariage, Q. Cao, K. Watanable, T. Taniguchi, B.M. Hunt, and D. Snoke, *ACS Photonics* 7, 7 (2020).

Iran J Sci Technol Trans Sci
https://doi.org/10.1007/s40995-022-01283-9

RESEARCH PAPER

# Relaxation and Transport of Excitonic Polaron in Monolayer Transition Metal Dichalcogenides

A. Kitio Teguimfouet[1] · C. Kenfack-Sadem[2] · J. Valère Nguepnang[1] · A. Kenfack-Jiotsa[3] · K. Bhattacharyya[4]

Received: 5 June 2021 / Accepted: 12 March 2022


**Abstract**
The relaxation and the transport of excitonic polaron are theoretically investigated in two-dimensional (2D) monolayer (ML) transition metal dichalcogenides (TMDCs): $MoSe_2$, $WSe_2$, $WS_2$, $MoS_2$. It is found that the exciton-polaron relaxation time occurs when the exciton effective kinetic energy is higher than phonon energy. For each TMDC, it decreases with the enhancement of temperature, confinement length and carrier concentration above the critical value, whereas it increases for concentrations below. The temperature effect is well pronounced in xy-plane than in z-direction and $MoS_2$ relaxes the least. In addition, the electrical conductivity decreases with the temperature, but increases with exciton-polaron energy and the concentration of charge carriers. Seebeck coefficient increases for low temperatures, but it decreases in high temperatures. It is seen that in the presence of exciton-polaron, the Seebeck coefficient strongly depends on temperature. For the electrical conductivity and Seebeck effect, $MoSe_2$ is the most interesting. Also, the optical conductivity occurs for some values of the frequency for each TMDC. It is observed that the optical conductivity varies from one TMDC to another. The highest amplitude is observed in $MoS_2$ at low values of frequency and the lowest in $WSe_2$ at large values of frequency.

**Keywords** Relaxation · Exciton-polaron · Conductivity · Seebeck coefficient · TMDCs

## 1 Introduction

One of the two-dimensional (2D) interesting materials is transition metal dichalcogenides (TMDCs) because of their various applications which are mainly due to their structures. Their general formula is in the form $MX_2$ in which the atoms of the transition metal M are sandwiched between atoms of two layers of chalcogen X coupled to each other by the interactions of Van der Waals. They became particularly promising due to their semiconducting characteristics with large flexibility and high stability (Kormányos et al. 2014; Song et al. 2015; Pearce and Burkard 2017), their electronic and optical properties (Fiori et al. 2014; Bernardi et al. 2017) which indicate applications in transistors, photovoltaics, optoelectronics, molecular sensing and photodetectors (Mak et al. 2013; Qiu et al. 2015; Yang et al. 2018), in spintronic and valleytronic effects (Wang et al. 2017; Dey et al. 2017), in photoluminescence experiments (Ono and Tomohiro 2018).

Yang et al. (2014) studied the layer-dependence on electricity and optoelectronic properties. It is shown that the number of layers considerably influences these properties. The band gap increases when decreases the number of layers and single-layers provide best performance. Chen et al. (2014) demonstrated that the electrical conductivity increases with the decrease in thickness layer. That implies the probable surface dominance of electrical conduction in TMDC layer structures results from either the intrinsic high surface conductivity or the anisotropic conductivity. Qin

✉ C. Kenfack-Sadem
christian.kenfack@univ-dschang.org

[1] Laboratoire de Mécanique-Matériaux et Structures, Département de Physique, Faculté Des Sciences, Université de Yaoundé 1, P.O. Box 812, Yaoundé, Cameroun

[2] Laboratory of Condensed Matter and Nanomaterials, Department of Physics, Faculty of Science, University of Dschang, P.O.Box 67, Dschang, Cameroon

[3] Département de Physique, Ecole Normale Supérieure, Université de Yaoundé 1, BP 42, Yaoundé, Cameroun

[4] School of Physics, University of Hyderabad, Hyderabad 500046, India

Published online: 21 March 2022

et al. (2018) studied the effect of electron (hole) concentration at 300 K of the transport coefficient along the x and y directions. Anisotropic behavior is observed for thermopower and electrical conductivity. The electrical conductivity increases when enhances the carrier concentration, whereas it is decreasing for Seebeck coefficient. They found a larger asymmetry of the Seebeck coefficient for p-type doping than for n-type doping. High amplitudes of Seebeck coefficient are seen, and a peak is observed as the carrier concentration reaches $1.25 \times 10^{11}$ cm$^{-2}$. In addition, recently Ge et al. (2020) have combined first principle calculations and Boltzmann theory to demonstrate that TMDC materials have possibility of high-performance carrier transport. High Seebeck coefficient at low temperature and low electrical conductivity at high temperatures are observed. They showed that carrier transport can be due to the modest carrier effective mass and the weak electron (hole)—phonon coupling.

As the material is subject to an excitation, it generates electrons and holes which propagate in opposite directions with the same velocity. Since an exciton-polaron results from the interaction of a pair of electron–hole with phonons in the structure, then the relaxation phenomenon is determinant to understand such systems limited by the process of dressing with phonons (Favero et al. 2003; Jacak et al. 2003; Krummheuer et al. 2002). Relaxation is a good concept in the study of excitonic polaron systems precisely optical excitation, exciton formation and recombination (Jankovic and Vukmirovic 2015; Brem et al. 2018). Authors experimentally studied this time, and it appears that the range of relaxation time is around the femtoseconds (fs) and picosecond (ps) (Maidannyk and Roos 2016; Singh et al. 2014; Foglia et al. 2019). The exciton generation and the relaxation of intraconduction band are investigated in quantum dot (El-Ballouli et al. 2014). It is shown that the confinement has an important role in this process (Kandada and Silva 2020) and also in optical conductivity (Jia et al. 2016). The appearance of excitonic signal in optical conductivity has been demonstrated by Khoirunnisa and Majidi (2018) and Havener et al. (2014) revealed that the effects of exciton play a crucial role in the optical spectra. For energies below the gap, it appears as a well-defined peak in the absorption spectra, in the region within the energy gap. For energies above the gap, a renormalization of the band and an enhancement of the optical conductivity are observed and attributed to the Coulomb-mediated scattering between the electron–hole pair (Haug and Koch 1989; Ell et al. 1989). In addition, Peres et al. (2010) showed that excitonic resonances are responsible for several features of the experimentally measured midinfrared response of graphene such as the increase in the conductivity beyond the universal value above the Fermi blocked regime, the broadening of the absorption at the threshold and the decrease in the optical conductivity at higher frequencies.

Excitonic polaron systems have been modeled, but sometimes operators are not diagonally shaped and the techniques of diagonalization become necessary (Akay 2018, 2021; Kandemir and Akay 2018). In this context, Thilagam (2015) presented a model of the system and determined the effective mass, the ground state energy of monolayer (ML) TMDCs. Kenfack et al. (2021) investigated the exciton-polaron dynamics via the entropy, the lifetime, the mobility and the optical absorption for some TMDC materials: molybdenum diselenide ($MoSe_2$), molybdenum disulfide ($MoS_2$), tungsten diselenide ($WSe_2$) and tungsten disulfide ($WS_2$). It is seen that the entropy increases when the temperature and dot radius are increased, the lifetime decreases with the enhancement of temperature and then either the polaron or the exciton can exist separately in the structure. The excitonic polaron mobility decreases with an increase in the quantum confinement and temperature. Also, the absorption of photon begins when the photon energy reaches the energy of two phonons. Highest mobility and absorption are observed for $MoS_2$. It is shown that temperature and confinement influence considerably these optical properties. However, to explore the phenomenon of carrier transport, it is clear that the relaxation time, the electrical conductivity, the Seebeck coefficient and the optical conductivity are useful properties.

In this paper, we investigate the excitonic polaron transport properties for these four ML TMDCs. Section 2 is devoted to the model and calculations. Here, we derive the analytical expressions of relaxation time, electrical conductivity, Seebeck coefficient and optical conductivity. In Sect. 3, we present the numerical results and discussion. A comparison is made among the selected TMDC materials. The temperature effect, the confinement effect and the influence of carrier concentration are evaluated. We end with a conclusion which summarizes the results.

## 2 Model and Calculations

We consider an exciton moving in a slab representing a monolayer TMDC, interacting with longitudinal optical phonons in two dimensions. The total Hamiltonian is taken as (Thilagam and Singh 1996):

$$\hat{H} = \hat{H}_{ex}^{2D} + \hat{H}_z + \hat{H}_{ph} + \hat{H}_{ex-ph} \tag{1}$$

The first term of Eq. 1 is the Hamiltonian of exciton in the $xy-$ plane given by:

$$\hat{H}_{ex}^{2D} = \sum_{K_{//}} E_{K_{//}} C_{K_{//}}^{+} C_{K_{//}} \tag{2}$$

where $C_{K_{//}}^{+}$ and $C_{K_{//}}$ denote the creation and annihilation operators, whereas $K_{//}$ is the 2D exciton wave vector. $E(K_{//})$ is the exciton energy in the layered slab given explicitly by (Thilagam 2015):

$$E_{K_{//}} = \frac{\hbar^2 K_{//}^2}{2M} + E_g - E_b \tag{3}$$

$E_g$ and $E_b$ are, respectively, the band gap and exciton binding energies in the monolayer TMDC with the effective mass of the exciton $(M = m_e^* + m_h^*)$. $\hat{H}_z$ descripts the particles motion in the z-direction, and it takes the form:

$$\hat{H}_z = \frac{P_{e,z}^2}{2m_e^*} + \frac{P_{h,z}^2}{2m_h^*} + v_e(z_e) + v_h(z_h) \tag{4}$$

$P_{e,z}(P_{h,z})$ is the electron (hole) momentum and $m_e^*(m_h^*)$ is the effective mass of electron (hole). $v_e(z_e)$ and $v_h(z_h)$ are confinement potential of electron and hole, respectively, for a quantum well of width $(L)$ and infinite depth. The third term in Eq. 1 represents the Hamiltonian of optical phonon $(\hat{H}_{ph} = \sum_q \hbar\omega_0 b_q^+ b_q)$ with wave vector $(q)$ and $b_q^+(b_q)$ the phonon's creation (annihilation) operator.

The Hamiltonian of exciton–phonon interaction is given by:

$$\hat{H}_{ex-ph} = \sum_{K,q} \Xi(q) C_{K+q}^{+} C_K \left(b_q + b_{-q}^{+}\right) \tag{5}$$

where the exciton–phonon coupling function can be taken as (Shree et al. 2018):

$$\Xi(q) = (D_c - D_v)\sqrt{\frac{\hbar q}{2S\rho u}} \tag{6}$$

with $S$, the normalization area, $\rho$ being the area mass density and $u$ the sound velocity of the phonon mode.$D_c$ and $D_v$ denote, respectively, the deformation potential constant for electron-optical phonon interaction at the critical points $(K, K')$ in the conduction band and the corresponding expression for hole in the valence band.

The exiton-polaron ground state energy appears on the form:

$$\varepsilon = \varepsilon^{2D} + \varepsilon^{z} \tag{7}$$

where $\varepsilon^{2D}$ is the exciton-polaron energy in the $xy$-plane given by (Thilagam 2015):

$$\varepsilon^{2D}(K_{//}) = \left(\frac{\hbar^2 K_{//}^2}{2M}\right)\left(1 - \tilde{B}_{ex2}\right) + E_g - E_b - B_{ex1} \tag{8}$$

with

$$B_{ex1} = \frac{\pi\sqrt{\hbar\omega_0}\left(D_c^{op} - D_v^{op}\right)^2}{\sqrt{2}\,\hbar^2\rho u}\left(m_e^* + m_h^*\right)^{3/2},\ \tilde{B}_{ex2} = \frac{3\pi\left(D_c^{op} - D_v^{op}\right)^2}{4\sqrt{2}\,\hbar^2\rho u}\frac{\left(m_e^* + m_h^*\right)^{3/2}}{\sqrt{\hbar\omega_0}} \tag{9}$$

and the corresponding energy in the z-direction is taken as:

$$\varepsilon^{z} = \frac{\hbar^2\pi^2}{2\mu L^2} = \frac{\hbar^2 K_z^2}{2\mu} \tag{10}$$

here, the motion of the exciton reduced mass $(1/\mu = 1/m_e^* + 1/m_h^*)$ with a momentum $P_z = \hbar K_z$ is observed.

## 2.1 Relaxation Time

The transport and dynamics of polaronic systems are governed by the fact that the time of optical phonon is finite and approximately constant in materials. The exciton-polaron relaxation time $(\tau)$ can be written in the form (Ge et al. 2020):

$$\frac{1}{\tau} = \frac{2\pi}{\hbar}\sum_q |\Xi(q)|^2 \{ (n_B + f_{K+q})\delta(\varepsilon - \varepsilon_{K+q} + \hbar\omega_0) + (n_B + 1 - f_{K+q})\delta(\varepsilon - \varepsilon_{K+q} - \hbar\omega_0)\} \tag{11}$$

where $n_B$ is the Bose–Einstein distribution function and $f(\varepsilon, E_F)$ is the Fermi–Dirac distribution function with the Fermi energy $(E_F)$ which is related to the concentration of charge carriers $n$ (Al-Jaber 1999).

We first evaluate the relaxation time in the $xy$-plane as:

$$\frac{1}{\tau^{2D}} = \frac{2\pi}{\hbar}\sum_{q_{//}} \left|\Xi(q_{//})\right|^2 \Big\{ (n_B + f_{K_{//}+q_{//}})\delta(\varepsilon_{K_{//}}^{2D} - \varepsilon_{K_{//}+q_{//}}^{2D} + \hbar\omega_0) + (n_B + 1 - f_{K_{//}+q_{//}})\delta(\varepsilon_{K_{//}}^{2D} - \varepsilon_{K_{//}+q_{//}}^{2D} - \hbar\omega_0)\Big\} \tag{12}$$

Let use the following relation:

$$\delta[g(q)] = \sum_i \frac{\delta(q - q_i)}{|g'(q_i)|} \tag{13}$$

where $q_i$ are the roots of the function $g$. Therefore, with respect to Eq. 8, the Dirac delta functions are transformed as:

$$\delta(\varepsilon_{K_{//}}^{2D} - \varepsilon_{K_{//}+q_{//}}^{2D} + \hbar\omega_0) = \frac{M}{\hbar^2(1 - \tilde{B}_{ex2})} \frac{\delta(q_{//} - q_1) + \delta(q_{//} - q_2)}{\sqrt{K_{//}^2\cos^2\theta + 2M\hbar\omega_0/\hbar^2(1 - \tilde{B}_{ex2})}} \tag{14}$$

and

$$\delta(\varepsilon^{2D}_{K_{//}} - \varepsilon^{2D}_{K_{//}+q_{//}} - \hbar\omega_0) = \frac{M}{\hbar^2(1-\tilde{B}_{ex2})} \frac{\delta(q_{//}-q_3)+\delta(q_{//}-q_4)}{\sqrt{K_{//}^2\cos^2\theta - 2M\hbar\omega_0/\hbar^2(1-\tilde{B}_{ex2})}} \tag{15}$$

where

$$\begin{cases} q_1 = -K_{//}\cos\theta + \sqrt{K_{//}^2\cos^2\theta + 2M\hbar\omega_0/\hbar^2(1-\tilde{B}_{ex2})} \\ q_2 = -K_{//}\cos\theta - \sqrt{K_{//}^2\cos^2\theta + 2M\hbar\omega_0/\hbar^2(1-\tilde{B}_{ex2})} \end{cases} \tag{16}$$

and

$$\begin{cases} q_3 = -K_{//}\cos\theta + \sqrt{K_{//}^2\cos^2\theta - 2M\hbar\omega_0/\hbar^2(1-\tilde{B}_{ex2})} \\ q_4 = -K_{//}\cos\theta - \sqrt{K_{//}^2\cos^2\theta - 2M\hbar\omega_0/\hbar^2(1-\tilde{B}_{ex2})} \end{cases} \tag{17}$$

The summation of Eq. 12 is converted into integration and we integrate over $q_{//}$ to obtain:

$$\frac{1}{\tau^{2D}(K_{//})} = \frac{M(D_c-D_v)^2}{\pi\rho u\hbar^2(1-\tilde{B}_{ex2})}\left[n_B + \left\{1+\exp\beta\left(\varepsilon^{2D}+\hbar\omega_0-E_F\right)\right\}^{-1}\right]K_{//}I^+ + \frac{M(D_c-D_v)^2}{\pi\rho u\hbar^2(1-\tilde{B}_{ex2})}\left[1+n_B - \left\{1+\exp\beta\left(\varepsilon^{2D}-\hbar\omega_0-E_F\right)\right\}^{-1}\right]K_{//}I^- \tag{18}$$

where

$$I^+ = \frac{4}{\sqrt{A_2}}\int_0^{\pi/2}\frac{A_1-\sin^2\theta}{\sqrt{1-A^2\sin^2\theta}}d\theta;\ I^- = \frac{4}{\sqrt{B_2}}\int_0^{\pi/2}\frac{B_1-\sin^2\theta}{\sqrt{1-B^2\sin^2\theta}}d\theta \tag{19}$$

with

$$A_1 = \frac{\hbar^2K_{//}^2(1-\tilde{B}_{ex2})+M\hbar\omega_0}{\hbar^2K_{//}^2(1-\tilde{B}_{ex2})};\ A_2 = \frac{\hbar^2K_{//}^2(1-\tilde{B}_{ex2})+2M\hbar\omega_0}{\hbar^2K_{//}^2(1-\tilde{B}_{ex2})};\ A^2 = 1/A_2 \tag{20}$$

$$B_1 = \frac{\hbar^2K_{//}^2(1-\tilde{B}_{ex2})-M\hbar\omega_0}{\hbar^2K_{//}^2(1-\tilde{B}_{ex2})};\ B_2 = \frac{\hbar^2K_{//}^2(1-\tilde{B}_{ex2})-2M\hbar\omega_0}{\hbar^2K_{//}^2(1-\tilde{B}_{ex2})};\ B^2 = 1/B_2 \tag{21}$$

One can see the two terms of Eq. 18 which are attributed, respectively, to electron and hole contributions on the excitonic polaron relaxation time.

Since $A^2 < 1$, $I^+$ can be solve using the elliptic integrals of the first and second kind. However, to integrate $I^-$ it is convenient to take ($B^2 \to 1$):

$$\hbar^2K_{//}^2(1-\tilde{B}_{ex2}) > > 2M\hbar\omega_0 \tag{22}$$

This leads to:

$$I^- \approx I^+ = 4\int_0^{\pi/2}\cos(\theta)d\theta \tag{23}$$

Then, the final expression of the 2D-relaxation time reads:

$$\frac{1}{\tau^{2D}(K_{//})} = \frac{4M(D_c-D_v)^2}{\pi\rho u\hbar^2(1-\tilde{B}_{ex2})}(1+2n_B)K_{//} \tag{24}$$

This time is proportional to the factor $(1+2n_B)$ which indicates both the phonon emission and absorption processes (Shree et al. 2018).

In the z-direction, we start from:

$$\frac{1}{\tau^z} = \frac{2\pi}{\hbar}\sum_{q_z}|\Xi(q_z)|^2\Big\{(n_B+f_{K_z+q_z})\delta(\varepsilon^z-\varepsilon^z_{K_z+q_z}+\hbar\omega_0) + (n_B+1-f_{K_z+q_z})\delta(\varepsilon^z-\varepsilon^z_{K_z+q_z}-\hbar\omega_0)\Big\} \tag{25}$$

In the same manner, we transform the Delta Dirac functions using:

$$\begin{cases} q_1' = K_z - \sqrt{K_z^2+2\mu\hbar\omega_0/\hbar^2} \\ q_2' = K_z + \sqrt{K_z^2+2\mu\hbar\omega_0/\hbar^2} \end{cases};\quad \begin{cases} q_3' = K_z - \sqrt{K_z^2-2\mu\hbar\omega_0/\hbar^2} \\ q_4' = K_z + \sqrt{K_z^2-2\mu\hbar\omega_0/\hbar^2} \end{cases} \tag{26}$$

and obtain a similar relation as Eq. 24 for the z-direction:

$$\frac{1}{\tau^z(K_z)} = \frac{\mu(D_c-D_v)^2}{\rho u\hbar^2}\left\{\frac{n_B+f_{K_z+\hbar\omega_0}}{\sqrt{K_z^2+2\mu\hbar\omega_0/\hbar^2}} + \frac{1+n_B-f_{K_z-\hbar\omega_0}}{\sqrt{K_z^2-2\mu\hbar\omega_0/\hbar^2}}\right\}K_z \tag{27}$$

The relaxation time is given by Eqs. 24 and 27, respectively, for xy-plane and z-direction. It is seen that the temperature, the concentration of charge carriers and the confinement length act on this property.

## 2.2 Seebeck Coefficient

The thermoelectric power (Seebeck's effect) of a material can be seen as its property to transform heat into electricity or the fact of generating a current when it is subjected to a thermal variation. The Seebeck coefficient can be written as (Huang et al. 2018):

$$S = \frac{e\beta}{\sigma}\int \lambda(E)\left(-\frac{\partial f}{\partial E}\right)(E - E_F)dE \tag{28}$$

$\sigma$ is the electrical conductivity taken in the relaxation time approximation as (Pizzi et al. 2014):

$$\sigma = e^2\int \lambda(E)\left(-\frac{\partial f}{\partial E}\right)dE \tag{29}$$

and $\lambda(E)$ is the transport function given by:

$$\lambda(E) = \frac{1}{S}\sum_K v_g^2\,\tau\,\delta(E-\varepsilon) \tag{30}$$

where $v_g$ represents the group velocity (Tomczak et al. 2010) taken, according to the total energy, as:

$$v_g = \frac{\partial\varepsilon}{\partial P} = \frac{\hbar K_{//}\left(1-\tilde{B}_{ex2}\right)}{M} + \frac{\hbar K_z}{\mu} = v_{//} + v_z \tag{31}$$

One gets, respectively:

$$\begin{aligned}\lambda^{2D} &= \frac{1}{S}\sum_{K_{//}} v_{//}^2\,\tau^{2D}\,\delta\left(E-\varepsilon^{2D}\right) \text{ and } \lambda^z \\ &= \frac{1}{S}\sum_{K_z} v_z^2\,\tau^z\,\delta(E-\varepsilon^z)\end{aligned} \tag{32}$$

According to Eq. 7 and using Eq. 13, we have:

$$\begin{aligned}\delta\left(E-\varepsilon^{2D}\right) = \frac{M}{\hbar^2\left(1-\tilde{B}_{ex2}\right)}\frac{1}{K_0}\{&\delta\left(K_{//}-K_0\right) \\ &+\delta\left(K_{//}+K_0\right)\}\end{aligned} \tag{33}$$

and

$$\delta(E-\varepsilon^z) = \frac{\mu}{\hbar^2}\frac{1}{K_0'}\left\{\delta(K_z-K_0') + \delta(K_z+K_0')\right\} \tag{34}$$

with

$$K_0 = \frac{\sqrt{2M\left(E+E_b+B_{ex1}-E_g\right)}}{\hbar\sqrt{1-\tilde{B}_{ex2}}} \text{ and } K_0' = \frac{\sqrt{2\mu E}}{\hbar} \tag{35}$$

Then, Eq. 32 becomes:

$$\begin{aligned}\lambda^{2D} = \frac{\left(1-\tilde{B}_{ex2}\right)}{2\pi M K_0}\int_0^\infty dK_{//}K_{//}^3\tau^{2D}(K_{//})\{&\delta(K_{//}-K_0) \\ &+\delta(K_{//}+K_0)\}\end{aligned} \tag{36}$$

After integrating with respect to Eq. 35, the 2D transport function gives:

$$\lambda^{2D} = \frac{\rho u\hbar(1-\tilde{B}_{ex2})^{3/2}}{2\sqrt{2}M^{3/2}(D_c-D_v)^2}\frac{\sqrt{E+E_b+B_{ex1}-E_g}}{(1+2n_B)} \tag{37}$$

In other hand, we have:

$$\begin{aligned}\lambda^z &= \frac{1}{2\pi\mu K_0'}\int_0^a dK_z\,K_z^2\tau^z(K_z)\left\{\delta(K_z-K_0')+\delta(K_z+K_0')\right\} \\ &= 0\end{aligned} \tag{38}$$

From the latest, the transport function is globally in the xy-plane for our 2D TMDCs. Then, considering the approximation of Boltzmann (Shree et al. 2018) in Eq. 29 that means $-\partial f/\partial E \approx \beta f$, the electrical conductivity reads:

$$\begin{aligned}\sigma^{2D} = &\frac{e^2\rho u\hbar(1-\tilde{B}_{ex2})^{3/2}}{2\sqrt{2}M^{3/2}(D_c-D_v)^2}\frac{\beta}{(1+2n_B)} \\ &\int_0^\infty dE f(E)\sqrt{E+E_b+B_{ex1}-E_g}\end{aligned} \tag{39}$$

Since the electrical conductivity depends on temperature, a variation of temperature can induce the Seebeck's effect.

Then, substituting Eq. 39 into Eq. 28, we obtain the Seebeck coefficient:

$$S = \frac{\beta}{e}\frac{C_1}{C_2} \tag{40}$$

where

$$\begin{aligned}C_1 = &\int_0^\infty dE\,f(E)(E-E_F)\sqrt{E+E_b+B_{ex1}-E_g};\; C_2 \\ &= \int_0^\infty dE\,f(E)\sqrt{E+E_b+B_{ex1}-E_g}\end{aligned} \tag{41}$$

## 2.3 Optical Conductivity

In an excitonic system, the excited electron can transit via an absorption or emission process of phonons. This motion of the electron (and its corresponding hole) contributes to the conductivity. Here, the optical conductivity represents the optical response of the TMDC materials and it can be expressed through the Kubo formula (Devreese 2018):

$$\sigma_{(\omega)} = i\frac{2e^2}{SM\omega} + \frac{1}{S\hbar\omega}\int_0^\infty dt\,e^{i\omega t}\langle[J_x(t),J_x(0)]\rangle \tag{42}$$

where $J_x$ is the $x$-component of the current operator $J$ which is related to the momentum operator of the charge carriers by:

$$J = \frac{q}{m}\sum_{j=1}^N p_j = \frac{e}{m_h}p_h - \frac{e}{m_e}p_e \tag{43}$$

The real part of the optical conductivity at zero temperature can be written as:

$$\mathrm{Re}\sigma_{(\omega)} = \frac{1}{S\hbar\omega}\mathrm{Im}\left\{\int_0^\infty dt\, e^{i\omega t}\left\langle \frac{e^2}{m_h^2}[p_{xh}(t), p_{xh}(0)] + \frac{e^2}{m_e^2}[p_{xe}(t), p_{xe}(0)]\right\rangle\right\} \tag{44}$$

From the vanish of the total momentum of the system, one gets:

$$p_e = p_h = p = -\frac{1}{2}\sum_q \hbar q b_q^+ b_q \tag{45}$$

Integrating by parts, we have:

$$\mathrm{Re}\sigma_{(\omega)} = \frac{-e^2\left(m_h^2 + m_e^2\right)}{Sm_e^2 m_h^2 \hbar\omega^3}\mathrm{Im}\left\{\int_0^\infty dt\, e^{i\omega t}\langle[F(t), F(0)]\rangle\right\} \tag{46}$$

where

$$F(t) = \frac{i}{\hbar}[H, p_x(t)] = \\ = \frac{-i}{2}\sum_q q_x \Xi(q)\, C_{K+q}^+(t) C_K(t)\left(b_q(t) - b_q^+(t)\right) \tag{47}$$

The operators are given by:

$$\begin{cases} b_q^+(t) = \exp(i\omega_0 t) b_q^+(0) \\ b_q(t) = \exp(-i\omega_0 t) b_q(0) \end{cases}$$

$$\text{and} \quad \begin{cases} C_{K+q}^+(t) = \exp(\frac{it}{\hbar}E_{K+q}) C_{K+q}^+(0) \\ C_K^+(t) = \exp(-\frac{it}{\hbar}E_K) C_K^+(0) \end{cases} \tag{48}$$

Substituting the latest relations in Eq. 46, the real part of the optical conductivity gives:

$$\mathrm{Re}\sigma_{(\omega)} = \frac{e^2\left(m_h^2 + m_e^2\right)}{4Sm_e^2 m_h^2 \hbar\omega^3}\mathrm{Im} \\ \left\{\int_0^\infty dt\, e^{i\omega t}\left\langle \sum_q q_x^2\, \Xi^2(q)\left\{U(t) - T(t)\right\} C_{K+q}^+(0) C_K(0)\right\rangle\right\} \tag{49}$$

with

$$T(t) = \exp\frac{it}{\hbar}\left(E_{K+q} - E_K - \hbar\omega_0\right) \quad \text{and} \quad U(t) \\ = \exp\frac{it}{\hbar}\left(E_{K+q} - E_K + \hbar\omega_0\right) \tag{50}$$

Let us average with $|\phi_0\rangle = U_{ex} C_K^+ |0\rangle_k |0\rangle_q$ and integrate over $t$, one gets for $\hbar = 1$:

$$\mathrm{Re}\sigma_{(\omega)} = \frac{Me^2\left(m_h^2 + m_e^2\right)(D_c - D_v)^2}{8\rho u S^2 m_e^2 m_h^2 \omega^3} \\ \sum_q q^3\left(\frac{1}{q^2 + 2kq\cos\theta + 2M(\omega + \omega_0)} \right. \\ \left. - \frac{1}{q^2 + 2kq\cos\theta + 2M(\omega - \omega_0)}\right) \tag{51}$$

Transforming the summation into integration and integrating over $\theta$, it gives:

$$\mathrm{Re}\sigma_{(\omega)} = \frac{e^2 M\left(m_h^2 + m_e^2\right)(D_c - D_v)^2}{16\pi\rho u S m_e^2 m_h^2 \omega^3} \\ \int_0^\infty dq\, q^4\left(\frac{1}{\sqrt{q^4 - 4k^2q^2 + 4Mq^2(\omega + \omega_0) + 4M^2(\omega + \omega_0)^2}} \right. \\ \left. - \frac{1}{\sqrt{q^4 - 4k^2q^2 + 4Mq^2(\omega - \omega_0) + 4M^2(\omega - \omega_0)^2}}\right) \tag{52}$$

The real part of the optical conductivity of exciton-polaron is finally obtained as:

$$\mathrm{Re}\sigma_{(\omega)} = \frac{n_0 e^2 M\left(m_h^2 + m_e^2\right)}{8\pi\rho u}\frac{(D_c - D_v)^2}{m_e^2 m_h^2}\frac{1}{\omega^3}\int_0^\infty dq\, q^4 \\ \left(\frac{1}{\sqrt{q^4 - 4k^2q^2 + 4Mq^2(\omega + \omega_0) + 4M^2(\omega + \omega_0)^2}} \right. \\ \left. - \frac{1}{\sqrt{q^4 - 4k^2q^2 + 4Mq^2(\omega - \omega_0) + 4M^2(\omega - \omega_0)^2}}\right) \tag{53}$$

## 3 Results and Discussion

The characteristics of each material that we have used for calculations are given in Table 1, and the mass of electron (hole) is in the free electron mass unit. From Eq. 22, it is seen that the relaxation appears when the exciton effective kinetic energy is very higher than the phonon energy, else it is an electron (or polaron) relaxation.

Figures 1 and 2 present the temperature dependence on the relaxation time in xy-plane and z-direction, respectively. The greatest amplitudes are observed for lower temperatures, and it decreases when the temperature is increased. In fact, the increase in temperature perturbs the electron (hole) distribution and increases the diffusion coefficient in the excitonic network of TMDC. This leads to the appearance of loss power in the system and then, the decrease in the exciton-polaron relaxation time. For high temperatures (T > 25 K in the plane and T > 150 K in z-direction), the relaxation time becomes constant and the

**Table 1** Parameters of monolayer TMDCs materials taken from (Thilagam 2015; Xiao et al. 2017)

| Material | $m_e(m_0)$ | $m_h(m_0)$ | $\hbar\omega_0(eV)$ | $D_c(eV)$ | $D_v(eV)$ | $E_b(eV)$ | $E_g(eV)$ |
|---|---|---|---|---|---|---|---|
| $MoSe_2$ | 0.64 | 0.71 | 0.0365 | 5.2 | 4.9 | 0.174 | 1.56 |
| $WSe_2$ | 0.39 | 0.51 | 0.0291 | 2.3 | 3.1 | 0.231 | 1.65 |
| $WS_2$ | 0.31 | 0.42 | 0.0435 | 3.1 | 2.3 | 0.19 | 2.10 |
| $MoS_2$ | 0.51 | 0.58 | 0.0443 | 5.8 | 4.6 | 0.313 | 1.87 |

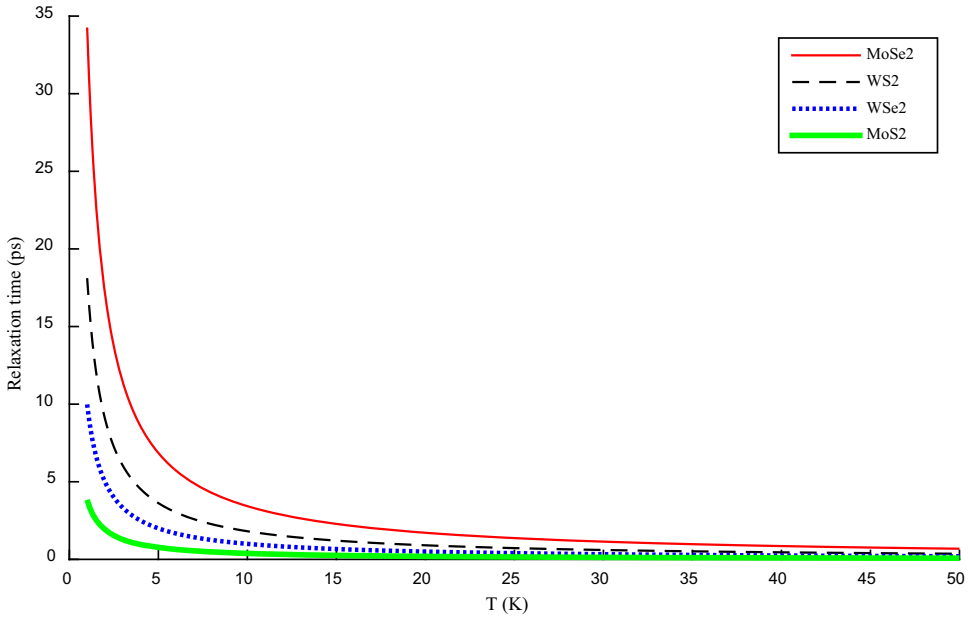


**Fig. 1** 2D excitonic polaron relaxation time as function of temperature for different TMDCs

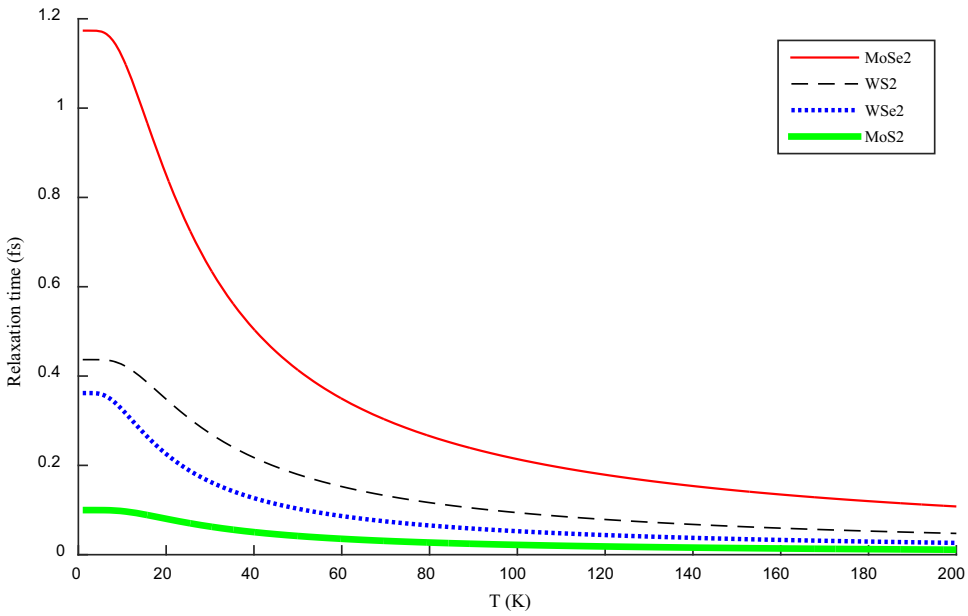


**Fig. 2** Exciton-polaron relaxation time in z-direction versus temperature for different TMDCs at L = 1 nm

system reaches the thermal equilibrium. The relaxation of exciton-polaron is related to the process of dressing with phonon: more the carriers interact with the structure and less they relax. One can say that due to temperature, the exciton interacts with more phonons and then, it takes few time to reach the equilibrium. The result agrees with the works of Glazov (2020) and Maidannyk et al. (2016). In addition, it is shown that the temperature effect is well pronounced in the plane because the drop observed in Fig. 1, while in Fig. 2 it is a low decrease. This difference

is related to the confinement since in the z-direction; the system needs more thermal energy (temperatures) to dominate the confinement energy and acts on confined exciton-polaron.

Figure 3 shows the influence of carrier concentration on the exciton-polaron relaxation. It is seen that due to the increase in the carrier concentration, the relaxation time does not have a monotonic behavior. This influence is observed only for concentrations around a critical value corresponding to the peak. The increase in the carrier concentration means the increase in electrons and holes number in the structure. It is seen that at a low fixed temperature there is a corresponding critical value of carrier concentration. Up to this value, the particles interact with phonons that lead to their cooling, contributing then to the increase in the relaxation time. However, above this critical value it is higher concentrations, the collisions between carriers can enhance the heat in the material and then decreases the relaxation time as seen for the previous figures. The latest is in agreement with the study of Huang et al. (2018). Also, $MoS_2$ has the lowest peak appearing at lowest critical value.

Figure 4 presents the confinement effect on the exciton-polaron relaxation time. It appears that the increase in the confinement length leads to a decrease in the relaxation time. This is explained by the fact that exciton-polaron is well confined in the structure for lower values of confinement length since it is inversely proportional to the energy. A great confinement does not obstruct the interaction with phonon. It is shown that for the excitonic polaron system, the time to return into equilibrium is reduced when the particles are confined. This result adheres with the ones of Singh et al. (2014) and (Tong and Wu 2018). In the other hand, the results indicate that $MoS_2$ is the most interesting for this first property since it has the lowest amplitude which can be attributed to its highest excitonic deformation potential $(D_c - D_v)$ according to Eqs. 24 and 27.

Figure 5 plots the electrical conductivity as function of the temperature for four materials. It is seen that the electrical conductivity of TMDCs decreases when increases the temperature. In fact, when raises the temperature in the medium, that enhances the lattice vibrations, modifies the particles direction and therefore reduces the electron (hole) motion. The enhancement of temperature creates a disorder that perturbs the electronic transitions. This is in agreement with the work of Xu et al. (2020). At very low temperature, it is highest conductivities in TMDCs, whereas at high temperatures it is lower conductivity, it becomes constant and can vanish. The curve presents two ranges of temperature: $T < 20$ K, a drop of conductivity is observed and it can be related to the appearance of conductor-semiconductor phase transition. $T > 20$ K, we observe a slowly decreasing of conductivity which characterize a metallic behavior. This joins the work of Meziane et al. (2016).

Figure 6 displays the electrical conductivity versus the excitonic polaron energy for four materials. It is observed that the electrical conductivity is an increasing function of the system energy. This is explained by the fact that particles in the valence band need to be energetic for transition toward the conduction band. Seen Eq. 38 and this figure, the conductivity appears when the energy of the system reaches to the gap energy and it increases to a maximum then becomes constant. Since there is a gap between valence and conduction bands in TMDCs, the electron with energy lower than the gap energy remains in the valence

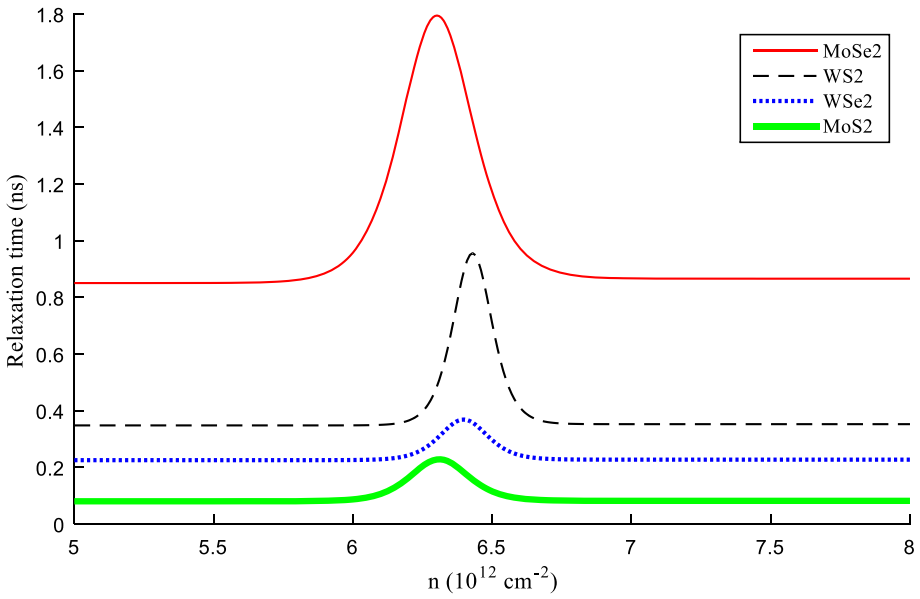


**Fig. 3** Exciton-polaron relaxation time in z-direction versus the carrier concentration for different TMDCs at T = 20 K and $L = 1\ \mu m$

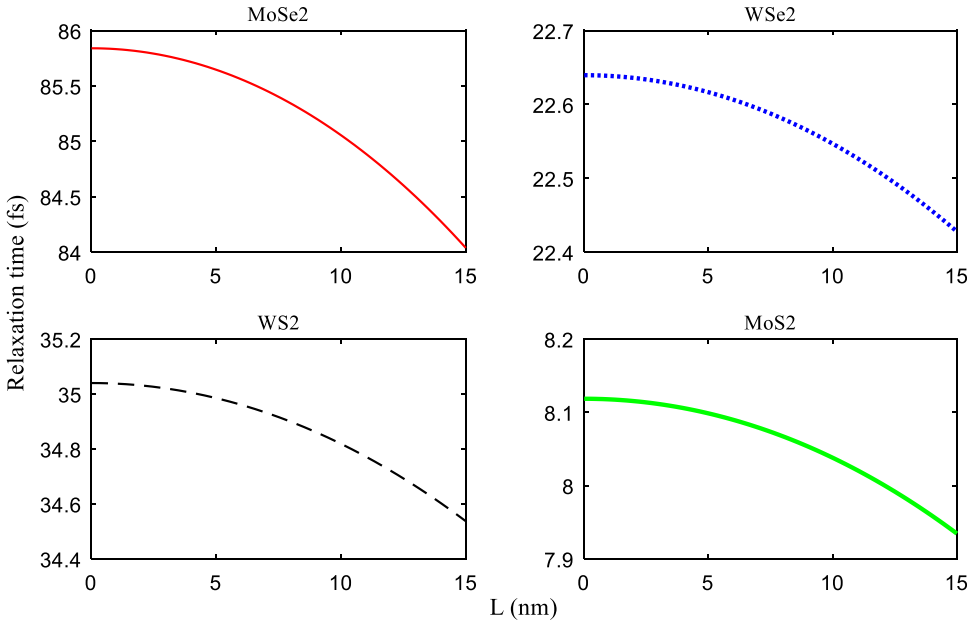


**Fig. 4** Exciton-polaron relaxation time in z-direction versus the confinement length for different TMDCs at T = 20 K

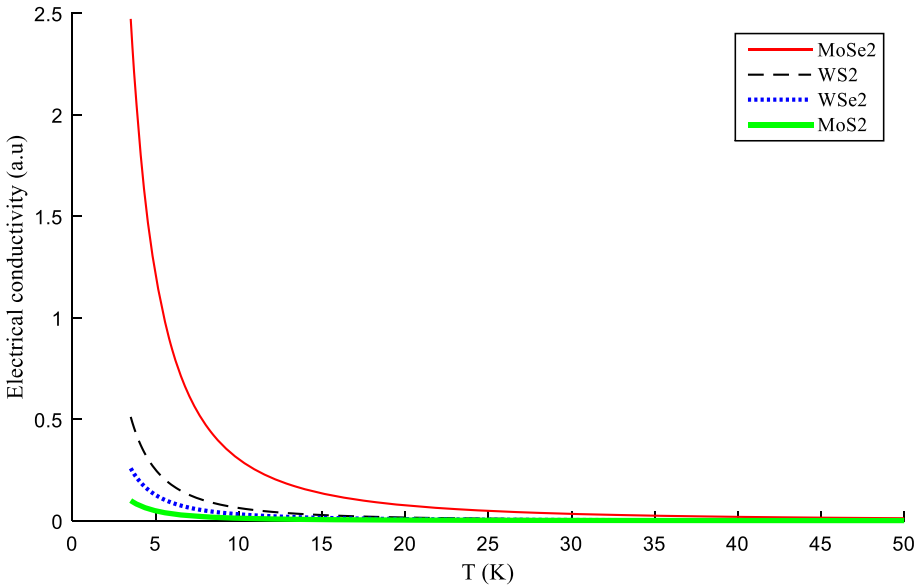


**Fig. 5** Electrical conductivity versus temperature for different TMDCs

band and, the more it gains in energy the more its possibility of reaching the conduction band enhances. Also from Fig. 7, it is shown that the conductivity increases when enhances charge carriers concentration. In fact, as the number of carriers increases, the particles move gradually toward the conduction band up to the Fermi energy and then, saturation occurs meaning that the conduction band is full. The number of particles increases the transitions, the more the energy of particles increases and it becomes easy to move toward the conduction band. Among the selected materials,$MoSe_2$ is the most interesting for electrical conductivity and is due to the fact that it has the lowest gap energy. This result is in accordance with (Wickramaratne et al. 2014; Ge et al. 2020). Moreover, as was pointed Seung-il (2012), it is seen from different TMDCs that the greater the relaxation time and the higher the electrical conductivity. Therefore, when the exciton-polaron lasts before reaching equilibrium that favors the electronic jumps in the material.

Figure 8 plots the Seebeck coefficient as function of the temperature for various ML TMDCs. It is seen that the Seebeck coefficient of TMDCs behaves differently at low temperature and high temperature. At very low temperature, the Seebeck coefficient approaches zero, meaning that the change of temperature is too weak and not sensitive for the material. It increases to a maximum when enhances

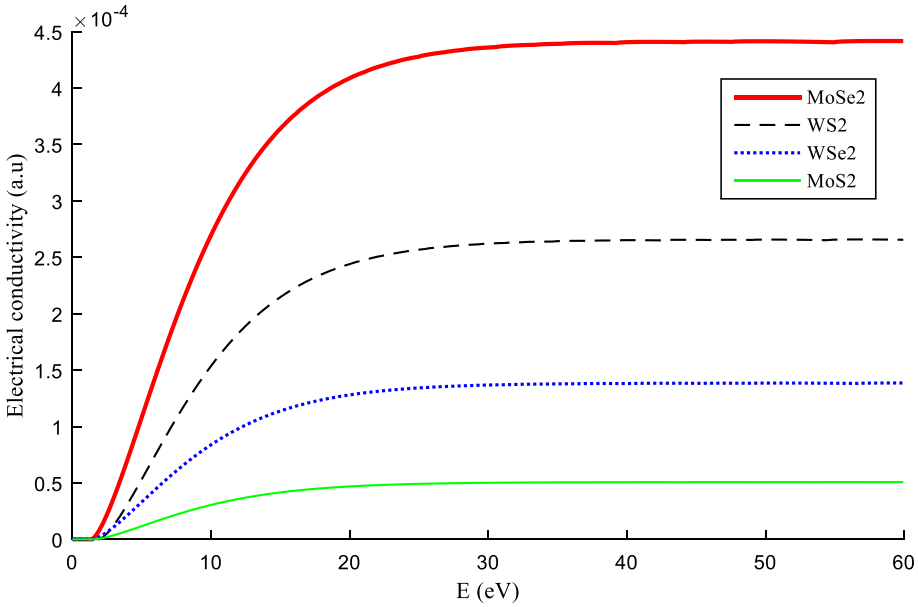


**Fig. 6** Electrical conductivity versus exciton-polaron energy for different TMDCs at $T = 5K$ and $n = 30\ \mathrm{cm}^{-2}$

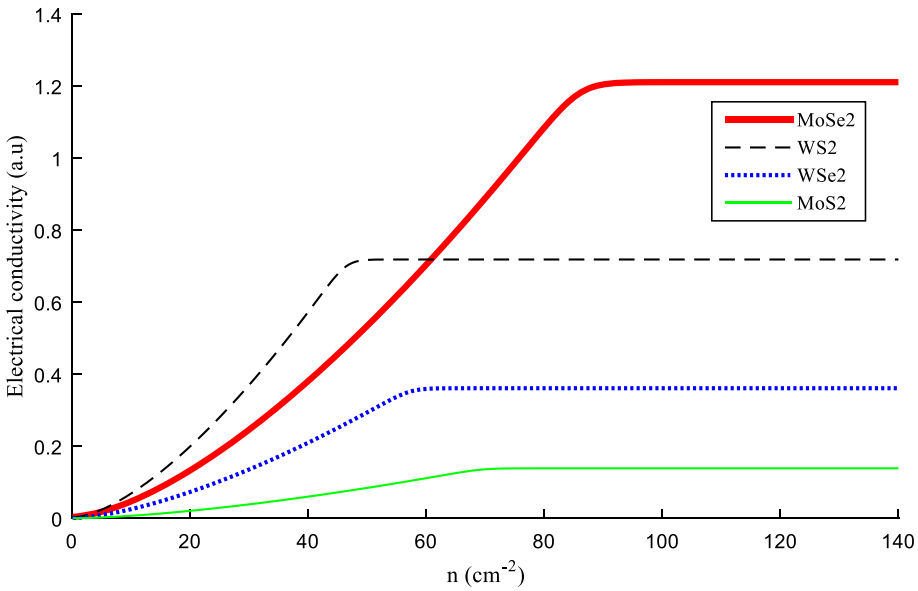


**Fig. 7** Electrical conductivity versus the concentration of charge carriers for different TMDCs at $T = 5K$

temperature and the peak is observed at temperature close to 15 K. The low change of temperature (T < 15 K) creates the movement of hot particles, inducing a voltage and then appears the Seebeck effect. This induction is attenuated in high temperatures range because particles are very hot and favor a collision motion in the structure. High temperatures (T > 15 K) act in the system as a perturbation which favors the disorder and then reduce the Seebeck voltage. Therefore, TMDCs generate an electric current when they are subject of temperature least than 15 K, but this current is dominated by the thermal disorder due to high temperatures. The result agrees with (Selvaggi 2019; Ashraf 2019).

Figure 9 plots the Seebeck coefficient versus the carrier concentration for various ML TMDCs. It is shown that the Seebeck coefficient is a decreasing function of the carrier concentration. In the case of exciton-polaron, we observe negative and positive values of the Seebeck coefficient which refer to the presence of electron and hole, respectively, in the system. The result indicates the dominance of the electrons in this thermoelectric property when enhances the carriers concentration. In fact, the Seebeck effect implies the creation of a low electric field and the electron's charge favors an electric force opposite to the field in direction. Then, more the structure is concentrated in electrons, and the stronger is the opposition to the appearance of the current induced by the temperature

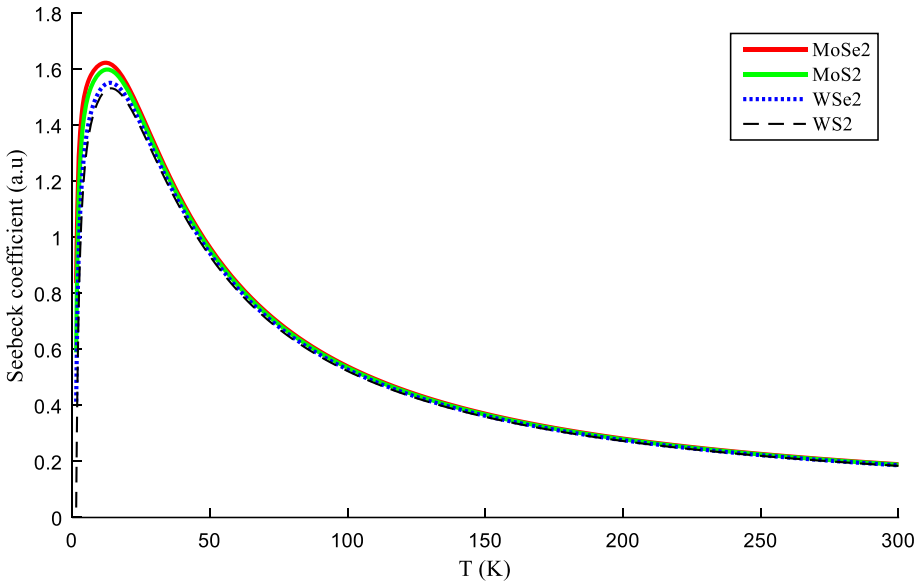


**Fig. 8** Seebeck coefficient versus temperature for different TMDCs

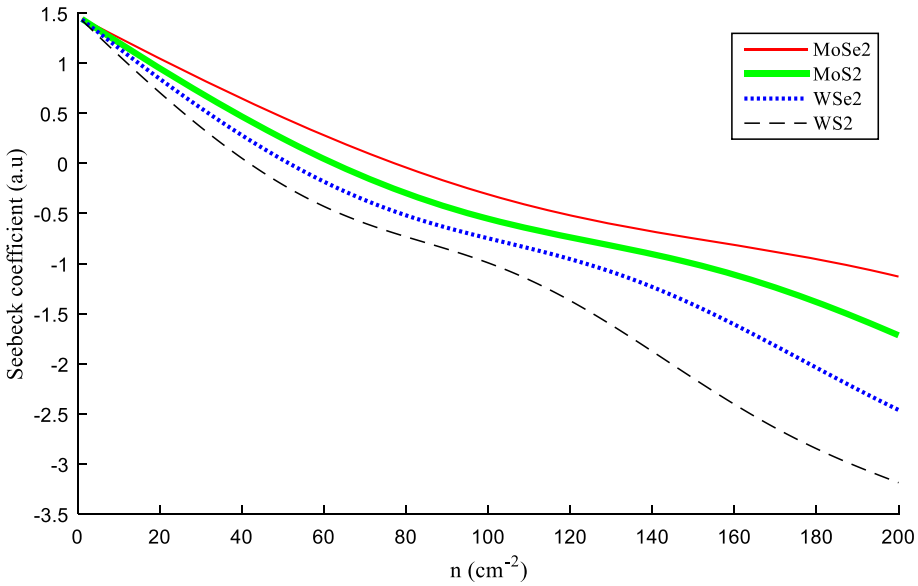


**Fig. 9** Seebeck coefficient versus the concentration of charge carriers for various TMDCs at T = 100 K

change; this explains the decrease observed on the curves. Also, $MoSe_2$ has the highest magnitude for this property and the result adheres with (Qin et al. 2018; Ge et al. 2020).

Figure 10 presents the real part of optical conductivity as a function of the frequency for different monolayer TMDCs. It is shown that the conductivity appears when the system absorbs the phonon and this is observed by the appearance of the peak which characterizes the first relaxed excited state. From Eq. 53, one can see that the optical conductivity is inversely proportional to the frequency and then, it falls when the frequency is increased. This result is in accordance with that obtained by previous authors (Huang et al. 2018; Glen et al. 2011). It is noticed that this behavior is observed for all materials, but the optical conductivity starts at a different value of frequency for each material showing the difference of vibration in these TMDCs. $MoS_2$ and $MoSe_2$ are interesting for optical conductivity because of their high magnitudes and it occurs at low frequencies.

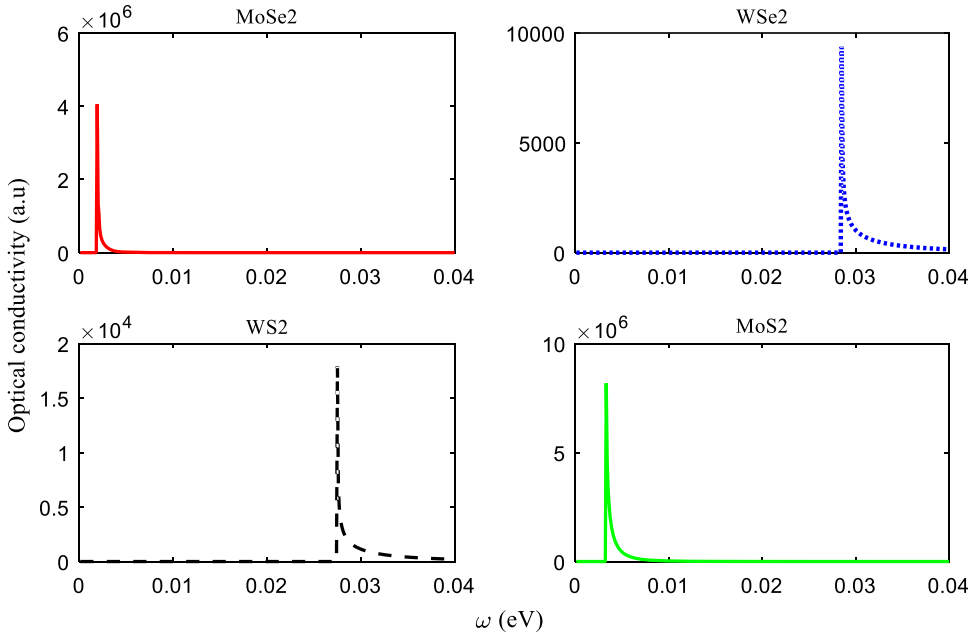


**Fig. 10** Optical conductivity versus frequency for various TMDCs

## 4 Conclusion

The investigation of exciton-polaron transport in quasi-two-dimensional transition metal dichalcogenides has been made. Electrical conductivity, optical conductivity and Seebeck coefficient have been determined analytically. We extend the study to four different monolayer TMDC materials ($MoSe_2$, $WSe_2, WS_2, MoS_2$) which parameters are registered in Table 1. It follows that the relaxation time of exciton-polaron decreases with higher carrier concentrations and when increase the temperature, the confinement length. $MoS_2$ is the most interesting for this property. In addition, the electrical conductivity is a decreasing function of temperature, whereas it increases when enhances the system energy and the carrier concentration. The highest magnitude of electrical conductivity is observed for very low temperatures and at high temperatures, it is low magnitude. The electrical conductivity appears when the energy of the system reaches the gap energy and the increase in carrier concentration favors this property up to a saturation. Seebeck coefficient increases for low temperatures ($T < 15$ K), but it decreases for high temperatures ($T > 15$ K) and carrier concentration. For these electric and thermoelectric power properties, $MoSe_2$ is the one having the highest amplitude. The optical conductivity is not a monotonic function of the frequency. It increases after absorbing phonons, and then, it falls. It starts at different value of frequency for each material showing the optical differences between the selected TMDC materials. Also, $MoS_2$ and $MoSe_2$ are more interesting for this last property.

**Author contributions** CKS and AKT designed the model and the computational framework and analyzed the data. AKJ carried out the implementation. AKT and JVN performed the calculations. CKS and AKT wrote the manuscript with input from all authors. KB, CKS and AKT contributed to the analysis of the results and performed the computations. All authors discussed the results and contributed to the final manuscript.

**Funding** No funds, grants, or other support was received.

## Declarations

**Conflict of interest** The authors declare that they have no conflict of interest.

**Data availability** Not applicable.

**Code availability** Matlab.

## References

Akay D (2018) Trigonal warping and photo-induced effects on zone boundary phonon in monolayer graphene. Superlattices Microstruct 117:18–24

Akay D (2021) Manipulating electronic dynamics of 8-Pmmn borophene with surface optical phonons. Semicond Sci Technol 36:045001

Al-Jaber MS (1999) Fermi gas in D-dimensional space. Int J Theor Phys 38(3):919–923

Ashraf S, Forsberg V, Mattsson CG, Thungström G (2019) Thermoelectric properties of n-type molybdenum disulfide MoS2 thin film by using a simple measurement method. Materials 12:3521

Bernardi M, Ataca C, Palummo M, Grossman JC (2017) Optical and electronic properties of two-dimensional layered materials. Nanophotonics 6:479

Brem S, Selig M, Berghaeuser G, Malic E (2018) Exciton relaxation cascade in two-dimensional transition metal dichalcogenides. Sci Rep 8(1):1–8

Chen RS, Tang CC, Shen WC, Huang YS (2014) Thickness-dependent electrical conductivities and ohmic contacts in transition metal dichalcogenides multilayers. Nanotechnology 25:415706

Devreese J T (2018) Frohlich polarons, lecture course including detailed theoretical derivation.arXiv1611.06122v3 [cond-mat.other]

Dey P, Yang L, Robert C, Wang G, Urbaszek B, Marie X, Crooker SA (2017) Gate controlled spin valley locking of resident carriers in WSe2 monolayers. Phys Rev Lett. https://doi.org/10.1103/PhysRevLett.119.137401

El-Ballouli AO, Alarousu E, Usman A, Pan J, Bakr OM, Mohammed OF (2014) Real time observation of ultrafast intraband relaxation and exciton multiplication in PbS quantum dots. ACS Photon 1(3):285–292

Ell C, Blank R, Benner S, Haug H (1989) Simplified calculations of the optical spectra of two and three dimensional laser excited semiconductors. J Opt Soc Am B 6(11):2006–2012

Favero CG, Ferreira R, Darson D, Voisin C, Tianon J, Delalande C (2003) Acoustic phonon sidebands in the emission line of single InAs/GaAs quantum dots. Phys Rev B 68(23):233301

Fiori G, Bonaccorso F, Iannccone G, Palacios T, Neumaier D, Seabaugh A, Banerjee SK, Colombo L (2014) Electronics based on two-dimensional materials. Nat Nanotechnol 9:768

Foglia L, Vempati S, Bonkano BT, Gierster L, Wolf M, Sadofev S, Stahler J (2019) Revealing the competing contributions of charge carriers, excitons and defects to the non-equilibrium optical properties of ZnO. Struct Dyn 6(3):034501

Ge Y, Wenhui W, Yulu R, Yong L (2020) Large thermoelectric power factor of high-mobility transition metal dichalcogenides with 1*T* phase. Phys Rev Res 2:013134

Glazov MM (2020) Quantum interference effect on exciton transport in monolayer semiconductors. Phys Rev Lett 124(16):166802

Glen L, Goodvin, Andrey S, Mishchenko, Berciu M (2011) Optical conductivity of the Holstein polaron. Phys Rev Lett 107, 076403

Haug H, Koch SW (1989) Semiconductor laser theory with many body effects. Phys Rev A 39(4):1887

Havener RW, Liang Y, Brown L, Yang L, Park J (2014) Van Hove singularities and excitonic effects in the optical conductivity of twisted bilayer graphene. Nano Lett 14(6):3353–3357

Huang S, Liu HJ, Fan DD, Jiang PH, Liang JH, Cao GH, Liang RZ, Shi J (2018a) First principle study of the thermoelectric properties of the Zintl compound KSnSb. J Phys Chem C 122(8):4217–4223

Huang S, Sanderson M, Tian J, Chen Q, Wang F, Zhang C (2018) Hot carrier relaxation in three dimensional gapped Dirac semimetals. J Phys D Appl Phys 51(1):015101

Jacak MP, Krasnyj J, Zoller P (2003) Coherent and incoherent phonon processes in artificial atoms. Eur Phys J D 22:319–331

Jankovic V, Vukmirovic N (2015) Dynamics of exciton formation and relaxation in photoexcited semiconductors. Phys Rev B 92:235208

Jia GY, Liu Y, Gong JY, Lei DY, Wang DL, Huang ZX (2016) Excitonic quantum confinement modified optical conductivity of monolayer and few-layered MoS2. J Mater Chem C 4:8822–8828

Kandada ARS, Silva C (2020) Exciton polarons in two-dimensional hybrid metal halide perovskites. J Phys Chem Lett 11(9):3173–3184

Kandemir BS, Akay D (2018) Photoinduced dynamical band gap in graphene, the effects of electron-phonon and spin-orbit interaction. Phys Stat Solidi B 225(10):1800163

Kenfack-Sadem C, Teguimfouet KA, Kenfack-Jiotsa A, Tsiaze RMK (2021) Dynamics and decoherence of exciton polaron in monolayer transition metal dichalcogenides. J Electron Mater. https://doi.org/10.1007/s11664-021-08808-9

Khoirunnisa H, Majidi MA (2018) Exploring excitonic signal in optical conductivity of ZnO through first order electron hole vertex correction. J Phys Conf Ser 1011:012073. https://doi.org/10.1088/1742-6596/1011/1/012073

Kormányos A, Zolyomi V, Drummond ND, Burkard G (2014) Spin-orbit coupling, quantum dots, and qubits in monolayer transition metal dichalcogenides. Phys Rev X 4:011034

Krummheuer B, Aavin VM, Kuhn T (2002) Theory of pure dephasing and resulting absorption line shape in semiconductor quantum dots. Phys Rev B 65(19):195313

Maidannyk VA, Roos YH (2016) Modification of the WLF model for characterization of the relaxation time temperature relationship in trehalose-whey protein isolate systems. J Food Eng 188:21–31

Mak KF, He K, Lee C, Lee GH, Hone J, Heinz TF, Shan J (2013) Tightly bound trions in monolayer $MoS_2$. Nat Mater 12:207–211

Meziane S, Faraoun HI, Esling C (2016) The layered transition metal dichalcogenides as materials for storage clean energy: ab initio investigations. Int J Energy Power Eng. https://doi.org/10.5281/zenodo.1126539

Ono S, Tomohiro O (2018) Anomalous energy shift of laterally confined two dimensional excitons. J Appl Phys 124(3):034301

Pearce AJ, Burkard G (2017) Electron spin relaxation in a transition-metal dichalcogenide quantum dot. 2D Mater 4:5114

Peres NMR, Ribeiro RM, Neto AHC (2010) Excitonic effects in the optical conductivity of gated graphene. Phys Rev Lett 105(5):055501

Pizzi G, Volja D, Kozinsky B, Fornari M, Marzari N (2014) Boltzwann, a code for the evaluation of thermoelectric and electronic transport properties with a maximally localized Wannier functions basis. Comput Phys Commun 185(1):422–429

Qin D, Yan P, Ding G, Ge X, Song H, Gao G (2018) Monolayer PdSe2 a promising two-dimensional thermoelectric material. Sci Rep 8:2764

Qiu DY, Cao T, Louie SG (2015) Nonanalyticity, valley quantum phases, and lightlike, exciton dispersion in monolayer transition metal dichalcogenides: theory and first-principles calculations. Phys Rev Lett 115:176801

Selvaggi JP (2019) Modeling the seebeck coefficient for organic materials with the Kubo-Greenwood integral and a Gaussian density of states. J Comput Electr 18(2):473–481

Seung-il N (2012) Electrical conductivity of quark matter at finite T under external magnetic field. Phys Rev D 86:033014

Shree S, Semina M, Robert C, Han B, Amand T, Balocchi A, Manca M, Courtade E, Marie X, Taniguchi T, Watanabe T, Glazov MM, Urbaszek B (2018) Observation of exciton phonon coupling in MoSe2 monolayers. Phys Rev B 98(3):035302

Singh I, Madan S, Kaur A, Kumar J, Bhatnagar PK, Mathur PC (2014) Study of relaxation dynamics of photogenerated excitons in CulnS2 quantum dots. MRS Commun 4(01):1–5

Song X-X, Liu Di, Mosallanejad V, You J, Han T-Y, Chen D-T, Li H-O, Cao G, Xiao M, Guo G-C, Guo G (2015) A gate defined quantum dot on the two-dimensional transition metal dichalcogenide semiconductor $WSe_2$. Nanoscale 7:16867–16873

Thilagam A (2015) Excitonic polarons in low-dimensional transition metal dichalcogenides. Physica B 464:44–50

Thilagam A, Singh J (1996) Excitonic polarons in quasi-two-dimensional structures. Appl Phys A 62(5):445–450

Tomczak MJ, Haule K, Miyake T, Georges A, Kotliar G (2010) Thermopower of correlated semiconductors, application to $FeAs_2$ and $FeSb_2$. Phys Rev B 82:085104

Tong H, Wu MW (2011) Theory of excitons in cubic III-V semiconductor GaAs, InAs and GaN quantum dots, fine structure and spin relaxation. Phys Rev B Condens Matter. https://doi.org/10.1103/PhysRevB.83.235323

Wang G, Robert C, Glazov MM, Cadiz F, Courtade E, Amand T, Lagarde D, Taniguchi T, Watanabe K, Urbaszek B, Marie X (2017) In-plane propagation of light in transition metal dichalcogenide monolayers, optical selection rules. Phys Rev Lett 119(4):047401

Wickramaratne D, Zahid F, Lake RK (2014) Electric and thermoelectric properties of few-layer TMDs. J Chem Phys 140:124710

Xiao Y, Li Z-Q, Wang Z-W (2017) Polaron effect on the bandgap modulation in monolayer transition metal dichalcogenides. J Phys Condens Matter 29:485001

Xu H, Wei J, Zhou H, Feng J, Xu T, Du H, He C, Huang Y, Zhang J, Liu Y, Wu H-C, Gu C, Wang X, Guang Y, Wei H, Peng Y, Jiang W, Yu G, Han X (2020) High spin hall conductivity in large-area type II Dirac semimetal $PtTe_2$. Adv Mater 32:2000513

Yang S, Tongay S, Li Y, Yue Q, Xia J-B, Li S-S, Li J, Wei S-H (2014) Layer-dependent electrical and optoelectronic responses of ReSe2 nanosheet transistors. Nanoscale 6(13):7226–7231

Yang L, Xie C, Jin J, Nauman RA, Feng C, Liu P, Xiang B (2018) Properties, preparation and applications of low dimensional transition metal dichalcogenides. Nanomaterials 8(7):463

Physica E 144 (2022) 115448

Contents lists available at ScienceDirect

Physica E: Low-dimensional Systems and Nanostructures

journal homepage: www.elsevier.com/locate/physe

# Magnetic barrier and temperature effects on optical and dynamic properties of exciton-polaron in monolayers transition metal dichalcogenides

A.K. Teguimfouet [a], C. Kenfack-Sadem [b,c,*], A. Kenfack-Jiotsa [d], F.C. Fobasso Mbognou [b], M. El-Yadri [e,**], L.M. Pérez [f], D. Laroze [g], E. Feddi [e,h]

[a] Laboratoire de Mécanique, Matériaux et Structures, Département de Physique, Université de Yaoundé 1, BP 812, Yaoundé, Cameroon
[b] Laboratory of Condensed Matter-Electronics and Signal Processing (LAMACET), Department of Physics, University of Dschang, P.O.Box 67, Dschang, Cameroon
[c] International Chair in Mathematical Physics and Applications, University of Abomey-Calavi, Cotonou, Benin
[d] Département de Physique, Ecole Normale Supérieure, Université de Yaoundé 1, BP 42, Yaoundé, Cameroon
[e] Group of Optoelectronic of Semiconductors and Nanomaterials, ENSAM, Mohammed V University in Rabat, Morocco
[f] Departamento de Física, FACI, Universidad de Tarapacá, Casilla 7 D, Arica, Chile
[g] Instituto de Alta Investigación, CEDENNA, Universidad de Tarapacá, Casilla 7 D, Arica, Chile
[h] Institute of Applied Physics, Mohammed VI Polytechnic University, Lot 660, Hay Moulay Rachid Ben Guerir, 43150, Morocco

ARTICLE INFO

*Keywords:*
Exciton-polaron
TMDs
Magnetic barrier
Temperature

ABSTRACT

We theoretically investigate the properties of exciton-polaron moving through a magnetic barrier in monolayers (1Ls) transition metal dichalcogenides (TMDs): $MoS_2$, $WS_2$, $MoSe_2$, and $WSe_2$. We find that the exciton-polaron has the highest ground state energy in $WS_2$ and the lowest one in $MoSe_2$. It is seen that the magnetic barrier stabilizes the excitonic polaron system subjected to thermal perturbation. We demonstrate that the entropy of the system is very sensitive to the type of monolayers TMDs, the length scale of the barrier, the temperature. We observe that the higher the magnetic length, the greater the disorder in exciton-polaron system and the highest entropy is in $MoSe_2$. Also, the mobility and the lifetime of exciton-polaron decrease with the enhancement of the magnetic length. We observe the highest mobility and lifetime in $WS_2$. Moreover, We show that the optical absorption appears when the photon energy is more than twice phonon energy and the absorption coefficient is higher when the incident photon induces an in plane field. $MoS_2$ presents the highest amplitude of optical absorption.

## 1. Introduction

In both molecular lattices (agregats) and large molecules, excitons play important roles as transmitting of informations, carrying energy and activating some chemical reactions. More recently, excitons in monolayers (1Ls) transition metal dichalcogenides (TMDs) [1,2] have grown very rapidly due to the optical and electronic characteristics. These structures are considered as one of the most interesting 2D materials due to their large band of applications such as fabrication of electronic devices [3], spintronics and valleytronic [4], preparation of qubit [5]. Additionally, the magneto-optical mechanisms of 1Ls TMDs [6–8] have stimulated some new opportunities for applications where a comprehensive insight of the action of a magnetic field affecting the excitons is desired. Indeed, excitons in TMD's monolayers submitted to a magnetic field show interesting optical and electronic characteristics [9–11] due to the large binding energy of the excitons [12–14]. It has been shown that the external magnetic field applied to a 1L TMD provides an experimental understanding of the characteristics of excitons, such as their spatial extent [15,16].

Unfortunately, in practice, the exciton does not spread freely, but it is constantly interacting with the other degrees of freedom in the crystal lattice. At a finite temperature, a strong coupling appears with low internal vibrations so called as phonons or polaronic effects [17,18]. The main idea is to say that phonons cause random fluctuations of energy from each local state. Therefore, identifying the nature and properties of the exciton's motion appear to be a difficult task, crucial for

* Corresponding author. Laboratory of Condensed Matter-Electronics and Signal Processing (LAMACET), Department of Physics, University of Dschang, P.O.Box 67, Dschang, Cameroon.
** Corresponding author.
*E-mail addresses:* kevinsadem@yahoo.fr (C. Kenfack-Sadem), md.yadri@gmail.com (M. El-Yadri).

https://doi.org/10.1016/j.physe.2022.115448
Received 6 March 2022; Received in revised form 30 June 2022; Accepted 20 July 2022
Available online 27 August 2022
1386-9477/

understanding its role in various transport processes.

The principle of exciton-polaron has been elaborated extensively by a number of authors who have demonstrated that the exciton behavior is modified according to the coupling with phonons [19–25]. In confined system, this interaction is more obvious and presents some interesting futures mainly in 2D materials. It has been thoroughly explored both theoretically and experimentally by several authors [26–30]. In low dimensional system, the interaction between electron-hole pair and phonon is recognized to change the real apparent mass of exciton and reduces its energy, leading to a shift of the energy difference. Confined particles are relevant in nanostructures applications [31–33], so, several potential models have been developed in order to describe and control the dynamics of quasiparticles. Several parameters as the width, the depth of Gaussian well and temperature turned out to be significant in the study of energy levels and lifetime of polaron [34]. In the latter, it is found that lifetime decays with temperature. Also, Li [35] revealed that one can adjust the polaron ground state lifetime by changing the temperature, the polaron radius, the pseudoharmonic potential and the external field. This is interesting for application in quantum computation.

Inspired by the invention of an exceptional optical and electronic system [36–38], the class of 2D monolayers TMDs has attracted the attention of the scientific community. The dynamics of excitons and carriers in monolayers TMDs were examined by absorption or reflectivity of the pump-probe experiences [39–43]. Owing to a high temporal resolution (~100 fs), these experimental results have highlighted a complex dynamic generally described by multi-exponential decay times [44]. Wu et al. [45] examined the optical absorption of cross-layer excitons in TMD heterolayers, they showed a diversity of cross-layer excitons in the two directions of optical activity and energies occur at any given valley. It has been demonstrated that excitons between layers possess a long-lived and easily electro-tunable energy due to their spatially indirect character [46]. However, they continue to exhibit a fairly high electron-hole binding energy. Moreover, the large band gap confers to TMD materials the possibility of high charge carrier mobility and high absorption coefficient [47]. From the work of Li et al. [48], the optical absorption appears when the incident photon energy exceeds the energy of optical phonon. Also, Thilagam [49] studied the ground state energy and the mass change of exciton-polaron for some monolayers. It is shown that under impurity effect, the exciton is localized in a quantum well. In this nanostructure, the transport of excitons is mostly quasi-2D and the variation in the size of the exciton alters the impact of its interplay with phonons. Consequently, it is advisable to explore how the features of an exciton-polaron in TMDs subjected to magnetic barrier.

As mentioned by several authors, exciton-polarons are ideal candidates for transmitting information and carrying energy. This inspires us to derive the lifetime, mobility, Tsallis entropy and the optical absorption coefficient. These are important properties necessary to describe the behavior of exciton-polaron in TMDs in order to ameliorate and understand the transport properties. In this paper, we determine theoretically the above properties of exciton-polaron in various monolayer TMD materials under magnetic field characterized by a magnetic length scale. The paper is organized as follows: in Sec. 2, we present the theory in which we describe the model of exciton-polaron system and derive the analytical expressions while in Sec. 3, we present our main results on energy, lifetime, mobility, entropy and optical absorption coefficient for the common 1Ls TMDs ($MoSe_2$, $WSe_2$, $WS_2$, $MoS_2$). Finally, in Sec. 4, we provide the conclusion.

## 2. Theoretical model

### 2.1. Hamiltonian of the system

Let us consider the motion of an exciton through a panel depicting a 1L TMD which interacts with longitudinal optical (LO)-phonons in presence of a magnetic strength. The total Hamiltonian of the system can be written as:

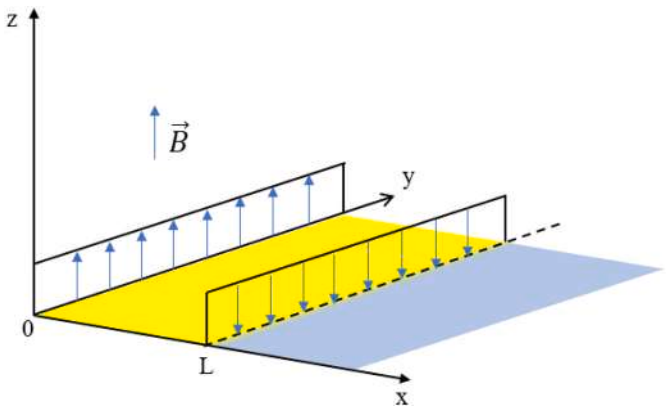


**Fig. 1.** Magnetic barrier using two long narrow magnetic stripes perpendicular to the monolayer TMD.

$$\widehat{H} = \widehat{H}_{ex}^{2D} + \widehat{H}_{ph} + \widehat{H}_{ex-ph}^{2D} \tag{1}$$

where $\widehat{H}_{ex}^{2D}$ is the Hamiltonian of electron and hole [50,51] taken here as:

$$\widehat{H}_{ex}^{2D} = \frac{1}{2m_e^*}\left(\vec{P}_e + e\vec{A}_e\right)^2 + \frac{1}{2m_h^*}\left(\vec{P}_h - e\vec{A}_h\right)^2 - \frac{e^2}{\varepsilon\left|\vec{\rho}_e - \vec{\rho}_h\right|} \tag{2}$$

where $\vec{P}_e$ ($\vec{P}_h$) is respectively the momentum vector of electron (hole) while $\vec{\rho}_e$ ($\vec{\rho}_h$) represents the electron (hole) position-vector in the xy-plane. $m_e^*$ ($m_h^*$) is the effective mass of electron (hole). The last term of Eq. (2) is the coulomb interaction between electron and hole in the monolayer TMD. The magnetic barrier [52] is characterized by the field $\vec{B} = (0, 0, B_z)$ with $B_z(x) = B_0\, l_B[\delta(x) - \delta(x - L)]$. $L$ is the barrier width taken at 150 nm, $l_B$ indicates a length measure based on a standard magnetic flux field given by $B_0 = \hbar/(el_B^2)$.

From the definition of the Dirac delta function, this magnetic field can also take the form:

$$B_z = \begin{cases} B_0\, l_B\ ;\ if\ x = 0 \\ -B_0\, l_B\ ;\ if\ x = L \\ 0\ ;\ otherwise \end{cases} \tag{3}$$

Such barrier can be constructed as shows Ghosh et al. [53] and Fig. 1 illustrates the present case. Here, two long narrow magnetic stripes are placed perpendicular to the TMD layer respectively at $x = 0$ (with $B_0\, l_B$) and $x = L$ (with $-B_0\, l_B$). It is convenient to use the relation $\vec{B} = rot\vec{A}$ to obtain the vector potential of the magnetic barrier as $\vec{A} = (0, A_y, 0)$:

$$A_y(x) = B_0\, l_B\, [\Theta(x) - \Theta(x - L)] = \begin{cases} A\ ; & 0 < x < L \\ 0\ ; & otherwise \end{cases} \tag{4}$$

where $A = \hbar/(el_B)$ and $\Theta$ is the Heaviside function.

The phonon energy operator appear as:

$$\widehat{H}_{ph} = \sum_q \hbar\omega\, b_q^+ b_q \tag{5}$$

with $b_q^+$ and $b_q$ denote the creation and annihilation operators of phonon, $q$ the phonon wave vector with component $q_{//}$ in the xy-plane.

The last term of Eq. (1) stands for the Hamiltonian of exciton-phonon interaction given by Ref. [49]:

$$\widehat{H}_{ex-ph}^{2D} = \sum_{K,q_{//}} \Xi^{op}\left(q_{//}\right) C_{K+q_{//}}^+ C_K \left(b_{q_{//}} + b_{-q_{//}}^+\right) \tag{6}$$

where $C_K^+(C_K)$ denotes the creation (annihilation) operator of an exciton

and $K$ is the two-dimensional exciton wave vector. The exciton-optical phonon coupling function is taken as:

$$\Xi^{op}\left(q_{//}\right)=\left(D_c^{op}-D_v^{op}\right)\sqrt{\frac{\hbar q_{//}}{2\eta u S_{2D}}} \tag{7}$$

where $S_{2D}$ represents the area of the layer plane, $\eta$ denotes the area mass density and $u$ is the sound velocity of the mode. $D_c^{op}$ and $D_v^{op}$ are respectively the deformation potential constant for electron-LO phonon coupling at some critical points $(K,K')$ inside conduction band and the corresponding expression for hole in the valence band. These critical points are used to better estimate the polaronic effect on excitons.

Eq. (2) can be rewritten as:

$$\widehat{H}_{ex}^{2D}=\frac{\left(P_{e,x}^2+P_{e,y}^2\right)}{2m_e^*}+\frac{\left(P_{h,x}^2+P_{h,y}^2\right)}{2m_h^*}+\frac{e^2A^2}{2\mu^*}-\frac{e^2}{\varepsilon\left|\overrightarrow{\rho}_e-\overrightarrow{\rho}_h\right|} \tag{8}$$

$\mu^*$ is the effective exciton reduced mass given by:

$$\frac{1}{\mu^*}=\frac{1}{m_e^*}+\frac{1}{m_h^*} \tag{9}$$

Using the center of mass ($\overrightarrow{R}=\frac{m_e^*}{M^*}\overrightarrow{\rho}_e+\frac{m_h^*}{M^*}\overrightarrow{\rho}_h$) and the relative coordinate ($\overrightarrow{\rho}=\overrightarrow{\rho}_e-\overrightarrow{\rho}_h$),Eq. (8) becomes:

$$H_{ex}^{2D}=\frac{-\hbar^2}{2M^*}\nabla_R^2-\left(\frac{\hbar^2}{2\mu^*}\nabla_\rho^2+\frac{e^2}{\varepsilon\rho}-\frac{e^2A^2}{2\mu^*}\right)=H_R-H_{\rho,A} \tag{10}$$

$M^*=m_e^*+m_h^*$ represents the effective mass of an exciton. Let us check the 2D energy so that:

$$\widehat{H}_{ex}^{2D}=\sum_K\lambda C_K^+C_K \tag{11}$$

This leads to the Schrodinger equation:

$$H_{ex}^{2D}\,\Psi_{ex}=\lambda\,\Psi_{ex} \tag{12}$$

The exciton wave function is considered as [51,54]:

$$\Psi_{ex}=\varphi\,(R)\,\varphi_{1s}(\rho)=\exp\left(i\overrightarrow{K}^*.\,\overrightarrow{R}\right)\sqrt{\frac{2}{\pi}}\,\frac{1}{a}\exp\left(-\frac{\rho}{a}\right) \tag{13}$$

with $\overrightarrow{K}^*=\overrightarrow{K}-\frac{e}{\hbar}\overrightarrow{A}$ and $a$ the exciton Bohr radius.

For the center of mass, we have:

$$\frac{-\hbar^2}{2M^*}\nabla_R^2\,\varphi(R)=E(K,l_B)\,\varphi(R) \tag{14}$$

Here, $E_b$ comes from the general formula $E_b=\frac{R_y}{(n-0.5)^2}$, $n=1$ being the principal quantum number and $R_y$ the Rydberg's constant. Then according to Eqs. (15) and (16), one gets:

$$\lambda=E(K,l_B)+E_b(l_B) \tag{17}$$

We obtain the expression of the exciton eigen energy as:

$$\lambda(K,\xi)=E_g+\frac{\hbar^2K^2}{2M^*}-E_b+\xi^2 \tag{18}$$

where $\xi$ is the magnetic parameter given by:

$$\xi=\frac{\hbar}{l_B}\left(\frac{1}{2M^*}+\frac{1}{2\mu^*}\right)^{1/2} \tag{19}$$

It is seen that the magnetic barrier contributes on kinetic and binding energies respectively.

We use the following unitary transformation [49] to diagonalize the Hamiltonian of the system:

$$U_{ex}=\exp(iS) \tag{20}$$

with

$$S=\sum_{K,q_{//}}C_{K+q_{//}}^+C_K\left[f_{ex}^*\left(K,q_{//}\right)b_{-q_{//}}^++f_{ex}\left(K,q_{//}\right)\,b_{q_{//}}\right] \tag{21}$$

$U_{ex}$ is called the displaced-oscillator which is related to the phonon operators via Eq. (20). This transformation enables us to consider the dressed electron states due to the phonon field. It generates coherent states from the phonon vacuum. The variational functions $f_{ex}$ and $f_{ex}^*$ provide the phonon distribution function induced by the electron dynamics are determined as:

$$f_{ex}^*\left(K,q_{//}\right)=\frac{\Xi^{op}\left(q_{//}\right)}{\lambda\left(K+q_{//},\xi\right)-\lambda(K,\xi)+\hbar\omega}\,and\,f_{ex}\left(K,q_{//}\right)=\frac{\Xi^{op}\left(q_{//}\right)}{\lambda\left(K+q_{//},\xi\right)-\lambda(K,\xi)-\hbar\omega} \tag{22}$$

Theses functions shift the position of the vibrational modes quantifying the strength of the coupling between electron and lattice displacement.

According to Eq. (20), the transformed Hamiltonian gives:

$$\widehat{H}^T=U_{ex}^{-1}\widehat{H}U_{ex}\approx\widehat{H}_{ex}^{2D}+\widehat{H}_{ph}+\widehat{H}_{ex-ph}^{T2D} \tag{23}$$

where

$$\widehat{H}_{ex-ph}^{T2D}=\sum_{K,K',q_{//}}\left|\Xi^{op}\left(q_{//}\right)\right|^2\left[\frac{1}{\lambda\left(K+q_{//},\xi\right)-\lambda(K,\xi)+\hbar\omega}-\frac{1}{\lambda\left(K+q_{//},\xi\right)-\lambda(K,\xi)-\hbar\omega}\right]C_{K+q_{//}}^+C_KC_{K'+q_{//}}^+C_{K'} \tag{24}$$

Thus

$$E(K,l_B)\approx E_g+\frac{\hbar^2}{2M^*}\left(K^2+\frac{1}{l_B^2}\right) \tag{15}$$

$E_g$ stands for the gap energy in the $MX_2$ monolayer.

Also, for the relative coordinate, we have:

$$-\langle\varphi_{1s}|H_{\rho,\,A}\,|\varphi_{1s}\rangle=-E_b+\frac{\hbar^2}{2\mu^*l_B^2}=E_b(l_B) \tag{16}$$

We can now use the approximate diagonalized form of the Hamiltonian given by Eq. (23) to easily obtain the properties of the system like energy, mobility, entropy, optical absorption. Let us proceed by the calculation of entropy.

### 2.2. Tsallis entropy

In this section, we will evaluate the Tsallis entropy which depends of

a degree ($j$) [55–58] as:

$$S_j = \frac{1 - \sum_{i=1} P_i^j}{j-1} \tag{25}$$

The probabilities are $P_1$ for ground state and $P_2$ for the first excited state given by:

$$P_1 = \frac{\left[1-\beta(1-j)E^0_{ex-pol}\right]^{\frac{1}{1-j}}}{Z_j} \text{ and } P_2 = \frac{\left[1-\beta(1-j)E^1_{ex-pol}\right]^{\frac{1}{1-j}}}{Z_j} \tag{26}$$

and the partition function is defined as:

$$Z_j = \left[1-\beta(1-j)E^0_{ex-pol}\right]^{\frac{1}{1-j}} + \left[1-\beta(1-j)E^1_{ex-pol}\right]^{\frac{1}{1-j}} \tag{27}$$

the parameter $j$ is a real number and represents the entropy degree and $\beta$ is the inverse of temperature. $E^0_{ex-pol}$ and $E^1_{ex-pol}$ are respectively the fundamental state and the first excited level energies of the excitonic polaron. For the ground state, we have:

$$E^0_{ex-pol} = \langle \Psi_0 | \widehat{H}^T | \Psi_0 \rangle \tag{28}$$

with the ground state wave function

$$|\Psi_0\rangle = C_K^+ |0\rangle_k |0\rangle_{ph} \tag{29}$$

$|0\rangle_k$ and $|0\rangle_{ph}$ represent respectively the exciton's and phonon's vacuum state vectors. The state energies are obtained after straightforward calculations made in Eq. (23).

$$E^0_{ex-pol} = E_g + \left(\frac{\hbar^2 K^2}{2M}\right)(1-\widetilde{G}_{ex2}) - E_b - G_{ex1} + \xi^2 \tag{30}$$

where

$$G_{ex1} = \frac{\pi\sqrt{\hbar\omega}\left(D_c^{op}-D_v^{op}\right)^2}{\sqrt{2}\,\hbar^2\eta u}\left(m_e^* + m_h^*\right)^{3/2} \text{ and } \widetilde{G}_{ex2} = \frac{3\pi\left(D_c^{op}-D_v^{op}\right)^2}{4\sqrt{2}\,\hbar^2\eta u}\frac{\left(m_e^*+m_h^*\right)^{3/2}}{\sqrt{\hbar\omega}} \tag{31}$$

Using $|\Psi_1\rangle = C_K^+ |1\rangle_k |0\rangle_{ph}$, the first excited state energy is obtain as:

$$E^1_{ex-pol} = 4E_g + 4\left(\frac{\hbar^2 K^2}{2M}\right)(1-2\widetilde{G}_{ex2}) - 4E_b - 8G_{ex1} + 4\xi^2 \tag{32}$$

Inserting Eqs. (30) and (32) in Eq. (23), we obtain the entropy of the system.

### 2.3. Lifetime and mobility of the excitonic polaron

The form of energies obtained allows to investigate the lifetime of exciton-polaron in TMDs under magnetic field. To calculate this property, the following expression [59] is used:

$$\frac{\hbar}{\tau} = 2\pi \sum_q \left|\langle n_{q'}, K | H^{2D}_{ex-ph} | K, n_q\rangle\right|^2 \delta\left[\lambda_K - \lambda_{K+q} + \hbar\omega\right] \tag{33}$$

where

$$n_{q'} = n_q - 1 \tag{34}$$

For the ground state, we have:

$$\frac{\hbar}{\tau} = 2\pi \sum_q \left|\langle n_q - 1 | \langle 0 | C_K H^{2D}_{ex-ph} C_K^+ | 0\rangle | n_q\rangle\right|^2 \delta\left[\lambda_K - \lambda_{K+q} + \hbar\omega\right] \tag{35}$$

After averaging, Eq. (33) gives:

$$\frac{\hbar}{\tau} = 2\pi \sum_{q_{//}} \overline{n}\left(\Xi^{op}_{(q_{//})}\right)^2 \delta\left[\frac{\hbar^2}{2M}\left(q_{//}^2 + 2K.\,q_{//} - \frac{2M\hbar\omega}{\hbar^2}\right)\right] \tag{36}$$

According to Eq. (7) and converting the summation into integration, we obtain:

$$\frac{\hbar}{\tau} = \frac{M}{2\hbar\pi\eta u}\left(D_c^{op}-D_v^{op}\right)^2 \int_0^{2\pi} d\theta \int_0^{\infty} dq_{//}\,\overline{n}\,q_{//}^2\,\delta\left[q_{//}^2 + 2Kq_{//}\cos\theta - \frac{2M\hbar\omega}{\hbar^2}\right] \tag{37}$$

The Dirac function is transformed by using $\delta[g(q)] = \sum_i \frac{\delta(q-q_i)}{|g'(q_i)|}$ with $q_i$ the roofs of $g$.

One gets:

$$\frac{\hbar}{\tau} = \frac{M\left(D_c^{op}-D_v^{op}\right)^2}{4\pi\eta u}\int_0^{2\pi}\frac{d\theta}{\sqrt{\hbar^2K^2\cos^2\theta + 2M\hbar\omega}}\int_0^{\infty} dq_{//}\,\overline{n}\,q_{//}^2\left[\delta\left(q_{//}-q_1\right) + \delta\left(q_{//}-q_2\right)\right] \tag{38}$$

where

$$q_1 = -k\cos\theta + \frac{1}{\hbar}\sqrt{\hbar^2K^2\cos^2\theta + 2M\hbar\omega} \text{ and } q_2 = -k\cos\theta - \frac{1}{\hbar}\sqrt{\hbar^2K^2\cos^2\theta + 2M\hbar\omega} \tag{39}$$

The mean number of phonons in the ground state is taken from the quantum statistics as:

$$\overline{n} = \left[\exp\left(\beta\, E^0_{ex-pol}\right) - 1\right]^{-1} \tag{40}$$

The integration over $q_{//}$ gives:

$$\frac{\hbar}{\tau} = \frac{M\left(D_c^{op}-D_v^{op}\right)^2}{4\pi\eta u}\overline{n}\int_0^{2\pi}\frac{d\theta}{\sqrt{\hbar^2K^2\cos^2\theta + 2M\hbar\omega}}\left(q_1^2 + q_2^2\right) \tag{41}$$

Thus, the expression of exciton-polaron lifetime is:

$$\frac{1}{\tau} = \frac{M\left(D_c^{op}-D_v^{op}\right)^2}{\hbar^3\pi\eta\, u}\overline{n}\int_0^{2\pi} d\theta\frac{\left(\hbar^2K^2\cos^2\theta + M\hbar\omega\right)}{\sqrt{\hbar^2K^2\cos^2\theta + 2M\hbar\omega}} \tag{42}$$

The mobility can be related to the mean number of phonons as [60]:

$$\mu \approx \frac{1}{\overline{n}} = \left[\exp\left(\beta\, E^0_{ex-pol}\right) - 1\right] \tag{43}$$

From here we observe that the lifetime and the mobility depend on the magnetic barrier and the TMD's characteristics. Thus, these properties can be affected by those parameters.

### 2.4. Optical absorption coefficient

When the exciton-polaron absorbs the light of frequency ($\Omega$), the optical absorption coefficient $\Gamma(\hbar\Omega)$ is related to the probability $P(\hbar\Omega)$ of absorbing a photon in the ground state [61]:

**Table 1**
The performed physical parameters of 1L TMD materials used in calculation taken from Refs. [63,64]. $\hbar\omega$, $D_c^{op}$, $D_v^{op}$, $E_b$ and $E_g$ are given in unit of (eV); $m_e$ and $m_h$ are in unit of free electron mass.

| Materials | $m_e$ | $m_h$ | $\hbar\omega$ | $D_c^{op}$ | $D_v^{op}$ | $E_b$ | $E_g$ |
|---|---|---|---|---|---|---|---|
| $MoSe_2$ | 0.64 | 0.71 | 0.0365 | 5.2 | 4.9 | 0.174 | 1.56 |
| $WSe_2$ | 0.39 | 0.51 | 0.0291 | 2.3 | 3.1 | 0.231 | 1.65 |
| $WS_2$ | 0.31 | 0.42 | 0.0435 | 3.1 | 2.3 | 0.19 | 2.10 |
| $MoS_2$ | 0.51 | 0.58 | 0.0443 | 5.8 | 4.6 | 0.313 | 1.87 |

$$\Gamma(\hbar\Omega) = \frac{\Omega}{cn\varepsilon_0(2E^2)} P(\hbar\Omega) \tag{44}$$

where $\varepsilon_0$ is the vacuum's permittivity, $c$ is the light's velocity, $n$ is the medium's refractive index and $E$ represents the strength of the electric field vector of the incident photon. The transition probability is taken as [48]:

$$P(\hbar\Omega) = 2\pi \sum_f \langle\Psi|\, V|\Psi_f\rangle\langle\Psi_f|\, V|\Psi\rangle \delta(E_0 + \hbar\Omega - E_f) = 2\mathrm{Re}\, R(\hbar\Omega) \tag{45}$$

$\Psi$ ($\Psi_f$) is the ground state (possible final) wave function with energy $E_0$ ($E_f$) and $R(\hbar\Omega)$ is given by:

$$\mathrm{Re}\, R(\hbar\Omega) = \left(\frac{1}{\hbar\Omega}\right)^2 \int_{-\infty}^{0} dt\, e^{-it(i\varepsilon+\hbar\Omega)} \langle\Psi|\, [H,V]_0 [H,V]_t |\Psi\rangle \tag{46}$$

$V$ is the time-dependent perturbation describes by the electric dipole interaction $V = eE.r$.

According to Eq. (8), the previous equation gives [62]:

$$\mathrm{Re}R(\hbar\Omega) = \left(\frac{e}{\hbar\Omega}\right)^2 \int_{-\infty}^{0} dt e^{-it(i\varepsilon+\hbar\Omega)} \langle\Psi|E.\left\{\frac{p_e(0)}{m_e} + \frac{p_h(0)}{m_h}\right\} E.\left\{\frac{p_e(t)}{m_e} + \frac{p_h(t)}{m_h}\right\} |\Psi\rangle \tag{47}$$

Now, let us apply the unitary transformation:

$$\mathrm{Re}\, R(\hbar\Omega) = \left(\frac{e}{\hbar\Omega}\right)^2 \int_{-\infty}^{0} dt\, e^{-it(i\varepsilon+\hbar\Omega)} \langle\Psi|E.\, U_{ex}^{-1} \left\{\frac{p_e(0)}{m_e} + \frac{p_h(0)}{m_h}\right\} U_{ex}\, E.\, U_{ex}^{-1} \left\{\frac{p_e(t)}{m_e} + \frac{p_h(t)}{m_h}\right\} U_{ex} |\Psi\rangle \tag{48}$$

We have for P = 0:

$$U_{ex}^{-1} p U_{ex} = p + [iS,p] = p + i\left[\sum_{K,q} C_{K+q}^{+} C_K \left(f_{ex}^{*} b_{-q}^{+} + f_{ex} b_q\right), P - \sum_q \hbar\omega q b_q^{+} b_q\right]$$
$$= p - i\hbar\omega \sum_{K,q} q C_{K+q}^{+} C_K \left(f_{ex} b_q - f_{ex}^{*} b_{-q}^{+}\right) \tag{49}$$

Therefore:

$$R(\hbar\Omega) = \left(\frac{e}{\hbar\Omega}\right)^2 \int_{-\infty}^{0} dt\, e^{-it(i\varepsilon+\hbar\Omega)} \langle\Psi|\, E.\left\{\frac{p_e}{m_e} + \frac{p_h}{m_h} - \frac{i\hbar\omega}{\mu} \sum_{K,q_{//}} q_{//} C_{K+q_{//}}^{+} C_K \left(f_{ex} b_{q_{//}} - f_{ex}^{*} b_{-q_{//}}^{+}\right)\right\} \times$$
$$E.\left\{\frac{p_e(t)}{m_e} + \frac{p_h(t)}{m_h} - \frac{i\hbar\omega}{\mu} \sum_{K,q_{//}} q_{//} C_{K+q_{//}}^{+}(t) C_K(t) \left(f_{ex} b_{q_{//}}(t) - f_{ex}^{*} b_{-q_{//}}^{+}(t)\right)\right\} |\Psi\rangle \tag{50}$$

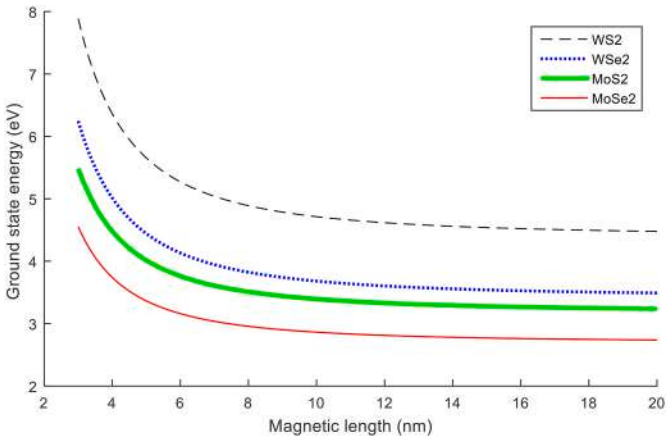


**Fig. 2.** Exciton-polaron ground state energy versus the length scale $l_B$ of magnetic barrier for various 1Ls TMDs.

By using the relation $\frac{dC(t)}{dt} = i\,[H, C(t)]$, the time dependence of the different operators is

Obtained as:

$$C_{K+q}^{+}(t) C_K(t) = C_{K+q}^{+} C_K\, e^{-it\left(\lambda_K - \lambda_{K+q}\right)} : b_{-q}^{+}(t) = b_{-q}^{+}\, e^{it\hbar\omega} \text{ and } p\,(t) = p\,(0)$$
$$= p \tag{51}$$

with the previous relation and after averaging with respect to Eq. (29), the real part is written as:

$$\mathrm{Re}R(\hbar\Omega) = \left(\frac{e}{\hbar\Omega}\right)^2 \int_{-\infty}^{0} dt\, e^{-it(i\varepsilon+\hbar\Omega)} \left\{\frac{2\hbar^2 E^2 K^{*2}}{M^2} - \frac{\hbar^2 E^2 \left(m_e^2 + m_h^2\right)}{m_e^2 m_h^2 a^2} + \frac{\hbar^2\omega^2}{\mu^2} \sum_{q_{//}} \left(E.\, q_{//}\right)^2 f_{ex} f_{ex}^{*}\, e^{-ig}\right\} \tag{52}$$

where

$$g = \left(\lambda_K - \lambda_{K+q_{//}} - \hbar\omega\right) \tag{53}$$

We consider the ratio of frequencies $\chi = \Omega/\omega$. The optical absorption coefficient reads:

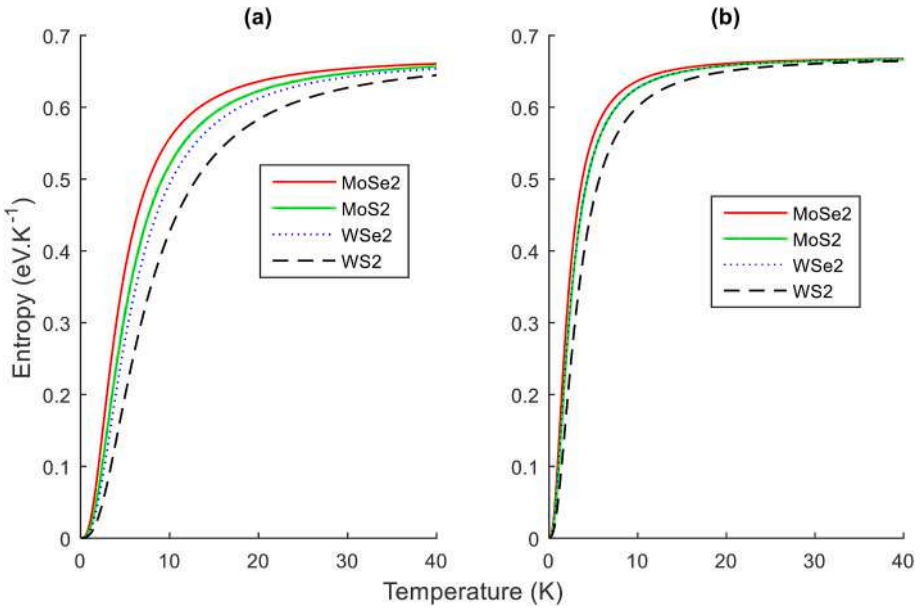


**Fig. 3.** Exciton-polaron entropy as function of the temperature for various 1L TMDs at $j = 1.1$ (a) $l_B = 5\ nm$ and (b) $l_B = 50\ nm$.

$$\Gamma(\chi) = \frac{\pi e^2}{cn\varepsilon_0\hbar(\hbar\omega)^2\chi}\left\{\frac{2\hbar^2K^{*2}}{M^2} - \frac{\hbar^2\left(m_e^2+m_h^2\right)}{m_e^2m_h^2a^2}\right\}\delta(\chi)$$
$$+\frac{\pi e^2\omega}{cn\varepsilon_0\mu^2E^2\chi}\sum_{q_{//}}\left(E.\,q_{//}\right)^2 f_{ex}f_{ex}^{*}\,\delta\left[-\frac{\hbar^2}{2M}\left(q_{//}^2+2kq_{//}\cos\theta\right)+\hbar\omega(\chi-1)\right] \tag{54}$$

Transforming the summation into an integration, one gets:

$$\Gamma(\chi) = \frac{\pi e^2}{cn\varepsilon_0\hbar(\hbar\omega)^2\chi}\left\{\frac{2\hbar^2}{M^2}\left(k^2+\frac{1}{l_B^2}\right) - \frac{\hbar^2\left(m_e^2+m_h^2\right)}{m_e^2m_h^2a^2}\right\}\delta(\chi)$$
$$+\frac{M\hbar\omega e^2\left(D_c^{op}-D_v^{op}\right)^2}{4\pi cn\varepsilon_0\eta u\hbar^2\mu^2\chi}\sin^2(\gamma)\int_0^{2\pi}d\theta\int_0^{\infty}dq_{//}\frac{q_{//}^4\,\delta\left[q_{//}^2+2kq_{//}\cos\theta-\frac{2M\hbar\omega(\chi-1)}{\hbar^2}\right]}{\frac{\hbar^4}{4M^2}\left(q_{//}^2+2kq_{//}\cos\theta\right)^2-(\hbar\omega)^2} \tag{55}$$

$\gamma$ is the angle between the field induced by incident photon ($E$) and the normal of TMD.

Let us take $q_0^2 = 2M\hbar\omega(\chi-1)/\hbar^2$ for $\chi > 1$ ;

We first integrate over $q_{//}$ in Eq. (55), it gives:

$$\Gamma(\chi) = \frac{e^2\sqrt{\pi}}{cn\varepsilon_0\hbar(\hbar\omega)^2}\left\{\frac{2\hbar^2}{M^2}\left(k^2+\frac{1}{l_B^2}\right) - \frac{\hbar^2\left(m_e^2+m_h^2\right)}{m_e^2m_h^2a^2}\right\}\frac{\exp(-\chi^2/\alpha^2)}{|\alpha|\chi} + \frac{M\hbar\omega e^2\left(D_c^{op}-D_v^{op}\right)^2}{8\pi cn\varepsilon_0\eta u\hbar\mu^2}\times$$
$$\frac{\sin^2(\gamma)}{\chi}\int_0^{2\pi}\frac{d\theta}{\sqrt{\hbar^2k^2\cos^2\theta+2M\hbar\omega(\chi-1)}}\left\{\frac{q_3^4}{\frac{\hbar^4}{4M^2}\left(q_3^2+2kq_3\cos\theta\right)^2-(\hbar\omega)^2}+\frac{q_4^4}{\frac{\hbar^4}{4M^2}\left(q_4^2+2kq_4\cos\theta\right)^2-(\hbar\omega)^2}\right\} \tag{56}$$

where

$$q_3 = -k\cos\theta+\frac{1}{\hbar}\sqrt{\hbar^2k^2\cos^2\theta+2M\hbar\omega(\chi-1)}\ :\ q_4$$
$$= -k\cos\theta-\frac{1}{\hbar}\sqrt{\hbar^2k^2\cos^2\theta+2M\hbar\omega(\chi-1)} \tag{57}$$

This leads to:

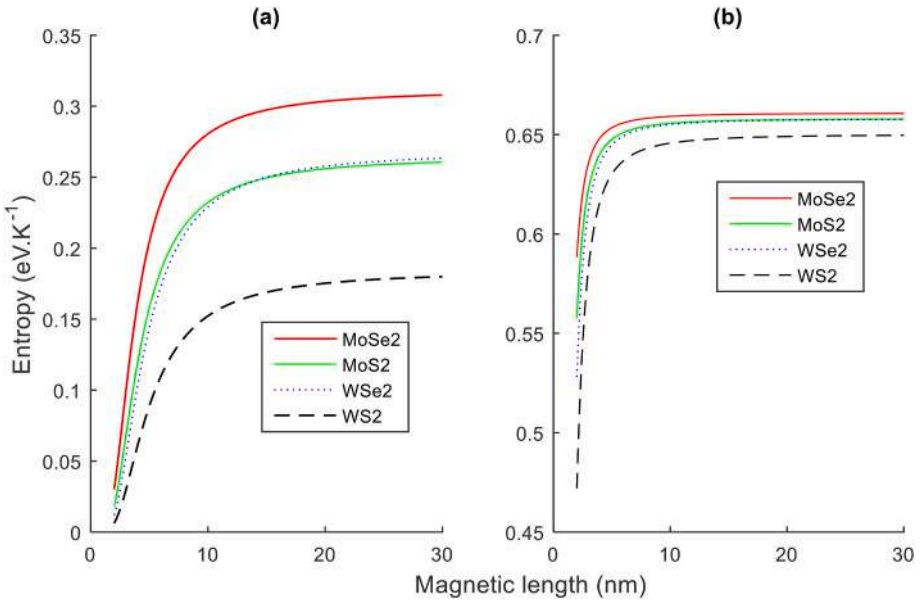


**Fig. 4.** Excitonic polaron entropy versus the length scale ($l_B$) of the magnetic barrier for various monolayers TMDs for $j = 1.1$ (a) $T = 2K$ and (b) $T = 20K$.

$$\Gamma(\chi) = \frac{e^2\sqrt{\pi}}{cn\varepsilon_0\hbar(\hbar\omega)^2}\left\{\frac{2\hbar^2}{M^2}\left(k^2+\frac{1}{l_B^2}\right)-\frac{\hbar^2\left(m_e^2+m_h^2\right)}{m_e^2m_h^2a^2}\right\}\frac{\exp(-\chi^2/\alpha^2)}{|\alpha|\chi}+\frac{Me^2\left(D_c^{op}-D_v^{op}\right)^2}{8\pi cn\varepsilon_0\eta u\hbar(\hbar\omega)\mu^2}\times$$
$$\frac{\sin^2(\gamma)}{\chi^2(\chi-2)}\int_0^{2\pi}d\theta\,\frac{16k^4\cos^4\theta+32M\hbar\omega(\chi-1)k^2\cos^2\theta/\hbar^2+4M^2(\hbar\omega)^2(\chi-1)^2/\hbar^4}{\sqrt{\hbar^2k^2\cos^2\theta+2M\hbar\omega(\chi-1)}} \tag{58}$$

The final expression of the absorption coefficient is obtained by integrating the previous equation over $\theta$. It is proportional to the photon's incidence, the photon's frequency, the magnetic length and the TMD's parameters.

## 3. Results and discussion

We have derived the analytical expression of Tsallis entropy, mobility, lifetime and optical absorption coefficient of an exciton-polaron in 1L TMDs submitted to a magnetic barrier. The Fröhlich unit and the data of each material are given in Table 1.

Fig. 2 displays the fundamental state energy of an exciton-polaron versus magnetic length for different monolayers. As we can see from this figure, the exciton polaron ground state energy is very sensitive to the applied magnetic field in all considered 2D materials. The variation of magnetic field in the increasing direction enhances the ground state energy of the system. Therefore, since the magnetic length is a function of $1/B$, the exciton-polaron interaction becomes stronger as well as the magnetic length reduces and inversely. It is seen that the fundamental state energy drops with the expansion of $l_B$ and there is a shift between the monolayers. The magnetic field plays an interesting role on the energy of an exciton-polaron in TMDs. Due to magnetic barrier, the interaction between particles is strengthened and the exciton-polaron is more confined in TMDs. This result is in accordance with what was found by Myoung et al. [52]. The authors have proved that magnetic gate is suitable for use as base elements for one-electron tunneling systems or spin-polarized devices. In fact, the decrease in the length scale enhances the barrier height and the exciton-polaron is well confined in the ground state. This assumption is found spectacularly in systems like TMDs where the electronic structure changes abruptly when they are stripped down from few to a single atomic layer [65]. $WS_2$ has the highest ground state energy and $MoSe_2$ the lowest one.

In Fig. 3, we have plotted the entropy of an excitonic polaron versus temperature for some monolayers respectively for $l_B = 5\ nm$ Fig. 3a and $l_B = 50\ nm$ Fig. 3b. Each figure shows the increase of entropy with temperature and an approximately change in evolution for all considered monolayers when the magnetic length is modified. From the figures, it becomes evident that the entropy for all compounds expands up to T = 25 K and then remains constant. The entropy starts from zero and increases until reaches the thermodynamic equilibrium which confirms the principle of the third law of thermodynamic and it is in accordance with physics laws and the work of [19]. The main explanation of the increasing entropy can also be due to the fact that phonons cause random fluctuations of energy from each local state. These fluctuations break the coherence of the excitonic states and lead to a process of relaxation at the origin of various phenomena like decoherence. Then, as a result, the system is decoherent for T < 25 K, coherent for T > 25 K and $MoSe_2$ has the highest entropy. From Fig. 3b, it can be seen that the magnetic barrier modifies the entropy behavior. We may see that, the entropy of the system is very sensitive to monolayers TMDs, magnetic length and temperature. We find that the magnetic barrier controls the system disorder. This result is in accordance with the one obtained by Fobasso et al. [66].

We observe in Fig. 4 that entropy increases and reaches an equilibrium state with the enhancement of magnetic length. The higher the magnetic length, the longer the disorder until a certain period and then, coherence can be restored in the system. Then it is possible to control the information of the system. This means that it is possible to encode quantum information on the high-frequency vibrations of excitonic

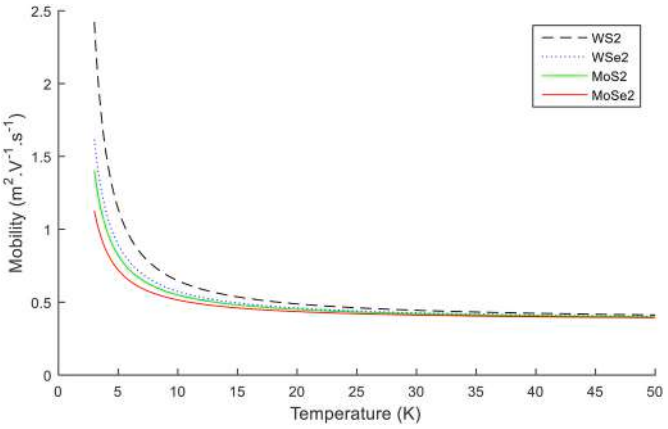


**Fig. 5.** Exciton-polaron mobility versus the temperature for different 1L TMD materials at $l_B = 5\ nm$.

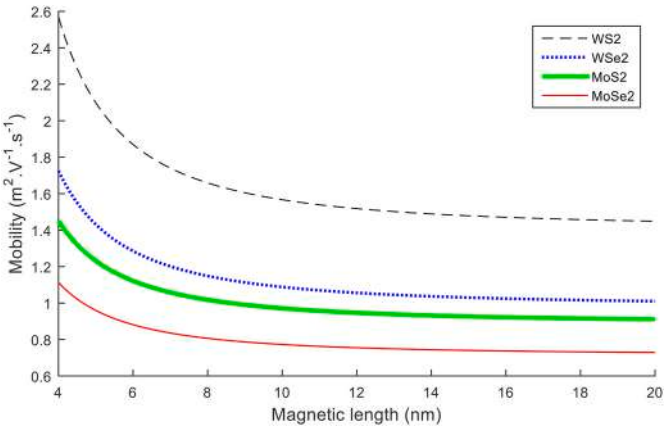


**Fig. 6.** Exciton-polaron mobility versus the magnetic barrier length ($l_B$) for different 1L TMD materials at T = 5 K.

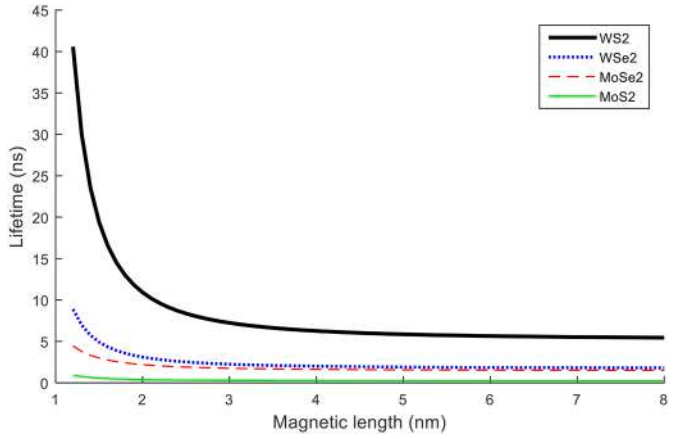


**Fig. 7.** Exciton-polaron lifetime versus the length scale ($l_B$) of the magnetic barrier for different monolayers TMDs.

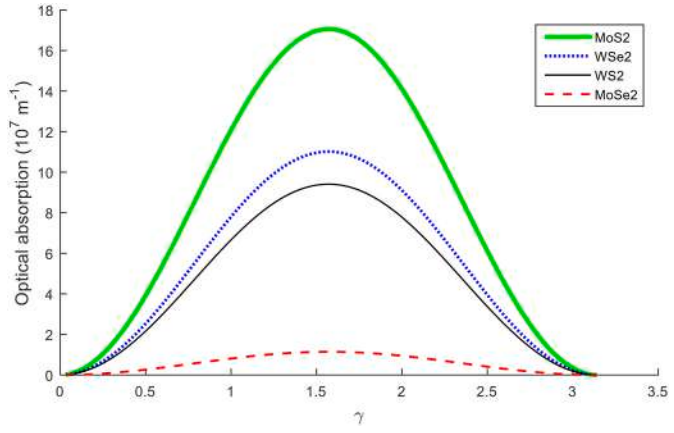


**Fig. 8.** Optical absorption coefficient versus the incidence angle of photon for different TMDs at $\chi = 2.01$ and $l_B = 10\ nm$.

polaron in quantum communication protocol. The exciton-polaron is confined in TMD materials when $l_B$ decreases (as seen in Fig. 2) and the disorder can be control by the temperature and magnetic length. It is well recognized that an accumulation of entropy signifies the deficiency of information within the system. The variation of the magnetic length plays an essential role in the coherence control of systems [67–69].

In Fig. 5, we present the exciton-polaron mobility as function of the temperature. It is observed that the mobility of exciton-polaron decreases with the increase in temperature. This behavior is understood when we look at the entropy. In fact, as the temperature enhances that generates disorder in excitonic network and then perturbs the motion of particles. In presence of temperature, the exciton-polaron has a random movement leading to the reduction of this transport property. Also, as for Fig. 3, at very high temperatures (T > 25 K) the mobility becomes constant and the movement of electron (hole) is dominated by high disorder contributing then to the lowest values of mobility. The result is in agreement with [70] and with Djomou et al. [71] who show that it is possible to accelerate the movement of a quasiparticle in nanostructures. Contrary to the entropy case, the highest mobility is obtained for $WS_2$ and the lowest for $MoSe_2$. In addition, Fig. 6 represents the mobility of an excitonic polaron versus magnetic length. It is observed that mobility decreases slowly with the magnetic length. As it was seen for energy, the exciton-polaron in TMDs is localized and its motion is modified by the magnetic barrier. In fact, from Eq. (15), it follows that low values of the magnetic length (high magnetic field) enhance the kinetic energy of exciton-polaron and as the magnetic length increases its influence on kinetic energy vanishes. One can say that for high values of the magnetic length, the magnetic barrier doesn't more act on the excitonic polaron mobility. Among the selected TMD materials, the mobility is most sensible for $WS_2$ and this result is in accordance with the one of Pouthier [72].

Fig. 7 presents the exciton-polaron lifetime as function of the magnetic length for the four TMDs. It is observed that the exciton-polaron lifetime decreases with the increase of the length scale. This is in agreement with [28]. This can be explained through the confinement of exciton motion. In the presence of magnetic field, the distance between particles is reduced, the binding energy is enhanced and electron (hole) better interacts with the structure. This interaction is reduced when enhances the magnetic length and then the existence of excitonic polaron becomes weak in the barrier. We can confirm that the change in exciton-polaron can alter the interplay effects with phonons, thus affects the decay time. The more the particle is confined in the barrier, the higher the mobility and the higher the lifetime. As it was predicted with mobility, the monolayer with long decay time is $WS_2$. At low magnetic length, the exciton-polaron has a long decay time and great energy, this result is in agreement with [47,48]. These characteristics make the TMD sheets a robust system for performing indirect exciton-polaron condensation in space.

Fig. 8 displays the behavior of the optical absorption as function of the photon incidence. It is observed that the peak of absorption appears at $\gamma = \pi/2$ corresponding to the incident photon in the plane. In fact, for this value of the angle, the total strength of the field induced by incident photon interactes with exciton-polaron in TMD materials. Also, the lowest absorption of photon by excitonic polaron is obtained for

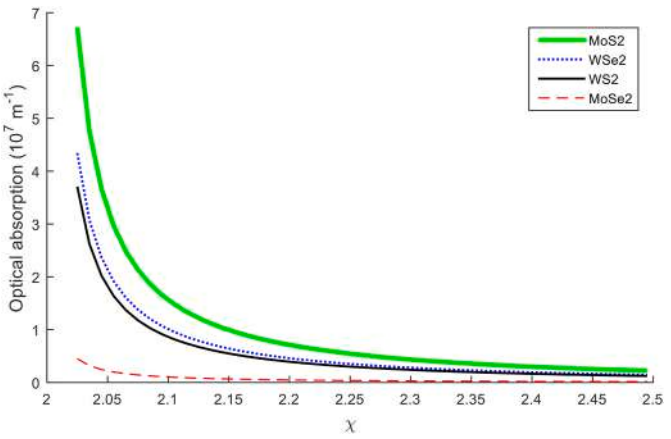


**Fig. 9.** Optical absorption coefficient as function of the incident photon energy for different TMDs at $l_B = 10\ nm$ and $\gamma = \pi/2$.

incidence normal to the plane. The result indicates that as the angle varies from the normal to $\pi/2$, the stronger the interaction with photon and then increases the probability of absorbing photon. Moreover, from Eq. (58) one can see that for $\chi < 2$ it is negative values of absorption coefficient and also $\chi = 2$ leads to $\Gamma \to \infty$. It is also convenient to take $\chi > 1 - (\hbar^2 k^2 \cos^2\theta / 2M\hbar\omega)$ due to the presence of the square root. Therefore, the result reveals that the absorption of light by exciton-polaron starts when the photon energy is more than twice phonon energy ($\chi > 2$) and it falls as shown Fig. 9. This is in agreement with the recent work of [62]. We can say that exciton-polaron may have similar properties as polaron alone. The result also quantifies the photonic impact on the exciton. This result is linked with the experimental one of Lengers et al. [73]. The optical absorption coefficient is highest for $MoS_2$ and lowest for $MoSe_2$.

Fig. 10 presents the reduction of the optical absorption with the increase of magnetic length since it is proportional to $1/(l_B^2)$ as shows Eq. (58). The spectra of absorption in 1Ls TMDs exhibits strong signatures of the unusually pronounced exciton-polaron interference in such materials of short magnetic length. This good absorption at low magnetic length delivers a useful utility for quantifying absorption spectra in popular monolayers materials. This result is in agreement with existing theoretical explanations of optical devices that are focused mainly on basic excitonic resonances by using a simple Wannier scheme for correlated electron-hole couples [74–76] or the Ab-initio Bethe-Salpeter equation [77–79]. But in these works, the linear form of the excitonic resonance tends to be incorporated phenomenologically like a Lorentzian. As the source of line forms is diverse [80], some works are dedicated to the description of the impact of excitonic phonon interaction [81]. Here, we add the influence of magnetic barrier on the spectra since the presence of magnetic field enhances the probability of absorbing the photon by exciton-polaron in the ground state. Thus, the results show that as the electron and hole need more phonon energy to absorb light, the absorption can be adjusted by the magnetic barrier.

## 4. Conclusion

The exciton-polaron properties have been studied in monolayers TMDs. We precisely investigated the Tsallis entropy, the mobility, the entropy and the optical absorption coefficient of the system through magnetic barrier. The results are obtained for different TMD materials ($MoSe_2$, $WSe_2$, $WS_2$, $MoS_2$) for comparison. We found that the exciton-polaron is confined in the magnetic barrier and the energy of exciton-polaron is lower than that of the polaron states. This favorable energy could have impact on other properties of the excitonic polaron. Also, the entropy increases with temperature and approximately changes in evolution for the different monolayers when the magnetic length is modified. We showed that the entropy of the system is very sensitive to monolayers TMDs, magnetic length and temperature. The magnetic barrier can be used to restore order in a system subject of thermal perturbation, control experimental disorder and influence quantitative measurements. It is seen that the exciton-polaron lifetime decreases with the increase of the length scale. We confirm that the transport of exciton-polaron affects the decay time. A good absorption at short magnetic length supplies a valuable tool for quantifying the absorption spectra in widely used single-layer substrates. The orientation of the field induced by the incident photon modifies the amplitude of the optical absorption coefficient. These results are useful for the improvement of electronic and optic devices.

## Declaration of competing interest

The authors declare that they have no known competing financial interests or personal relationships that could have appeared to influence the work reported in this paper.

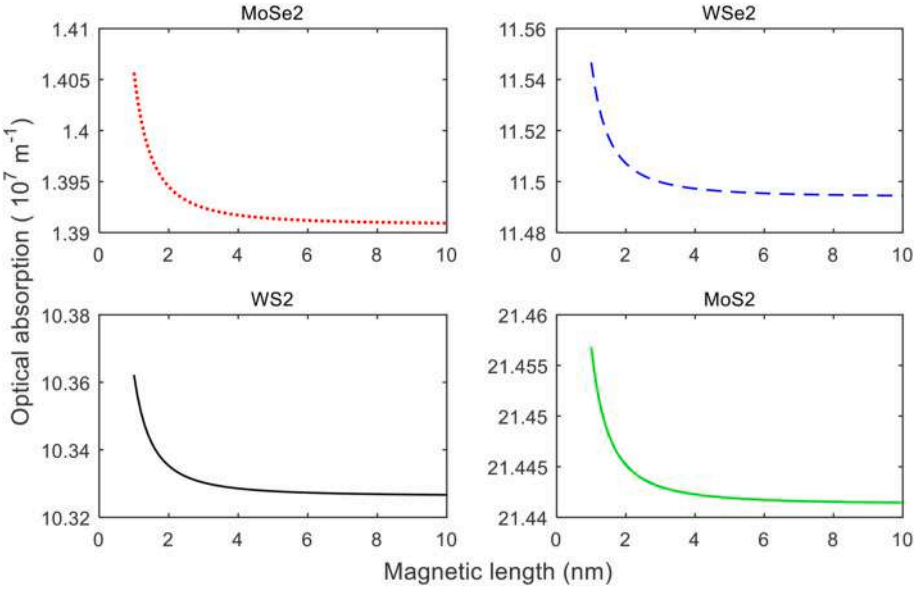


**Fig. 10.** Optical absorption coefficient versus the magnetic length for various TMDs at $\chi = 2.01$ and $\gamma = \pi/2$.

## Acknowledgments

LMP acknowledges ANID through Convocatoria Nacional Subvención a Instalación en la Academia Convocatoria Año 2021, Grant SA77210040. DL acknowledges partial financial support from Centers of Excellence with BASAL/ANID financing, Grant AFB180001, CEDENNA. CKS acknowledges support from the Deutscher Akademischer Austauchdienst German Academic Exchange Service through the Staff Exchange Fellowships in Sub-Saharan-Africa.

## References

[1] S. Ayari, A. Smiri, A. Hichri, S. Jaziri, T. Amand, Radiative lifetime of localized excitons in transition-metal dichalcogenides, Phys. Rev. B 98 (2018), 205430.
[2] J.V. Nguepnang, C. Kenfack-Sadem, A. Kenfack-Jiotsa, C. Guimapi, A.J. Fotue, A. E. Merad, Electron-phonon coupling contribution on the optical absorption and the dynamic of exciton-polaron in monolayer transition meta dichalcogenides, Opt. Quant. Electron. 53 (2021) 654.
[3] S.V. Mandyam, H.M. Kim, M. Drndic, Large area few-layer TMD film growths and applications, J. Phys. Mater. 3 (2020), 024008.
[4] H.G. Ji, P.S. Fernandez, U. Erkilic, H. Ago, Stacking orientation-dependent photoluminescence pathways in artificially stacked bilayer $WS_2$ nanosheets grown by chemical vapor deposition: implications for spintronics and valleytronics, ACS Appl. Nano Mater. 4 (2021) 3717–3724.
[5] A.J. Pearce, G. Burkard, Electron spin relaxation in a transition metal dichalcogenide quantum dot, 2D Mater. 4 (2017), 025114.
[6] N.D. Hien, C.V. Nguyen, N.N. Hieu, S.S. Kubakaddi, C.A. Duque, M.E. Mora-Ramos, L. Dinh, T.N. Bich, H.V. Phuc, Magneto-optical transport properties of monolayer transition metal dichalcogenides, Phys. Rev. B 101 (2020), 045424.
[7] Z. Wang, J. Shan, K.F. Mak, Valley and spin polarized Landau levels in monolayer $WSe_2$, Nat. Nanotechnol. 12 (2017) 144–149.
[8] C.V. Nguyen, N.N. Hieu, D. Muoi, C.A. Duque, E. Feddi, H.V. Nguyen, L.T. T. Phuong, B.D. Hoi, H.V. Phuc, Linear and nonlinear magneto-optical properties of monolayer $MoS_2$, J. Appl. Phys. 123 (2018), 034301.
[9] W. Liu, Z. Lin, S. Tian, Y. Huang, H. Xue, K. Zhu, C. Gu, Y. Yang, J. Li, Plasmonic effect on the magneto-optical property of monolayer $WS_2$ studied by polarized-Raman spectroscopy, Appl. Sci. 11 (2021) 1599.
[10] J. Forste, N.V. Tepliakov, S.Y. Kruchinin, J. Lindlau, V. Funk, M. Forg, K. Watanable, T. Taniguchi, A.S. Baimuratov, A. Hogele, Exciton g-factors in monolayer and bilayer $WSe_2$ from experiment and theory, Nat. Commun. 11 (2020) 1–8.
[11] E. Liu, J.V. Baren, C.T. Liang, T. Taniguchi, K. Watanabe, N.M. Gabor, Y.C. Chang, C.H. Lui, Multipath optical recombination of intervalley dark excitons and trions in monolayer $WSe_2$, Phys. Rev. Lett. 124 (2020), 196802.
[12] Z.W. Wang, W.P. Li, Y. Xia, R.Z. Li, Z.Q. Li, Influence of exciton-phonons coupling on the exciton binding energy in monolayer transition metal dichalcogenides, Appl. Phys. Lett. 110 (2017), 231603.
[13] E. Jung, J.C. Park, Y.S. Seo, J.H. Kim, J. Hwang, Y.H. Lee, Unusually large exciton binding energy in multilayered 2H-MoTe2, Sci. Rep. 12 (2022) 1–10.
[14] A.J. Chaves, R.M. Ribeiro, T. Frederico, N.M.R. Peres, Excitonic effects in the optical properties of 2D materials: an equation of motion approach, 2D Mater. 4 (2017), 025086.
[15] A.V. Stier, N.P. Wilson, K.A. Velizhanin, J. Kono, X. Xu, S. Crooker, Magneto-optics of exciton Rydberg states in a monolayer semiconductor, Phys. Rev. Lett. 120 (2018), 057405.
[16] J. Zipfel, J. Holler, A.A. Mitioglu, M.V. Ballottin, P. Nagler, A.V. Stier, T. Taniguchi, K. Watanabe, S.A. Crooker, P.C.M. Christiansen, T. Korn, A. Chernikov, Spatial extent of the excited exciton states in $WS_2$ monolayers from diamagnetic shifts, Phys. Rev. B 98 (2018), 075438.
[17] S. Helmrich, R. Schneider, A.W. Achtstein, A. Arora, B. Herzog, S.M. de Vasconcellos, M. Kolarczik, O. Schops, R. Bratschitsch, U. Woggon, N. Owschimikow, Exciton-phonon coupling in mono-and bilayer $MoTe_2$, 2D Mater. 5 (2018), 045007.
[18] D. Christiansen, M. Selig, G. Berghauser, R. Schmidt, I. Niehues, R. Schneider, A. Arora, S.M. de Vasconcellos, R. Bratschitsch, E. Malic, A. Knorr, Phonon sidebands in monolayer transition metal dichalcogenides, Phys. Rev. Lett. 119 (2017), 187402.
[19] I. Niehues, R. Schmidt, M. Druppel, P. Marauhn, D. Christiansen, M. Selig, G. Berghauser, D. Wigger, R. Schneider, L. Braasch, R. Koch, A. Castellanos-Gomez, T. Kuhn, A. Knorr, E. Malic, M. Rohlfing, S.M. de Vasconcellos, R. Bratschitsch, Strain control of exciton phonon coupling in atomically thin semiconductors, Nano Lett. 18 (2018) 1751–1757.
[20] W.P.D. Wong, J. Yin, B. Chaudhary, X.Y. Chun, D. Cortecchia, S.-Z.A. Lo, A. C. Grimsdale, O.F. Mohammed, G. Lanzani, C. Soci, Large polaron self-trapped states on three dimensional metal Halide Perovskites, ACS Materials Lett 2 (2020) 20–27.
[21] A. Simbula, R. Pau, Q. Wang, F. Liu, V. Sarritzu, S. Lai, M. Lodde, F. Mattana, G. Mulla, A.G. Lehmann, I.D. Spanopoulos, M.G. Kanatzidis, D. Marongiu, F. Quochi, M. Saba, A. Mura, G. Bongiovanni, Polaron plasma in equilibrium with bright excitons in 2D and 3D hybrid Perovskites, Adv. Opt. Mater. 9 (2021), 2100295.
[22] D. Li, C. Trovatello, S.D. Conte, M. Nub, G. Soavi, G. Wang, A.C. Ferrari, G. Cerullo, T. Brixner, Exiton phonon coupling strength in single layer $MoSe_2$ at room temperature, Nat. Commun. 12 (2021) 954.
[23] T. Wang, M.S. Niu, J.J. Guo, K.N. Zhang, Z.C. Wen, J.Q. Liu, C.C. Qin, X.T. Hao, 3D charge transport pathway in organic solar cells via incorporation of discotic liquid crystal columns, Solar RRL 4 (2020), 2000047.
[24] S. Shree, M. Semina, C. Robert, B. Han, T. Amand, A. Balocchi, M. Manca, E. Courtade, X. Marie, T. Taniguchi, K. Watanabe, M.M. Glazov, B. Urbaszek, Observation of exciton phonon coupling in $MoSe_2$ monolayers, Phys. Rev. B 98 (2018), 035302.
[25] C. Trovatello, H.P.C. Miranda, A.M. Sanchez, R.B. Varillas, C. Manzoni, L. Moretti, L. Ganzer, M. Maiuri, J. Wang, D. Dumcenco, A. Kis, L. Wirtz, A. Marini, G. Soavi, A.C. Ferrari, G. Cerullo, D. Sangalli, S.D. Conte, Strongly coupled coherent phonons in single-layer $MoS_2$, ACS Nano 14 (2020) 5700–5710.
[26] S. Ono, T. Ogura, Anomalous energy shift of laterally confined two dimensional excitons, J. Appl. Phys. 124 (2018), 034301.
[27] Y. Liu, H. Li, C. Qiu, X. Hu, D. Liu, Layer dependent signatures for exciton dynamics in monolayer and multilayer $WSe_2$ revealed by fluorescence lifetime imaging measurement, Nano Res. 13 (2020) 661–666.
[28] Y.J. Zheng, Y. Chen, Y.L. Huang, P.K. Gogoi, M.Y. Li, L.J. Li, P.E. Trevisanutto, Q. Wang, S.J. Pennycook, A.T.S. Wee, S.Y. Quek, Point defects and localized excitons in 2D $WSe_2$, ACS Nano 13 (2019) 5.
[29] L. Du, M. Liao, J. Tang, Q. Zhang, H. Yu, R. Yang, K. Watanable, T. Taniguchi, D. Shi, Q. Zhang, G. Zhang, Strongly enhanced exciton phonon coupling in two dimensional $WSe_2$, Phys. Rev. B 97 (2018), 235145.
[30] M.C. Gelvez-Rueda, E.M. Hutter, D.H. Cao, N. Renaud, C.C. Stoumpos, J.T. Hupp, T.J. Savenije, M.G. Kanatzidis, F.C. Grozema, Interconversion between free charges and bound excitons in 2D hybrid lead Halide Perovskites, J. Phys. Chem. C 121 (2017) 47.
[31] M. Tiotsop, A.J. Fotue, G.K. Fautso, C.S. Kenfack, H.B. Fotsin, L.C. Fai, Decoherence time, hydrogenic-like impurity effect and Shannon entropy on polaron in RbCl triangular quantum dot qubit, Superlattice. Microst. 103 (2017) 70–77.
[32] S.C. Kenfack, A.J. Fotue, M.F.C. Fobasso, G.N. Bawe, L.C. Fai, Shannon entropy and decoherence of polaron in asymmetric polar semiconductor quantum wire, Superlattice. Microst. 111 (2017) 32–44.
[33] D.V. Tuan, M. Yang, H. Dery, Coulomb interaction in monolayer transition metal dichalcogenides, Phys. Rev. B 98 (2018), 125308.
[34] R. Khordad, S. Goudarzi, H. Bahramiyan, Effect of temperature on lifetime and energy states of bound polaron in asymmetrical Gaussian quantum well, Indian J. Phys. 90 (2016) 659–664.
[35] Z. Li, The ground state lifetime of polaron in a two-dimensional quantum pseudodot system, Indian J. Phys. 93 (2018) 707–711.
[36] T. Mueller, E. Mallic, Exciton physics and device application of two-dimensional transition metal duchalcogenide semiconductors, npj 2D Mater, Apple 2 (2018) 1–12.
[37] X. Xi, Z. Wang, W. Zhao, J.H. Park, K.T. Law, H. Berger, L. Forro, J. Shan, K.F. Mak, Ising pairing in superconducting $NbSe_2$ atomic layers, Nat. Phys. 12 (2016) 139–143.
[38] Z. Fei, T. Palomaki, W. Wu, S. Zhao, X. Cai, B. Sun, P. Nguyen, J. Finney, X. Xu, D. H. Cobden, Edge conduction in monolayer $WTe_2$, Nat. Phys. 13 (2017) 677–682.
[39] Z.E. Eroglu, O. Comegys, L.S. Quintanar, N. Azam, S. Elafandi, M.M. Samani, A. Boulesbaa, Ultrafast dynamics of exciton formation and decay in two-dimensional tungsten disulfide 2D-$WS_2$ monolayers, Phys. Chem. Chem. Phys. 22 (2020) 17385–17393.
[40] A. Rodek, T. Hahn, J. Kasprzak, T. Kazimierczuk, K. Nogajewski, K.E. Polczynska, K. Watanabe, T. Taniguchi, T. Kuhn, P. Machnikowski, M. Potemski, D. Wigger, P. Kossacki, Local field effects in ultrafast light-matter interaction measured by pump-probe spectroscopy of monolayer $MoSe_2$, Nanophotonics 10 (2021) 2717–2728.
[41] Y. Hu, F. Zhang, M. Titze, B. Deng, H. Li, G.J. Cheng, Straining effects in $MoS_2$ monolayer on nanostructured substrates: temperature dependent photoluminescence and exciton dynamics, Nanoscale 10 (2018) 5717–5724.
[42] Y.Y. Yue, H.Y. Wang, L. Wang, L.Y. Zhao, H. Wang, B.R. Gao, H.B. Sun, Direct observation of room temperature intravalley coherent coupling processes on monolayer $MoS_2$, Laser Photon. Rev. 16 (2022), 2100343.
[43] H. Liu, A. Pau, D.K. Efimkin, Hybrid dark excitons in monolayer $MoS_2$, Phys. Rev. B 104 (2021), 165411.
[44] H. Shi, R. Yan, S. Bertolazzi, J. Brivio, B. Gao, A. Kis, D. Jena, H.G. Xing, L. Huang, Exciton dynamics in suspended monolayer and few layer $MoS_2$ 2D crystals, ACS Nano 7 (2013) 1072–1080.
[45] F. Wu, T. Lovorn, A.H. MacDonald, Theory of optical absorption by interlayer excitons in transition metal dichalcogenides heterobilayers, Phys. Rev. B 97 (2018), 035306.
[46] P. Rivera, J.R. Schaibley, A.M. Jones, J.S. Ross, S. Wu, G, P. Klement, K. Seyler, G. Clark, N.J. Ghimire, J. Yan, D.G. Mandrus, W. Yao, X. Xu, Observation of long-lived interlayer excitons in monolayer $MoSe_2$ –$WSe_2$ heterostructures, Nat. Commun. 6 (2015) 6242.
[47] Q.H. Wang, K. Zadeh, K. Kourosh, C. Andras, N.J. Strano, S. Michael, Electronics and optoelectronics of two-dimensional transition metal dichalcogenides, Nat. Nanotechnol. 7 (2012) 699–712.
[48] P.F. Li, Z.W. Wang, Optical absorption of Frohlich polaron in monolayer transition metal dichalcogenides, J. Appl. Phys. 123 (2018), 204308.
[49] A. Thilagam, Excitonic polarons in low dimensional transition metal dichalcogenides, Phys. B Condens. Matter 464 (2015) 44–50.

[50] S. Zielinska-Raczynska, D.A. Fishman, C. Faugeras, M.M.P. Potemski, P.H.M. V. Loosdrecht, K. Karpinski, G. Czajkowski, D. Ziemkiewicz, Magneto-excitons in $Cu_2O$: theoretical model from weak to high magnetic fields, New J. Phys. 21 (2019), 103012.
[51] G. Kankan Cong, N. Timothy, J. Kono, Excitons in magnetic fields, Encyclo. Modern Opt. II 2 (2018).
[52] N. Myoung, G. Ihm, S. Lee, Transport in armchair graphene nanoribbons modulated by magnetic barriers, Physica 42 (2010) 2808–2811.
[53] S. Ghosh, M. Sharma, Electron optics with magnetic vector potential barriers in graphene, J. Phys. Condens. Matter 21 (2009), 292204.
[54] V.K. Kozin, V.A. Shabashow, A.V. Kavokin, I.A. Shelykh, Anomalous exciton Hall effect, Phys. Rev. Lett. 126 (2021), 036801.
[55] C. Kenfack-Sadem, S. Mounbou, S.I. Fewo, M.F.C. Fobasso, A.J. Fotue, L.C. Fai, Optical absorption and Tsallis entropy of polaron in monolayer graphene, J. Low Temp. Phys. 200 (2020) 173–186.
[56] R. Khordad, H.R.R. Sedehi, Study of non-extensive entropy of bound polaron in monolayer graphene, Indian J. Phys. 92 (2018) 979–984.
[57] R. Khordad, Ar Firoozi, H.R.R. Sedehi, Simultaneous effects of temperature and pressure on the entropy and the specific heat of a three-dimensional quantum wire: Tsallis formalism, J. Low Temp. Phys. 202 (2021) 185–195.
[58] R. Khordad, H.R.R. Sedehi, Magnetic susceptibility of graphene in non-commutative phase-space: extensive and non-extensive entropy, Eur. Phys. J. A 134 (2019) 133.
[59] D. Kozawa, R. Kumar, A. Carvalho, K.K. Amara, W. Zhao, S. Wang, M. Toh, R. M. Ribeiro, A.H. Castro Neto, K. Matsuda, G. Eda, Photocarrier relaxation pathway in two dimensional semiconducting transition metal dichalcogenides, Nat. Commun. 5 (2014) 4543.
[60] M.F.C. Fobasso, C. Kenfack-Sadem, E. Baloitcha, A.J. Fotue, L.C. Fai, Lifetime and dynamics of polaron and bipolaron in graphene nanoribbon under laser, Eur. Phys. J. A 135 (2020) 471.
[61] J.T. Devreese, Frohlich Polarons: Lecture Course Including Detailed Theoretical Derivations, eighth ed., 2018. Antwerpen, Belgium.
[62] C. Kenfack-Sadem, A.K. Teguimfouet, A. Kenfack Jiotsa, R.M.K. Tsiaze, Dynamics and decoherence of exciton polaron in monolayer transition metal dichalcogenides, J. Electron. Mater. 50 (2021) 5.
[63] A.K. Teguimfouet, C.K. Sadem, J.V. Nguepnang, A.K. Jiotsa, K. Bhattacharyya, Relaxation and transport of excitonic polaron in monolayer transition metal dichalcogenides, Iran, J. Sci. Technol. Trans. Sci. 46 (2022) 717–730.
[64] Y. Xiao, Z.Q. Li, Z.W. Wang, Polaron effect on the bandgap modulation in monolayer transition metal dichalcogenides, J. Phys. Condens. Matter 29 (2017), 485001.
[65] A. Splendiani, L. Sun, Y. Zhang, T. Li, J. Kim, C.Y. Chim, G. Galli, F. Wang, Emerging photoluminescence in monolayer $MoS_2$, Nano Lett. 10 (2010) 1271–1275.
[66] M.F.C. Fobasso, A.J. Fotue, S.C. Kenfack, L.C. Fai, Thermal properties of magnetopolaron in GaAs delta potential under Rashba effect, Phys. E Low-dimens. Syst. Nanostruct. 118 (2020), 113941.
[67] A.V. Stier, N.P. Wilson, G. Clark, X. Xu, S.A. Crooker, Probing the influence of dielectric environment on excitons in monolayer $WSe_2$: insight from high magnetic fields, Nano Lett. 16 (2016) 7054–7060.
[68] A.A. Mitioglu, K. Galkowski, A. Surrente, L. Klopotowski, D. Dumcenco, A. Kis, D. K. Maude, P. Plochocka, Magnetoexcitons in large area CVD grown monolayer $MoS_2$ and $MoSe_2$ on sapphire, Phys. Rev. B 93 (2016), 165412.
[69] A.V. Stier, K.M. McCreary, B.T. Jonker, J. Kono, S.A. Crooker, Exciton diamagnetic shifts and valley Zeeman effects in monolayer $WS_2$ and $MoS_2$ to 65 tesla, Nat. Commun. 7 (2016), 10643.
[70] J. Moore Frost, Calculating polaron mobility in halide perovskites, Phys. Rev. B 96 (2017), 195202.
[71] J.R.D. Djomou, S.C. Kenfack, A.J. Fotue, M.F.C. Fobasso, L.C. Fai, Contribution of bulk and surface phonons to the properties of polaron in $Zn_{1-x}Cd_xSe/ZnSe$ heterojunction confined in a triangular potential, Physica B: Phys. Condens. Matter 548 (2018) 58.
[72] V. Pouthier, Quantum decoherence in finite size exciton phonon systems, J. Chem. Phys. 134 (2011), 114516.
[73] F. Lengers, T. Kuhn, D.E. Reiter, Theory of the absorption line shape in monolayer of transition metal dichalcogenides, Phys. Rev. B 101 (2020), 155304.
[74] G. Berghauser, E. Malic, Analytical approach to excitonic properties of $MoS_2$, Phys. Rev. B 89 (2014), 125309.
[75] E. Malic, M. Selig, M. Feierabend, S. Brem, D. Christiansen, F. Wendler, A. Knorr, G. Berghauser, Dark excitons in transition metal dichalcogenides, Phys. Rev. Mater. 2 (2018), 014002.
[76] L. Meckbach, T. Stroucken, S.W. Koch, Influence of the effective layer thickness on the ground state and excitonic properties of transition metal dichalcogenide systems, Phys. Rev. B 97 (2018), 035425.
[77] D.Y. Qiu, F.H. da Jornada, S.G. Louie, Screening and many body effects in two dimensional crystals: monolayer $MoS_2$, Phys. Rev. B 93 (2016), 235435.
[78] T. Deilmann, K.S. Thygesen, Dark excitations in monolayer transition metal dichalcogenides, Phys. Rev. B 96 (2017), 201113.
[79] M. Druppel, T. Deilmann, J. Noky, P. Marauhn, P. Kruger, M. Rohlfing, Electronic excitations in transition metal dichalcogenide monolayers from an LDA+GdW approach, Phys. Rev. B 98 (2018), 155433.
[80] G. Moody, C. Kavir Dass, K. Hao, C. Chen, L. Li, A. Singh, G. Tran, K. Clark, X. Xu, G. Berghauser, E. Malic, A. Knorr, X. Li, Intrinsic homogeneous linewidth and broadening mechanisms of excitons in monolayer transition metal dichalcogenides, Nat. Commun. 6 (2015) 8315.
[81] M. Selig, G. Berghauser, A. Raja, P. Nagler, C. Schuller, T.F. Heinz, T. Korn, A. Chernikov, E. Malic, A. Knorr, Excitonic linewidth and coherence lifetime in monolayer transition metal dichalcogenides, Nat. Commun. 7 (2016), 13279.

# Magnetic barrier and electric field effects on exciton-polaron relaxation and transport properties in transition metal dichalcogenide monolayers

C. Kenfack-Sadem,[1,2,*] A. K. Teguimfouet,[3] A. B. Moubissi,[4] Natalia Cortés,[5] M. F. C. Fobasso,[1] M. Masale,[6] and A. Kenfack-Jiotsa[7]

[1]*Laboratory of Condensed Matter and Nanomaterials, Department of Physics, University of Dschang, P.O. Box 67, Dschang, Cameroon*

[2]*International Chair in Mathematical Physics and Applications (ICMPA-UNESCO Chair), University of Abomey-Calavi, 072 P.O. Box 50, Cotonou, Republic of Benin*

[3]*Laboratoire de Mécanique-Matériaux et Structures, Département de Physique, Université de Yaoundé I, BP 812, Yaoundé, Cameroon*

[4]*Faculté des Sciences, Université des Sciences et Techniques de Masuku B.P. 901, Franceville, Gabon*

[5]*Instituto de Alta Investigación, Universidad de Tarapacá, Casilla 7D, Arica, Chile*

[6]*University of Botswana, P/Bag 0022, Gaborone, Botswana*

[7]*Département de Physique, Ecole Normale Supérieure, Université de Yaoundé I, BP 42, Yaoundé, Cameroon*

(Received 31 May 2022; revised 9 September 2022; accepted 23 January 2023; published 14 February 2023)

The relaxation of excitonic polaron and the transport properties in two-dimensional monolayers of transition metal dichalcogenides (TMDCs) such as $MoS_2$, $MoSe_2$, $WSe_2$, and $WS_2$ are investigated under the influence of a magnetic barrier and an electric field using the relaxation-time approximation and the Kubo formula. We find that the presence of magnetic barrier strengthens the electron-hole interaction and stabilizes the exciton-polaron while the electric field alters this stability. In addition, exciton-polaron is more relaxed as the electric field increases but due to the magnetic barrier it quickly returns into its equilibrium. Moreover, the electrical conductivity of TMDCs is favored by the electric field and a barrier of high magnetic lengths. $MoSe_2$ is the compound that presents the highest relaxation time and electrical conductivity. The result indicates that the electrical conductivity grows when the system is relaxed. The thermoelectric power of TMDCs falls when the electric field increases, whereas it does not present a monotonic behavior in the magnetic barrier. It globally decreases for weak values of the magnetic length and enhances for high values. The highest thermoelectricity is obtained in $MoSe_2$. A high optical conductivity is observed in TMDCs. The result shows that optical transitions rise as the magnetic strength of the barrier increases, but the electric field presents an opposite effect. The probability of absorb energy $\hbar\omega$ by the exciton-polaron steps up when the magnetic length and electric field increase. The highest value of optical conductivity and oscillator strength is observed for $MoS_2$. We demonstrate that the magnetic barrier and electric field are suitable parameters which can be used to improve the performance of TMDCs materials.

DOI: 10.1103/PhysRevB.107.075134

## I. INTRODUCTION

Due to their structures and different applications, transition metal dichalcogenides (TMDCs) are suitable two-dimensional (2D) materials with formula $MX_2$, where the transition metal atoms $M$ are sandwiched between two layers of chalcogen atoms $X$, and the $MX_2$ layers are coupled to each other by van der Waals interactions. Their semiconductor characteristics presenting high stability and flexibility [1–3] makes them highly interesting in many areas [4–6]. Their optical and electronic properties [7,8] reveal applications in valleytronics and spintronics [9,10], as well as in photoluminescence experiments [11].

An exciton-polaron is a quasiparticle resulting from the interaction of exciton (pair of electron-hole) with phonons, which are present in TMDCs [12,13]. Some authors have developed excitonic polaron systems where diagonalization techniques are needed for suitable energy spectra and properties in 2D materials [14–16]. Excitonic systems are limited by the process of dressing with phonons [17–19], which itself can be understood through the relaxation phenomenon. The relaxation time is a good concept to study these systems due to the fact that exciton generation and recombination, and optical excitation depend on it [20,21]. Experimentally, it is found that the relaxation-time range is around femtosecond (fs) and picosecond (ps) [22–24]. The relaxation and the exciton generation are studied in PbS quantum dots [25]. It is seen that the confinement has an important role in these processes [26], and also in optical conductivity [27]. The appearance of an excitonic signal in the optical conductivity response has been demonstrated in ZnO [28] and graphene [29], revealing that exciton effects play an important role in the optical spectra. In semiconductors GaAs [30,31], the excitonic signal is observed for energies below the gap, by a peak in the absorption spectra. Above the gap, a renormalization of the band and the increase of the optical conductivity occur due to the scattering between electrons and holes. In addition, Peres *et al.* [32]

*kevinsadem@yahoo.fr

 

proved that an excitonic resonance in graphene is responsible for the measured midinfrared response, the broadening of the absorption at the threshold, the increase of the conductivity beyond the universal value above the Fermi blocked regime, and the reduction of the conductivity at high frequencies.

Yang *et al.* [33] studied the layer dependence on electrical and optoelectronic properties in $ReSe_2$. It is shown that the number of layers considerably influences these properties. For example, the band gap increases when the number of layers decreases, and a single layer provides best performance for mobility. Chen *et al.* [34] demonstrated the increase of electrical conductivity with the decrease in thickness layer. This implies the probable surface dominance of electrical conduction in TMDC layers resulting from either the intrinsic high surface conductivity or the anisotropic conductivity. Qin *et al.* [35] studied the in-plane effect of electron (hole) concentration at 300 K on the transport coefficients. Anisotropic behavior is observed for the thermopower and electrical conductivity. The electrical conductivity enhances when the carrier concentration increases, whereas the Seebeck coefficient decreases. They found that the Seebeck coefficient presents a lower asymmetry for $n$-type doping than for $p$-type doping. High amplitudes for the Seebeck coefficient are seen and a peak is observed at a carrier concentration of $1.25 \times 10^{11}\text{cm}^{-2}$. In addition, recently Ge *et al.* [36] have combined first-principles calculations and Boltzmann theory to demonstrate the high performance for the carrier transport in TMDCs. High Seebeck coefficient at low temperature and low electrical conductivity at high temperature are observed. They showed that the carrier transport can be due to the modest carrier effective mass and the weak electron (hole)-phonon coupling. It is clear that these properties are crucial in the study of charge-carrier transport in TMDC materials. It is well known that the behavior of quasiparticles such as polaron and exciton is considerably influenced by its environment, which can be an external magnetic field [37,38] or an electric field [39,40].

It has been shown that the applying of magnetic field on TMDCs leads to the increase of exciton binding energy with the magnetic strength [41]. Nam *et al.* [42] proved that the role of external magnetic field is minor on the electrical conductivity for very strong magnetic strength, and it becomes relatively significant for temperatures less than 200 K. Das *et al.* [43] showed a reduction of the Seebeck coefficient with an applied magnetic field and it enhances globally when the chemical potential and temperature increase. Tahir *et al.* [44] showed that the magneto-optical transport properties in monolayer (1L) 2D phosphorene are very influenced by a magnetic field. It is found that the optical conductivity has an oscillatory dependence on the magnetic field and the strength of optical transitions is a function of the $xy-$plane momentum operator. The magneto-optical response in TMDCs can be tuned in the visible, in the range of microwave to terahertz, contrary to graphene or a 2D electron gas, which are limited to the terahertz range. Reference [45] revealed that the real part of the optical conductivity is an increasing function of the temperature for $WTe_2$. In TMDCs [46], the attractive branch of excitonic polaron is not influenced enough by the magnetic strength, while the repulsive ones exhibit magnetic peaks and oscillations reflecting combined exciton-cyclotron resonance. In 2D materials, the anomalous transport of exciton in response to an in-plane electric field is studied [47]. It is shown that during a very short time, there is a regime in which the velocities of electron and hole (which constitute the exciton) are in the same direction. The electron and hole initially move in separate directions until reaching an equilibrium, in which the Coulomb interaction is closer to the force of the electric field. In addition, applying an electric field considerably increases the relaxation time [48] and reduces the optical absorption [49] in GaAs quantum wells. The exciton binding energy decreases with the increase of the electric field and quantum-dot radius [50].

In this paper, we theoretically investigate the transport properties in typical 1L TMDCs: $MoSe_2$, $WS_2$, $WSe_2$, and $MoS_2$. The paper organization is as follows: the second section is the model and calculations in which we derive the analytical expressions of the ground-state (GS) energy, the relaxation time, the electrical conductivity, the optical conductivity, the Seebeck coefficient, and the oscillator strength. In Sec. III, we present the results and discussion of the magnetic barrier and in-plane electric field effects on these properties, whereas the conclusion summarizes in the last section.

## II. MODEL AND CALCULATIONS

The system is taken as an exciton under the influence of a magnetic barrier and an electric field, interacting with longitudinal optical (LO) phonons in a 1L TMDC. The total Hamiltonian is written as

$$\hat{H} = \hat{H}_{ex}^{2D} + \hat{H}_{ph} + \hat{H}_{ex-ph}^{2D}. \tag{1}$$

Here, $\hat{H}_{ex}^{2D}$ represents the Hamiltonian of the exciton (electron-hole) [49,51] in the TMDC $xy$ plane, including the magnetic barrier and the electric field as

$$\hat{H}_{ex}^{2D} = \frac{\left(P_{e,x}^2 + P_{e,y}^2\right)}{2m_e} - eE_{el}\, y_e + \frac{\left(P_{h,x}^2 + P_{h,y}^2\right)}{2m_h} + eE_{el}\, y_h + \frac{e^2 A_y^2}{2\mu} - \frac{e^2}{\varepsilon|\rho_e - \rho_h|}. \tag{2}$$

where $\vec{P}_h(\vec{P}_e)$ is the hole (electron)-momentum vector, $\rho_e(\rho_h)$ represents the electron (hole) coordinate in the TMDC $xy$ plane, and $E_{el}$ is the electric field along the $y$ direction. $m_e(m_h)$ is the effective mass of electron (hole), $\mu$ is the effective reduced mass of the exciton $(1/\mu) = (1/m_e) + (1/m_h)$, $e(-e)$ is the hole (electron) charge, and $\varepsilon$ is the TMDC permittivity.

The magnetic barrier is characterized by the magnetic strength [52] $\vec{B}(0, 0, B_z)$, with $B_z(x) = B_0 l_B[\delta(x) - \delta(x-L)]$. The width of the barrier is denoted by $L$ taken at 150 nm, and $l_B$ is the magnetic length related to a standard magnetic field given by $B_0 = \hbar/(el_B^2)$. From the Dirac delta function, the magnetic field can also take the form

$$B_z(x) = \begin{cases} B_0\, l_B; & \text{if } x = 0 \\ -B_0\, l_B; & \text{if } x = L \\ 0; & \text{otherwise} \end{cases}. \tag{3}$$

Such magnetic barrier can be constructed as shown by Ghosh *et al.* [53]. Figure 1 illustrates the present case where two long narrow magnetic stripes are placed perpendicular

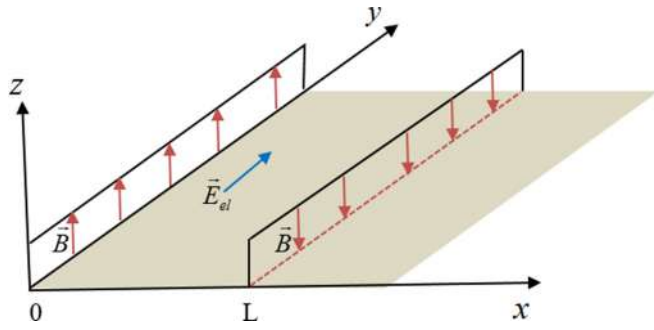


FIG. 1. Schematic of a TMDC system (light-brown 2D plane) under a magnetic barrier using two long narrow magnetic stripes with a magnetic field $B$ (red arrows) along the $z$ axis, and an electric field $E_{el}$ along the $y$ axis (blue arrow).

to the TMDC layer, respectively, at $x = 0$ (with $B_0 l_B$) and $x = L$ (with $-B_0 l_B$). The magnetic vector potential $\vec{A}(0, A_y, 0)$ is given by

$$A_y(x) = B_0\, l_B\, [\Theta(x) - \Theta(x - L)] = \begin{cases} A; & 0 < x < L \\ 0; & \text{otherwise} \end{cases}, \tag{4}$$

where $A = \hbar/(el_B)$ and $\Theta$ is the Heaviside function.

The phonon's Hamiltonian appears as $\hat{H}_{ph} = \sum_q \hbar\omega_0\, b_q^+ b_q$. $\hbar\omega_0$ denotes the phonon's energy while $b_q$ and $b_q^+$ are, respectively, the annihilation and creation phonon operators, $q$ is the phonon wave vector. The third term of Eq. (1) denotes the Hamiltonian of the exciton-phonon interaction taken as [54,55]

$$\hat{H}^{2D}_{ex-ph} = \sum_{K,q} \Xi^{op}(q)\, C^+_{K+q} C_K\, (b_q + b^+_{-q}), \tag{5}$$

where $C_K^+(C_K)$ denotes the creation (annihilation) operator of an exciton, and $K$ is the 2D wave vector of the exciton. The exciton-optical phonon-coupling function is given by

$$\Xi^{\text{op}}(q) = \left(D_c^{\text{op}} - D_v^{\text{op}}\right)\sqrt{\frac{\hbar q}{2S\eta u}}. \tag{6}$$

$S$ represents the area of the TMDC layer, $\eta$ denotes the area mass density, and $u$ is the sound velocity. The deformation potential constant is $D_v^{\text{op}}(D_c^{\text{op}})$ for hole (electron)–LO phonon coupling at some critical points $(K', K)$ inside the valence (conduction) band.

In order to simplify the calculations, we can do a useful transformation for the exciton Hamiltonian term in Eq. (2) as

$$\hat{H}^{2D}_{ex} = \sum_K \lambda\, C_K^+ C_K. \tag{7}$$

We use the relative coordinate ($\vec{\rho} = \vec{\rho}_e - \vec{\rho}_h$), the center of mass ($\vec{R} = \frac{m_e}{M}\vec{\rho}_e + \frac{m_h}{M}\vec{\rho}_h$), and the 2D wave function $\Psi^{2D} = \exp(i\vec{K}^*.\vec{R})\sqrt{\frac{2}{\pi}\frac{1}{a}}\exp(-\frac{\rho}{a})$, with $\vec{K}^* = \vec{K} - \frac{e}{\hbar}\vec{A}$, $a$ the exciton Bohr radius [51,56]. Then, the eigenenergy $\lambda$ for the 2D exciton is obtained as

$$\lambda(K, l_B, E_{el}) = E_g + \frac{\hbar^2 K^2}{2M} - E_b + \xi_B - \xi_{el}. \tag{8}$$

The exciton energy is then quantified. $E_g$ stands for the gap energy of the 1L $MX_2$, the second term of Eq. (8) is the kinetic energy with the exciton effective mass $M = m_e + m_h$, $E_b$ is the free-exciton binding energy, while $\xi_{el}$ and $\xi_B$ represent, respectively, the electric and magnetic parameters appearing as

$$\xi_B = \frac{\hbar^2}{l_B^2}\left(\frac{1}{2M} + \frac{1}{2\mu}\right);\ \xi_{el} = 2eaE_{el}/\pi. \tag{9}$$

In the latest equation, the terms $\frac{\hbar^2}{2M}$ and $\frac{\hbar^2}{2\mu}$ refer, respectively, to the kinetic and binding energies. The magnetic barrier contributes both in the kinetic and binding energies of exciton, whereas the electric field which is directly linked to the charge ($e$) modifies the Coulomb interaction of the electron-hole pair. The barrier acts as an effective potential for the exciton motion and modifies the kinetic-energy operator. Moreover, the field is along the $z$ direction confining the particles in the plane; then, electron and hole can acquire great kinetic energy.

We use an approximate method to diagonalize the full Hamiltonian (see Appendix A). The transformed Hamiltonian ($\hat{\Gamma}$) is averaged with the GS wave function $|\Psi_0\rangle = C_K^+|0\rangle_k|0\rangle_{ph}$ to obtain the energy as

$$E_K = \left(\frac{\hbar^2 K^2}{2M}\right)(1 - G_{ex2}) - G_{ex1} + E_g - E_b + \xi_B - \xi_{el}. \tag{10}$$

One can see that the magnetic barrier and electric field modify the GS energy of excitonic polaron.

### A. Relaxation time

The dynamic of polaronic systems is related to the fact that the time of optical phonons is approximately constant and finite. The presence of both electric and magnetic fields perturbs the excitonic states and the behavior of the system. The relaxation time ($\tau$) of the exciton-polaron can take the form [37]

$$\frac{1}{\tau} = \frac{2\pi}{\hbar}\sum_q \{|\Xi(q)|^2\{[n_B + f(E_{K+q})]\delta(E_K - E_{K+q} + \hbar\omega_0) + [1 + n_B - f(E_{K+q})]\delta(E_K - E_{K+q} - \hbar\omega_0)\}, \tag{11}$$

where $n_B$ is the Bose-Einstein function and $f$ is the Fermi-Dirac distribution with the Fermi energy ($E_F$),

$$n_B = [\exp(\beta E_K) - 1]^{-1}$$
$$f(E_{K+q}) = [1 + \exp\beta(E_{K+q} - E_F)]^{-1}. \tag{12}$$

$\beta$ denotes the inverse of the temperature. We develop the Dirac delta functions to obtain suitable forms for calculations (see Appendix B). Then, converting the summation of Eq. (11) into an integration, and integrating over $q$, one gets

$$\frac{1}{\tau} = \frac{M\left(D_c^{\text{op}} - D_v^{\text{op}}\right)^2}{\pi\eta u(1 - G_{ex2})\hbar^2} K\{[n_B + f(E_K + \hbar\omega_0)]\, I_K^+ + [1 + n_B - f(E_K - \hbar\omega_0)]\, I_K^-\}, \tag{13}$$

where the integrals $I_K^+$ and $I_K^-$ are given by

$$I_K^+ = \int_0^{2\pi} d\theta \frac{\cos^2\theta + \frac{M\hbar\omega_0}{\hbar^2 K^2(1-G_{ex2})}}{\sqrt{\cos^2\theta + \frac{2M\hbar\omega_0}{\hbar^2 K^2(1-G_{ex2})}}}, \tag{14}$$

$$I_K^- = \int_0^{2\pi} d\theta \frac{\cos^2\theta - \frac{M\hbar\omega_0}{\hbar^2 K^2(1-G_{ex2})}}{\sqrt{\cos^2\theta - \frac{2M\hbar\omega_0}{\hbar^2 K^2(1-G_{ex2})}}}. \tag{15}$$

These integrals are solved using the elliptic integrals of the first and second kind. This leads to

$$I_K^+ \approx \pi\left[\frac{\sqrt{\hbar^2 K^2(1-G_{ex2}) + 2M\hbar\omega_0}}{\hbar K\sqrt{1-G_{ex2}}} + \frac{\hbar^3 K^3(1-G_{ex2})^{3/2} + M\hbar\omega_0\,\hbar K\sqrt{1-G_{ex2}}}{2(\hbar^2 K^2(1-G_{ex2}) + 2M\hbar\omega_0)^{3/2}}\right], \tag{16}$$

$$I_K^- \approx \pi\left[\frac{2\hbar^2 K^2(1-G_{ex2}) - 2M\hbar\omega_0}{\hbar^2 K^2(1-G_{ex2})} + \frac{2(M\hbar\omega_0)^2 - M\hbar\omega_0\hbar^2 K^2(1-G_{ex2})}{2\hbar^4 K^4(1-G_{ex2})^2}\right]. \tag{17}$$

Therefore, the relaxation time for the exciton-polaron is obtained since $I_K^+$ and $I_K^-$ are determined analytically according to Eq. (13).

### B. Electrical conductivity and Seebeck coefficient

The electrical conductivity evaluates the motion of charge carriers in TMDC materials responsible for the current. As for each semiconductor, applying an external field modifies this property. Based on the relaxation-time approximation, the electrical conductivity is given by [57]

$$\sigma_{el} = e^2 \int \Lambda(E)\left(-\frac{\partial f}{\partial E}\right)dE, \tag{18}$$

where $\Lambda(E)$ is the transport function taken as

$$\Lambda(E) = \frac{1}{S}\sum_K v_g^2\,\tau\,\delta(E - E_K). \tag{19}$$

$v_g$ corresponds to the group velocity [58] obtained as

$$v_g = \frac{\hbar K(1-G_{ex2})}{M}. \tag{20}$$

After the integration over $K$, one gets

$$\Lambda = \frac{(1-G_{ex2})K_0^2}{2\pi M}\{\tau(K_0) - \tau(-K_0)\}, \tag{21}$$

with

$$K_0 = \frac{\sqrt{2Md}}{\hbar\sqrt{1-G_{ex2}}};$$
$$d = E + E_b + G_{ex1} - E_g - \xi_B + \xi_{el}. \tag{22}$$

Then, substituting the latest relations in Eq. (18), the electrical conductivity reads

$$\sigma_{el} = \frac{32\eta u\hbar^4(1-G_{ex2})^3}{\pi M^3\left(D_c^{\rm op} - D_v^{\rm op}\right)^4}\beta e^2\int_0^\infty dE\,\frac{(d-\hbar\omega_0)\sqrt{d}}{\gamma^2-\chi^2}f(E), \tag{23}$$

where

$$\gamma = [n_B + f(E+\hbar\omega_0)]\left(\frac{8d^2 + 9\hbar\omega_0 d + 4(\hbar\omega_0)^2}{(d+\hbar\omega_0)^{3/2}}\right) + 2[1 + n_B - f(E-\hbar\omega_0)]\left(\frac{5d-\hbar\omega_0}{\sqrt{d-\hbar\omega_0}}\right), \tag{24}$$

and

$$\chi = 4[1 + n_B - f(E-\hbar\omega_0)]\left(\frac{\hbar\omega_0 - d}{\sqrt{d}}\right). \tag{25}$$

Since the electrical conductivity depends on temperature, it is convenient to explore the Seebeck effect (or thermoelectric power) which evaluates the electric current generated by a gradient of temperature. The Seebeck coefficient takes the form [59]

$$S = \frac{\beta}{e}\frac{C_1}{C_2}, \tag{26}$$

where

$$C_1 = \int_0^\infty dE\,\frac{(d-\hbar\omega_0)\sqrt{d}}{\gamma^2-\chi^2}f(E)(E-E_F)$$
$$C_2 = \int_0^\infty dE\,\frac{(d-\hbar\omega_0)\sqrt{d}}{\gamma^2-\chi^2}f(E). \tag{27}$$

### C. Optical conductivity and oscillator strength

The optical conductivity represents the optical response of the TMDC materials and it can be expressed through the Kubo formula [60] at zero temperature by

$$\sigma_{(\omega)} = i\frac{2e^2}{SM\omega} + \frac{1}{S\hbar\omega}\int_0^\infty dt\,e^{i\omega t}\langle[J(t), J(0)]\rangle. \tag{28}$$

$J$ is the total current operator. Taking into account the electron- and hole-current operators [61], $\sigma_{(\omega)}$ becomes

$$\sigma_{(\omega)} = i\frac{2e^2}{SM\omega} + \frac{1}{S\hbar\omega}\int_0^\infty dt\,e^{i\omega t}\left\langle\frac{e^2}{m_h^2}[p_h(t), p_h(0)] + \frac{e^2}{m_e^2}[p_e(t), p_e(0)]\right\rangle. \tag{29}$$

After integrating by parts [60], one gets

$$\sigma_{(\omega)} = i\frac{2e^2}{SM\omega} - \frac{e^2}{S\hbar\omega}\frac{1}{\omega^2}\int_0^\infty dt\,e^{i\omega t}\left\langle\frac{1}{m_e^2}[F_e(t), F_e(0)] + \frac{1}{m_h^2}[F_h(t), F_h(0)]\right\rangle. \tag{30}$$

As shown in Appendix C, we evaluate the commutators of Eq. (30) and the average is done with respect

to the ground state. We get

$$\sigma_{(\omega)} = i\frac{2e^2}{SM\omega} + \frac{e^2}{S\hbar\omega}\frac{1}{\omega^2}\int_0^\infty dt\, e^{i\omega t}\left\{-i\sum_q\left(\frac{e^2B^2\left(m_e^3+m_h^3\right)}{2m_e^3m_h^3} - \frac{eE_{el}\left(m_h^2-m_e^2\right)}{2m_e^2m_h^2}\right)q\Xi(q)(f_{ex}^*-f_{ex})\right.$$
$$\left. + i\sum_q\left(\frac{e^2B^2\left(m_e^3+m_h^3\right)}{2m_e^3m_h^3} - \frac{eE_{el}\left(m_h^2-m_e^2\right)}{2m_e^2m_h^2}\right)q\Xi(q)(U(t)f_{ex}^* - T(t)f_{ex}) + \frac{\left(m_h^2+m_e^2\right)}{m_e^2m_h^2}\sum_q q^2\Xi^2(q)(U(t)-T(t))\right\}. \tag{31}$$

The imaginary part of the optical conductivity is obtained after integrating over $t$ as

$$\mathrm{Im}\left[\sigma(\omega)\right] = \frac{2e^2}{SM\omega} + \frac{\hbar e^2}{S\hbar\omega}\frac{\left(m_h^2+m_e^2\right)}{m_e^2m_h^2\omega^2}\sum_q q^2\Xi^2(q)\left(\frac{1}{\lambda_{K+q}-\lambda_K+\hbar\omega-\hbar\omega_0} - \frac{1}{\lambda_{K+q}-\lambda_K+\hbar\omega+\hbar\omega_0}\right). \tag{32}$$

It is seen that the imaginary part represents the optical conductivity out of any field. For the present case in which we investigate the effect of fields, we will focus on the real part. It reads

$$\mathrm{Re}\left[\sigma_{(\omega)}\right] = \frac{e^2}{S\hbar\omega}\frac{1}{\omega^2}\left\{\frac{1}{\omega}\sum_{q_{//}}\left(\frac{e^2B^2\left(m_e^3+m_h^3\right)}{2m_e^3m_h^3} - \frac{eE_{el}\left(m_h^2-m_e^2\right)}{2m_e^2m_h^2}\right)q\Xi(q)(f_{ex}^*-f_{ex})\right.$$
$$\left. + \hbar\sum_q\left(\frac{e^2B^2\left(m_e^3+m_h^3\right)}{2m_e^3m_h^3} - \frac{eE_{el}\left(m_h^2-m_e^2\right)}{2m_e^2m_h^2}\right)q\Xi(q)\left(\frac{f_{ex}}{\lambda_{K+q}-\lambda_K+\hbar\omega+\hbar\omega_0} - \frac{f_{ex}^*}{\lambda_{K+q}-\lambda_K+\hbar\omega-\hbar\omega_0}\right)\right\}. \tag{33}$$

The final expression of the real part of optical conductivity is determined by replacing the summation into integration. It takes the form

$$\mathrm{Re}\left[\sigma(\omega)\right] = \sigma_B(\omega) - \sigma_{el}(\omega), \tag{34}$$

with

$$\sigma_B(\omega) = \frac{e^2\left(D_c^{\mathrm{op}}-D_v^{\mathrm{op}}\right)^2}{16S\eta u\pi^2\hbar\omega}\frac{\hbar^3\left(m_e^3+m_h^3\right)}{m_e^3m_h^3\omega^2l_B^2}\int_0^\infty dq\int_0^{2\pi}d\theta\, q^3\left\{\frac{1/\omega}{\frac{\hbar^2q^2}{2M}+\frac{\hbar^2}{M}Kq\cos\theta-\hbar\omega_0} - \frac{1/\omega}{\frac{\hbar^2q^2}{2M}+\frac{\hbar^2}{M}Kq\cos\theta+\hbar\omega_0}\right.$$
$$+\frac{\hbar}{\left(\frac{\hbar^2q^2}{2M}+\frac{\hbar^2}{M}Kq\cos\theta+\hbar\omega+\hbar\omega_0\right)\left(\frac{\hbar^2q^2}{2M}+\frac{\hbar^2}{M}Kq\cos\theta-\hbar\omega_0\right)}$$
$$\left.-\frac{\hbar}{\left(\frac{\hbar^2q^2}{2M}+\frac{\hbar^2}{M}Kq\cos\theta+\hbar\omega-\hbar\omega_0\right)\left(\frac{\hbar^2q^2}{2M}+\frac{\hbar^2}{M}Kq\cos\theta+\hbar\omega_0\right)}\right\}, \tag{35}$$

and

$$\sigma_{el}(\omega) = \frac{e^3\left(D_c^{\mathrm{op}}-D_v^{\mathrm{op}}\right)^2}{16S\eta u\pi^2}\frac{\left(m_h^2-m_e^2\right)}{m_e^2m_h^2\omega^3}E_{el}\int_0^\infty dq\int_0^{2\pi}d\theta\, q^3\left\{\frac{1/\omega}{\frac{\hbar^2q^2}{2M}+\frac{\hbar^2}{M}Kq\cos\theta-\hbar\omega_0} - \frac{1/\omega}{\frac{\hbar^2q^2}{2M}+\frac{\hbar^2}{M}Kq\cos\theta+\hbar\omega_0}\right.$$
$$+\frac{\hbar}{\left(\frac{\hbar^2q^2}{2M}+\frac{\hbar^2}{M}Kq\cos\theta+\hbar\omega+\hbar\omega_0\right)\left(\frac{\hbar^2q^2}{2M}+\frac{\hbar^2}{M}Kq\cos\theta-\hbar\omega_0\right)}$$
$$\left.-\frac{\hbar}{\left(\frac{\hbar^2q^2}{2M}+\frac{\hbar^2}{M}Kq\cos\theta+\hbar\omega-\hbar\omega_0\right)\left(\frac{\hbar^2q^2}{2M}+\frac{\hbar^2}{M}Kq\cos\theta+\hbar\omega_0\right)}\right\}. \tag{36}$$

Now that the optical conductivity is obtained, let us evaluate the strength of optical transitions by the formula [62]

$$F_{osc}(\omega) = \frac{2\pi\varepsilon_0M}{ne^2\omega^2}\frac{1}{\tau_l}. \tag{37}$$

$F_{osc}$ is the oscillator strength and $\tau_l$ is the ground-state exciton-polaron lifetime taken as [63]

$$\frac{1}{\tau_l} = \frac{2\pi}{\hbar}\sum_q\left|\left\langle n_{q'},K\left|H_{ex-ph}^{2D}\right|K,n_q\right\rangle\right|^2\delta[\lambda_K-\lambda_{K+q}+\hbar\omega_0]. \tag{38}$$

TABLE I. Characteristics of each TMDC taken from Refs. [14,65].

| | $m_e$ ($m_0$) | $m_h$ ($m_0$) | $\hbar\omega_0$ (eV) | $D_c^{op}$ (eV) | $D_v^{op}$ (eV) | $E_b$ (eV) | $E_g$ (eV) |
|---|---|---|---|---|---|---|---|
| $MoSe_2$ | 0.64 | 0.71 | 0.0365 | 5.2 | 4.9 | 0.174 | 1.56 |
| $WSe_2$ | 0.39 | 0.51 | 0.0291 | 2.3 | 3.1 | 0.231 | 1.65 |
| $WS_2$ | 0.31 | 0.42 | 0.0435 | 3.1 | 2.3 | 0.19 | 2.10 |
| $MoS_2$ | 0.51 | 0.58 | 0.0443 | 5.8 | 4.6 | 0.313 | 1.87 |

Here we consider $n_{q'} = n_q - 1$ and the summation is transformed into integration. The integration over $q$, after averaging with $|\Psi_0\rangle$, gives

$$\frac{1}{\tau_l} = \frac{M\left(D_c^{op} - D_v^{op}\right)^2}{\hbar^3\,\pi\,\eta u}\bar{N}_0 \int_0^{2\pi} d\theta \frac{(\hbar^2 K^2\cos^2\theta + M\hbar\omega_0)}{\sqrt{\hbar^2 K^2\cos^2\theta + 2M\hbar\omega_0}}, \tag{39}$$

where $\bar{N}_0$ is the mean number of phonons [64] and the final expression of the oscillator strength is determined by substituting the latest relation in Eq. (37). This leads to

$$F_{osc} = \frac{2\varepsilon_0\left(D_c^{op} - D_v^{op}\right)^2 M^2}{n\eta u e^2\,\hbar^3}\frac{1}{[\exp(\beta\,E_K) - 1]\,\omega^2} \times \int_0^{2\pi} d\theta \frac{(\hbar^2 K^2\cos^2\theta + M\hbar\omega_0)}{\sqrt{\hbar^2 K^2\cos^2\theta + 2M\hbar\omega_0}}. \tag{40}$$

From Eqs. (13), (23), (26), (34), and (40) it is clear that the relaxation time, the electrical conductivity, the Seebeck coefficient, the optical conductivity, and the oscillator strength calculated for 1Ls TMDCs are influenced by both the magnetic barrier and the electric field acting on the TMDC monolayer.

## III. RESULTS AND DISCUSSION

For calculations of the properties we have described above, we use the following data showing some materials characteristics (see Table I).

Figures 2 and 3 plot the variation of the exciton-polaron ground-state energy for various monolayers TMDCs. Figure 2

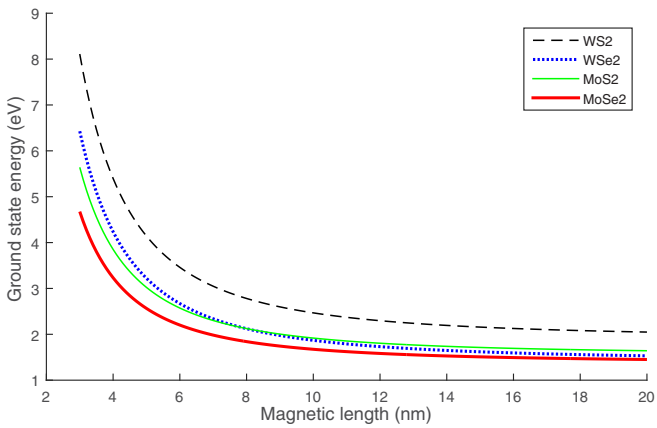


FIG. 2. GS energy of exciton-polaron as function of the magnetic length for zero electric field.

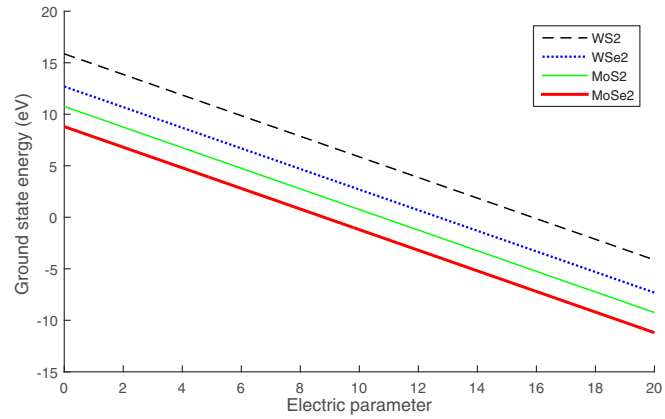


FIG. 3. GS energy of exciton-polaron vs the electric parameter for $l_B = 2$ nm.

shows the decrease of the exciton-polaron energy when enhancing the magnetic length and one can say that the energy is sensitive to the applied magnetic barrier.

Since the magnetic strength is inversely proportional to the magnetic length, it follows that the excitonic polaron energy increases with the enhancement of the magnetic field. In fact, the magnetic field reduces the interparticle distance and increases the Coulomb interaction of the electron-hole pair [41]. This leads to the increase of the binding energy. The excitonic polaron is then confined in the magnetic barrier and that favors its stability. Also, for $l_B > 15$ nm the energy becomes constant, meaning that the magnetic barrier loses its influence and it corresponds to weak magnetic range.

However, from the curves of Fig. 3, we observe a monotonic decrease of the GS energy when the electric parameter increases. Even if the excitonic polaron is a neutral set, it remains a two-particle system of opposite charges and then the presence of electric field affects the excitonic components.

In fact, the hole tends to move in the electric field direction, whereas its corresponding electron moves against the electric field. Because of this opposition in direction, one can say that due to the applied electric field the binding energy is reduced and it brings down the excitonic polaron stability. It adheres with the work of Oukerroum *et al.* [66]; Ref. [50] predicts the dissociation of exciton by electric field. The highest GS energy is obtained in $WS_2$ and the lowest in $MoSe_2$.

Figures 4 and 5 show the relaxation time of the exciton-polaron as a function of the magnetic length ($l_B$) and the electric parameter ($\xi_{el}$) respectively. The result indicates that the relaxation time increases as the magnetic length and electric parameter increase, and it saturates for high values of the parameters.

The relaxation of exciton-polaron is related to the process of phonons' absorption-emission in TMDCs. This process is influenced by the interaction with phonons: the less the exciton interacts in the structure, the more it relaxes. In fact, from the results of GS energy, it is shown that the enhancement of the magnetic length leads to the reduction in exciton binding energy. As the binding energy decreases, the interplay between exciton and phonon is lowered. This justifies the increase of the relaxation time observed in Fig. 4 and it adheres with Ref. [67]. In addition, it is observed that the

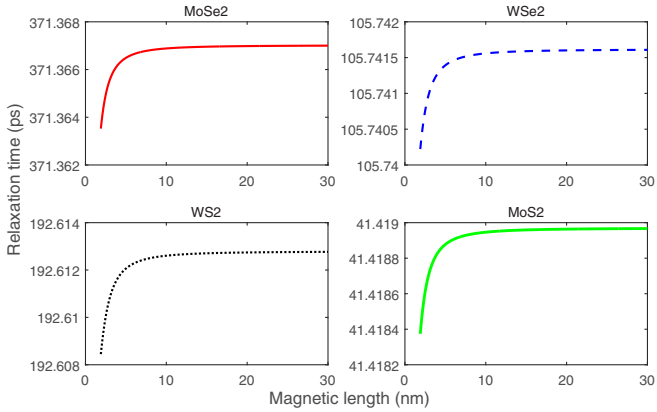


FIG. 4. Exciton-polaron relaxation time vs the magnetic length at $T = 70$ K.

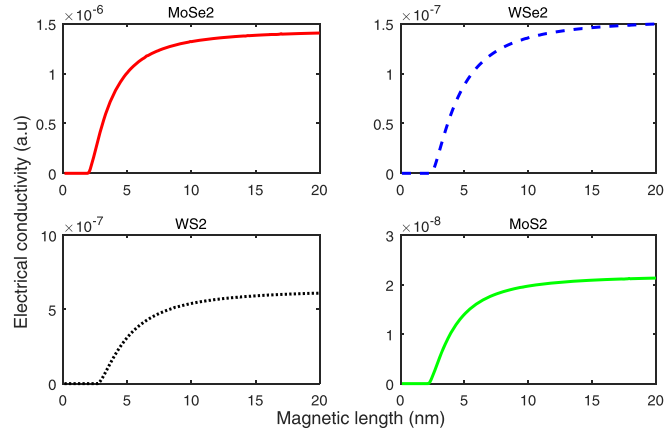


FIG. 6. Electrical conductivity vs the magnetic length at $T = 25$ K.

saturation occurs at $l_B = 15$ nm, meaning that the exciton-polaron reaches its maximum relaxation time and one can say that the phenomenon of relaxation is sensitive to the magnetic barrier. In the same way, as the electric field is applied, it delocalizes the hole and electron toward different directions. This generates the decrease of exciton binding energy contributing to the reduction of particle interactions. Therefore, the electron and hole are more relaxed in the presence of an external electric field and the exciton-polaron relaxation time enhances as shown in Fig. 5. The lowest relaxation time is observed in $MoS_2$ and the highest in $MoSe_2$. Also, Yan *et al.* [68] used a spectroscopic method in $WSe_2$ and found the relaxation time of free exciton about 2 ps at 70 K. Here, the relaxation time for $WSe_2$ is about 105 ps. Thus, we predict that the relaxation time of exciton-polaron in the presence of electric field and magnetic barrier is 50 times larger than that of free exciton.

Figures 6 and 7 present the electrical conductivity for TMDCs as a function of the magnetic length and electric parameter, respectively. One can see from Eq. (23) that the electrical conductivity is proportional to $\sqrt{d}$ and according to Eq. (22), we have $\sqrt{d} = \sqrt{E + E_b + G_{ex1} - E_g}$ when the fields are zero. Then, in the absence of any field, the electrical conductivity appears when the system's energy overpasses the band-gap energy, so that the electron can transit toward the conduction band.

Now from Fig. 6, it follows that there is no electrical conductivity for low values of the magnetic length. This result indicates that at very high magnetic strength, there is no electrical conductivity in TMDCs. Moreover, the system's energy should be greater than the band gap and the magnetic parameter since the electrical conductivity becomes proportional to $\sqrt{E + E_b + G_{ex1} - E_g - \xi_B}$ according to Eq. (22).

As the magnetic length increases, it favors the attenuation of the magnetic strength, and the electrical conductivity becomes possible. This occurs when the magnetic length reaches a value around 2.5 nm and from this value the electrical conductivity increases as the magnetic length increases. This enhancement of the electrical conductivity is in accordance with Refs. [69,70]. Also, applying the magnetic field along the $z$ direction induces the confinement and carriers' concentration in the $xy$ plane. Then, as $l_B$ increases, electron- and hole interactions with phonons grow because the particles motion increases. In Ref. [71] it is shown that the polaron motion is fast with higher magnetic barrier lengths.

Figure 7 shows the enhancement of electrical conductivity when the electric parameter increases. Reference [50]

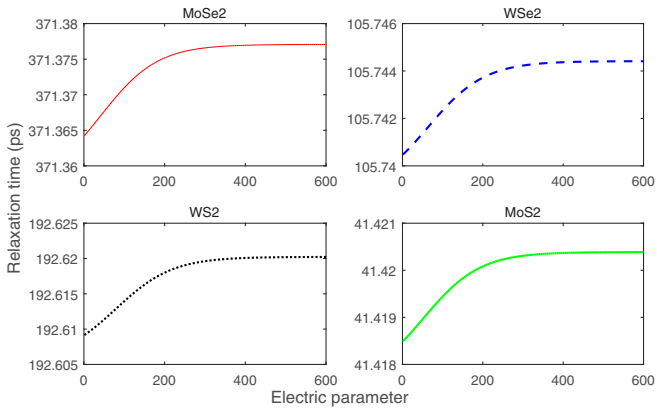


FIG. 5. Exciton-polaron relaxation time vs the electric parameter at $T = 70$ K.

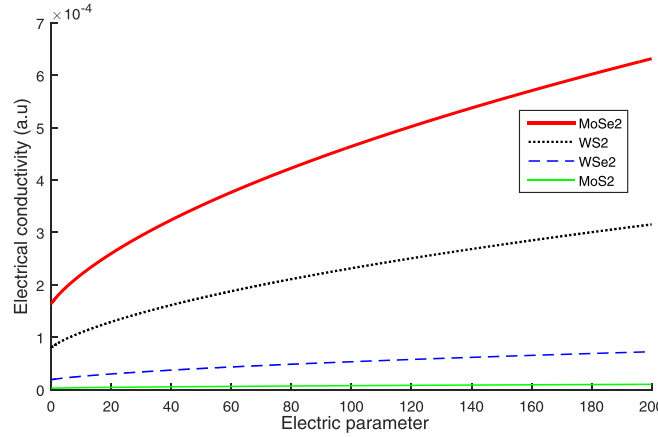


FIG. 7. Electrical conductivity vs the electric parameter at $T = 25$ K.

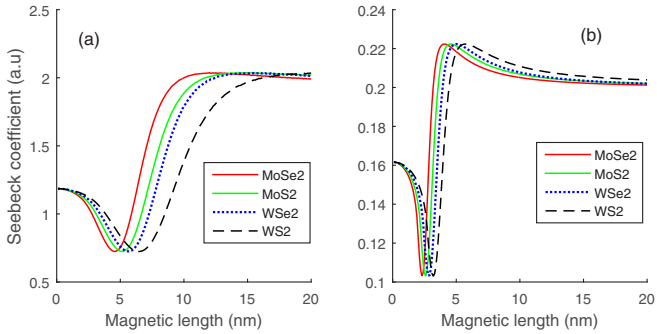


FIG. 8. Seebeck coefficient vs the magnetic length for (a) $T = 5$ K and (b) $T = 150$ K.

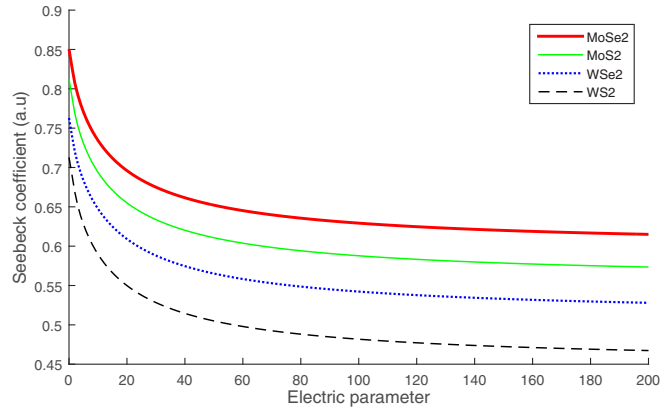


FIG. 9. Seebeck coefficient vs the electric parameter at $T = 25$ K.

demonstrated that the exciton energy level decreases when the electric field increases. In addition, the applied electric field induces an electric force responsible for the increase of electron's motion in TMDCs. Thus, the electric field facilitates the electronic transitions and it agrees with Ref. [72]. In addition, Fig. 7 shows a very low electrical conductivity in $MoS_2$ for $\xi_{el} = 0$ ($E_{el} = 0$) at 25 K. This is a good result, adhering with the experiment of Kim *et al.* [73]. The latest observed the increase of electrical conductivity with temperature and a weak value (close to zero) in 1L $MoS_2$ without heterostructure at 300 K.

Among the selected TMDCs, $MoSe_2$ has the greatest amplitude and its electrical conductivity begins at a low value ($l_B \approx 2$ nm), meaning that it is a suitable TMDC for studies in high magnetic fields. This can be due to its lowest bandgap energy which favors the electronic transition between valence- and conduction bands. This result of $MoSe_2$, also suggested by Figs. 4 and 5, fits with Ref. [42], which showed that the electrical conductivity rises when the relaxation time increases.

The Seebeck coefficient as a function of the magnetic length for low- and high temperatures and diverse TMDCs is presented in Figs. 8(a) and 8(b), respectively. It is observed that the curves do not present monotonic shapes. The Seebeck coefficient falls until to a critical value of the magnetic length, and above this value it increases. In fact, as the temperature changes in TMDCs, it generates excitations and increases the motion of particles. This leads to the appearance of a voltage responsible for the Seebeck effect. At a fixed temperature and for low values of the magnetic length, which means high magnetic field, the magnetic influence dominates. Then, electron (hole) is more confined than subjected to thermal perturbation and it explains the decrease of this property.

In the opposite way, above the critical value of the magnetic length, which means low magnetic field, the temperature effect dominates and enhances the Seebeck coefficient. It is in agreement with Refs. [70,74].

Also, the result shows that the magnetic effect is less significant in high-temperature range since one can observe the regression of the critical value range [from 5–7 nm in Fig. 8(a) to 2.5–3.5 nm in Fig. 8(b)] and the reduction of the Seebeck coefficient values regarding Fig. 8(a) and Fig. 8(b). In addition, for very high values of the magnetic length ($l_B >$ 18 nm) in Fig. 8(a) and $l_B > 10$ nm in Fig. 8(b)), the Seebeck coefficient becomes constant and the magnetic barrier does not influence this property more. At $T = 5$ K, the highest amplitude is obtained for $WS_2$ at low magnetic length and for $MoSe_2$ at high magnetic length.

Figure 9 presents the evolution of the Seebeck coefficient of TMDCs in the presence of the external electric field. The result shows the highest amplitudes of the coefficient at zero electric field. It decreases gradually as the field increases. This decrease of $S_b$ is in agreement with Ref. [75] and the experiment of Ref. [76]. Thus, the Seebeck effect as a thermoelectric power property is favored by the absence of the electric field. In this case, when the temperature changes, the electron (hole) moves directed only by the temperature gradient from the hot source to the cold source, and then it generates the Seebeck voltage.

In the presence of the electric field, the particles' motion is governed by the field. As the strength of the electric field increases, it overcomes the temperature gradient and the curves of the Seebeck coefficient decrease.

Figures 10 and 11 present the real part of the optical conductivity of TMDCs versus the magnetic length and electric field, respectively. The optical conductivity of TMDCs presents a high amplitude and this is also observed at room temperature by Kravets *et al.* [77]. The figures show that this

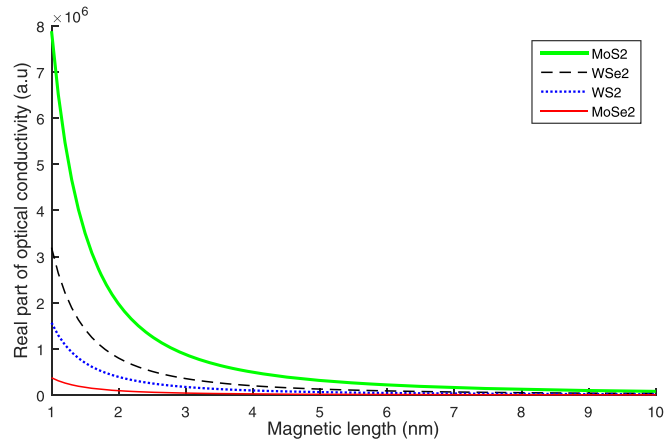


FIG. 10. Real part of the optical conductivity vs the magnetic length at $\hbar\omega = 0.1$ eV and $E_{el} = 0$.

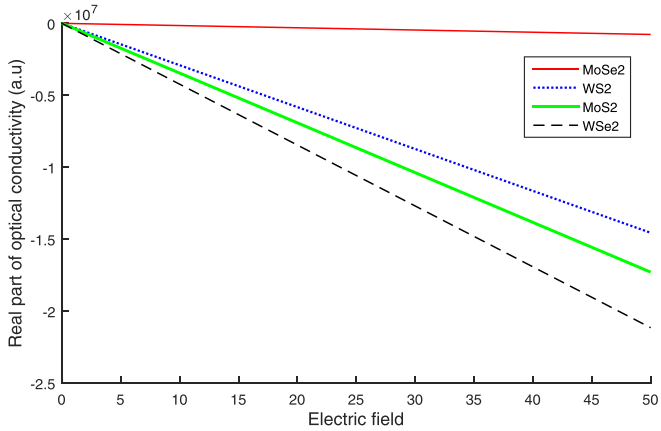


FIG. 11. Real part of optical conductivity vs the electric field for $l_B = 2$ nm and $\hbar\omega = 0.1$ eV.

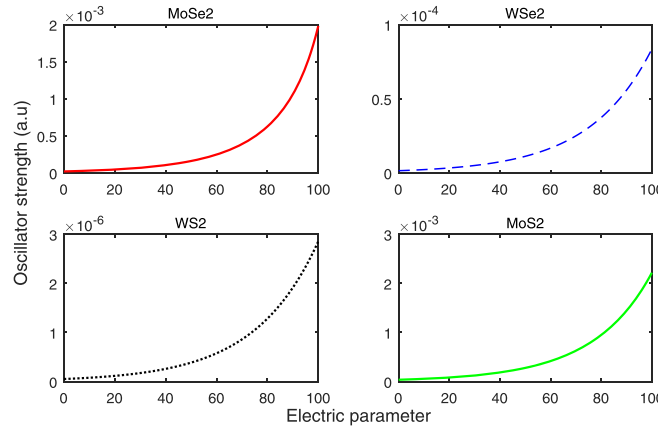


FIG. 13. Oscillator strength vs the electric parameter at $T = 25$ K.

property decreases when the magnetic length and electric field increase. It adheres, respectively, with Refs. [61,49]. As the applied energy $\hbar\omega$ is more than twice the phonon energy, the exciton-polaron becomes more energetic and then optical transitions can occur [55,78].

Moreover, the particles are well confined in the presence of the magnetic barrier favoring the growth of their energies. The increase of the magnetic length has the effect of reduce the exciton-polaron energy, then decreasing the optical conductivity as pointed out in Fig. 10. The highest optical conductivity is obtained for $MoS_2$.

Also, the presence of the electric field modifies the Coulomb force between electrons and holes reducing the exciton binding energy. In addition, according to Eq. (10) it is seen that the increase of the electric field leads to the decrease of the system energy. Therefore, the electric field does not favor the optical transitions. The negative sign in Fig. 11 is justified by the dominance of the electric field effect against the magnetic barrier according to Eq. (34).

Figures 12 and 13, respectively, show the evolution of the excitonic polaron oscillator strength when the magnetic length and the electric parameter change. The results indicate that it increases with the magnetic length and electric field. One can say that this property is very sensitive to low magnetic lengths

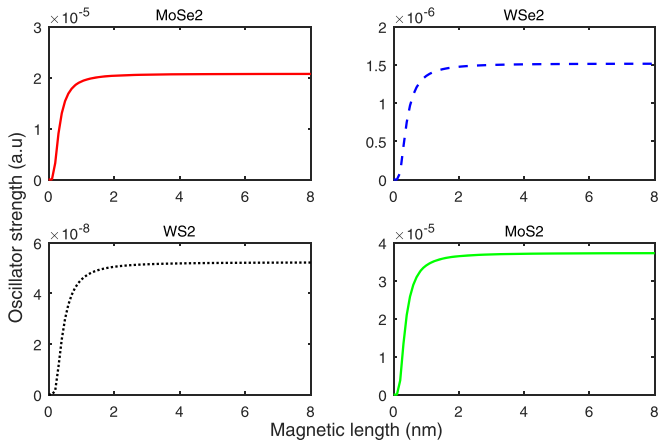


FIG. 12. Oscillator strength vs the magnetic length at $T = 25$ K.

(high magnetic strength) due to the rapid growth observed in Fig. 12.

From Eq. (37), it is seen that the lifetime is inversely proportional to the oscillator strength. The curve presents a saturation when $l_B > 2$ nm; the oscillator strength reaches its maximum and becomes constant. This range also corresponds to the shortest lifetime characterizing the lowest stability of exciton-polaron, since when the lifetime is zero it means the death of this quasiparticle [54]. Hence, the result shows that the less the exciton is confined, the lower its lifetime, the greater the oscillator strength, and it joins the work of Ref. [79]. From Fig. 13, it is seen that as the electric field increases, the particles' motions grow and the optical transition is faster. Moreover, it is in agreement with Ref. [72] which shows the decrease of lifetime when the electric field rises. Among the TMDCs, the highest value of oscillator strength is observed in $MoS_2$.

## IV. CONCLUSION

The relaxation of exciton-polaron and the transport properties under a magnetic barrier and an electric field have been investigated in various TMDCs. The analytical study of the relaxation time, the electrical conductivity, the Seebeck coefficient, the optical conductivity, and the oscillator strength has been done. It follows that the relaxation time of the exciton-polaron grows when the magnetic length and electric field increase. Also, the electrical conductivity increases as the magnetic length and electric field increase. It reaches at different values of the magnetic length characterizing each TMDC material. In addition, the Seebeck coefficient presents a monotonic decrease under the electric field, whereas the magnetic barrier changes its behavior. The low values of the magnetic length favor the decrease of this coefficient while the high values increase it. Moreover, the optical conductivity of TMDCs decreases with increasing both the magnetic length and electric field. The oscillator strength of the excitonic polaron is an increasing function of both magnetic length and electric field. It increases gradually as the electric field increases. This work shows that the magnetic barrier and the electric field can be used to adjust these transport properties and relaxation of the exciton-polaron in TMDCs. This could be useful to improve optical- and electronic device properties.

## ACKNOWLEDGMENTS

This research was supported by the Deutscher Akademischer Austauchdienst German Academic Exchange Service through the Staff Exchange Fellowships in Sub-Saharan-Africa under the funding Programme No. 57588199. N.C. acknowledges also support from ANID Fondecyt Iniciación en Investigación Project No. 11221088.


## APPENDIX A: DIAGONALIZATION METHOD

Let us use the unitary transformation:

$$U_{ex} = \exp(iS_a), \tag{A1}$$

with

$$S_a = \sum_{K,q} C^+_{K+q} C_K [f^*_{ex} b^+_{-q} + f_{ex}\, b_q]. \tag{A2}$$

The $f_{ex}$ functions are variational parameter. We apply the unitary transformation to the full Hamiltonian and get

$$\hat{\Gamma} = U^{-1}_{ex} \hat{H} U_{ex} \approx \hat{H}^{2D}_{ex} + \hat{H}_{ph} + \hat{\Gamma}^{2D}_{ex-ph}. \tag{A3}$$

The transformed Hamiltonian can be separated as

$$\hat{\Gamma} = \hat{H}_0 + \hat{\Gamma}^{2D}_{ex-ph}, \tag{A4}$$

where the free part $\hat{H}_0$ and the interacting part $\hat{\Gamma}^{2D}_{ex-ph}$ of $\hat{\Gamma}$ are given by

$$\hat{H}_0 = \hat{H}^{2D}_{ex} + \hat{H}_{ph}, \tag{A5}$$

$$\hat{\Gamma}^{2D}_{ex-ph} = \sum_{K,K',q} |\Xi^{\rm op}(q)|^2 (f^*_{ex} - f_{ex}) C^+_{K+q} C_K C^+_{K'+q} C_{K'}. \tag{A6}$$

Using a series expansion of (A4) and the perturbation theory [14], we obtain the $f_{ex}$ functions as

$$f^*_{ex} = \frac{\Xi^{\rm op}(q)}{\lambda(K+q, l_B, E_{el}) - \lambda(K, l_B, E_{el}) + \hbar\omega_0}$$

$$f_{ex} = \frac{\Xi^{\rm op}(q)}{\lambda(K+q, l_B, E_{el}) - \lambda(K, l_B, E_{el}) - \hbar\omega_0}. \tag{A7}$$

Therefore, according to (A7) and Eq. (6), we evaluate the summation over $q$ in (A6). This leads to

$$\hat{\Gamma}^{2D}_{ex-ph} = -\sum_{K,K'} [\tilde{G}_{ex2} + G_{ex1}] C^+_{K+q} C_K C^+_{K'+q} C_{K'}, \tag{A8}$$

with

$$G_{ex1} = \frac{\pi\sqrt{\hbar\omega_0}\left(D^{\rm op}_c - D^{\rm op}_v\right)^2}{\sqrt{2}\,\hbar^2\eta u}(m_e + m_h)^{3/2}, \tag{A9}$$

$$\tilde{G}_{ex2} = \left(\frac{\hbar^2 K^2}{2M}\right)\frac{3\pi\left(D^{\rm op}_c - D^{\rm op}_v\right)^2}{4\sqrt{2}\,\hbar^2\,\eta u}\frac{(m_e + m_h)^{3/2}}{\sqrt{\hbar\omega_0}}$$

$$= \left(\frac{\hbar^2 K^2}{2M}\right) G_{ex2}. \tag{A10}$$

Thus, the Hamiltonian in its approximate diagonalized form, taking into account Eq. (7), becomes

$$\hat{\Gamma} = \sum_K \lambda\, C^+_K C_K + \hat{H}_{ph} - \sum_{K,K'} [\tilde{G}_{ex2} + G_{ex1}] C^+_{K+q} C_K C^+_{K'+q} C_{K'}. \tag{A11}$$

## APPENDIX B: DEVELOPMENT OF THE DIRAC DELTA FUNCTION

Let us use the following relation:

$$\delta[g(q)] = \sum_i \frac{\delta(q - q_i)}{|g'(q_i)|}, \tag{B1}$$

where $q_i$ are the roots of the $g$ functions contained in the Dirac delta function and $g'$ its derivative. From Eq. (12), we consider

$$g_1 = E_K - E_{K+q} + \hbar\omega_0, \tag{B2}$$

$$g_2 = E_K - E_{K+q} - \hbar\omega_0. \tag{B3}$$

According to Eqs. (10) and (B1), we establish

$$\delta(g_1) = \frac{M}{\hbar^2(1 - G_{ex2})}\frac{\delta(q - q_1) + \delta(q - q_2)}{\sqrt{K^2\cos^2\theta + 2M\hbar\omega_0/\hbar^2(1 - G_{ex2})}}, \tag{B4}$$

$$\delta(g_2) = \frac{M}{\hbar^2(1 - G_{ex2})}\frac{\delta(q - q_3) + \delta(q - q_4)}{\sqrt{K^2\cos^2\theta - 2M\hbar\omega_0/\hbar^2(1 - G_{ex2})}}, \tag{B5}$$

with

$$q_1 = -K\cos\theta + \sqrt{K^2\cos^2\theta + 2M\hbar\omega_0/\hbar^2(1 - G_{ex2})}$$

$$q_2 = -K\cos\theta - \sqrt{K^2\cos^2\theta + 2M\hbar\omega_0/\hbar^2(1 - G_{ex2})}, \tag{B6}$$

$$q_3 = -K\cos\theta + \sqrt{K^2\cos^2\theta - 2M\hbar\omega_0/\hbar^2(1 - G_{ex2})}$$

$$q_4 = -K\cos\theta - \sqrt{K^2\cos^2\theta - 2M\hbar\omega_0/\hbar^2(1 - G_{ex2})}. \tag{B7}$$

These expressions (B4) and (B5) of the Dirac delta functions are suitable for integration or summation.

## APPENDIX C: COMMUTATOR OF FORCE OPERATORS AND AVERAGING

The force operator is defined as $F_\alpha(t) = (i/\hbar)[H, p_\alpha]$, with the linear momentum operator taken in the second quantization as $p_\alpha = \hbar K_\alpha C^+_{K\alpha} C_{K\alpha}$ [60], $\alpha$ standing for electron ($e$) or hole ($h$).

Thus,

$$F_e(t) = -i\left\{\left(\frac{e^2 B^2}{2m_e} - eE_{el}\right) C^+_{Ke}(t) C_{Ke}(t) + \sum_q q\,\Xi(q)\, C^+_{K+q}(t) C_K(t)\,(b_q(t) + b^+_{-q}(t))\right\}, \tag{C1}$$

$$F_h(t) = -i\left\{\left(\frac{e^2B^2}{2m_h} + eE_{el}\right)C^+_{Kh}(t)C_{Kh}(t) + \sum_q q\,\Xi(q)\,C^+_{K+q}(t)C_K(t)\,(b_q(t) + b^+_{-q}(t))\right\}. \tag{C2}$$

Also, the time dependence of the operators is given by

$$b_q(t) = e^{-i\omega_0 t}b_q(0); \quad b^+_{-q}(t) = e^{i\omega_0 t}b^+_{-q}(0), \tag{C3}$$

and

$$\begin{aligned} C^+_{K\alpha}(t)C_{K\alpha}(t) &= e^{(it/\hbar)\lambda_K}C^+_K(0)\,e^{[(-it)/\hbar]\lambda_K}C_K(0) \\ C^+_{K+q}(t)C_K(t) &= e^{(it/\hbar)\lambda_{K+q}}C^+_{K+q}(0)\,e^{[(-it)/\hbar]\lambda_K}C_K(0). \end{aligned} \tag{C4}$$

After straightforward calculations made in Eq. (30), we evaluate the commutator taking into account (C1), (C2), and the time dependence of the operators. This leads to

$$\begin{aligned} \left\langle \frac{1}{m_e^2}[F_e(t), F_e(0)] + \frac{1}{m_h^2}[F_h(t), F_h(0)]\right\rangle = \Bigg\langle \Bigg\{ &\sum_q \left(\frac{e^2B^2\left(m_e^3 + m_h^3\right)}{2m_e^3\,m_h^3} - \frac{eE_{el}\left(m_h^2 - m_e^2\right)}{2m_e^2\,m_h^2}\right) q\Xi(q)C^+_{K+q}C_K(b_q + b^+_{-q}) \\ &- \sum_q \left(\frac{e^2B^2\left(m_e^3 + m_h^3\right)}{2m_e^3\,m_h^3} - \frac{eE_{el}\left(m_h^2 - m_e^2\right)}{2m_e^2\,m_h^2}\right) q\Xi(q)C^+_{K+q}C_K(U(t)b_q + T(t)b^+_{-q}) \\ &- \frac{\left(m_h^2 + m_e^2\right)}{m_e^2\,m_h^2}\sum_q q^2\,\Xi^2(q)C^+_{K+q}C_KC^+_{K+q}C_K(U(t) - T(t))\Bigg\}\Bigg\rangle, \end{aligned} \tag{C5}$$

where

$$\begin{aligned} T(t) &= \exp\frac{it}{\hbar}(\lambda_{K+q} - \lambda_K + \hbar\omega_0); \\ U(t) &= \exp\frac{it}{\hbar}(\lambda_{K+q} - \lambda_K - \hbar\omega_0). \end{aligned} \tag{C6}$$

We then apply the unitary transformation and obtain

$$\begin{aligned} \left\langle \frac{1}{m_e^2}[F_e(t), F_e(0)] + \frac{1}{m_h^2}[F_h(t), F_h(0)]\right\rangle = \Bigg\langle \Bigg\{ &\sum_q \left(\frac{e^2B^2\left(m_e^3 + m_h^3\right)}{2m_e^3\,m_h^3} - \frac{eE_{el}\left(m_h^2 - m_e^2\right)}{2m_e^2\,m_h^2}\right) \\ &\times\ q\Xi(q)C^+_{K+q}C_K(b_q + b^+_{-q} + iC^+_{K+q}C_K(f^*_{ex} - f_{ex})) \\ &- \sum_q \left(\frac{e^2B^2\left(m_e^3 + m_h^3\right)}{2m_e^3\,m_h^3} - \frac{eE_{el}\left(m_h^2 - m_e^2\right)}{2m_e^2\,m_h^2}\right) \\ &\times\ q\Xi(q)C^+_{K+q}C_K\,(U(t)b_q + T(t)b^+_{-q} + iU(t)C^+_{K+q}C_Kf^*_{ex} - iT(t)C^+_{K+q}C_Kf_{ex}) \\ &- \frac{\left(m_h^2 + m_e^2\right)}{m_e^2\,m_h^2}\sum_q q^2\,\Xi^2(q)C^+_{K+q}C_KC^+_{K+q}C_K(U(t) - T(t))\Bigg\}\Bigg\rangle. \end{aligned} \tag{C7}$$

The average is done using the ground-state wave function. We have

$$\begin{aligned} \left\langle \frac{1}{m_e^2}[F_e(t), F_e(0)] + \frac{1}{m_h^2}[F_h(t), F_h(0)]\right\rangle = \Bigg\{ &i\sum_q \left(\frac{e^2B^2\left(m_e^3 + m_h^3\right)}{2m_e^3\,m_h^3} - \frac{eE_{el}\left(m_h^2 - m_e^2\right)}{2m_e^2\,m_h^2}\right) \\ &\times\ q\Xi(q)(f^*_{ex} - f_{ex}) - i\sum_q \left(\frac{e^2B^2\left(m_e^3 + m_h^3\right)}{2m_e^3\,m_h^3} - \frac{eE_{el}\left(m_h^2 - m_e^2\right)}{2m_e^2\,m_h^2}\right) q\Xi(q)(U(t)f^*_{ex} \\ &- T(t)f_{ex}) - \frac{\left(m_h^2 + m_e^2\right)}{m_e^2\,m_h^2}\sum_q q^2\,\Xi^2(q)(U(t) - T(t))\Bigg\}. \end{aligned} \tag{C8}$$

[1] A. Kormányos, V. Zolyomi, N. D. Drummond, and G. Burkard, Spin-Orbit Coupling Quantum Dots and Qubits in Monolayer Transition Dichalcogenides, Phys. Rev. X **4**, 011034 (2014).

[2] X. X. Song, D. Liu, V. Mosallanejad, J. You, T. Y. Han, D. T. Chen, H. O. Li, G. Cao, M. Xiao, G. C. Guo, and G. P. Guo, A gate defined quantum dot on the two-dimensional transition metal dichalcogenide semiconductor $WSe_2$, Nanoscale **7**, 16867 (2015).

[3] A. J. Pearce and G. Burkard, Electron spin relaxation in a transition metal dichalcogenide quantum dot, 2D Mater. **4**, 025114 (2017).

[4] K. F. Mak, K. He, C. Lee, G. H. Lee, J. Hone, T. F. Heinz, and J. Shan, Observation of tightly trions in monolayer $MoS_2$, Nat. Mater. **12**, 207 (2013).

[5] D. Y. Qiu, T. Cao, and S. G. Louie, Nonanalyticity Valley Quantum Phases and Lightlike Exciton Dispersion in Monolayer Transition Metal Dichalcogenides: Theory and First Principles Calculations, Phys. Rev. Lett. **115**, 176801 (2015).

[6] L. Yang, C. Xie, J. Jin, R. N. Ali, C. Feng, P. Liu, and B. Xiang, Properties preparation and applications of low dimensional transition metal dichalcogenides, Nanomaterials **8**, 463 (2018).

[7] G. Fiori, F. Bonaccorso, G. Iannccone, T. Palacios, D. Neumaier, A. Seabaugh, S. K. Banerjee, and L. Colombo, Electronics based on two dimensional materials, Nat. Nanotechnol. **9**, 768 (2014).

[8] M. Bernardi, C. Ataca, M. Palummo, and J. C. Grossman, Optical and electronic properties of two dimensional layered materials, Nanophotonics **6**, 479 (2017).

[9] G. Wang, C. Robert, M. M. Glazov, F. Cadiz, E. Courtade, T. Amand, D. Lagarde, T. Taniguchi, K. Watanabe, B. Urbaszek, and X. Marie, In-plane Propagation of Light in Transition Metal Dichalcogenide Monolayers: Optical Selection Rules, Phys. Rev. Lett. **119**, 047401 (2017).

[10] P. Dey, L. Yang, C. Robert, G. Wang, B. Urbaszek, X. Marie, and S. A. Crooker, Gate Controlled Spin Valley Locking of Resident Carriers in $WSe_2$ Monolayers, Phys. Rev. Lett. **119**, 137401 (2017).

[11] S. Ono and Tomohiro, Anomalous energy shift of laterally confined two dimensional excitons, J. Appl. Phys. **124**, 034301 (2018).

[12] S. Shree, M. Semina, C. Robert, B. Han, T. Amand, A. Balocchi, M. Manca, E. Courtade, X. Marie, T. Taniguchi, K. Watanabe, M. M. Glazov, and B. Urbaszek, Observation of exciton phonon coupling in $MoSe_2$ monolayers, Phys. Rev. B **98**, 035302 (2018).

[13] A. Chernikov, T. C. Berkelbach, H. M. Hill, A. Rigosi, Y. Li, Ö. B. Aslan, D. R. Reichman, M. S. Hybertsen, and T. F. Heinz, Exciton Binding Energy and Nonhydrogenic Rydberg Series in Monolayer $WS_2$, Phys. Rev. Lett. **113**, 076802 (2014).

[14] A. Thilagam, Excitonic polarons in low dimensional transition metal dichalcogenides, Phys. B: Condens. Matter **464**, 44 (2015).

[15] D. Akay, Trigonal warping and photoinduced effects on zone boundary phonon in monolayer graphene, Superlattices Microstruct. **117**, 18 (2018).

[16] B. S. Kandemir and D. Akay, Photoinduced dynamical band gap in graphene: The effects of electron phonon and spin orbit interaction, Phys. Status Solidi B **255**, 1800163 (2018).

[17] I. Favero, G. Cassabois, R. Ferreira, D. Darson, C. Voisin, J. Tignon, C. Delalande, G. Bastard, P. Roussignol, and J. M. Gerard, Acoustic phonon sidebands in the emission line of single InAs/GaAs quantum dots, Phys. Rev. B **68**, 233301 (2003).

[18] B. Krummheuer, V. M. Axt, and T. Kuhn, Theory of pure dephasing and the resulting absorption line shape in semiconductor quantum dots, Phys. Rev. B **65**, 195313 (2002).

[19] P. Machnikowski Jacak, J. Krasnyj, and P. Zoller, Coherent and incoherent phonon processes in artificial atoms, Eur. Phys. J. D **22**, 319 (2003).

[20] V. Jankovic and N. Vukmirovic, Dynamics of exciton formation and relaxation in photoexcited semiconductors, Phys. Rev. B **92**, 235208 (2015).

[21] S. Brem, M. Selig, G. Berghaeuser, and E. Malic, Exciton relaxation cascade in two dimensional transition metal dichalcogenides, Sci. Rep. **8**, 8238 (2018).

[22] V. A. Maidannyk and Y. H. Roos, Modification of the WLF Model for characterization of the relaxation time-temperature relationship in trehalose whey protein isolate systems, J. Food Eng. **188**, 21 (2016).

[23] I. Singh, S. Madan, A. Kaur, J. Kumar, P. K. Bhatnagar, and P. C. Mathur, Study of relaxation dynamics of photogenerated excitons in $CuInS_2$ quantum dots, MRS Commun. **4**, 1 (2014).

[24] L. Foglia, S. Vempati, B. T. Bonkano, L. Gierster, M. Wolf, S. Sadofev, and J. Stahler, Revealing the competing contributions of charge carriers excitons and defects to the non-equilibrium optical properties of ZnO, Struct. Dyn. **6**, 034501 (2019).

[25] A. O. El-Ballouli, E. Alarousu, A. Usman, J. Pan, O. M. Bakr, and O. F. Mohammed, Real time observation of ultrafast intraband relaxation and exciton multiplication in PbS quantum dots, ACS Photonics **1**, 285 (2014).

[26] A. R. S. Kandada and C. Silva, Exciton polarons in two dimensional hybrid metal halide perovskites, J. Phys. Chem. Lett. **11**, 3173 (2020).

[27] G. Y. Jia, Y. Liu, J. Y. Gong, D. Y. Lei, D. L. Wang, and Z. X. Huang, Excitonic quantum confinement modified optical conductivity of monolayer and few layered $MoS_2$, J. Mater. Chem. C **4**, 8822 (2016).

[28] H. Khoirunnisa and M. A. Majidi, Exploring excitonic signal in optical conductivity of ZnO through first order electron-hole vertex correction, J. Phys.: Conf. Ser. **1011**, 012073 (2018).

[29] R. W. Havener, Y. Liang, L. Brown, L. Yang, and J. Park, Van Hove singularities and excitonic effects in the optical conductivity of twisted bilayer graphene, Nano Lett. **14**, 3353 (2014).

[30] H. Haug and S. W. Koch, Semiconductor laser theory with many-body effects, Phys. Rev. A **39**, 1887 (1989).

[31] C. Ell, R. Blank, S. Benner, and H. Haug, Simplified calculations of the optical spectra of two and three dimensional laser excited semiconductors, J. Opt. Soc. Am. B **6**, 2006 (1989).

[32] N. M. R. Peres, R. M. Ribeiro, and A. H. C. Neto, Excitonic Effects in the Optical Conductivity of Gated Graphene, Phys. Rev. Lett. **105**, 055501 (2010).

[33] S. Yang, S. Tongay, Y. Li, Q. Yue, J. B. Xia, S. S. Li, J. Li, and S. H. Wei, Layer dependent electrical and optoelectronic responses of $ReSe_2$ nanosheet transistors, Nanoscale **6**, 7226 (2014).

[34] R. S. Chen, C. C. Tang, W. C. Shen, and Y. S. Huang, Thickness dependent electrical conductivities and ohmic contacts in transition metal dichalcogenides multilayers, Nanotechnology **25**, 415706 (2014).

[35] D. Qin, P. Yan, G. Ding, X. Ge, H. Song, and G. Gao, Monolayer $PdSe_2$: A promising two dimensional thermoelectric material, Sci. Rep. **8**, 2764 (2018).
[36] Y. Ge, W. Wenhui, R. Yulu, and L. Yong, Large thermoelectric power factor of high mobility transition metal dichalcogenides with 1T phase, Phys. Rev. Res. **2**, 013134 (2020).
[37] J. P. Ansermet and S. D. Brechet, Magnetic contribution to the Seebeck effect, Entropy **20**, 912 (2018).
[38] U. I. Erkaboev, G. Gulyamov, J. I. Mirzaev, and R. G. Rakhimov, Modeling on the temperature dependence of the magnetic susceptibility and electrical conductivity oscillations in narrow gap semiconductors, Int. J. Mod. Phys. B **34**, 2050052 (2020).
[39] Y. Jiang, Shula Chen, W. Zheng, B. Zheng, and A. Pan, Interlayer exciton formation relaxation and transport in TMD van der Waals heterostructures, Light: Sci. Appl. **10**, 72 (2021).
[40] V. Kattoor, K. Awasthi, E. Jokar, E. W. G. Diau, and N. Ohta, Enhanced dissociation of hot excitons with an applied electric field under low power photoexcitation in two dimensional perovskite quantum wells, J. Phys. Chem. Lett. **10**, 4752 (2019).
[41] M. Van der Donck, M. Zarenia, and F. M. Peeters, Excitons trions and biexcitons in transition metal dichalcogenides: Magnetic field dependence, Phys. Rev. B **97**, 195408 (2018).
[42] S. I. Nam, Electrical conductivity of quark matter at finite $T$ under external magnetic field, Phys. Rev. D **86**, 033014 (2012).
[43] A. Das, H. Mishra, and R. K. Mohapatra, Magneto Seebeck coefficient and Nernst coefficient of a hot and dense hadron gas, Phys. Rev. D **102**, 014030 (2020).
[44] M. Tahir, P. Vasilopoulos, and F. M. Peeters, Magneto optical transport properties of monolayer phosphorene, Phys. Rev. B **92**, 045420 (2015).
[45] C. C. Homes, M. Ali, and R. J. Cava, Optical properties of the perfectly compensated semimetal $WTe_2$, Phys. Rev. B **92**, 161109(R) (2015).
[46] D. K. Efimkin and A. H. MacDonald, Exciton polarons in doped semiconductors in a strong magnetic field, Phys. Rev. B **97**, 235432 (2018).
[47] S. Chaudhary, C. Knapp, and G. Refael, Anomalous exciton transport in response to a uniform in-plane electric field, Phys. Rev. B **103**, 165119 (2021).
[48] A. Balocchi, Q. H. Duong, P. Renucci, B. Liu, C. Fontaine, T. Amand, D. Lagarde, and X. Marie, Full Electrical Control of the Electron Spin Relaxation in GaAs Quantum Wells, Phys. Rev. Lett. **107**, 136604 (2011).
[49] E. Kasapoglu, H. Sari, M. Bursal, and I. Sokmen, Exciton absorption in quantum well wires under the electric field, Physica E **16**, 237 (2003).
[50] E. M. Proupin and C. T. Giner, Electric field and exciton structure in CdSe nanocrystals, Phys. Rev. B **69**, 125336 (2004).
[51] K. Cong, G. T. Noe II, and J. Kono, Excitons in magnetic fields, Encycl. Mod. Optics II **2**, 63 (2018).
[52] N. Myoung, G. Ihm, and S. J. Lee, Transport in armchair graphene nanoribbons moduled by magnetic barriers, Physica E **42**, 2808 (2010).
[53] S. Ghosh and M. Sharma, Electron optics with magnetic vector potential barriers in graphene, J. Phys.: Condens. Matter **21**, 292204 (2009).
[54] C. Kenfack-Sadem, A. K. Teguimfouet, A. Kenfack-Jiotsa, and R. M. K. Tsiaze, Dynamics and decoherence of exciton polaron in monolayer transition metal dichalcogenides, J. Electron. Mater. **50**, 2911 (2021).
[55] A. Thilagam and J. Singh, Excitonic polarons in quasi two dimensional structures, Appl. Phys. A **62**, 445 (1996).
[56] V. K. Kozin, V. A. Shabashow, A. V. Kavokin, and I. A. Shelykh, Anomalous Exciton Hall Effect, Phys. Rev. Lett. **126**, 036801 (2021).
[57] G. Pizzi, D. Volja, B. Kozinsky, M. Fornari, and N. Marzari, An updated version of Boltzwann: A code for the evaluation of thermoelectric and electronic transport properties with a maximally localized Wannier functions basis, Comput. Phys. Commun. **185**, 2311 (2014).
[58] M. J. Tomczak, K. Haule, T. Miyake, A. Georges, and G. Kotliar, Thermopower of correlated semiconductors: Application to $FeAs_2$ and $FeSb_2$, Phys. Rev. B **82**, 085104 (2010).
[59] S. Huang, H. J. Liu, D. D. Fan, P. H. Jiang, J. H. Liang, G. H. Cao, R. Z. Liang, and J. Shi, First principles study of the thermoelectric properties of the Zintl compound KSnSb, J. Phys. Chem. C **122**, 4217 (2018).
[60] J. T. Devreese, *Frohlich Polarons: Lecture Course Including Detailed Theoretical Derivation* (Antwerp, Belgium, 2018).
[61] M. Oliva-Leyva and C. Wang, Magneto optical conductivity of anisotropic two dimensional Dirac Weyl materials, Ann. Phys. **384**, 61 (2017).
[62] C. Meier, S. Lüttjohann, M. Offer, H. Wiggers, and A. Lorke, Silicon nanoparticles: Excitonic fine structure and oscillator strength, Adv. Solid State Phys. **48**, 79 (2009).
[63] D. Kozawa, R. Kumar, A. Carvalho, K. K. Amara, W. Zhao, S. Wang, M. Toh, R. M. Ribeiro, A. H. C. Neto, K. Matsuda, and G. Eda, Photocarrier relaxation pathway in two dimensional semiconducting transition metal dichalcogenides, Nat. Commun. **5**, 4543 (2014).
[64] M. F. C. Fobasso, C. Kenfack-Sadem, E. Baloitcha, A. J. Fotue, and L. C. Fai, Lifetime and dynamics of polaron and bipolaron in graphene nanoribbon under laser, Eur. Phys. J. Plus **135**, 471 (2020).
[65] Y. Xiao, Z. Q. Li, and Z. W. Wang, Polaron effect on the bandgap modulation in monolayer transition metal dichalcogenides, J. Phys.: Condens. Matter **29**, 485001 (2017).
[66] A. Oukerroum, E. Feddi, J. B. Bailach, J. M. Pastor, F. Dujardin, and E. Assaid, On the anomalous Stark effect in a thin disc-shaped quantum dot, J. Phys.: Condens. Matter **22**, 375301 (2010).
[67] M. Ghali, J. Kossut, E. Janik, F. Teppe, M. Vladimirova, and D. Scalbert, Spin precession in a model structure for spintronics, AIP Conf. Proc. **772**, 1383 (2005).
[68] T. Yan, S. Yang, D. Li, and X. Cui, Long valley relaxation time of free carriers in monolayer $WSe_2$, Phys. Rev. B **95**, 241406(R) (2017).
[69] H. Xu, J. Wei, H. Zhou, J. Feng, T. Xu, H. Du, C. He, Y. Huang, J. Zhang, Y. Liu, H. C. Wu, C. Guo, X. Wang, Y. Guang, H. Wei, Y. Peng, W. Jiang, G. Yu, and X. Han, High spin Hall conductivity in large area type II Dirac semimetal $PtTe_2$, Adv. Mater. **32**, 2000513 (2020).
[70] A. Das, H. Mishra, and R. K. Mohapatra, Electrical conductivity and Hall conductivity of a hot and dense hadron gas in a magnetic field: A relaxation time approach, Phys. Rev. D **99**, 094031 (2019).
[71] J. R. Djomou, S. C. Kenfack, A. J. Fotue, M. F. C. Fobasso, and L. C. Fai, Contribution of bulk and surface phonons to

the properties of polaron in a $Zn_{1-x}Cd_xSe/ZnSe$ heterojunction confined in a triangular potential, Phys. B: Condens. Matter **548**, 58 (2018).

[72] J. V. Nguepnang, A. K. Teguimfouet, C. S. Kenfack, and A. J. Kenfack, Polaron dynamic and decoherence in transition metal dichalcogenides under electric field, Indian J. Phys. **96**, 2001 (2022).

[73] S. Kim, C. Lee, Y. S. Lim, and J. H. Shim, Investigation for thermoelectric properties of the $MoS_2$ monolayer-graphene heterostructure: Density functional theory calculations and electrical transport measurements, ACS Omega **6**, 278 (2021).

[74] B. Skinner and L. Fu, Large nonsaturating thermopower in a quantizing magnetic field, Sci. Adv. **4**, eaat2621 (2018).

[75] J. Hong, C. Lee, J. S. Park, and J. H. Shim, Control of valley degeneracy in $MoS_2$ by layer thickness and electric field and its effect on thermoelectric properties, Phys. Rev. B **93**, 035445 (2016).

[76] M. Buscema, M. Barkelid, V. Zwiller, H. S. J. Van der Zant, G. A. Steele, and A. C. Gomez, Large and tunable photothermoelectric effect in single layer $MoS_2$, Nano Lett. **13**, 358 (2013).

[77] V. G. Kravets, V. V. Prorok, L. V. Poperenko, and I. A. Shaykevich, Ellipsometry and optical spectroscopy of low dimensional family TMDs, Semiconductor Phys.-Quantum Electron. Optoelectron. **20**, 284 (2017).

[78] P. F. Li and Z. W. Wang, Optical absorption of Frohlich polaron in monolayer transition metal dichalcogenides, J. Appl. Phys. **123**, 204308 (2018).

[79] M. Baira, M. Aljaghwani, B. Salem, N. A. Madhar, and B. Ilhi, Investigation of GeSn/Ge quantum dots optical transitions for integrated optics on Si substrate, Results Phys. **12**, 1732 (2019).